

Innovative optical lactate biosensing through the design of nanostructured materials

THÈSE N° 6520 (2015)

PRÉSENTÉE LE 8 OCTOBRE 2015

À LA FACULTÉ DES SCIENCES ET TECHNIQUES DE L'INGÉNIEUR
LABORATOIRE DE TECHNOLOGIE DES POUDRES
PROGRAMME DOCTORAL EN SCIENCE ET GÉNIE DES MATÉRIAUX

ÉCOLE POLYTECHNIQUE FÉDÉRALE DE LAUSANNE

POUR L'OBTENTION DU GRADE DE DOCTEUR ÈS SCIENCES

PAR

Oswaldo Javier PÉREZ ANGUIANO

acceptée sur proposition du jury:

Prof. P. Muralt, président du jury
Prof. H. Hofmann, Dr E. Scolan, directeurs de thèse
Prof. F. Nüesch, rapporteur
Dr R. Steiger, rapporteur
Dr G. Suarez, rapporteur



ÉCOLE POLYTECHNIQUE
FÉDÉRALE DE LAUSANNE

Suisse
2015

Todo libro, como todo recorrido, cobra sentido hasta su término.
Las primeras páginas de una historia, como los primeros pasos que damos al empezar un
viaje, nos parecen incomprensibles hasta no saber como acaba.
Un rostro también es una historia y requiere tiempo; demorarnos, llegar hasta el final.
— Valeria Luiselli, *Papeles falsos*

Dedicado a mis padres

Acknowledgements

Every book, like every journey, only makes sense when it ends. This line sums up in a simplistic way my own experience during this academic journey. Never did I imagine to find myself in such a privileged position in my life, with many inspiring people around, and with so many opportunities to learn, from nanotechnology and materials science, and from life. I have evolved, not only as a scientist, but as a human being, and I am very thankful for this gift.

First of all I would like to thank this country which has welcomed me and changed my life forever. The possibility to do a PhD at EPFL is a dream of many, and I am deeply grateful for this opportunity. But also I am very appreciative of my very own experience living in Switzerland, from the views of Lac Léman serving as a mirror to the Alpes (which I watched from my seat every morning on the train), to the politeness, correctness and respect from the people. True: not everything is perfect in Switzerland, particularly for a lactose-intolerant Mexican. In many occasions my social interactions during coffee breaks or outings have ended up with a bloated belly: milk chocolate, fondue, luxemburgerli, and all the most delicious creamy and fluffy desserts that contain dairy products. It has been the price I had to pay, and which I will keep paying.

I would like to thank:

* my supervisors, Prof. Heinrich Hofmann and Dr. Emmanuel Scolan. I thank Prof. Hofmann for offering me the opportunity to enrol at EPFL under his supervision. His support was endless, as well as his sense of humor. During my PhD I felt part of LTP despite of working most of the time in Neuchâtel, and this was due to his constant invitations to join the activities from his lab. I thank Manu for introducing me to the world of sol-gel technology and wine tasting. His know-how and guidance during my PhD at CSEM combined with his well known gourmand personality and generous apéros made all the fun at work double. Thank you both for your support and patience.

* the jury members from my PhD exam: Prof. Paul Mural, Prof. Frank Nüesch, Dr. Rolf. Steiger and Dr. Guillaume Suárez for the time spent reviewing my thesis and their comments to improve it.

*Prof. Frank Caruso, from the University of Melbourne in Australia, for allowing me to perform part of my PhD at his lab.

* CSEM for the possibility to do my PhD there. Apart from the freedom and the good environment to work, I had the opportunity to undertake other activities such as launching a PhD student club, and doing some sport for which the company was very supportive. Particularly

Acknowledgements

I would like to thank Ms. Anne-Marie van Rampaey for her approachability, which I very much appreciated. I reckon that my experience at CSEM on how directors interact with their employees independently of their job function should be emulated, as it makes the workplace more human. I also would like to thank Ms. Dominique LeRoux-Morger for her assistance with the more than usual administrative tasks I had to go through. Also I thank Dr. Raphaël Pugin for the opportunity to join his team to perform my PhD there.

* Dr. Bernard Wenger for serving in many occasions as a second CSEM supervisor. My discussions with you, specially those regarding the design of a biosensor, were very important to focus my efforts during the second half of my project. In the same sense, I would like to thank Dr. Stéphanie Boder-Pasche for the invitation to join a CSEM internal project, which gave direction to the final applications of my PhD work.

* Dr. Rolf Steiger for the many inspirational and interesting discussions we had, from archeology, languages, to science. I have never met anyone so eager to keep learning and with such a deep knowledge on diverse fields. After my conversations with you I felt very inspired and full of drive to keep going with my PhD project.

* Dr. Nicolas Blondiaux, Nico, who was a very neighborly engineer who happened to be my office mate. I appreciated very much your positive vibe and friendly personality in the lab or at the office.

* my LTP fellows : the Abhishek (Tewari and Kumar), June, Sandra, Gaby, Lionel, Vianney, Débora. My visits to EPFL were always fun because of you.

* my CSEM fellows and colleagues, which are many: Bastien, Sher, Tobias, Alex (my fellow PhD students) Gaëlle, Greg, Véro, Noémie, Lolo, Aurélie (my section colleagues), David, Johan, Jiamwen, Fabian (my fellow PhD Club committee members), Martha, Harry, Marta, Réal, Mélanie, Olga, Cristina, Ludo, , Rolf, Silvia, Bane (my Divison colleagues) and more. Thank you all for the nice moments, talks and adventures shared and for all the help received.

* Sophie and Patricia, our friendly and efficient secretaries, to whom I enjoyed very much working with. I am very thankful for all your support along my PhD at CSEM (and for the chocolates at your office too).

* the friends from Melbourne: Blaise, Katelyn (Lupe), Markus, Martin, Suma, Mattias, Jiwei, Junling, Alessia, Kristian, Julia, Sher Leen, David, Cathy, Sylvia, Ada, for the fun times, banana breads, and meals together in the lab or somewhere else. I want to thank very specially to you Mona for making my stay in Melbourne amazing. I could not have asked for a better place to stay and a better company to have. I am so grateful to you. I dedicate to you guys these lines to thank you for the wonderful welcome I received and the great memories I have. You should know that meeting you and spending time with you has been a highlight from my PhD, and all the moments and experiences we shared I cherish them greatly.

Finally, I want to thank my friends and family. Your support and advice was always constant and it definitely was a source of constant motivation for me during my PhD.

Geneva, 20 July 2015

O.

Abstract

The scope of this thesis is the synthesis of nanostructured materials, their functionalization and use for optical lactate biosensing applications. Rapid detection of L-lactate is important in many applications in the clinical sector, in the food industry, or in biotechnology. The formation of enzyme loaded nanostructured materials is a promising approach to obtain performing, reliable and stable enzyme-based optical biosensors. Two different sensing schemes are proposed: the development of lactate-responsive films (patches) and the development of a microparticle based lactate detection system.

The content of this work can be divided in three main tasks: (i) the synthesis of relevant nanostructured support materials for enzyme immobilization, (ii) the functionalization of these materials towards lactate detection, and (iii) the assessment of the performance and sensitivity of these enzyme-loaded films and particles for biosensor applications. For the synthesis of nanostructured supports for enzyme immobilization suitable for optical biosensing, several constraints must be met: The design of porous supports aims at providing large surface area for enzyme loading. Additionally, the porosity design must take into account that enzymes are large biomolecules, requiring tailored pore sizes to be transported and immobilized within the inner surface of the material. In this work, the synthesis of large mesoporous silica films with pore sizes ranging from 10 to 50 nm was explored by two different methodologies. Firstly, a bottom up approach was followed using amphiphilic block copolymers as porogenic templates and silicon alkoxides as silica precursors. Secondly, a powder approach using pre-synthesized silica particles in form of agglomerates was employed to obtain stable silica dispersions, which after casting resulted in porous silica films with pore sizes within the large-mesopore range. To further improve the performance of these materials for enzyme immobilization, multi-scale porous films including large mesopores and macropores were synthesised by the powder approach, where polymer particles as additional macroporous templates were used.

The functionalization of nanostructured silica films for L-lactate biosensing was explored using two different enzymes. As a first alternative, lactate dehydrogenase (LDH) was immobilized on amino-functionalized silica surfaces, and its immobilization and performance towards lactate detection was compared between monomodal (mesoporous) and bimodal (meso-macroporous) films. Adsorption and desorption of LDH using quartz crystal microbalance measurements confirmed higher enzyme loadings and better stability against desorption for the hierarchical films. Enzyme activity tests suggested that additional advantages from the use of multi-scale porous enzyme supports were obtained: increased enzyme loading, better stability, and stronger and faster response compared to mesoporous-only films, allowing more sensitive and more robust detection of L-lactate.

A novel concept for L-lactate biosensing is finally presented using a second enzyme, lactate oxidase (LOx); unlike LDH, it does not require a cofactor. This detection scheme is based on

Abstract

a combination of a powder approach for the synthesis of the enzyme's silica support and a layer-by-layer assembly of polyelectrolytes. These hybrid systems incorporate cytochrome C (CytC) as a biosensing element. Its optical properties depend on its oxidation state and can be coupled to the oxidation of L-lactate via the generation of hydrogen peroxide by LOx. The kinetic and structural aspects of the resulting materials are presented and discussed. In addition to the film-based detection schemes, a final part of the thesis focuses on the formation of LOx-CytC particles using porous calcium carbonate particles as sacrificial templates. The resulting protein-based particles can be used directly for facile optical detection of lactate; moreover, they are interesting materials for future developments of optical detection methods based on liquid suspensions, for example in cell media.

Key words: biosensors, coatings, sol-gel chemistry, enzyme immobilization, amphiphilic block copolymers, large mesopores, thin films, layer-by-layer assembly, polyelectrolyte multilayers, lactate dehydrogenase, lactate oxidase, cytochrome C

Résumé

Cette thèse porte sur la synthèse de matériaux de silice nanostructurés ainsi que sur la modification de ces matériaux en vue de leur utilisation pour des applications biocapteurs enzymatiques pour la mesure du L-lactate .

La détection rapide du L-lactate est importante pour de nombreuses applications dans le secteur clinique, dans l'industrie alimentaire, ou dans la biotechnologie. La formation de matériaux nanostructurés est une approche prometteuse pour obtenir des biocapteurs optiques performants à base d'enzymes. Deux différents schémas sont proposés : le développement des couches minces (patch) sensibles au lactate et le développement d'un système pour la mesure du lactate à base de microparticules.

Le contenu de cette thèse peut être divisé en trois tâches principales : (i) la synthèse de supports nanostructurés pertinents pour l'immobilisation d'enzymes, (ii) la fonctionnalisation de ces matériaux en vue de la détection du L-lactate, et (iii) l'évaluation de la performance et de la sensibilité des films et des particules pour les applications biocapteurs. La conception des supports poreux vise à fournir une grande surface pour héberger les biocatalyseurs. Cependant, la conception de la porosité doit tenir compte du fait que les enzymes sont de grandes molécules biologiques. Par conséquent, des tailles de pores adaptées sont nécessaires pour permettre le transport contrôlé et l'immobilisation de l'enzyme à la surface des pores. Dans cet objectif, des films mésoporeuses de silice avec des tailles de pores de 10 à 50 nm ont été synthétisés.

Une approche 'bottom-up' a été suivie en utilisant des copolymères à blocs amphiphiles comme agents porogènes et des alcoxydes de silicium comme précurseurs de silice. Une deuxième approche a été développée en utilisant des particules de silice pré-synthétisées afin d'obtenir des dispersions stables de silice. Ces dispersions ont ensuite été déposées sur des supports solides pour former des films mésoporeux. Afin d'améliorer les performances de ces matériaux pour l'immobilisation des enzymes, des films à porosité hiérarchique ont été synthétisés. A cet effet, des particules polymères ont été utilisées comme générateurs de macropores.

Les films de silice nanostructurés ont été fonctionnalisés avec deux enzymes différentes pour la détection du L-lactate. Dans une première variante, la lactate déshydrogénase (LDH) a été immobilisée sur les surfaces de silice amino-fonctionnalisées. Sa performance en vue de la détection du lactate a été comparée entre des couches mésoporeuses et hiérarchiques. L'influence de la porosité sur la détection de lactate a été déterminé : les couches hiérarchiques permettent une adsorption plus importante de l'enzyme, une meilleure stabilité et une ré-

Abstract

ponse plus rapide par rapport aux couches mésoporeuses. Dans une deuxième approche, un nouveau concept pour la détection du lactate a été développé en utilisant la lactate oxydase (LOx) en combinaison avec le cytochrome C (CytC). Contrairement à la lactate déshydrogénase, le mécanisme réactionnel de cette enzyme ne nécessite pas de cofacteur. En utilisant des films multicouches à base de polyélectrolytes, cette approche hybride comprend le CytC comme indicateur optique. Ses propriétés optiques dépendent de son état d'oxydation et il est lié à l'oxydation du L-lactate par la production de peroxyde d'hydrogène par la lactate oxydase. Les aspects cinétiques et structurels des films hybrides sont présentés et discutés.

En plus des systèmes de détection à base de films, la dernière partie de la thèse porte sur la formation des particules hybrides LOx-CytC. Elles sont formées en utilisant des microsphères poreuses de carbonate de calcium comme agents porogènes sacrificiels. Les particules à base de protéines ainsi obtenues peuvent être utilisées directement pour la détection optique du lactate. Elles sont également intéressantes pour les futurs développements de méthodes de détection optique dans des suspensions liquides, par exemple dans les milieux de culture cellulaire.

Mots clés : biocapteurs, chimie sol-gel, immobilisation d'enzymes, mésopores, films minces, assemblage couche par couche, multicouches de polyélectrolytes, lactate déshydrogénase, lactate oxydase, cytochrome C

Zusammenfassung

Die vorliegende Arbeit befasst sich mit der Synthese, Funktionalisierung und Anwendung nanostrukturierter Materialien für Biosensor-Anwendungen zur optischen Bestimmung von L-Lactat. Schnellmethoden zum Nachweis von L-Lactat sind von Bedeutung in zahlreichen Anwendungen im klinischen Bereich, in der Lebensmittelindustrie sowie in der Biotechnologie. Die Synthese nanostrukturierter organisch/anorganischer Hybridmaterialien ist ein vielversprechender Ansatz für die Entwicklung empfindlicher, zuverlässiger und stabiler optisch-enzymbasierter Biosensoren. Die hier vorgestellten Ansätze beruhen auf zwei verschiedenen Biosensor-Konzepten: es wurden sowohl L-Lactat-empfindliche Filme (patches) als auch enzymatisch aktive Mikropartikeln zur Lactatbestimmung entwickelt.

Der Inhalt dieser Arbeit ist in die folgenden Schwerpunkte unterteilt: (i) die Synthese nanostrukturierter Trägermaterialien für die Enzymimmobilisierung, (ii) die Funktionalisierung dieser Materialien für bioanalytische Anwendungen, und (iii) die Beurteilung der Wirksamkeit und Empfindlichkeit der so hergestellten enzymbeladenen Filme und Partikeln für Biosensor-Applikationen.

Für das Design der porösen Trägermaterialien ist die Bereitstellung einer grossen spezifischen Oberfläche für die Enzymbeladung wichtig. Jedoch muss daneben auch berücksichtigt werden, dass Enzyme grosse Biomoleküle sind, die eine massgeschneiderte Porenstruktur erfordern, um den Stofftransport innerhalb des Films zu erleichtern. In dieser Arbeit wurde deshalb die Synthese mesoporöser Siliciumdioxid-Filme mit Porengrössen im Bereich von 10 bis 50 nm untersucht. Zum einen wurde ein 'bottom up' Ansatz mit amphiphilen Blockcopolymeren als porogenen Matrizen und Siliciumalkoxiden als Siliciumdioxid-Vorstufen entwickelt. Zweitens wurde eine pulverbasierte Methode verwendet, bei der stabile Disersionen vorsynthetisierter SiO₂-Agglomerate als Beschichtungsmedium verwendet wurden. Die dadurch entstandenen Filme enthalten Porengrössen im oberen Mesoporenbereich. Um die Anwendbarkeit dieser Materialien für die Enzymimmobilisierung zu verbessern, wurden multiskalig-poröse Filme einschliesslich grosser Mesoporen sowie Makroporen durch eine modifizierte Pulvermethode synthetisiert, bei der zusätzlich Polymerpartikeln als makroporöse Matrizen verwendet wurden.

Die Funktionalisierung der nanostrukturierten Siliciumdioxidfilme für die analytische Bestimmung von L-Lactat wurde anhand zwei verschiedener Enzymsysteme untersucht. Als erste Alternative wurde Lactatdehydrogenase (LDH) in aminofunktionalisierten Siliciumdioxidfilmen immobilisiert, wobei rein mesoporöse mit hierarchisch strukturierten Filmen verglichen wurden. Messungen der Adsorption und Desorption von LDH mit der Methode der Quarzkristall-Mikrowaage bestätigten höhere Enzymbeladungen und bessere Stabilität gegenüber Enzym-Desorption im Fall der hierarchisch strukturierten Filme. Enzymaktivi-

Abstract

tätstests zeigten, dass zusätzliche Vorteile aus der Verwendung von hierarchisch-porösen Enzymträgern erreicht wurden: erhöhte Enzymbeladung, eine bessere Stabilität und eine stärkere und schnellere Sensorantwort im Vergleich zu rein mesoporösen Filmen, wodurch empfindlichere und robustere Nachweismethoden für L-Lactat ermöglicht werden.

Ein neuartiges Konzept für L-Lactat-Biosensoren wurde mit einem alternativen Enzym, der Lactat-Oxidase (LOx) erarbeitet; im Gegensatz zu LDH erfordert der Reaktionsmechanismus von LOx keinen Cofaktor. Dieser Ansatz beruht auf der Kombination einer Nanopulvermethode für die Synthese von Siliciumdioxid-Trägerfilmen und einer nachfolgenden Layer-by-Layer-Beschichtung mittels Polyelektrolyten. Diese Hybrid-Systeme ermöglichen die Integration von Cytochrom C (CytC) als Indikatormolekül. Dessen optischen Eigenschaften sind abhängig vom Oxidationszustand, wodurch die Oxidation von L-Lactat anhand der Bestimmung der produzierten Wasserstoffperoxid durch LOx quantitativ verfolgt werden kann.

Zusätzlich zu den filmbasierten Biosensor-Materialien befasst sich der letzte Teil der Arbeit mit der Entwicklung hybrider LOx-CytC-Mikropartikeln anhand poröser Calciumcarbonat-Matrizen. Die resultierenden proteinbasierten Partikeln können direkt zur optischen Detektion von Lactat verwendet werden; ausserdem sind sie interessante Materialien für zukünftige Entwicklungen optischer Nachweismethoden in flüssigen Suspensionen, beispielsweise in Zellkulturmedien.

Keywords: Biosensoren, Sol-Gel-Chemie, Enzymimmobilisierung, Mesoporen, Hierarchisch-poröse Materialien, Beschichtungen, Coatings, Layer-by-Layer-Verfahren, Lactatdehydrogenase, Lactatoxidase, Cytochrom C

The research described in this thesis was performed at CSEM (Centre Suisse d'Electronique et de Microtechnique) in Neuchâtel and at the Powder Technology Laboratory at EPFL. Additional work was performed at the University of Melbourne, Australia, with the support of a doc.mobility fellowship from the Swiss National Science foundation (SNSF). The SNSF is acknowledged for funding via the NCCR and a doc.mobility fellowship; CSEM is acknowledged for direct funding.

Contents

Acknowledgements	v
Abstract (English/Français/Deutsch)	i
List of figures	xiii
List of tables	xvii
List of symbols	xix
1 Introduction	1
1.1 The role of lactate biosensing in health care, biotechnology and industry	1
1.2 Lactate biosensors: State of the art	3
1.3 Overview of the lactate biosensing concept developed in this thesis	10
1.4 Objectives and outline of the thesis	11
2 Background	15
2.1 Enzymes: definition, mechanisms and immobilization	16
2.1.1 Definitions and composition of enzymes	16
2.1.2 L-Lactate consuming enzymes and other biomolecules	17
2.1.3 Enzyme kinetics	25
2.1.4 Enzyme immobilization	27
2.2 Synthesis of porous materials	30
2.2.1 Sol-gel chemistry for thin film formation	30
2.2.2 Synthesis of particles as enzyme supports	33
2.2.3 Multi-scale porosity design	33
2.3 Mass Transport in Enzyme-based Biosensor Systems	36
3 Mesopore Size and Processability of Transparent Enzyme-Loaded Silica Films	41
3.1 Introduction	42
3.2 Experimental section: materials and methods	44
3.2.1 Materials	44
3.2.2 Micellar suspensions	44
3.2.3 Sol-gel formulation and film deposition	44
3.2.4 Micelle size measurements	44
3.2.5 Rheology	45
3.2.6 Nanostructure characterization	45
3.2.7 Post-functionalization	45

Contents

3.2.8	Estimation of available amino groups	45
3.2.9	Enzyme immobilization and enzymatic activity	45
3.3	Results and discussion	46
3.3.1	Synthesis of silica sol	46
3.3.2	Formation and characterization of block-copolymer micelles as pore templates	46
3.3.3	Formulation of silica-PS-P2VP mixtures	52
3.3.4	Effect of solvent evaporation during spin coating	55
3.3.5	Film post-functionalization	55
3.3.6	Enzyme immobilization and enzymatic test	56
3.4	Conclusions	60
4	Hierarchically porous silica films: screening of approaches	61
4.1	Introduction	62
4.2	Powder approach for the formation mesoporous silica films	62
4.2.1	Experimental section	62
4.2.2	Results and discussion	64
4.3	Silica powder dispersions combined with polymeric macropore templates	65
4.4	PS-P2VP block copolymer templating	66
4.5	Porous silica particles in combination with micellar pore templates	66
4.6	Hierarchically nanostructured films formed by emulsion templating	68
4.7	Electrospinning-based approaches: direct deposition and template fibers	69
4.8	Conclusion	71
5	Lactate detection based on nanostructured and transparent hybrid silica films	73
5.1	Introduction	74
5.2	Materials and methods	76
5.2.1	Film synthesis and casting	76
5.2.2	Film characterization	76
5.2.3	Post-functionalization of silica films	76
5.2.4	Streaming potential	77
5.2.5	Quartz crystal microbalance measurements	77
5.2.6	Thermogravimetry (TGA) measurements	77
5.2.7	Enzymatic tests	77
5.2.8	Visual modelling of enzyme and solute transport	78
5.3	Results and discussion	79
5.3.1	Nanostructure and Porosity	79
5.3.2	Tracking of enzyme adsorption and desorption by QCM	83
5.3.3	Streaming potential	85
5.3.4	Themogravimetry analysis	87
5.3.5	Characterization of the enzymatic response of lactate dehydrogenase in solution	88
5.3.6	Enzymatic response of the lactate dehydrogenase-loaded transparent silica films	90
5.3.7	Discussion of mass transport in porous silica films	93
5.3.8	Visual modelling of enzyme immobilization and solute transport	95
5.4	Summary and Conclusions	101

6 Layer-by-layer assembled films and particles for lactate biosensors	103
6.1 Introduction	104
6.2 Materials and methods	106
6.2.1 Film synthesis, casting and characterization	106
6.2.2 Post-functionalization of silica films	106
6.2.3 Layer-by-layer deposition of cytochrome C	107
6.2.4 Detection of lactate in porous silica films	107
6.2.5 Assembly of LOx-CytC particles	107
6.2.6 Detection of lactate using protein particles	108
6.3 Results and discussion	109
6.3.1 Lactate responsive LOx-CytC hybrid patches	109
6.3.2 Micrometric lactate-responsive particles	116
6.4 Summary and conclusions	122
7 Conclusions and Outlook	123
A Supporting Information for Chapter 3	131
B Supporting Information for Chapter 4	135
C Supporting Information for Chapter 5	137
D Supporting Information for Chapter 6	143
Bibliography	166

List of Figures

1.1	Overview of the role of L-lactate in different fields of application	2
1.2	Schematics and classifications of biosensors	4
1.3	Overview of the biosensing approaches developed and investigated in this work	10
2.1	Amino acids synthesized by the cell with color-coded functionalities used for immobilization	17
2.2	“Key and lock” model of enzymatic reactions	17
2.3	Structures and physicochemical details of the biomolecules used in this work .	18
2.4	Structure of Nicotinamide Adenine Dinucleotide	19
2.5	Mechanism of reaction of L-lactate dehydrogenase	20
2.6	Active site from L-lactate oxidase	21
2.7	Mechanism of reaction of L-lactate oxidase I	21
2.8	Mechanism of reaction of L-lactate oxidase II	22
2.9	heme	24
2.10	Reaction between hydrogen peroxide and the iron center (heme group) from horseradish peroxidase	24
2.11	Reduction-oxidation of the heme group of horseradish peroxidase	25
2.12	Graphic representation of the Michaelis-Menten equation	26
2.13	Most common strategies to immobilize enzymes	28
2.14	Examples of enzyme immobilization schemes	29
2.15	Parameters to consider for a successful enzyme immobilization strategy	30
2.16	Casting techniques for sol-gel films	31
2.17	Silica synthesis under basic or acidic catalysis	32
2.18	Correction factor κ for diffusion through a liquid-filled pore	39
2.19	Schematic representation of tortuosity	40
3.1	Flow curves of block copolymer micelle solutions	49
3.2	Limiting cases of rheological behavior	50
3.3	TEM and AFM images of micelles of samples	51
3.4	Micelle mean diameter as a function of the PS block molecular weight	52
3.5	Silica thin film nanostructures obtained from PS-P2VP micelle templating . . .	53
3.6	Pore diameter distribution of nanoporous films	54
3.7	Mean pore diameter as a function of the original micelle size	54
3.8	Schematization of a PS-P2VP micelle	55
3.9	Estimation of available amino groups	57
3.10	Conversion of TMB into its diimine derivative in an acidic medium	58

List of Figures

3.11	Monitoring of the oxidation of 3,3',5,5'-tetramethylbenzidine (TMB) from HRP-loaded porous silica films.	58
3.12	Equivalent concentration of immobilized HRP in mesoporous silica films . . .	59
4.1	Representation of the method followed for the synthesis of mesoporous silica films via a top-down approach	63
4.2	Top-down approach for the synthesis of multi-scale porous films based on a powder method	65
4.3	A formulation of silica sol/PS-P2VP micelles of different sizes cast into films . .	66
4.4	Polymer particles in combination with PS-P2VP micelles used as templates for porous silica particles and ultimately cast as nanostructured silica films	67
4.5	Example of an emulsion-templated silica film	69
4.6	Electrospinning setup and nanostructures obtained using this technique	70
5.1	SEM images of hierarchically nanostructured films	80
5.2	Pore size distributions of mesoporous structured silica films	80
5.3	Pore size distribution (relative volume) from MIP measurements	82
5.4	QCM analysis of LDH adsorption and desorption on mesoporous and hierarchically porous films	84
5.5	Streaming potential measurements	86
5.6	TGA analysis of functionalized hierarchically nanostructured films	87
5.7	Effect of the pH on the activity of LDH	89
5.8	Response curves of enzymatic activity for LDH immobilized in mesoporous and hierarchically porous films	90
5.9	Sensor response curves for lactate detection with LDH immobilised on mesoporous and hierarchically structured films	91
5.10	Mesoporous silica films visualized by 3D modelling with enzyme diffusion . . .	96
5.11	Profiles of adsorbed enzyme amount vs. film depth obtained from particle-based visual modelling	98
5.12	Brownian motion of LDH inside and outside a porous film	99
5.13	Visualization of diffusion and substrate/enzyme contact during biosensing . .	100
6.1	Schematic of the approach developed in this study to assemble a hybrid functionalized porous silica film for lactate detection	109
6.2	Layer-by-layer adsorption on QCM sensors and spectra of nanoporous mesoporous films with immobilized LOx and coated with PEI-PAA-CytC	110
6.3	QCM study of polymer adsorption on top of a silica coated sensor	112
6.4	Images of glass slides coated with LOx-loaded mesoporous and hierarchically porous silica films	112
6.5	Response curves of mesoporous and hierarchically porous silica films functionalized for lactate detection	114
6.6	Oxidation coefficient over time for LOx-CytC functionalized mesoporous and hierarchically porous films	115
6.7	Initial slope of the oxidation coefficient vs. time curves for LOx-CytC functionalized mesoporous and hierarchically porous films	115
6.8	Preparation of CaCO ₃ -templated LOx-CytC particles	117
6.9	LOx-CytC protein particles.	117

6.10	Time course of the dissolution of CaCO ₃	118
6.11	TEM micrographs of CaCO ₃ particles after LOx–CytC absorption and following removal of CaCO ₃ by EDTA	119
6.12	Oxidation of CytC in solution by LOx–CytC particles: spectra and fluorescence decay	120
6.13	Oxidation of CytC due to H ₂ O ₂ formed by LOx activity, tracked by fluorescence microscopy of LOx–CytC particles in the presence of L-lactate	120
6.14	Evolution of the normalized fluorescence intensity obtained by image analysis of fluorescence micrographs	121
7.1	Outlook: schematic overview of possible implementations of the biosensing materials developed in this thesis	128
A.1	Images of PS-P2VP-silica coatings deposited by spin coating on silicon substrates	131
A.2	Calibration curve from Coomassie brilliant blue G for the estimation of available amino groups in mesoporous silica films	132
A.3	Calibration curve from TMB after acidification of the medium	132
A.4	Slope of the absorbance vs. time curves for the oxidation of TMP from HRP-loaded porous silica films	133
B.1	PVA cross-linking with boric acid	135
C.1	Absorbance spectra of transparent silica films synthesised by a powder approach	137
C.2	Calibration and Michaelis-Menten curve for LDH	137
C.3	Example for the numerical derivation of the initial reaction rate from product concentration vs. time data	138
C.4	SEM image of a hierarchically porous silica film	138
C.5	SEM image with higher amplification of a hierarchically porous film	138
C.6	SEM image of the cross section from a hierarchically porous silica film	139
C.7	Examples for the mesh structure used to model silica aggregates and enzyme molecules	139
C.8	Examples for a sequence of images from the visual modelling approach.	140
C.9	Examples for a sequence of images from the visual modelling approach.	141
C.10	Calibration of Brownian motion for visual modelling	142
C.11	Actual size of L-lactate vs. LDH	142
C.12	Close-up images of the visual modelling performed visualized using the Blender™ software	142
D.1	Reference spectra of reduced and oxidized CytC	143
D.2	Reference images for the CaCO ₃ particles: nanocrystal branches and pore sizes	143

List of Tables

1.1	Examples of commercially available lactate detection systems	8
2.1	Difference in reactivity of silicon alkoxides and transition metal alkoxides.	32
2.2	Overview of diffusivities D and effective diffusivities D_{eff}	38
3.1	Overview of the PS–P2VP block copolymers used to form micellar pore templates	46
3.2	Solubility data for P2VP	47
3.3	Flory–Huggins parameters of ethanol and 1-butanol with respect to polystyrene	48
3.4	Summary of size measurements for PS-P2VP block copolymer micelles in ethanol and 1-butanol by different techniques.	50
3.5	Description of samples used for enzyme immobilization	56
4.1	Overview of the HLB scale and values for specific surfactants	68
4.2	Overview of different approaches screened to synthesize hierarchically porous films	72
5.1	Summary of porosity and surface area measurements	79
5.2	Summary of TGA results. Evaluation of the functionalization steps of hierarchically porous films towards enzyme functionalization.	87
5.3	Approximation of enzyme coverage in the hierarchical and mesoporous films	88
5.4	Summary of effective diffusivity in mesoporous and hierarchically porous silica films	94
7.1	Overview of challenges, approaches and achievements	127
A.1	Calibration curve data from Commassie brilliant blue G solutions	131
A.2	Spectrophotometric measurements of desorbed Commassie brilliant blue G from amino-functionalized porous silica films	132
A.3	Spectrophotometric measurements from the oxidation of TMB by HRP immobilized in porous silica films and measured at 650 nm	132
A.4	Apparent concentration of HRP in the films obtained from calibration curve	133
A.5	Equivalent enzyme activity normalized with film thickness	133
A.6	Physical properties of solvents present in the sol-gel formulations	133

List of symbols and abbreviations

Abbreviations

AFM	atomic force microscopy
APTES	(3-aminopropyl)triethoxysilane
BCP	block copolymer
BET	Brunauer-Emmett-Teller (sorption isotherm)
CBB	Commassie brilliant blue G
CytC	cytochrome C
DLS	dynamic light scattering
EC	Enzyme Commission number
EDTA	ethylenediaminetetraacetic acid
EISA	evaporation-induced self-assembly
HLB	hydrophobic- lipophilic balance
HRP	horseradish peroxidase
IEP	isoelectric point
LDH	lactate dehydrogenase
LOx	lactate oxidase
MIP	mercury intrusion porosimetry
NADH	nicotinamide adenine dinucleotide
NAD ⁺	nicotinamide adenine dinucleotide (oxidized)
PBS	phosphate buffered saline
PBST	phosphate buffered saline Tween-20
PMMA	poly(methyl methacrylate)
PS	polystyrene
PTFE	polytetrafluoroethylene
PVA	polyvinyl alcohol
PVP, P2VP, P4VP	polyvinylpyrrolidone
QCM	quartz crystal microbalance
SEM	scanning electron microscopy
TEM	scanning electron microscopy
TEOS	tetraethoxysilane
TGA	thermogravimetric analysis
TMB	3,3',5,5'-tetramethylbenzidine
VMD	Visual Molecular Dynamics

List of symbols

Symbols and units

c	molar concentration (mol/l, M)
d_p	average pore diameter (nm)
Δf	relative frequency shift in QCM experiments (Hz)
G'	elastic modulus (Pa)
G''	viscous modulus (Pa)
K_M	Michaelis-Menten constant (mM)
MW	molecular weight (g/mol)
[P]	product concentration (mM)
[S]	substrate concentration (mM)
S_S	specific surface area (m ² /g)
t	time (s, min, h)
U	enzymatic activity unit
v	reaction rate ($\mu\text{mol}/\text{min}$)
v_0	initial reaction rate ($\mu\text{mol}/\text{min}$)
V_{max}	maximum rate ($\mu\text{mol}/\text{min}$)
V_p	pore volume (cm ³ /g)
$\langle x^2 \rangle$	mean square displacement (m ²)
χ	Flory-Huggins parameter (-)
ϵ	porosity (-)
$[\eta]$	intrinsic viscosity (-)
λ_{max}	wavelength at absorption maximum (nm)
τ	tortuosity (-)

1 Introduction

1.1 The role of lactate biosensing in health care, biotechnology and industry

L-lactate is an important metabolite and a target of attention in diverse fields of application, including clinical and sports medicine, bioprocess engineering and food manufacturing (Figure 1.1). In the last years several efforts have been made to determine in a fast and quantitative manner the concentration of lactate in different media. Some of the approaches explored have successfully led to their commercial exploitation in biosensing applications. Indeed, available options to determine lactate in some specific media can be found in many reports in the concerned literature¹⁻¹² and as commercial products in the market^{13;14}, particularly for medical applications. However, despite these successful efforts and their translation into commercially available products, many limitations are still encountered and challenges remain to be tackled, particularly with regards to the field of application, the versatility, and the convenience of use of current technologies. Therefore, research on this topic is mostly directed towards the exploration of better alternatives (covering more application fields, with cost effective, versatile, easy to use materials) to overcome the current limitations.

In this chapter, a motivation of the present work is explained through the importance of determining L-lactate for a wide range of applications. The state of the art regarding the available methods to determine lactate is presented. An analysis of the current limitations and remaining challenges regarding the available methodologies for lactate measurement is made. Finally, the approaches proposed in this work to contribute to overcome these limitations are presented.

L-lactate in the medical field

Lactic acid is an α -hydroxy acid, which in aqueous solutions and under physiological conditions dissociates almost completely to lactate with a pKa of 3.9²⁵. The terms lactic acid and

Chapter 1. Introduction

lactate are used almost indistinctively. L-lactate is a highly relevant molecule within the clinical sector as it is a key metabolite formed from the anaerobic metabolism of glucose in cells. Under abnormal situations, L-lactate concentrations in the blood can rise, indicating localized O₂ deprivation and representing a potential development of a wide range of pathological conditions derived from insufficient oxygen supply⁶. Specifically, lactate detection can be used for the prompt diagnosis of shock, different metabolic disorders, respiratory insufficiency, and heart failure²⁶ and to monitor the overall performance of sportsmen⁸. Lactate monitoring is an essential activity performed in patients in intensive care or during surgery¹⁷. An elevated lactate level in blood is a major indicator of insufficient blood circulation and consequently low oxygen supply in tissues. Additionally, abnormal lactate levels can be caused by other metabolic diseases such as diabetes or absorptive irregularities of short-chain fatty acids in the colon¹⁹.

L-lactate in the food industry

Despite the numerous reports on determining lactate in biologically relevant samples, the importance of lactate is not limited to the medical sector. Lactate can be found naturally in food goods such as dairy products, meat, vegetables or wine and its concentration can be interpreted as an indicator of freshness and quality in general. Lactic acid is produced by

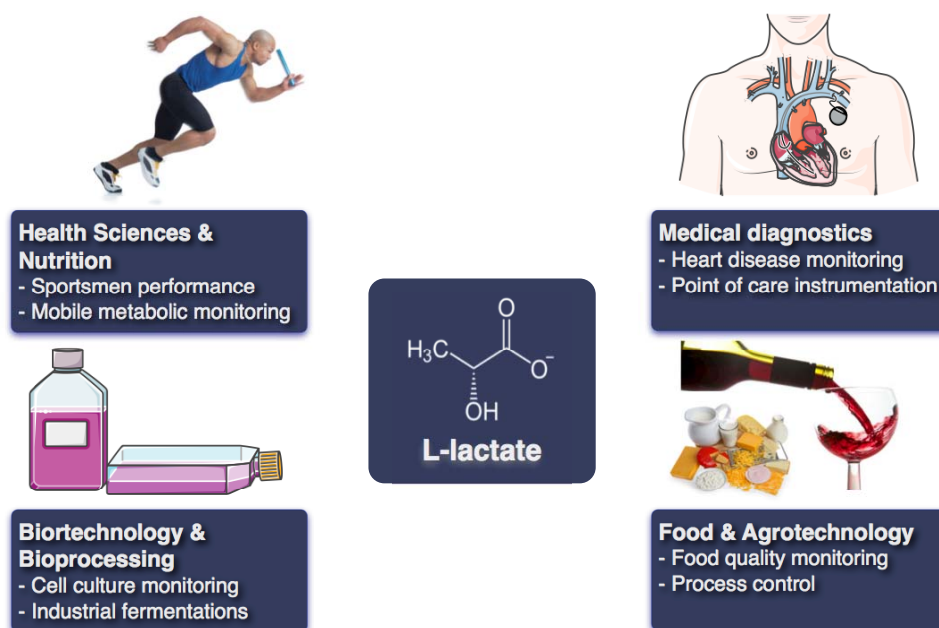


Figure 1.1 – Overview of the role of L-lactate in different fields of application. Top: in medical and health-related applications, lactate detection is useful in sports performance monitoring and heart disease diagnostics^{8;15–19}. Bottom: industrial applications include cell and enzyme-based biotechnology on the laboratory, pilot and industrial scale. L-lactate monitoring is also relevant in food raw materials and product quality assessment and food process control^{19–23}. Images adapted from Servier Medical Art²⁴.

lactic acid bacteria during the manufacturing of many fermented food products derived from milk (yogurt, cheese, buttermilk, etc.), vegetables (Sauerkraut, a German specialty or *tesgüino*, a Mexican traditional drink), cured meat products (chorizo, salami, etc.) and wine. In these examples, the presence of lactic acid has a positive effect. For instance, lactic acid acts as a natural preservative for food products^{27;28}. Most foodborne bacteria grow at a pH value around 4.5-7.3²⁹. The production of lactic acid lowers the pH of food and thus inhibits the proliferation of these microorganisms. Additionally, lactic acid has a characteristic acidic and astringent flavor, which imparts specific organoleptic properties to the foods. In contrast, lactic acid can be also an indication of contamination of milk, beer, fruit and vegetable juices by the same lactic acid bacteria, which in these cases is not desirable. For instance in wine, the balance between malic and lactic acid is used to determine its acidification and softening. Higher malic acid concentrations are usually desired¹⁹.

L-lactate in fermentation cultures

Cell cultures are industrially relevant for the production of therapeutic proteins. Effective ways to produce proteins using host cells (recombinant proteins) are extremely important as many of the applications of these proteins require both a large amount and high quality. The attention to production costs to achieve this becomes very relevant, aiming to produce them efficiently and to make the products commercially viable. As a general framework, the genetic information necessary for the codification (synthesis) of proteins from diverse origins is inserted into the host cell by diverse molecular biology techniques³⁰ (plasmids, viral vectors, chromosomal integration, etc.). The successful synthesis of these proteins by the host cells (protein expression) will depend on the molecular technique chosen³¹, but also on the manipulation of the cell culture to promote growth and expression of the proteins of interest.

The composition of the media where cells grow is crucial at finding the best conditions to express these recombinant proteins. Indeed, the accumulation of side metabolic products such as lactate from cell metabolism has an influence on their growth and on their overall production yields. A control over the growth rate of cells in continuous batches is relevant for maintaining a regular cell growth. By altering the feed of nutrients, cells can express differently proteins and this has an impact on the efficiency of the process. According to a recent study²¹, the accumulation of lactate in such media is linked to the cell reproduction cycle and it reaches a peak during cells exponential growth. Moreover, lactate is consumed during the stationary phase and its concentration varies according to the medium choice. In this field, lactate detection can provide information about the overall cell growth stage and its determination can lead to the optimisation of the media aiming at higher protein production yields²¹.

1.2 Lactate biosensors: State of the art

Biosensors: Definition and classification

According to IUPAC^a, a biosensor is a device that uses specific biochemical reactions mediated by isolated enzymes, immunosystems, tissues, organelles or whole cells to detect chemical

^aInternational Union of Pure and Applied Chemistry

Chapter 1. Introduction

compounds, usually by electrical, thermal or optical signals³². These signals are transduced through an electronic system into a readable outcome or display (Figure 1.2). The global biosensor market has been valued around 13 million USD in 2014 and it has been predicted that it will grow yearly at about 10% within the next 5 years, reaching a value of 22.5 million USD by 2020³³.

Biosensors are classified according to three criteria (Figure 1.2):

1. By the field of application they envisage: food, environment & agriculture, medical, etc.
2. By the targeted end-use: home and point of care diagnostics, research, biodefense and security
3. By the transducer technology: electrochemical, optical, thermal, piezoelectric, etc.

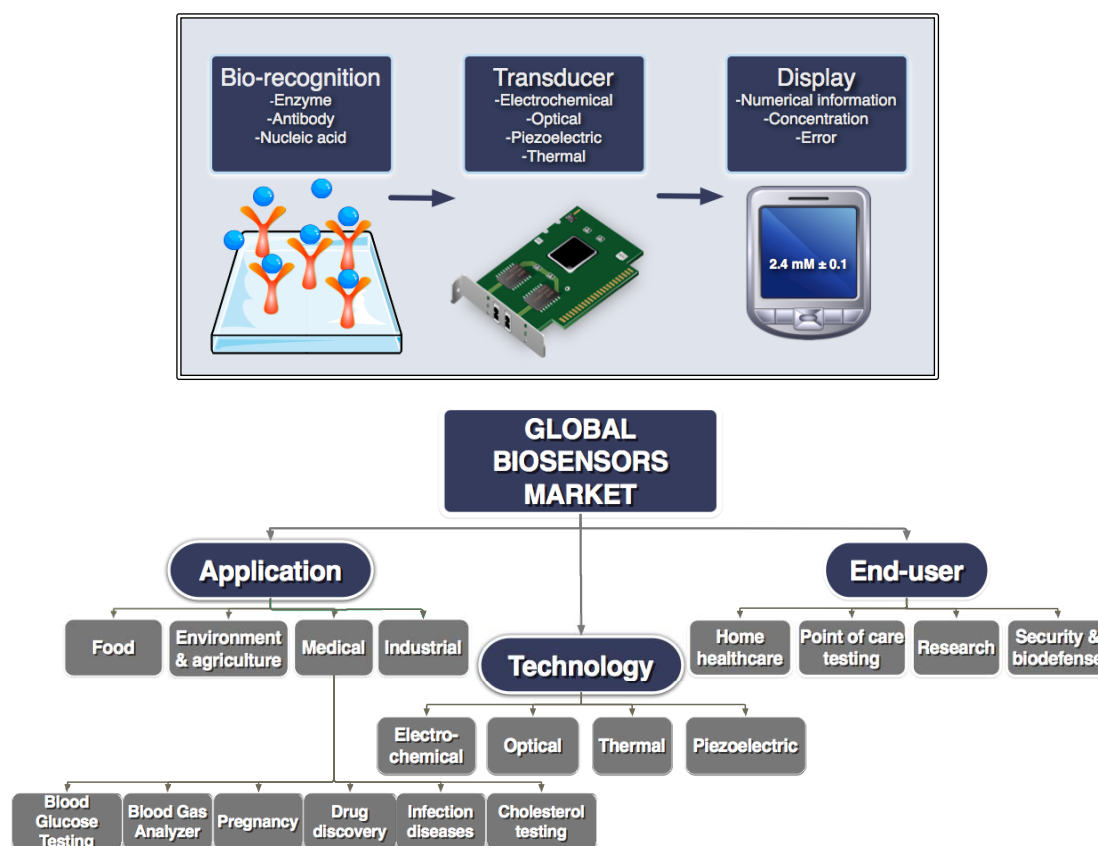
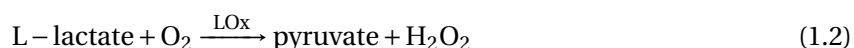
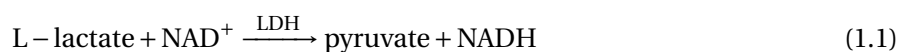


Figure 1.2 – *Top:* Schematic of a typical biosensor including the bio-recognition approach, transducer technology, and data processing, storage and display. *Bottom:* Classification of biosensors in the global market by application, end-user and transducer technology used. 90 % of the commercially available solutions are dominated by medical applications, mainly for blood glucose testing.

Medical applications dominate the market of biosensors, particularly those where blood samples are analyzed as a method to determine glucose levels, representing about 90% of

the global biosensor market³⁴. However, according to recent market research reviews^{33;35}, the demand in biosensors in other fields is expected to grow sharply within the next years, owing to their capability to bring convenient solutions to issues in diverse areas such as medicine, biotechnology, food & agriculture, safety and biodefense, among others. Specifically, a rising demand for detection methods in early disease diagnosis within the healthcare sector and in industrial applications is expected to drive the overall biosensors market during the forecast period. In this regard, lactate can be considered a highly relevant molecule linked to health state, food quality and bioprocess monitoring, and thus its measurement becomes very pertinent in more than one field of applications. In another category, biosensors are employed by end-users in areas such as home healthcare, point of care testing, research purposes in both industry and academia, and finally for nation security and defense. In this category, lactate biosensors become relevant in home and point of care diagnostics and for research purposes. Moreover, options for these applications are currently in demand. Finally, biosensors can be grouped by the kind of technology used to transduce the biological event between the analyte of interest and the biorecognition element into a readable outcome. Electrochemical and optical based approaches to determine lactate have been the predominant methods explored due to the suitable alternatives to follow and measure the biochemical reactions that lead to its quantification.

The most widely studied and economically established biosensors utilize immobilized enzymes onto supports as biorecognition elements. The nature of the support depends on the biosensing scheme. Enzymes are biomacromolecules, which catalyze chemical reactions in biological systems. The high specificity that enzymes exhibit regarding the reactions they catalyze, and the higher turnover rates, which are indisputably more effective than any equivalent chemical reaction, make enzymes the most convenient alternative in biosensing. Their immobilization may allow their utilization for more than one measurement, depending on the followed immobilization strategy. Furthermore, the large-scale production of industrially relevant enzymes makes them readily available for biosensing applications, and with progressively lower costs due to the optimization of the manufacturing processes and the increase in their demand. Two lactate-consuming enzymes are the most commonly reported in lactate biosensing applications: L-lactate dehydrogenase (LDH) and L-lactate oxidase (LOx), which catalyze the following reactions^b:



Numerous studies^{4;18;19;23;26;36-41} have been reported for the detection of lactate using enzymes mainly through electrochemical approaches. Although optical approaches have been also explored, their utilization for practical and commercial applications is less frequent. Over-

^bNAD: Nicotinamide Adenine Dinucleotide. An enzyme cofactor required for LDH to work. Generic abbreviation for either the oxidised (NAD⁺) or reduced form (NADH)

all, these solutions only cover a limited range of applications, predominantly in the medical field. An overview of these existing methodologies, and their advantages and disadvantages is presented in the next section. Further information can be consulted in recent market surveys^{33;35} and review articles^{19;41;42}.

Electrochemically based lactate biosensing

Most lactate biosensors described in the literature are based on an amperometric detection^{19;41;42}. Amperometric biosensors measure the current resulting from the electrochemical oxidation or reduction of an electroactive species. The resulting current is directly correlated to the concentration of the electroactive species or its production or consumption rate¹⁹. For instance, amperometric biosensors can be used for *in-situ* measurements of lactate in cell culture media^{13;43}. In a typical implementation, this concept relies on the enzymatic oxidation of lactate into pyruvate and the production of hydrogen peroxide coupled to an electrode, which is catalyzed by the enzyme L-lactate oxidase^{44;45}. Although lactate has been successfully measured following the production of hydrogen peroxide in cell cultures, the outcome values obtained for such inhomogeneous media and their significance are questionable. Cells tend to sediment owing their size and the action of gravity forming a layer at the bottom of the bottle or tank where they are contained. The detection probe to measure accurately the concentration of metabolites, i.e. lactate in cell cultures must be of a size close to the cell's dimensions (10-100 μm diameter), and should be able to reach the source of lactate production (the cell) to give a correct and significant concentration value of lactate near the cell. Several probes of this nature could be used to obtain a more realistic concentration of lactate through all the cell culture (mapping). A technology offering a solution in this sense is not yet available and gives a strong motivation to investigate possibilities to offer alternatives for this important biotechnological application.

Another area for which lactate biosensors have been studied and applied is the pre-clinical data acquisition and analysis for the Central Nervous System. Such sensors are capable of providing real-time changes in lactate concentration in the brains of rodents^{3;14}. In this case, lactate is monitored as a biomarker for sleep¹⁵ and in memory processing studies¹⁶. Still in another implementation, the enzyme L-lactate dehydrogenase and NAD were embedded in a conductive polymer with carbon nanotubes on the surface of an electrode. The reduction of NAD^+ into NADH was followed and used as an indirect way to measure the amount of lactate in milk and human serum⁴⁶.

Other amperometric biosensors to detect and quantify L-lactate are frequently found in the literature for diverse applications such as perspiration during exercise⁸, wine quality⁴⁷ and general human health care^{18;46}.

Amperometric biosensors are generally renowned for their accuracy and reliability. However, there are common issues confronted by users. These problems include the maintenance complexity and the frequency of calibration, which may require extra time and training. In addition, the sample's flow dependence can often pose problems for an accurate reading⁴⁸. Moreover, amperometric biosensors suffer from interference in the presence of high levels of hydrogen, this often results in negative readings and an unreliable measurement method⁴⁸. Finally, it is also known that the change of signal over time (drift), which is often associated with

sensor degradation, can be a major drawback where effort and cost associated to minimize these errors become significant. For these reasons, alternative methods to overcome these challenges are required. Optical biosensors can be an option to overcome some of these drawbacks. Their design becomes simpler and straightforward than amperometric counterparts. Optical approaches for lactate detection are much less reported than amperometric solutions, offering at the same time more opportunities to investigate potential new configurations for different applications. In the next section, an overview of the existing reports in optical lactate biosensing is presented.

Optically based lactate biosensing

Optical lactate biosensors depend on spectrophotometric, fluorimetric or chemoluminescence methods. Following the first optical sensor for lactate detection in whole blood reported by Broder and Weil⁴⁹, which was based on photospectrometry, fluorescence techniques gained in importance as they provide lower detection limits.

Fluorimetric biosensors rely on the measurement of the luminescence of a substrate on excitation by an appropriate light source. Analytes with luminescent capability respond strongly to incident light of a distinct wavelength by emitting more intensely at another specific wavelength. The distinct wavelengths allow both excitation and detection at the same location (e.g., via a fiber-optic cable) and result in high specificity for a particular substrate. Commonly the fluorescence is generated by the enzyme co-factors (i.e. NAD) or by other species, which react with by-products from the enzymatic reaction. The applications in which this approach has been explored involve environmental⁵ and medical applications for detection of lactate in blood¹⁰, and in cancer cells²². For this later case, the use of a microfabricated needle has been developed for the detection of lactate close the cell. The nanoscale fiber was able to measure lactate within the range of 0.06 to 1 mM. However, the resort to microfabrication techniques and heavy facilities significantly increases the final sensor cost.

Alternatively, the decay of fluorescence of some molecules such as cytochrome C (CytC) can be used to monitor the production of lactate. CytC is an electron carrier biomolecule with fluorescence properties in its reduced state. The oxidation state of CytC has been monitored directly in single cells to identify the reduced (CytC_{red}) form the oxidized species (CytC_{ox}), which have different roles in the cell⁵⁰. Whereas CytC_{red} displays fluorescence properties, CytC_{ox} does not, contributing to its differentiation by optical means. In another example, CytC has been used as a probe to detect hydrogen peroxide (H₂O₂) in stressed cells^{51;52}. In this case, the concept does not rely on the fluorescence properties of CytC, but on its light absorption in the visible range. While CytC_{red} absorbs light with a maximum at 550 nm, the oxidized species does not. Regarding lactate biosensing applications, the optical properties of CytC can be useful to quantify lactate. The coupling of LOx reaction (which produces H₂O₂) with CytC has not yet been reported. Although advantageous, the addition of CytC in a biosensing scheme requires a strategy to incorporate both enzyme and CytC in the same system, where different alternatives need to be considered.

Chemoluminescent biosensors rely on the emission of light, principally as a consequence of an oxidation reaction involving oxygen or H₂O₂. Luminol is a molecule, which exhibits chemoluminescence, which has been used in combination with enzymes to detect lactate¹¹. Although

Chapter 1. Introduction

the high sensitivity of this approach is an advantage, the reaction to generate chemoluminescence requires specific conditions of pH and temperature⁵³, which limits the application of this method. In addition to this, the incorporation of several species into the sensing scheme makes the approach more complex to be implemented for real applications.

Overview of commercially available technologies

Some of the electrochemical and in a less extend the optical methods outlined above have allowed the successful development and manufacture of commercially available devices for lactate detection. Table 1.1 gives example of some of these products and provides information regarding their analysis time, the limits in lactate concentration for a linear response and the followed transduction approaches, which are predominantly based in electrochemical methods. Accutrend[®] by Roche provides a point of care tool following an optical method for lactate detection in blood. The device consists of a portable spectrophotometer and single-use strips. Each strip is a multilayer system: an absorbent material for blood deposition, a mesh for blood filtration, and a final layer coated with LOx and other chemicals⁵⁴. The plastic support has a hole where the spectrophotometer can read from below the sample in reflectance mode. According to Karapinar et al.⁵⁵, Accutrend[®] showed limitations in the upper range from the specification of this system (Table 1.1), and dilutions were required for a correct measurement.

Table 1.1 – Examples of commercially available lactate detection systems with specifications and detection method (adapted from Rassaei et al.⁴¹)

Product name	Pro2 LT-1730 Arkray Inc.	Lactate scout+ EKF diagnostics	LaboTRACE compact Trace analytics	Accutrend [®] Roche	CITSens Bio Lactate Sensor PG13.5 C-cit AG
Country	Japan	Germany	Germany	Switzerland	Switzerland
Sample volume	0.3 μ L	0.5 μ L	0.5mL	15-50 μ L	–
Analysis time	15s	10s	45s	60s	–
Sample type	Whole blood	Whole blood	Cell culture	Whole blood	Cell culture
Linear response	0.5-25mM	0.5-25mM	0.5-30mM	0.8-22mM	1-60mM
Detection system	Electrochemical	Electrochemical	Electrochemical	Optical	Electrochemical

Despite significant technological improvements and innovations, the implementation of biosensing solutions in markets other than the medical field has been gradual. This situation opens the possibility to explore these and other technological approaches for lactate detection in different media, targeting different applications. For this purpose, it is important to understand the specifications required in designing lactate biosensors, taking into account the current drawbacks and limitations from existing technologies. This information will have an impact on the biosensor concept, which is based on the following design parameters:

- *Response and processing time:* Current commercially available products can determine lactate concentrations in a given sample within a minute. Any other proposed approach must target a response time within the same time interval.
- *Specificity:* Molecules such as α -hydroxy acids and/or their conjugate bases (citrate, tartaric acid, malic acid, glycolic acid and oxamate) have all similar chemical structures to lactic acid. The selection of enzymes can impart specificity to the sensing scheme. All of the existing commercial products utilize enzymes as bioreceptors.

- *Sensitivity*: Specifications regarding limits of detection for lactate depends strongly on the desired application. For instance, normal plasma lactate concentrations range from 0.3 to 1.3 mM in healthy individuals¹⁷. Lactate concentrations in plasma higher than 5 mM are an indication of severe acidosis and predict high mortality of patients¹⁷. Lactate concentration in cell cultures can reach concentrations up to 25 mM⁵⁶. Lactate concentrations in wine depend strongly on the fermentation process, and the kind of grape used. For instance, sweet wine, independently of the grape variety, have lower content of lactic acid than dry ones, overall lactate concentrations in wine can range from 0.1 to 20 mM²³.
- *Miniaturization*: According to biosensor market reviews^{33;57} on industrial research trends in biosensing, companies have been focusing on technological advances in order to achieve miniaturization and increased sensitivity and precision, especially on nanotechnology-based biosensors. In response to market demands, industrial research efforts aim at the development of devices suitable for multiple analyses, miniaturization in view mobile sensing, and improvement of readout time and energy efficiency.
- *In situ & continuous monitoring*: According to current trends and limitations, there is a need for approaches to quantify lactate both *in situ* and for continuous monitoring. Sensing applications in inhomogeneous media such as cell cultures require an adapted sensing probe able to detect in a sensitive and reliable way the production of lactate, and to give an indication of the real concentration at the source.
- *Costs of devices and consumables*: Enzymes are expensive raw materials in biosensing fabrication. The processes to integrate these biomolecules into devices and the necessary electronics to obtain a readable output can increase considerably the manufacturing process. Selection of low-cost starting materials is economically advisable, together with an optimization of enzymes efficiency and possible reusability.
- *Biocompatibility*: Regarding applications requiring direct contact with human tissues and/or body fluids, the sensing material must be harmless and biocompatible.

In summary, the design of a successful enzyme-based biosensor for lactate requires the assembly of enzymes onto a solid support and the selection of an appropriate transduction strategy between the enzyme reaction and the support. The enzyme support must be biocompatible and inexpensive to limit as much as possible the fabrication costs. At the same time, the enzyme support must be capable of bearing a high amount of enzyme, which will translate into a fast responsive and sensitive material towards lactate, able to detect between 0 and 20 mM of lactate and covering targeted applications in the medical, and agro-biotechnological fields. Given the opportunities in optical lactate biosensing derived from the less extensive commercially available options, the suggested transduced biochemical reaction between the analyte and the enzyme can then be optically measured. The sensing approach and the components to fabricate a responsive lactate material should be selected based on the previous requirements.

1.3 Overview of the lactate biosensing concept developed in this thesis

The concepts proposed in this work consist on the optical detection of lactate based on the utilization of two commercially available enzymes immobilized in porous materials for a high enzyme loading. The first objective is to appropriately design and functionalize porous supports for their immobilization.

By exposure of these functionalized porous supports to lactate, the concentration can be quantified following optical methods. Two different sensing schemes are proposed (Figure 1.3):

1. The development of lactate-responsive patches targeting applications in the medical/a-grofood field. Two concepts are presented:
 - (a) In the first case, the enzyme lactate dehydrogenase oxidizes lactate into pyruvate, with the concomitant reduction of its cofactor, the NAD, which is required for the enzyme activity. NAD optical properties depend on the oxidation state of the molecule. Only the reduced species, NADH shows fluorescence properties. Additionally, NADH absorbs light strongly in the UV visible range with a maximum at 340nm. The monitoring of the optical properties of NADH is correlated to the LDH activity and lactate concentration.
 - (b) The second enzyme, LOx catalyzes the same reaction but utilizing O_2 as co-reactive. The products in this reaction are pyruvate and H_2O_2 . For this second detection concept, CytC is included in the sensing scheme to react with the hydrogen peroxide produced by LOx⁵¹, as described in Section 1.2. Similarly to NAD, CytC optical

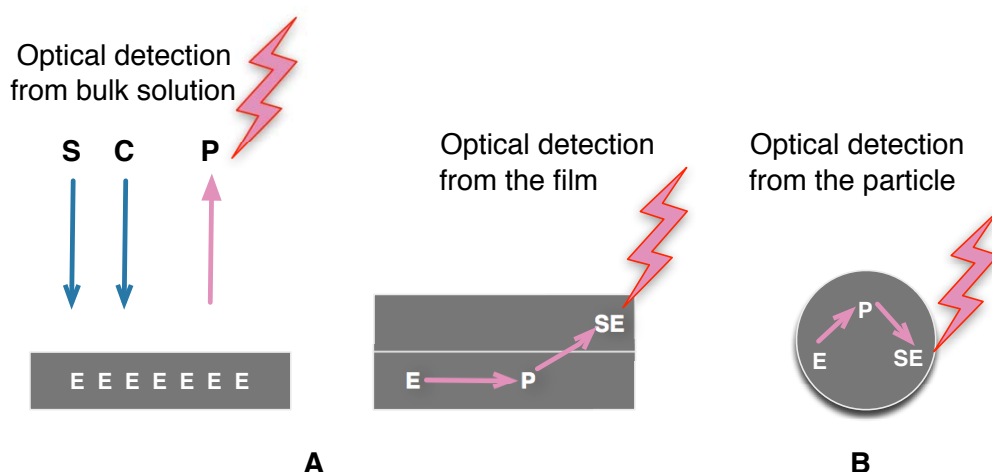


Figure 1.3 – Overview of the two different biosensing approaches developed and investigated in this work. A. Lactate detection in thin films. B. Lactate detection in micrometric particles. S: substrate (lactate); C: cofactor (NAD); E: enzyme (LOx, LDH); P: product (NADH; H_2O_2), SE: sensing element (CytC).

properties depend on its oxidation state. The reduced species of CytT (CytC_{red}) has fluorescence properties and absorbs light strongly in the visible range, with maximum at 550 nm. In contrast, the oxidised species (CytC_{ox}) does not show fluorescence properties nor absorb light at the same wavelength. The optical change in absorbance and fluorescence enables the quantitative monitoring of the Lox activity and lactate concentration.

2. The second scheme involves the synthesis of micrometric particles for lactate detection, aiming at applications in the bioprocessing/cell culture field. This concept proposes the integration of the enzyme LOx and CytC in the same particle, with the potential of synthesizing a particle able to respond to lactate in solution. In this sense, the particle becomes a micrometric *in-situ* lactate probe.

1.4 Objectives and outline of the thesis

The research presented in this thesis is reported into three scientific steps: (i) design of suitable support materials and porosity design for enzyme immobilization; (ii) functionalization of the supports for lactate biosensing; (iii) performance characterization of these biosensing materials. The specific challenges and approaches will be explained in detail in the following chapters. However, an introductory description is explained in this section as follows:

(i) Design of the support materials

Thin porous silica films are synthesized for the patch-based biosensing scheme (Figure 1.3, scheme A). These films are optically transparent allowing measurements at the surface by spectroscopic methods. They offer a high specific surface area for the immobilization of a high amount of biocatalyst in the thin film to achieve high sensitivity. Enzymes are large macromolecules with sizes up to 20 nm, imposing additional constraints on the porosity design: pores have to be large enough to enable enzyme loading into the pores by diffusion. Therefore, the first challenge is to robustly produce films with pores enabling the immobilization of the enzymes. A fine tuning of the pore-size and connectivity is required. Large mesoporous size range (20-50 nm) to macropores (>50 nm) and multiple length scales within the same support matrix are targeted.

Two wet chemistry approaches will be investigated to synthesize these silica films with the appropriate porous structure: (i) colloidal templating using block copolymer micelles as pore formers in combination with sol-gel chemistry to form silica films; and (ii) a powder-based method of film formation from porous silica particles in combination with polymeric macropore templates. Formulation and casting parameters have to be adjusted to reproducibly generate highly interconnected pores with one or two different scales.

Similar porosity design challenges have to be fixed in the particle-based biosensing scheme (Figure 1.3, scheme B). Calcium carbonate particles with multiscale porosity are synthesized and used as initial supports for the formation of enzyme-based particles. A co-precipitation approach in combination with polymer templating is used to create pores with different length scales in the CaCO₃ spheres.

(ii) Functionalization

Silica and calcium carbonate were also selected for their biocompatibility, specifically for enzyme hosting. The selected immobilization scheme is designed as the best compromise between the selection of biocompatible raw materials for enzyme coupling, the immobilization efficiency (e.g. mainly to prevent the release of enzyme in the probed medium), and the enzyme performance. In particular, the loading of the biocatalysts into the porous films during functionalization strongly depends on the pore size design and the pore wall chemistry. These aspects will be addressed using *in-situ* techniques (i.e. streaming potential characterization, quartz crystal microbalance measurements) during enzyme adsorption on the inorganic films.

The detailed functionalization approach depends on the chemistry of the enzyme reaction and the necessary cofactors and products used for detection: (i) for the case of biosensors based on lactate dehydrogenase (Chapter 4), the cofactor NADH and the product used for optical detection are present in solution; (ii) for films and particles based on the enzyme lactate oxidase (Chapter 5), hydrogen peroxide is formed as a reaction product, and the detected optical signal is caused by the oxidation of CytC, which will be co-embedded as a biosensing element in the same films (Figure 1.3).

(iii) Performance characterization and improvement

Since the use of enzymes as extremely selective biocatalysts is obviously the key for highly selective and sensitive biosensors, the main objectives are to maintain their intrinsic activity to a high degree even upon immobilization, to achieve high enzyme loadings in the films and particles, and to provide short transport distances for the substrate and the products for an efficient and fast response.

The transparency of the thin film supports is a main challenge in combination with high enzyme loadings and robustness of the materials. To synthesize transparent films and micro-metric particles, the key control parameters are the thickness (for films), the diameter (for particles), and the pore size (as potential scattering element).

Finally, the range of lactate concentrations of 0-20 mM was chosen, as it is relevant for health-care, food, and biotechnology applications.

In summary, the key objectives of the work described in this thesis are:

- to develop robust and reproducible methods for the synthesis of transparent, porous silica films and CaCO₃ porous particles, focusing on the synthesis of multi-scale porous systems with large mesopores (10-50 nm) and macropores (50-300 nm), and to study their suitability for enzyme immobilization.
- to functionalize the as-synthesized porous systems towards the optical detection of lactate within a concentration range of physiological relevance (here: L-lactate concentrations up to 20 mM), utilizing the enzymes lactate dehydrogenase and lactate oxidase.
- to develop optical detection schemes using different configurations of enzymes and

cofactor elements and to assess their performance in view of the support's structure and functionalization.

The thesis is structured as follows:

Chapter 2 summarizes the relevant background for the formation of supports with controlled porosity and presents concepts of mass transport, in particular the relationship between diffusion and reaction. Since the details of the support design and functionalization strategy depend on some of the biochemical aspects of the enzymes and the cofactors, an overview of the structures and mechanisms for the biocatalysts (lactate dehydrogenase; lactate oxidase) and the cofactors (NAD, cytochrome C) used here will be provided as well. Additional relevant literature will be summarized in each of the subsequent chapters.

Chapter 3 describes the synthesis of thin porous silica films as enzyme supports for biosensing applications. The first part of the chapter focuses on an approach using block copolymer micelle templates to form large mesopores for enzyme immobilization. A specific focus is on the challenge to form thin films or coatings with pores in the large mesoporous size range. Additionally, a demonstration of the concept for amino-functionalized silica films with immobilized horseradish peroxidase as a model enzyme is presented and discussed. In the second part of the chapter, alternative approaches to generate mesoporous and hierarchically porous films from silica particles are outlined.

An exploratory screening of various alternative approaches to form hierarchically porous silica materials is summarized in Chapter 4, including 'bottom-up' methods based on sol-gel synthesis and 'top-down' methods based on pre-formed dispersed silica particles. In particular, the methods screened include emulsion templating, electrospinning and powder-based methods. This last approach will also be the basis for the design of the enzyme-loaded biosensing films in the subsequent chapters

In Chapter 5 the enzyme-based detection of L-lactate is explored using the enzyme lactate dehydrogenase (LDH) immobilized on transparent silica thin films. An approach to form hierarchically structured silica films containing both mesopores and macropores is developed, and the structure, composition and surface charge behavior of these films is analyzed. Protein adsorption and desorption is investigated using quartz crystal microbalance experiments. The performance of hierarchical films is compared to traditional mesoporous films. Their characteristics for lactate biosensing are investigated and the enzyme kinetics and the response for lactate biosensing are discussed.

Chapter 6 is concerned with the utilization of the enzyme lactate oxidase (LOx) to build a hybrid multilayer scheme for lactate detection in films and protein-based lactate microparticle probes. In the patch-based scheme, the enzyme does not need the addition of a cofactor, and it is covalently immobilized within the silica porous structure. Cytochrome C (CytC) is then co-immobilized by adsorption using a polyelectrolyte layer-by-layer technique. A second approach that is complementary to the patch-based biosensing system developed in this thesis will be adapted to create particle-based detection systems by forming LOx-CytC protein particles instead of films. The biocatalytic activity of LOx in these particles will be assessed using fluorescence-based methods. This last part demonstrates that the detection schemes

Chapter 1. Introduction

for lactate biosensing developed in this thesis are not limited to film-based systems, but can be applied to other geometries as well.

Chapter 7 presents general conclusions and recommendations towards the implementation of the nanostructured materials developed in this work in the area of biosensing for a wide range of potential applications.

2 Background

The design and implementation of the biosensing concepts outlined in Chapter 1 involve the understanding and integration of principles, mechanisms, and methodologies from a broad range of disciplines. Among them, the enzymes' properties and reaction mechanisms, including methodologies for their immobilization, the approaches for the synthesis of porous materials, and diffusion considerations during their performance in biosensing are of particular relevance. In this second chapter, key information covering the important features of the enzymes and other biomolecules utilized for the development of lactate biosensing materials is presented. The strategies to incorporate these biological agents within the porous materials are summarized. Finally, the background for the approaches followed in this work to synthesize multiscale porous systems and the basics on diffusion in porous matrices is described.

2.1 Enzymes: definition, mechanisms and immobilization

2.1.1 Definitions and composition of enzymes

Enzymes are predominantly proteins: sequences of amino acids (Figure 2.1) covalently bound by condensation reactions between carboxylic and amino groups. Proteins contain a wide range of functional groups. They are present in all cells, independently of their origin, and participate in metabolic transformations by catalyzing chemical reactions. Enzymes function by lowering the transition-state energy and energetic intermediates and by rising the ground-state energy in chemical reactions⁵⁸. Enzymes can contain other elements than amino acids: metal ions, polysaccharides and/or prosthetic groups^a. Enzyme molecular weights range from several thousand to several million, and still catalyzing reactions in molecules as small as CO₂.

The structure of enzymes is important for their biological relevance. These biomolecules fold into several conformations to be able to perform their catalytic function. The conformations are stabilized by both non-covalent and covalent interactions between side chains of amino acids (known as residues) namely hydrogen bonding, van der Waals forces, hydrophobic and ionic interactions and disulfide bonds. The sequence of amino acids in an enzyme is known as their primary structure. The interaction between amino acids by hydrogen bonding into regular 2D structures identified as alpha-helix and beta-strand are the secondary structure. When these regular structures fold between them into a 3D structure, then they are referred as the tertiary structure. Finally, the association of more than one three-dimensional structure receives the definition of quaternary structure of the protein/enzyme⁵⁹.

The three-dimensional structure of these biomolecules provides specificity to the enzyme to interact with only one molecule, as the amino acid residues form in most cases an environment to bind a specific substrate, with a specific chirality, size and charge and “lock it” into the active site. The model of a lock and a key established by Emil Fischer⁶⁰, although not completely accurate, represents in a simple and graphic manner the mechanism of reaction of enzymes (Figure 2.2). A substrate (key) fits into a cavity in the enzyme (lock); the enzyme changes its three-dimensional structure while performing its catalytic reaction to finally release a product. Three-dimensional structures of enzymes can be obtained by X-ray crystallography. Online free databases are available providing 3-D models of enzymes via the Protein Data Bank (PDB)⁶¹, and more specific details regarding their optimal conditions to perform their activity, inhibitors, origin, classification, reactions, etc can be found via BRENDA, an online enzyme information system⁶².

Enzymes that oxidize lactate in the cell as a step in the metabolism of glucose are relevant in biosensing applications for lactate detection. The two most reported and commercially available lactate consuming enzymes LDH and LOx are described in the following section. Additionally, the structures and mechanisms of two other biomolecules, which have been used in this work, the model enzyme HRP and the biomolecule CytC, are also discussed (Figure 2.3).

^aA prosthetic group is a tightly bound, specific non-polypeptide unit required for the biological function of some proteins

2.1. Enzymes: definition, mechanisms and immobilization

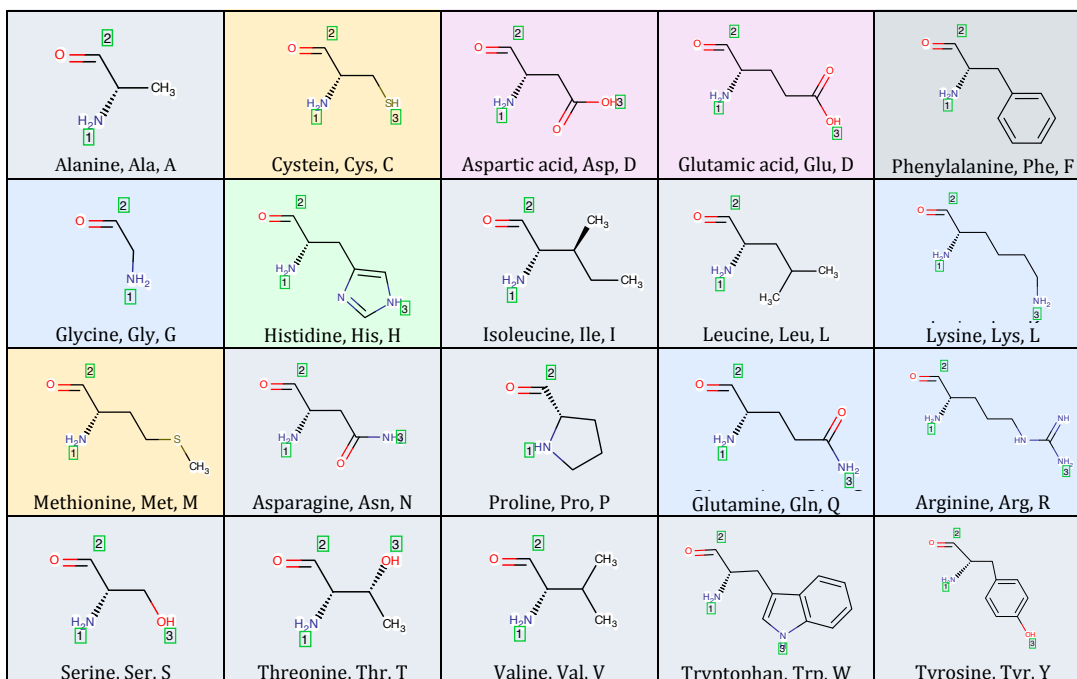


Figure 2.1 – Overview of the 20 amino acids synthesized by the cell color-coded by their functionalities used for immobilization. Blue: amino groups; red: carboxylic groups; orange: thiol groups; green: pyridine group used in his-tag for metal binding.

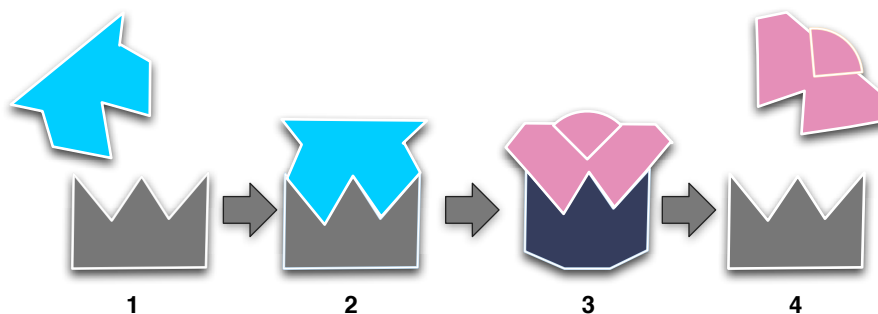


Figure 2.2 – “Key and lock” model of enzymatic reactions proposed by Emil Fisher. 1. The enzyme and substrate are present in the same medium 2. The enzyme recognizes the substrate and binds to it. 3. A conformational change occurs, the enzyme performs its catalytic reaction and 4. The enzyme returns to its original state, releasing a product of reaction.

2.1.2 L-Lactate consuming enzymes and other biomolecules

L-Lactate dehydrogenase

L-Lactate dehydrogenase (Figure 2.3) is an oxidoreductase^b with an Enzyme Commission Number (EC)^c 1.1.1.27^{62;63}. It is a 4-unit protein (quaternary structure, Figure 2.3) with a

^bAn oxidoreductase is a term used in biochemistry for an enzyme that catalyzes the transfer of electrons from one molecule to another. This group of enzymes usually utilizes NAD⁺ as cofactor.

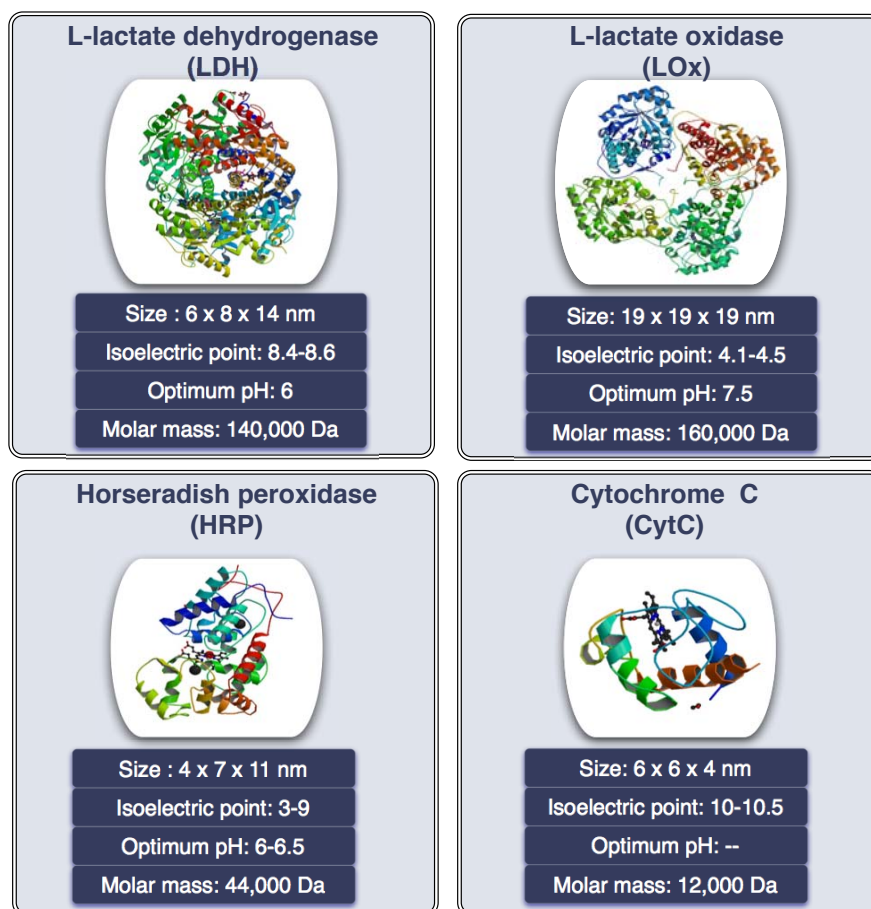


Figure 2.3 – Three-dimensional structures and physicochemical details of the biomolecules used in this work. LDH (PDB number 3H3F), LOx (PDB number 2DU2), HRP (1H1C) and CytC (PDB number 1HRC) accessed via <http://www.rcsb.org/pdb/>⁶¹

molecular weight of 140 kDa and with crystal dimensions of 6 x 8 x 14 nm⁶⁴. LDH has several isoenzymes and it is present in a wide range of organisms, both from animal and plant origin with slight changes in amino acid sequence, and therefore with different isoelectric points. The enzyme isolated from rabbit muscle, LDH-isoenzyme M (skeletal muscle) has been used in this work. It has an isoelectric point of 8.4-8.6 and an optimal catalytic pH of 6. It catalyzes the reversible oxidation of L-lactate in the presence of NAD⁺ into pyruvate with the concomitant reduction of the cofactor to NADH. NADH optical properties are exploited to follow the oxidation of lactate. The cofactor's reduced species absorbs light with a maximum at 340 nm⁶⁵ and it emits at 445 nm when excited at 350 nm⁶⁶. Only the reduced form of NAD has fluorescence properties. The enzyme cofactor is not an integral part of the enzyme and must be present in the medium where the enzyme is. For in-vitro studies, NAD⁺ is added at

⁶¹Nomenclature from the Committee of the International Union of Biochemistry and Molecular Biology. It is based on a number hierarchy of 4 digits. The first digit corresponds to the class: 1. Oxidoreductases; 2. Transferases; 3. Hydrolases; 4. Lyases; 5. Isomerases, and 6. Synthetases. Subsequent digits provide detailed information on specific function and reactants.

2.1. Enzymes: definition, mechanisms and immobilization

concentrations exceeding the concentration of substrate to avoid the limitation of cofactor to the enzyme. Both NAD^+ and NADH versions are commercially available with different purity degrees.



Each LDH subunit is able to bind a NAD molecule and a L-lactate molecule. According to binding dynamics studies⁶⁷, NAD^+ needs to bind first in order to proceed successfully to the binding of L-lactate. The protein's structure forms a loop at each subunit, which might be open or closed depending whether a NAD^+ molecule has bound or not. There are several conformations that can yield to multiple binding pathways. The enzyme structure fluctuates in shape due to internal rearrangements, mainly due to solvation/hydrogen bond formation between different amino acid residues. The binding pocket for NAD^+ and lactate is at the protein's interior. It is known that these rearrangements are necessary to allow the cofactor and the substrate to efficiently bind the active site.

NAD^+ is a dinucleotide: a ribose moiety bound to a nitrogenous base and a phosphate group (Figure 2.4). Only one of the nitrogenous bases, the nicotinamide base, is involved in the oxidation-reduction of lactate. The adenine base does not participate in this specific reaction.

LDH biocatalytic mechanism NAD^+ is a hydride acceptor (oxidizing agent). From crystallographic analysis⁶⁴, the histidine residue H192 (amino acid structure in Figure 2.1) from the enzyme takes a proton from the α -carbon in lactic acid, then the electrons from the O-H bond shift down and push out the hydride. Because of the proximity between lactate and NAD^+ , the NAD^+ molecule takes the leaving hydride becoming reduced (NADH). Arginine residues (Figure 2.1) R105 and R168 are responsible of forming hydrogen bonds with lactate, positioning the molecule to be attacked by the proximal histidine H192 and to transfer the hydride to NADH ⁶⁴. Once the reaction has taken place, pyruvate is released first, then the NADH (Figure 2.5).

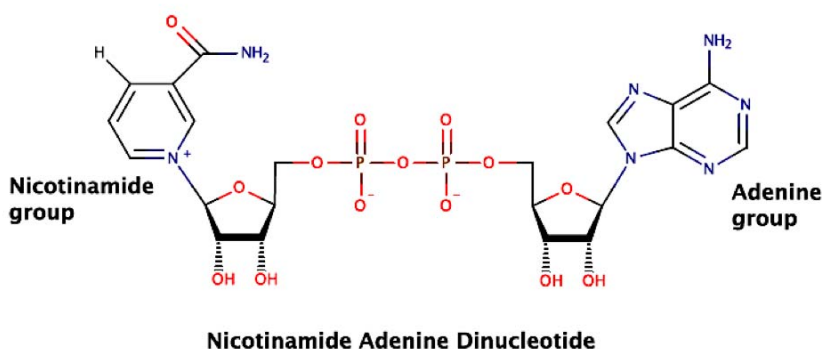


Figure 2.4 – Structure of Nicotinamide Adenine Dinucleotide, oxidised form (NAD^+). Only the nicotinamide base participates in the enzymatic reaction of LDH.

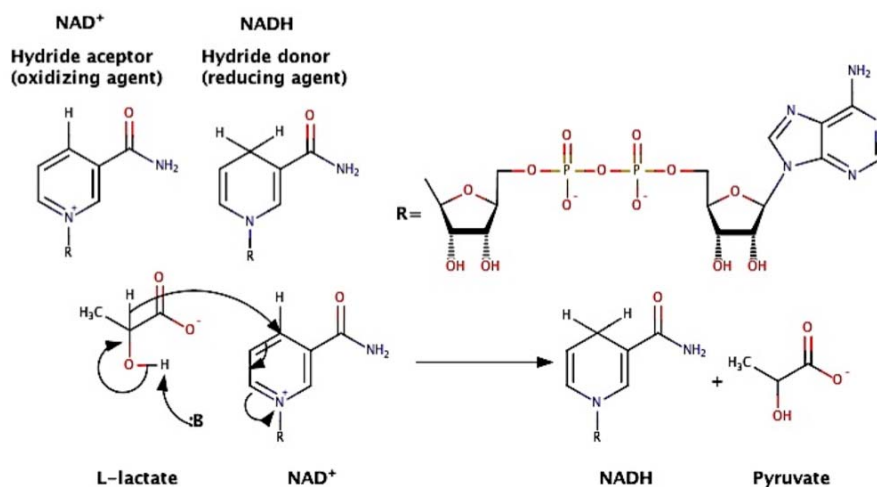


Figure 2.5 – Mechanism of reaction of L-lactate dehydrogenase. NAD^+ and NADH act as hydride acceptors and donors respectively. In the oxidation of lactate to produce pyruvate, NAD^+ accepts a hydride from the α -carbon in lactic acid. R represents the NAD moiety, which is not directly involved in the oxidation/reduction reactions. The reaction is reversible.

Lactate oxidase

EC 1.12.12.4 L-lactate oxidase (Figure 2.3) is an oxidoreductase with a tetrameric and almost symmetrical protein of 160 kDa size⁶⁸. Its crystallographic dimensions show a cubic structure of 19 nm in diameter⁶⁸. Each of the four subunits consists of 374 amino acids. It converts L-lactate into pyruvate and hydrogen peroxide with at an optimum pH of 7.5:



The commercial enzymes are isolated from microorganisms (predominantly bacteria). The lyophilized enzyme is a yellow highly hygroscopic powder. It is soluble in water and has a thermal stability up to 50 °C for 10 minutes⁶⁹. Whereas it can stay undamaged by surfactants such as Tween, Span and Triton-X at a concentration of 0.1% w/v, it becomes easily denaturated in the presence of SDS at 0.05%. This enzyme is used for the determination of lactate in diverse samples following different schemes for quantification of enzymatic activity.

LOx belongs to the family of flavoenzymes⁷⁰. Enzymes from this family require the participation of flavin cofactors to carry out their catalytic activity. In the case of LOx, a prosthetic group flavin mononucleotide (FMN, Figure 2.6 right) is an intrinsic and structural part of the enzyme, as it is involved in the selective recognition of L-lactate and its conversion into pyruvate in combination with molecular oxygen. Each subunit in the tetramer has a FMN molecule. Crystallographic studies^{68;71} have shown that the residues 190–220 form a lid-like structure for the active site, being a well conserved sequence among other enzymes with similar activity, such as glycolate oxidase (Figure 2.6 left). Arginine residue R268 fixes the

2.1. Enzymes: definition, mechanisms and immobilization

hydroxyl group from L-lactate's carboxylic group at the active site. A leucine residue L211, being hydrophobic fixes its methyl group. Tyrosine residues Y40, Y146 and Y215 are important to identify and fix via hydrogen bonding the right chirality of lactate.

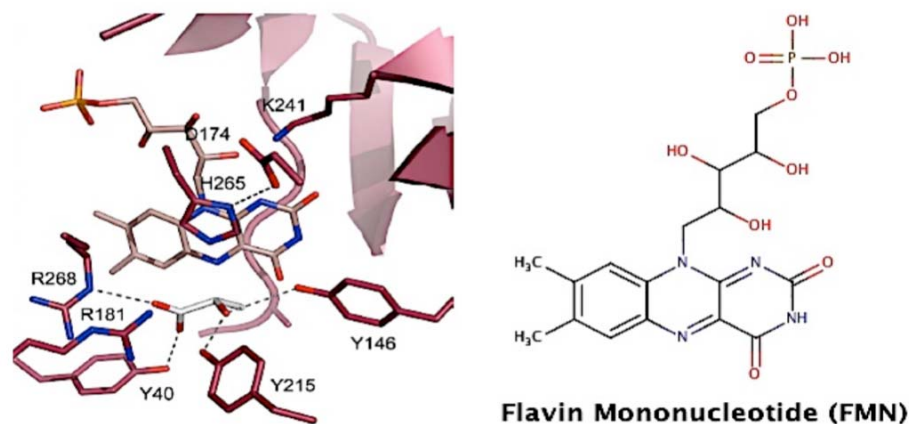


Figure 2.6 – Left: Active site from L-lactate oxidase. A flavin mononucleotide (FMN, right) is a constitutive part of the enzyme. L-lactate is fixed to the active site by covalent bonding and hydrophobic interactions from neighbouring amino acid residues, particularly tyrosine (Y), arginine (R) and leucine (L). Image taken from Leiros et al.⁷¹

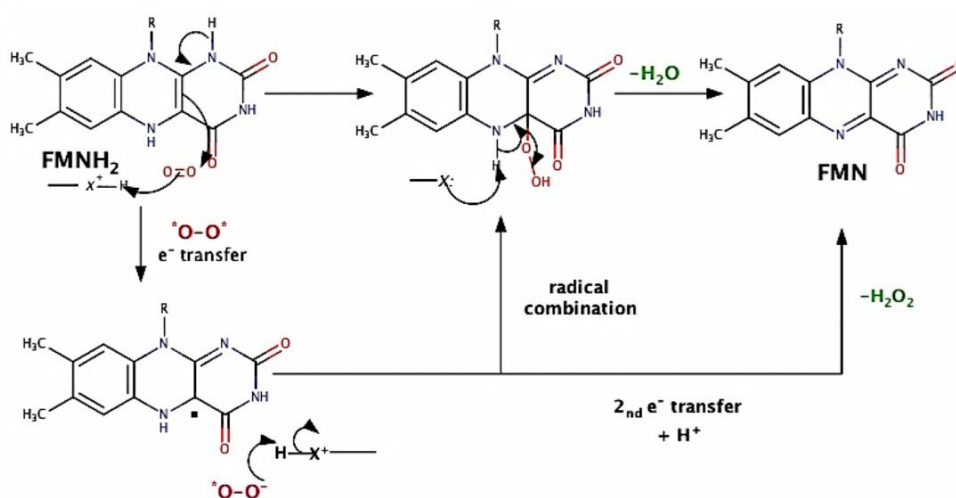


Figure 2.7 – Mechanism of reaction of L-lactate oxidase I. In a first step, molecular oxygen binds first the reduced flavin prosthetic group (FMNH₂) from the enzyme LOx in a two-single electron transfer mechanism, resulting in the production of hydrogen peroxide and the oxidised flavin, FMN.

LOx biocatalytic mechanism Although the details of the mechanism are still under debate⁷², it ultimately results in the transfer of two electrons and two protons from the reduced cofactor to molecular oxygen to generate hydrogen peroxide and the α -keto acid (pyruvate)

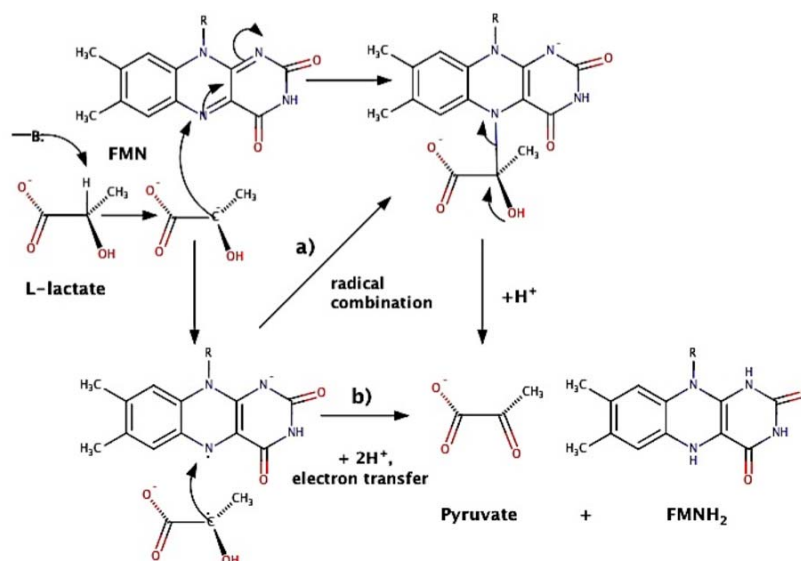


Figure 2.8 – Mechanism of reaction of L-lactate oxidase II. In a second step, the oxidation of lactate proceeds firstly with the formation of a carbanion by the subtraction of its acidic α -hydrogen. Two possible mechanisms are presented: a) a two electron transfer with the nucleophilic attack of the carbanion to the oxidised flavin or b) by a two-single electron transfer via radical formation. The final products of the reaction are pyruvate and the regeneration of FMN₂ to start a new cycle.

and ultimately to regenerate the oxidized cofactor. The reaction proceeds via a ping-pong mechanism⁵⁸ (a product is released before all the substrates are bound to the active site) with sequential reductive and oxidative steps⁷³. The reduced flavin (FMNH₂) is oxidized by molecular oxygen with the release of hydrogen peroxide (Figure 2.7). In the following step, a base abstracts a proton from the substrate α -carbon, and then a transfer of two electrons proceeds to the oxidized cofactor (FMN) to regenerate the reduced form (Figure 2.8). Flavin cofactors, as the nicotinamide adenine dinucleotide, can act as hydride acceptors and donors, transferring two electrons in the form of a hydride in these redox reactions. Flavin can also catalyze chemical reactions where only a single unpaired electron is transferred as in radical chemistry⁷⁴. This is due to the ability of flavin to form a stabilized radical intermediate called a semiquinone, formed when FMNH₂ donates a single electron, or when FMN accepts a single electron.

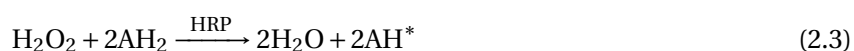
Horseradish peroxidase

EC 1.11.1.7 Horseradish peroxidase (HRP, Figure 2.3) with crystallographic dimensions of 4 x 7 x 12 nm⁷⁵ is a glycoprotein and a heme-containing enzyme with a molecular weight of 44 kDa. Almost a fifth part of its molecular weight corresponds to its carbohydrate moiety. It is isolated from horseradish roots (*Amoracia rusticana*) and it has several isoforms with isoelectric points ranging from 3 to 9 and an optimal pH value of 6-6.5. Compared to LDH and LOX, HRP is a single polypeptide chain (no quaternary structure). The heme group (Figure

2.1. Enzymes: definition, mechanisms and immobilization

2.9) is the active catalytic site. It is covalently bound to the enzyme via a nitrogen-iron bond between a proximal histamine residue in the protein and the iron center from the heme group. The second axial coordination side from the heme group (distal side) is available for reaction with oxygen species, among other small molecules such as CO, CN, etc.^{76;77}. The biological relevance of HRP is its ability to eliminate highly reactive oxygen species such as H₂O₂ which are toxic to cells. H₂O₂ is required by the enzyme to carry out its catalytic activity.

HRP Biocatalytic mechanism HRP catalyzes single-electron reduction reactions. A general equation for HRP activity can be expressed as⁷⁸:



where AH₂ and AH^{*} represent the reducing substrate and its radical product. Standard reducing substrates include aromatic phenols, indoles, amines, and sulfonates⁷⁸. The characteristic change of color of some of the substrates depending on their oxidation states is a widely employed in biochemistry to amplify and quantify the signal of relevant *in vitro* reactions, where HRP is usually conjugated to other biomolecules (such as antibodies, enzymes or other proteins of interest)⁷⁹.

The first step in the catalytic cycle is the reaction between hydrogen peroxide (H₂O₂) and ferric heme (Fe⁽³⁺⁾) in the resting or grounding state to generate compound I, a highly reactive intermediate state comprising a Fe⁽⁴⁺⁾ oxoferryl center and a porphyrin-based cation radical (Figure 2.10).

The complex I oxidizes a wide variety of hydrogen donors via a two-single electron transfer reactions. The generation of radical species in the two one-electron reduction steps results in a complex profile of reaction products, including dimers, trimers and higher oligomers that may themselves act as reducing substrates in subsequent turnovers⁷⁸ (Figure 2.11).

Cytochrome C

Cytochrome C (CytC) is another heme-containing protein with a diameter of 6 nm⁸⁰, a molecular weight of 12 kDa and an isoelectric point around 10-10.5. It is involved in the electron transfer in most eukaryotic organisms within the respiratory chain, acting as an electron-tunneling compound among the cell membrane. CytC is not an enzyme *per se*, however it is considered as a pseudo enzyme, as it is capable of reducing diverse aromatic compounds.

CytC is commercially available and is obtained from different sources, primarily from animal origin. It possesses a dark-red color in its oxidized state (the commercial form of CytC). Mild reducing agents such as ascorbic acid are capable of transferring single electrons to the iron center converting it from ferric cytochrome (Fe⁽³⁺⁾) to ferrous cytochrome (Fe⁽²⁺⁾)⁸¹. This change in oxidation state can be monitored with great specificity and sensitivity measuring the light absorbance change at 550 nm⁸². The importance of CytC for the sensing concepts presented in this work is its ability to react with hydrogen peroxide, the product of reaction of LOx⁸³

Chapter 2. Background

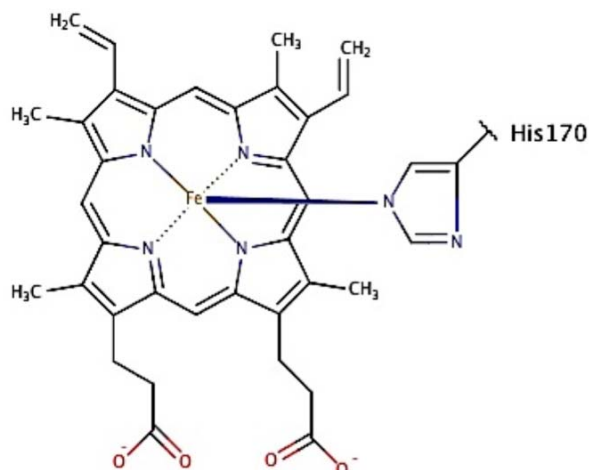


Figure 2.9 – Structure of heme group. In horseradish peroxidase, the heme group is attached to the enzyme via a histidine residue (His170) at the lower plane (from below). Another histidine residue resides at the upper plane (distal plane) and is ready to react to form hydrogen peroxide.

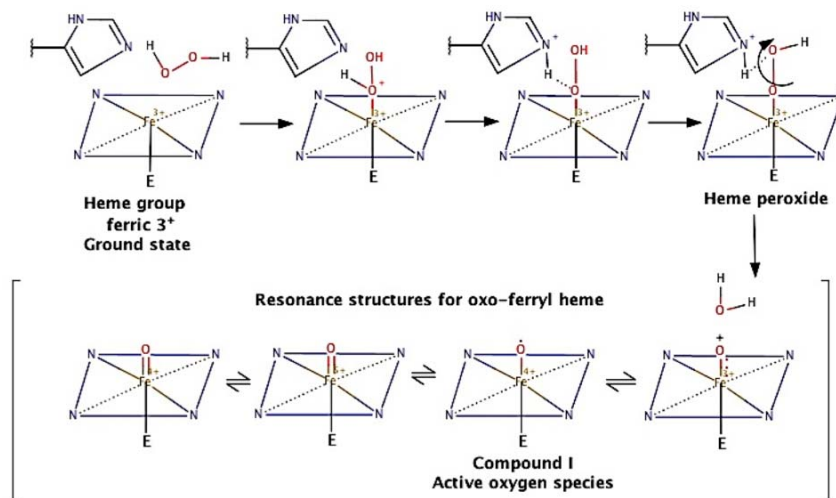


Figure 2.10 – Reaction between hydrogen peroxide and the iron center (heme group) from horseradish peroxidase. The formation of a highly reactive oxygen compound (complex I) is the first step towards the oxidation of several reducing substrates. Adapted from Silverman⁵⁸.

(Figures 2.7 and 2.8), changing its own oxidation state according to the reactions described in Figure 2.11. This change in oxidation state from the heme group can be monitored by optical means.

2.1. Enzymes: definition, mechanisms and immobilization

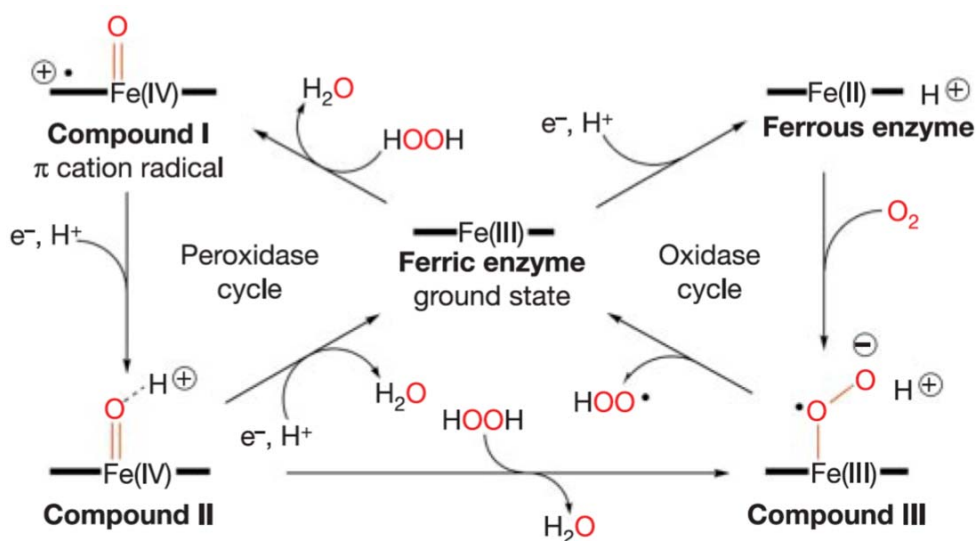


Figure 2.11 – Reduction-oxidation of the heme group. From Berglund et al.⁷⁵.

2.1.3 Enzyme kinetics

Kinetics is the study of the rates of chemical reactions. Enzymes catalyse most of the biological reactions that occur in the cells of living organisms⁸⁴. Considering the following unimolecular reaction:



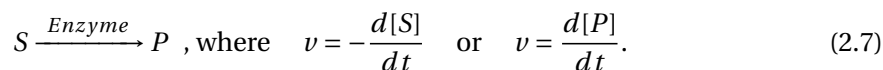
Since there is only one reactant, this reaction is of first order with respect to A. The rate or speed of this reaction is determined by the consumption of the reactant or the appearance of the product:

$$v = -\frac{d[A]}{dt} \quad \text{or} \quad v = \frac{d[B]}{dt}. \quad (2.5)$$

In this first order reaction, the rate is proportional to the concentration of reactant:

$$v = k[A], \quad (2.6)$$

where k is the rate constant. In enzymatic reactions, the reactant is called substrate (S) and it is converted into a product (P):



As the reaction progresses, the rate of reaction towards products competes with the rate of reaction towards substrate, until equilibrium is reached. At this point the rates become equal. The rate equation for an enzyme-catalysed reaction with one substrate is only the same as the rate equation for the simple non-enzymatic reaction, when the concentration of substrate is so low that the enzyme has barely a chance to convert it to product. Nevertheless this

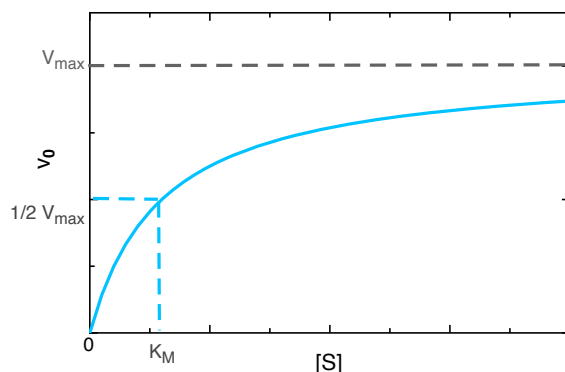
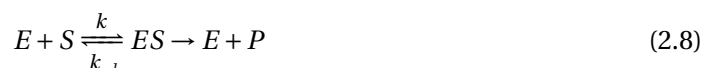


Figure 2.12 – Graphic representation of the Michaelis-Menten equation, which describes the kinetics of an enzyme. v_0 : initial reaction rate, $[S]$: substrate concentration, V_{max} : maximum speed of reaction, K_M : Michaelis-Menten constant.

special case is very restrictive and does not apply to biological systems. Enzyme kinetics can be studied when the concentration of the substrate is in excess compare to the concentration of the enzyme. Under this scenario, the rate reaction is called to be zero with respect to the substrate and any change in concentration will not affect the rate of the reaction. The model of an enzymatic reaction includes the formation of a substrate-enzyme complex:



At $[S] \gg [E]$, all the active sites of the enzyme are bound to substrate forming ES complexes. The rate of reaction does not depend on the concentration of substrate but on the enzyme concentration. In this case, the zero-order rate constant is the maximum speed of reaction, or V_{max} . Additionally, it is assumed that the disintegration of the ES leading to the product complex is irreversible. However, at concentrations of substrate or enzyme that are not saturating, another equation is needed to describe the kinetics of the reaction. The Michaelis-Menten equation describes a system where the initial rate of reaction is limited to the initial reaction rate v_0 , avoiding the effect of products accumulating in the medium and undergoing the inverse reaction. The Michaelis-Menten equation is

$$v_0 = \frac{V_{max}[S]}{K_M + [S]} \quad (2.9)$$

where K_M is a rate constant incorporating all the enzymatic constants for ES and P formation:

k_1 , k_{-1} and k_2 and it is equal to the concentration of substrate at half saturation of the enzyme. K_M is a ratio between the ES breakdown to S or P and the rate of ES formation and describes the dependence of v_0 on $[S]$ and the slope of the curve v_0 vs $[S]$. Graphically, it can be also noticed that K_M is the concentration at $\frac{1}{2}V_{max}$ (Figure 2.12).

K_M is inversely related to the concentration of enzyme that is in complex with substrate. The higher the K_M , the lower the fraction of enzyme bound to substrate. K_M describes the dependence of v_0 on S, and determines the slope of the Michaelis–Menten curve. The values of v_0 are obtained experimentally from different enzymatic assays maintaining $[E]$ constant

2.1. Enzymes: definition, mechanisms and immobilization

but changing $[S]$. To minimize the effect of ES converting into E and S (k_{-1}), v_0 is obtained from the slope at a short reaction time, to avoid the accumulation of the product, usually only after a few minutes of reaction, and in this limit the short-time rate is simply $v_0 = \Delta[P]/\Delta t$.

2.1.4 Enzyme immobilization

Immobilization of enzymes is one of the most important factors towards a stable biosensor. Different methods are known and widely used, varying in their degree of stability and specificity of attachment. Adsorption, covalent bonding, encapsulation or entrapments are some of the most common ways to immobilize enzymes (Figure 2.13).

Enzymes have been the target of efforts, initially to isolate them from their natural sources, and furthermore to find strategies to immobilize them. Enzyme immobilization aims at maintaining its biocatalytic function when it is out of its natural environment. The objective is to offer stability, mainly by confinement in a protective environment. At the same time, this confinement offers the possibility to preserve the enzyme with the potential to be reused several times.

Cross-linking of enzymes is a method consisting in the formation of enzyme aggregates by precipitation with a consequent chemical crosslinking, normally by glutaraldehyde, a bifunctional aldehyde crosslinker. This method does not require the use of a support, since the enzymes are linked one to each other forming particles of several microns of size. Adsorption is a popular method and very often reported as a means to immobilize enzymes due to its simplicity, because previous functionalization of the support is not required⁸⁵; however, the interactions between the enzyme and supports are relatively weak, with leaching of the enzyme occurring over time⁸⁶. Ionic binding involves the interaction of organic groups with opposite charges from the enzyme and the support. Positively charged amino acids like arginine, histidine, and lysine or negatively charged amino acids such as aspartic and glutamic acid for example can interact with carboxylic groups and amino groups from supports under specific pH ranges (Figure 2.14). Metal binding is another way to immobilize enzymes involving the genetic modification of an enzyme by attaching a *hist-tag* (Figure 2.1) moiety (several histidine groups, usually at the N- or C- end of the enzyme). By means of this modification, metal ions can bind to the enzyme as Ni^{2+} , Zn^{2+} , Cu^{2+} . At the same time, the support needs to be functionalized with chelating groups, being the most common nitriloacetic acid, andiminodiacetic acid or resacetophenone⁸⁷. Finally, the most stable method to immobilize enzymes is by covalent bonding (Figure 2.14). Organic functionalities at the support's surface are required, either naturally present or incorporated by means of post-functionalization steps. Some of the organic functionalities, which can participate in covalent bonding, are carbonates, aldehydes, epoxides, azides, isocyanates, amino and carboxylic groups. From the enzyme counterpart, amino acid residues containing carboxylic, amino, thiol or hydroxyl groups in the side chain and available at the surface of the enzyme are candidates for covalent bonding⁸⁸.

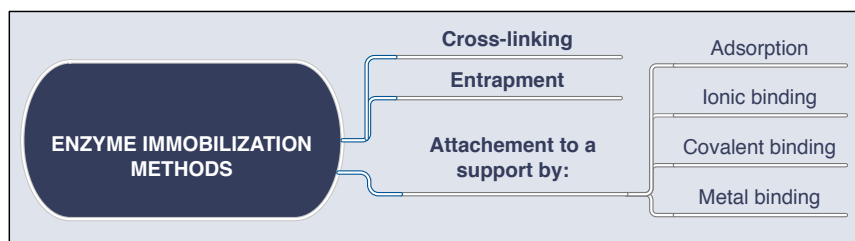


Figure 2.13 – Most common strategies to immobilize enzymes.

Enzyme supports

The choice of a relevant support for enzyme immobilization requires the consideration of several criteria, such as:

1. the mechanical stability of the support itself, which will protect the enzyme from denaturation
2. the surface functionalization and the available functional groups, which are important for the coupling of the enzyme to the support
3. the chemical/microbial resistance, relevant for the long-term stability and reusability, if required
4. the availability of raw materials for their synthesis and cost restrictions, which will influence the decision regarding their industrialization
5. the surface area and accessibility, which will determine their ability to host large amounts of enzymes

Different supports can serve as carriers to immobilize enzymes, both from inorganic and organic nature. The choice of one over another depends strongly on the final foreseen application^{84;89-91}.

Organic supports

Organic supports can occur naturally such as proteins (such as keratin, collagen, albumin, and gelatin) and carbohydrates (such as dextrans, celluloses, alginates, carrageenans, starch, agarose or chitosan)^{40;89;92}. Some of these materials are commercially available as enzyme supports. For example, Sephadex[®] and Sepharose[®] are products obtained from cross-linked dextran and agarose respectively. With further chemical modifications (activations), these materials can be used for covalent immobilization of enzymes. Alternatively, commercially available and already activated matrices are accessible too, for example Affi-Gel[®] (BioRad) which consists of crosslinked agarose and a customized selection of functional groups attach to it, depending on the target application⁹³.

2.1. Enzymes: definition, mechanisms and immobilization

Synthetic organic supports are diverse regarding their characteristics and they can be found commercially as well. Polystyrene, polyacrylate, polyvinyls, polyamides, polypropylene and copolymers of these are the most common synthetic support matrixes^{89;90;94}.

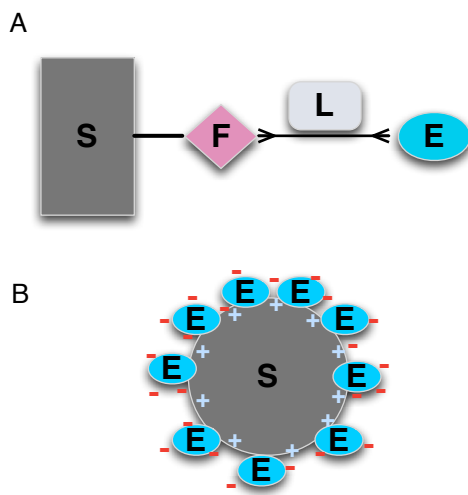


Figure 2.14 – Examples of enzyme immobilization schemes. A. Covalent immobilization involving the bonding between a functional group (F) from the support (S), the enzyme (E) and a linker (L) between enzyme and support. B. Ionic interactions between enzyme (E) and support (S) with opposite charges.

Inorganic supports

Inorganic carriers (e.g. glass, silica, alumina, bentonite, hydroxyapatite, nickel/nickel oxide, titania, zirconia, calcium carbonate) often show better mechanical properties, thermal stability, and resistance against microbial attack and organic solvents than organic supports. Inorganic supports are also better known for their mechanical stability as compared to the organic counterparts. However, for real applications, inorganic supports often require the combination with organic compounds, which are important part of the biosensing scheme. For example, inorganic supports are functionalized with organic functionalities, semipermeable polymer layers or with biological responsive components such as enzymes. This combination of inorganic-organic materials with enzymes in the same system can lead to the synthesis of suitable stimuli-responsive schemes with realistic applications^{95–97}. The term ‘hybrid material’ has been coined for this kind of materials with both organic and inorganic components on scale of less than 100 nm⁹⁸.

Enzyme immobilization strategy

The criteria for a successful immobilization of an enzyme must take into account the characteristics of the enzyme, the support and the immobilization conditions (Figure 2.15). Regarding the characteristics of the enzyme, parameters such as size, isoelectric point, available functional groups at the surface for covalent binding, and possible conformational changes during

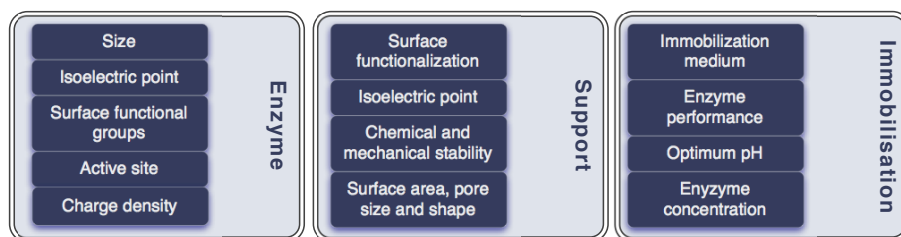


Figure 2.15 – Parameters to consider for a successful enzyme immobilization strategy.

the performance are important to evaluate. Some of these characteristics from the enzyme can be coupled to the features from the support. For example, the surface functionalization can be tailored to allow covalent binding between the available functional groups from the enzyme and the support. At the same time, these organic functionalities at the surface can be tuned to render the isoelectric point of the support compatible for the diffusion and immobilization of the enzyme. Electrostatic adsorption of the enzyme at the surface of the support can be a challenge during the immobilization. Finally, the concentration of enzyme, the immobilization medium chosen and the pH are factors that will influence the overall enzyme immobilization process.

2.2 Synthesis of porous materials

2.2.1 Sol-gel chemistry for thin film formation

Though nanostructured metal oxide and hybrid films are used in a large number of industrial applications, their design and preparation remain a challenge. Mesoporous silica films are known candidates for enzyme immobilization since they fulfill with the criteria listed before to become enzyme supports. The possibility to synthesize large surface area films (higher enzyme loadings), with controlled pore size, thickness, well defined pore geometry, homogeneous pore distribution along the films, together with their thermal and mechanical stability and their biocompatibility are among the key features. Furthermore, the inner surface of silica films can be chemically modified with various functional groups to match the intrinsic characteristics of the enzyme⁸⁵. Sol-gel chemistry is a very flexible approach for the synthesis of mesoporous silica films due to the availability of silica molecular precursors, the mild conditions for their synthesis and the opportunity to design and tune the porosity by a versatile combination of self-assembly principles and templating materials.

Sol-gel technology is a group of material synthesis processes starting from the formation of metal oxide colloidal particles with sizes ranging between 1 to 1000 nm. Sol-gel processes combine the control of the chemical composition of these colloidal particles at the molecular level with the ability to cast them or shape them into different forms such as bulks, powders, films, and fibers. The term sol-gel encloses then the formation of a colloidal suspension or sol of solid particles in a liquid, in which the dispersed phase particles can grow into a continuous solid network all along the liquid phase, forming a gel.

Sol-gel chemistry is the wet technique to prepare metal oxide materials from molecular

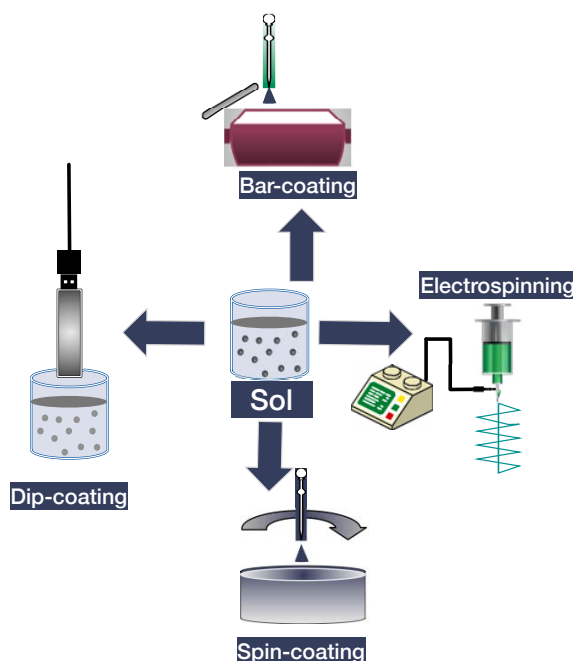
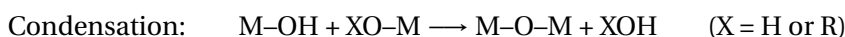
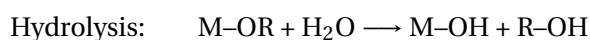


Figure 2.16 – Casting techniques for sol-gel films.

precursors. These precursors are involved in successive hydrolysis and condensation reactions leading to the formation of an oxide network. The growth of the metal oxide structure is assimilated to an inorganic polymerization. Starting from molecular precursors, sol-gel chemistry offers the opportunity to synthesize metal oxide materials under mild conditions in a solvent. Sol-gel casting processes enable the production of films via dip-coating, spin-coating, bar-coating, electrospinning, among others processes⁹⁹ (Figure 2.16).

Metal salts and alkoxides are typical metal oxide molecular precursors. Metal salts are used in water. Then, the oxidation state of the metal and the pH are predominant parameters determining the chemical composition of the grown metal oxide species in solution. Metal alkoxides are usually preferred precursors, since their reactivity towards water leading to metal oxide species can be monitored by the appropriate choice of the solvent, the alkoxide groups, and some additives and their relative concentrations.

The metal oxide network is formed by successive hydrolysis and condensation reactions from metal alkoxide precursors. Metal alkoxide molecules, $M(OR)_n$, R representing an alkyl group and n being the oxidation state of the metal, first react with water forming a hydroxyl group M-OH (hydrolysis reaction). Then, hydroxyl groups react with alkoxide or hydroxyl groups to form an oxide group between two metallic centers (condensation reaction).



The coordination numbers (N) of transition metal in thermodynamically stable crystallographic forms of the metal oxide are normally larger than their oxidation state (z). Moreover,

Chapter 2. Background

their electronegativity is lower, which make them prone to nucleophilic reactions. Therefore, transition metal alkoxides have a very high reactivity towards water. Commercial metal alkoxide flasks are filled in under Argon or nitrogen. Once opened, the metal alkoxide instantaneously forms oxide species by reacting with humidity.

Silicon alkoxides are less reactive towards water than other metal alkoxides (Table 2.1). Indeed, Silicon has a coordination number and an oxidation state of 4 in the alkoxide precursor and in crystalline silicon oxide respectively, and it shows relatively low electrophilicity: the partial charge of the silicon atom is lower than in transition metal atoms. Since $N=Z$, coordination expansion does not occur spontaneously as in the case of transition metals¹⁰⁰. For these reasons, they are not very reactive towards water. As a consequence, the addition of an acidic or basic catalyst such as mineral acids and bases is usually needed.

Table 2.1 – Difference in reactivity of silicon alkoxides and transition metal alkoxides.

Alkoxide	Electronegativity χ	Partial charge	Oxide	Coordination number N	N-z
Si(OPr ⁱ) ₄	1.74	+0.32	SiO ₂	4	0
Ti(OPr ⁱ) ₄	1.32	+0.60	TiO ₂	6	2
Zr(OPr ⁱ) ₄	1.29	+0.64	ZrO ₂	7	3

Silica sols obtained under basic or acidic catalysis show remarkable differences; under basic catalysis the hydrolyzed silica precursors will form dense particles, which will grow rapidly to a size dependent on precursor concentration and temperature. Under acidic conditions, the hydrolyzed silica precursors will form soft oligomers, which will eventually aggregate to form polymeric networks instead (Figure 2.17). The exact mechanism was described by Iler¹⁰¹. For the sake of the synthesis of porous silica films by sol-gel chemistry following a templating approach as described in the following section, the sols obtained under acidic catalysis are more suitable.

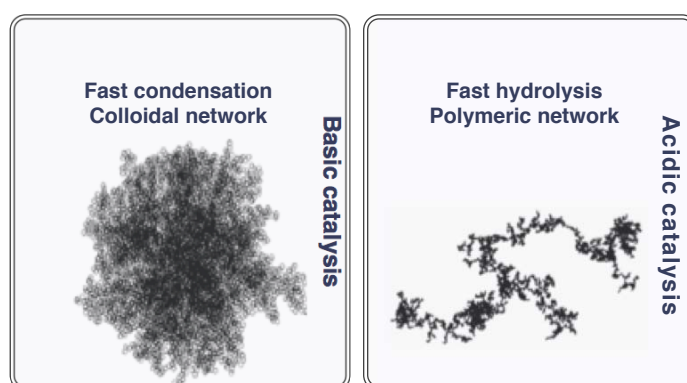


Figure 2.17 – Silica synthesis under basic or acidic catalysis. Under basic catalysis, spherical colloidal particles are formed whereas polymer networks are favored under acidic catalysis. Adapted from images published from Brinker et. al.¹⁰⁰

2.2.2 Synthesis of particles as enzyme supports

The biosensing concepts developed to form enzyme-loaded thin films can be extended to create enzyme-based biosensing microparticles, i.e. particles that respond optically to the presence of lactate in a liquid medium. In order to form those biosensing particles, a particle support will be needed onto which the enzyme can be immobilized, together with other biomolecules such as cytochrome C. Therefore, in this section the preparation of microparticles as supports for the formation of protein-based lactate probes will be briefly reviewed.

Well-defined metal salt microspheres have been described as supports for the formation of polymer multilayer capsules^{102;103} and for the formation of protein microspheres¹⁰⁴ by Sukhorukov, Möhwald and coworkers. The general concept of these approaches is to perform sequential adsorption of oppositely charged proteins or other polyelectrolyte material onto the surface of colloidal particles using Layer-by-Layer (LbL) adsorption¹⁰². If a pure protein-based microparticle is desired, the following step comprises the dissolution of the core material.

Volodkin et al.¹⁰⁴ demonstrated that monodisperse, uniform and spherical microparticles of a therapeutic protein (insulin) can be fabricated by adsorbing protein on calcium carbonate microparticles. The description and detailed characterization of the carbonate particles are described in previous publications^{103;105–107}. In particular, these particles are porous and such porosity has been discussed and found favorable for loading with biomolecules¹⁰⁷: average pore diameters measured by nitrogen sorption and BET analysis were found to be around 35 nm, with maximum pore diameters up to 80 nm¹⁰³. More recent modifications involve the formation of calcium carbonate microparticles with a radially grown backbone and pore structure consisting of CaCO₃ nanocrystals¹⁰⁸; whereas the pore sizes in these particles are very similar to the ones reported earlier by Sukhorukhov et al.¹⁰³, the radially grown structure of pores additionally facilitated the loading of organic molecules into the microparticles¹⁰⁸.

Other materials to create particles as enzyme supports have been described as well, including silica¹⁰⁹, gold¹¹⁰, polymers (e.g. melamine)¹¹¹. However, those alternatives usually encounter several drawbacks, among them the size of the particle smaller than half micron. Moreover, the most crucial drawback is the need of harsh conditions (organic solvents, or pH values below 1.6) to remove the particles. In contrast, the carbonate particles that will be used in this thesis can be dissolved under mild conditions, either at a weakly acidic pH value, or using complexation agents such as EDTA¹⁰⁶. As will be discussed in Chapter 6, this is a critical point because proteins, which are a key element for the biosensing concept developed here, are sensitive to the presence of acids or high salt concentrations, and protein denaturation needs to be avoided.

2.2.3 Multi-scale porosity design

Porosity is a fundamental aspect for the materials used as enzyme supports for biosensing purposes. It allows the immobilization and loading of higher amounts compared to non-porous counterparts. The incorporation of pores with more than one length scale is considered advantageous in biosensing, both for enzyme loading and performance. A hierarchically porous material can be defined as a structure containing interconnected pores on different length scales from micro- (<2 nm), meso- (2-50 nm) to macropores (>50 nm)¹¹². The classification

of pores into these three pore scales is associated to transport mechanisms: micropores are about the size of molecules and therefore the activated transport dominates. In mesopores, the size of the pores is the same or smaller to the path length of molecules and thus Knudsen diffusion and surface diffusion dictate the transport. Additionally, multilayer adsorption of molecules and capillary condensation can contribute to the transportation of molecules. Finally, in macropores the size of the pore is larger than the mean free path of molecules and bulk diffusion and viscous flow dominate¹¹³. By introducing a hierarchy of interconnected cavities at different length scales, the surface-to-volume ratio can be dramatically increased and the materials properties tailored accordingly. Such hierarchically porous systems have received special attention in recent years^{112;114}.

In a hierarchically porous material, all the pore scales have the potential to provide a specific effect for a final application: the microporosity controls the diffusion of molecules through percolation paths thereby increasing sensitivity and faster response in sensing¹¹⁵. Likewise, a material with interwoven meso- and macroporous structures can provide a high specific surface area and more interaction sites via small pores, whereas the presence of additional macropores can offer increased mass transport, increase storage volume and create easier accessibility to the active sites through the material¹¹⁶. In addition, transport phenomena of penetrating liquid media, as well as the diffusion of dispersed species, are fundamentally altered compared to a uniform pore architecture¹¹⁷.

The procedure to design porosity can follow a bottom-up or a top-down approach. In a bottom-up approach, different organic compounds are used as templating materials and a solid framework is built up around them from metal oxide molecular precursors. The incorporation of these organic compounds into a sol-gel matrix leads to the production of hybrid materials; such organic compounds are also called porogenic sacrificial agents. Their selective removal after being casted can yield nanostructured porous films, with a wide range of different pore sizes and shapes, depending on the sacrificial template used. In a top down approach, the solid framework around pores is not synthesized from molecular precursors but pre-fabricated nanoparticles, dispersed or in the form of powders (usually aggregated (nano)particles), are used instead. In this method, the porosity is not only determined by the size and shape of the templating materials used, but by the porosity from the particles themselves and the spaces or cavities among them when casted. Different reviews on nanostructuring of materials by different approaches have been reported and can be consulted for further information¹¹⁸⁻¹²³.

Microporosity (pore diameter < 2 nm)

Microporous materials, such as zeolites, possess well-defined crystallographic frameworks at the molecular level. The micropores occurring in these materials are produced by the utilization of molecules as directing agents, which after removal, notably by firing, can yield to a three dimensional network of pores. The micropores allow the diffusion of ions and small molecules. However, if larger molecules need to be transported through the porosity of the material, the incorporation of larger pores into the porous matrix are required.

Mesoporosity (2 nm < pore diameter < 50 nm)

The next scale in porosity, the meso-scale, demands the use of templating materials with larger sizes, i.e. molecular surfactants or block-copolymers, which self-organize producing micelles. The sizes of these micelles are larger than the size of single molecules and can therefore be used to structure larger pores. Using self-assembly principles to template structured metal oxide materials is consequently a highly flexible and efficient strategy to design materials with an enormous variety of structural features. Ordered mesoporous materials by surfactant-templating methods have dominated the first years of research on this field after their discovery¹²⁴. However, the pore size range achieved by these compounds is limited (< 10 nm in general).

Large mesoporous materials with pore sizes between 10-50 nm are somehow challenging from the design and synthesis point of view. One of the main challenges concerns the limitation of organic templates to produce large mesopores. The interest in large mesopores relies on their use to allow the diffusion and immobilization of larger molecules, like enzymes, since these biomolecules can have a size of several nanometers. Their diffusion and immobilization in nanoporous films can therefore be restricted. For instance, the crystallographic structure from LOx revealed a 4-subunit macromolecule with unit cell sizes of 11.7 nm, 11.34 nm and 18.5 nm at 90° angle each⁷¹. For this reason, the synthesis of large-mesopores in porous materials is pertinent for enzyme immobilization. Alternatively to the templating method in the synthesis of thin films, the casting from powders can also produce mesopores and this procedure will be explained in more detail in the following chapter.

Macroporosity (pore diameter > 50 nm)

Finally, the presence of macropores in porous media can enhance the mass transport, particularly in biosensing. Different templating materials can be used to produce macropores: micelles from large-molecular weight amphiphilic block copolymers, organic fibers, emulsions, and polymer particles, among others. Additionally, the combination of organic templating materials for macropores with powders is an effective and versatile way to produce not only macropores, but hierarchically nanostructured films, as explored in the following chapters.

2.3 Mass Transport in Enzyme-based Biosensor Systems

The conservation equation for mass transport of molecules in solution, including a reaction term and neglecting convection^{84;125} is:

$$\frac{\partial c}{\partial t} = D\nabla^2 c + Q \quad (2.10)$$

where c is the molar concentration, D is the self diffusivity of the molecule in the solvent, Q is a reaction term that describes the production of molecules per unit volume by reaction, and $\nabla^2 c = \frac{\partial^2 c}{\partial x^2} + \frac{\partial^2 c}{\partial y^2} + \frac{\partial^2 c}{\partial z^2}$ (in rectangular coordinates). This species balance is a partial differential equation that can only be solved in a few special cases, but in general the concentration $c=f(x,y,z,t)$ as a function of time and space needs to be obtained by computational methods¹²⁶.

For situations where diffusion occurs in combination with a heterogenous reaction, i.e. the reaction takes place not in the fluid, but at the surface of a catalyst particle or film, the reaction term in Eq. 2.10 is not included in the diffusion equation. In this case, the reaction is instead given as a boundary condition at the surface. For the case of a liquid solution with a heterogeneous reaction, with $\partial c/\partial t = 0$ (steady state assumption), the diffusion equation is simplified to^{125;127}

$$\frac{d^2 c}{dy^2} = 0 \quad (2.11)$$

and the reaction rate is included as a boundary condition at the solid surface as

$$r = -k_n'' c^n \quad (2.12)$$

where k_n'' is the rate constant and n is the order of the reaction. Here, y is the direction orthogonal to the surface. $y = 0$ is taken as the limit of the film of liquid with thickness L where the reaction becomes important. Even with these simplifications, the solution is usually an implicit equation for the concentration¹²⁵. For the concentration at the catalytic surface, the following relation can be used¹²⁷

$$Da \left(\frac{c}{c_0} \right)^n = 1 - \frac{c}{c_0} \quad (2.13)$$

2.3. Mass Transport in Enzyme-based Biosensor Systems

where

$$Da = \frac{k_n'' c_0^{n-1} L}{D} \quad (2.14)$$

is the Damköhler number^{84;128}, which gives the ratio of the intrinsic rate of the reaction velocity ($k_n'' c_0^{n-1}$) to the rate of diffusion (D/L). A simplified special case of Eq. 2.13 is a first order surface reaction (reaction constant k'')^{127;128}: then at the catalytic surface, $Da = k''L/D$, and the surface concentration is $c/c_0 = (Da+1)^{-1}$.

For $Da \ll 1$, the time for mass transport is much shorter than the reaction time. In this case, the reaction is not limited by transport through the medium to the surface. This means that the reaction is kinetically limited (observed rate = intrinsic rate of the reaction). In contrast, for $Da \gg 1$, the time scale for mass transport through the medium to the catalyst takes is much longer than the reaction time. In that case, the overall rate that is observed is controlled by mass transfer (here: diffusion).

From the diffusivity and the concentration gradient, the diffusive flux to or from the catalytic surface can be calculated using Fick's first law:

$$J = -D \frac{dc}{dy} \quad (2.15)$$

For a spherical molecule in a Newtonian fluid, D is related to the viscosity η and the sphere radius R by the Stokes-Einstein relationship⁸⁴:

$$D = \frac{k_B T}{f} \quad (2.16)$$

where $f = 6\pi\eta R$ is the drag coefficient for a sphere, and $k_B = 1.3806488 \cdot 10^{-23}$ J/K is Boltzmann's constant. This expression will be used here for molecules in dilute solution. Related expressions for non-spherical species are given in Truskey et al.⁸⁴.

An important relation between the distance travelled by molecule in a certain time in space (3D) is given by

$$\langle x^2 \rangle = 6Dt \quad (2.17)$$

where $\langle x^2 \rangle$ is the mean square displacement (MSD, the square of the distance travelled averaged over all molecules), i.e. the slope of $\langle x^2 \rangle / 6$ vs. t gives the diffusivity⁸⁴.

For mass transport through pores and gel-like media, D needs to be replaced by an effective diffusivity D_{eff} . In both cases, the behavior is controlled by the ratio of the dimensions of the molecule and a characteristic length scale of the pore (i.e. the pore diameter) or the polymer

Chapter 2. Background

network (i. e. free path length in a polymer gel network). Both these cases will be relevant in the following chapters for the following situations:

1. *transport of the enzyme* to the silica surface of the porous film during immobilization; we assume that this transport occurs by diffusion, and we will assess how the enzyme-to-pore ratio influences the process
2. *transport of the substrate* (L-lactate) and (optionally) the cofactor to the enzyme during sensing experiments
3. *transport of the product* of the enzymatic reaction away from the enzyme

Note that the last step is very different for the two approaches of biosensing films presented in Chapters 5 and 6, respectively: in Chapter 5, the product formed (NAD⁺) diffuses away from the film to the bulk solution, where its concentration is detected optically. In contrast, in Chapter 6 the immediate product of the enzyme reaction is hydrogen peroxide, which is detected using co-immobilized cytochrome C inside the multilayer film.

In comparison to dilute solutions, the observed values of D are lowered in media with a structure, such as gels, pores, or tissues, and in suspensions or concentrated solutions. For diffusion through liquid-filled pores, Anderson and Quinn¹²⁹ and Paine and Scherr¹³⁰ gave numerical results for the drag coefficient $f = 6\pi\eta R \cdot \kappa$, from which an effective diffusivity can be calculated. $\kappa(r_m/r_{pore})$ is a factor that needs to be computed numerically. Figure 2.18 shows the numerical results for this factor κ . These values are based on the simplification that the molecule and particle is at the center of the pore, and that no additional flow occurs.

For diffusion through polymer networks or hydrogels, hydrodynamic interactions between the solute and the surrounding water (described by a factor F with values between 0 and 1) and the steric exclusion due to the polymer network (described by another factor S) play a role, resulting in a reduction of the diffusivity as compared to the free solution, $D_{\text{eff}} = D_0 \cdot F \cdot S$. A summary of diffusivities of the molecules used in this thesis, including proteins, substrates and reaction products, is given in Table 2.2.

Table 2.2 – Overview of diffusivities D and effective diffusivities D_{eff} of the different species used in this work in the relevant media at 25 °C. ^afrom Fu et al.¹³¹; ^bfrom Zare and Golabi¹³²; ^cfrom Ribeiro et al.¹³³; ^dfrom Truskey et al.⁸⁴; ^eestimated from the Stokes-Einstein relationship with the dimensions from Figure 2.3.

Molecule	Medium	Diffusivity (m ² /s)
H ₂ O ₂ ^a	water	D = 1.0 · 10 ⁻⁹
NADH ^b	water	D = 3.24 · 10 ⁻¹⁰
lactate ^c	water	D = 9.70 · 10 ⁻¹⁰
lactate	plasma	D _{eff} = 8.87 · 10 ⁻¹⁰
lactate	cartilage	D _{eff} = 8.93 · 10 ⁻¹¹
Lactate dehydrogenase ^d	water	D = 4.99 · 10 ⁻¹⁰
Lactate oxidase ^e	water	D = 4.4 · 10 ⁻¹⁰
Horseradish peroxidase ^e	water	D = 1.6 · 10 ⁻⁹
Cytochrome C ^e	water	D = 5.8 · 10 ⁻⁹

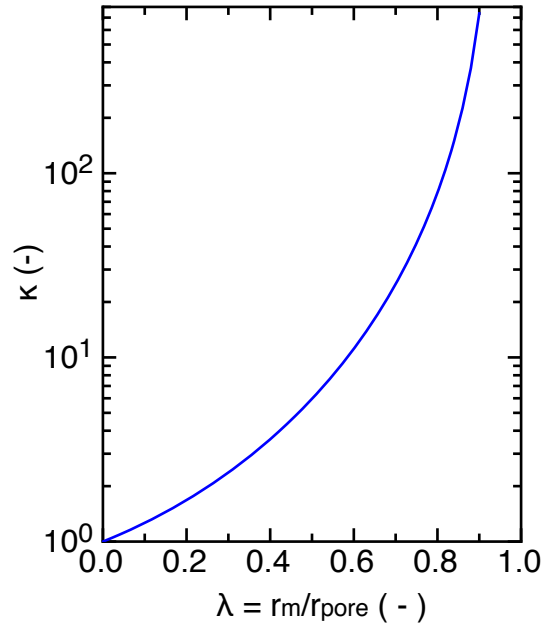


Figure 2.18 – Plot of the correction factor κ for diffusion through a liquid-filled pore from data by Paine and Scherr¹³⁰ as a function of the ratio of the molecule size to the pore size $\lambda = r_m/r_{pore}$. The effective diffusivity $D_{eff} = k_B T/f$ for a molecule with radius r_m in a pore with radius r_{pore} can then be obtained with the corrected friction factor $f = 6\pi\eta R \cdot \kappa$.

Most of the common formulations for mass conservation do not take into account the different time scale of diffusion as a function of porosity in porous media¹³⁴. In such systems, the restricted diffusion paths of species deviate from straight lines. Instead they follow trajectories which vary depending on the total porosity, pore size and degree of connectivity between pores in the material. A way to represent the role of these porosity effects in diffusion is to scale the diffusion coefficient with tortuosity¹³⁵. Tortuosity is the squared ratio of the shortest pathway between two points through connected pores to the straight-line between two points in a porous medium (Figure 2.19)¹³⁶. By definition, τ is always greater than or equal to unity.

$$\tau = \left(\frac{L_{eff}}{L} \right)^2 \quad (2.18)$$

Various theoretical and empirical relationships between porosity ϵ and τ are found in the literature obtained for different porous media^{137;138}. Typically used correlations include the ones proposed by Mackie and Meares¹³⁹, Wakao and Smith¹⁴⁰ and Suzuki and Smith¹⁴¹ in equations 2.19, 2.20 and 2.21, respectively:

$$\tau = \frac{(2 - \epsilon)^2}{\epsilon} \quad (2.19)$$

$$\tau = 1/\epsilon \quad (2.20)$$

$$\tau = \epsilon + 1.5(1 - \epsilon) \quad (2.21)$$

Although only empirical approximations, they all represent an increase in tortuosity with a decrease in the porosity¹⁴². The influence of tortuosity also depends on the time of observation and on the actual dimensions of the material: for very thin slices of material, or for short experimental times, the influence of tortuosity decreases (see Figure 2.19: if points A and B are very close, e.g. within the distance of a typical pore diameter, there are only direct paths between them) . This effect will also be pointed out in the thin film studies in Chapter 5.

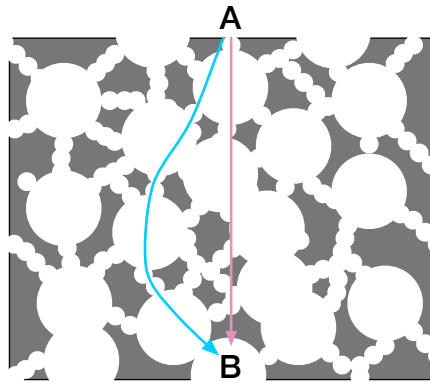


Figure 2.19 – Schematic representation of tortuosity⁸⁴. Red: direct path between A and B with length L , green: path through porous medium with length L_{eff} . The tortuosity is defined by the squared ratio $\tau=(L_{\text{eff}}/L)^2$.

3 Controlling Mesopore Size and Processability of Transparent Enzyme-Loaded Silica Films for Biosensing Applications

This chapter is dedicated to the design, synthesis and characterization of enzyme-loaded silica films using a bottom-up approach based on sol-gel chemistry with pore templates formed by block copolymer micelles. Silica-based nanoporous thin films including large mesopores are relevant as enzyme supports for applications in biosensing. The diffusion and immobilization of large biomolecules such as enzymes in such porous films require the presence of large mesopores. Creating such morphologies based on a bottom-up synthesis using colloidal templates is a challenge in view of the combination of desired material properties and the robustness of the casting process for the fabrication of thin films. Here a strategy to reproducibly synthesize transparent porous silica thin films with submicrometer thickness and homogeneously distributed porosity is presented. For this purpose, polystyrene-poly-2-vinylpyridine (PS-P2VP) amphiphilic block copolymers are used as porogenic templates. Low-chain alcohols are employed as both selective solvents for the P2VP blocks and reaction media for silica synthesis. Rheology measurements reveal a strong influence of the block copolymer length on the behavior of PS-P2VP micelles in suspension. The pore distribution and accessibility into the film are controlled by adjusting the silica to block copolymer weight ratio. The solvent choice is shown to control not only the micelle size and the generated pore morphology but also the structural homogeneity of the films. Finally, the suitability of the synthesized films as supports for enzymes is tested using a model enzyme, horseradish peroxidase EC 1.11.1.7. Our approach is innovative, robust, and reproducible and provides a convenient alternative to synthesize large mesopores up to small macropores (20–100 nm) in nanostructured thin films with applications in biosensing and functional coatings.^a

^aThis chapter was published as:

O. Pérez-Anguiano, B. Wenger, R. Pugin, H. Hofmann, E. Socolan, *ACS Applied Materials & Interfaces*, **2015**, *7*, 2960–2971. DOI: 10.1021/am508630c. All experimental work was performed entirely by the PhD candidate. Prof. Peter Fischer (ETH Zürich) is acknowledged for his help with preliminary experiments with rheology.

3.1 Introduction

Sol-gel derived thin films with controlled pore structures are materials which find applications as diverse as biosensing, drug delivery, catalysis, or solar cells¹⁴³⁻¹⁵⁰. Whereas their use and versatility for the mentioned applications has been shown, the control of homogeneity and pore size during their synthesis remains a challenge in particular for the upper end of the mesoporous size range (10-50nm). Larger pore sizes are desirable whenever these pores are aimed to host relatively large species such as proteins (e.g., enzymes) and to enable their diffusion through the porous medium. The large mesopore-size range is therefore of specific relevance to applications in the fields of biosensing, biomedical engineering¹⁵¹, or drug delivery¹⁵². Several methods have been explored to generate pores in sol-gel materials, from bubbling,¹⁵³ phase separation,¹⁵⁴⁻¹⁵⁶ emulsion templating,¹⁵⁷ and nanopowder deposition¹⁵⁸ to the embedding of sacrificial organic templates.^{159;160} Our goal here is the development of robust procedures to design and master adequate templating approaches to produce mesoporous films in the 20-100 nm size range.

Since the first report on the synthesis of ordered surfactant-templated mesoporous materials¹²⁴, numerous templating strategies to tailor the mesoporosity have been explored^{122;123;161;162}. Templating materials, e. g. molecular surfactants or block-copolymers (BCP), micro emulsions,¹⁶³ etc., self-organize onto large size 3D structures (e.g., micelles). Simultaneously, sol-gel chemistry is used to build a metal oxide framework around them. Using self-assembly principles to template nanostructured metal oxide materials is therefore a highly flexible and efficient strategy to design materials with an enormous variety of structural features.

Pluronic®-like block copolymers are based on polyethylene oxide (PEO, hydrophilic block) and polypropylene oxide (PPO, hydrophobic block) at different ratios and form stable micelles in solution. Therefore, they have been extensively used as directing agents for the design of porous materials; however, the range of pore sizes that can be obtained from them is rather limited to small mesopores, usually smaller than 12 nm.¹⁶⁴ This limitation is mainly due to the low HLB (hydrophilic-hydrophobic balance) between the PEO and PPO blocks and the limited size of the PPO block (70 units) in the available Pluronic®block copolymers.

Attempts to form larger pores have been explored. Organic compounds such as 1,3,5-trimethylbenzene (TMB) have been used to increase the micelle size of these polymers, acting as cosurfactants¹⁶⁵⁻¹⁶⁸. Recently it has been shown that this method can be optimized by careful selection of the swelling compound, based on its capability to be solubilized within the micelle, achieving a pore size up to 37 nm.¹⁵⁰ Nevertheless, the resulting materials suffer from the lack of homogeneity in porosity, the poor control over the pore shape, and the toxicity issues linked to the use of TMB.

Supercritical CO₂ has been also used as swelling agent of pluronic®-based micelles, avoiding the use of toxic organic compounds. However this synthesis is time-consuming (processing times of several days), is performed in stainless steel chambers at high pressure, and leads to bulk materials. This approach is therefore not adapted to the synthesis of porous films¹⁶⁹.

Hydrothermal/solvothermal synthesis is yet another commonly reported procedure based on the effect of high pressure and cosolvents to produce large mesopores from 10 to 30 nm^{159;170;171}; however, this approach is commonly only suitable to produce bulk materials

and the pore size reproducibility is poor^{172;173}.

Highly amphiphilic block copolymers have now emerged as versatile templating materials for the synthesis of mesoporous structures with controllable pore size, pore symmetry, and diverse chemical compositions. Hydrophilic segments such as PEO, P2VP or poly(4-vinylpyridine) (P4VP), and hydrophobic segments such as PS, polyisoprene (PI), polybutadiene (PB) and polyacrylonitrile (PAN) are examples of polymer blocks. Recently, Deng et al.¹⁶⁴ reviewed the synthesis of large mesoporous silica and metal oxides using highly amphiphilic block copolymers. According to the authors, chemical compositions, block sequences, molecular weights, and volume fractions of these templating materials can be designed, offering the possibility to be used as templates for the creation of novel mesoporous materials. Moreover, these copolymers can assemble into micelles of larger size compared to the pluronic types and thus are suitable to direct the organization of presynthesized nanocrystals without destruction of the mesostructures. The monitoring of these parameters leads to the synthesis of larger and more stable pores in the range of 10–50 nm with thicker pore walls. Nevertheless, controlling the morphologies in the large mesopore size range remains challenging, mostly because block copolymers with large molecular weights and high dispersibility are needed. Furthermore, methods enabling micelle formation along with the syntheses of metal oxide frameworks are also essential, in particular for the preparation of mesoporous coatings.

Reports about the utilization of highly amphiphilic block copolymers as templates in the synthesis of porous films mostly rely on evaporation induced self-assembly (EISA), a common strategy for the nanostructuring of films^{174;175}. In EISA, concentrations of block copolymers below their critical micelle concentration (CMC) are used. As the solvent evaporates, the template concentration increases, forming micelles.

Templating micelles self-organize with metal oxide precursors into highly ordered and interconnected structures. However, at diluted concentration of polymers, the thickness of the films obtained by this method is limited. Therefore, we propose an innovative approach to produce mesoporous films based on PS-P2VP block copolymer already organized into spherical micelles in a solvent suitable with the sol–gel synthesis of silica oligomers. Thus, the formation of stable and miscible sols of silica precursors and PS-P2VP micelles is the challenge to address.

In this work, we use PS-P2VP block copolymers as templating materials for the synthesis of nanoporous silica films with large mesopores up to small macropores (20–100 nm). More specifically, we established the relationship between the raw material features, the process parameters, and the resulting pore morphology after casting. The raw materials characteristics include BCP block lengths and ratios, solvent, and silica sol precursors. The process parameters comprise the one/two-pot method, the formulation content (e.g., silica to BCP ratio), the spinning speed, and the annealing procedure. In a first attempt to synthesize mesoporous films using PS-P2VP micelles as templates, a one-pot procedure was carried out, mixing molecular silica precursors and micelles at once: silica particles were obtained due to the basicity of the P2VP blocks. Consequently, the conditions to obtain highly homogeneous porosity in submicrometer-thick films with accessible and interconnected pores in a two-step procedure are described. Finally, the assessment of these films as enzyme supports was evaluated following the activity of immobilized HRP in different film structures, proving

Chapter 3. Mesopore Size and Processability of Transparent Enzyme-Loaded Silica Films

the suitability of the as-synthesized films in applications such as enzyme-based biosensing.

3.2 Experimental section: materials and methods

3.2.1 Materials

PS-P2VP block copolymers were purchased from Polymer Source Inc. (Canada). Any other chemical used in this work was obtained from Sigma Aldrich and used as received.

3.2.2 Micellar suspensions

4 mL glass vials covered with screw caps and PTFE seals were used. PS-P2VP with different molecular weights were weighed and dissolved in ethanol or 1-butanol at a concentration of 50 mg/mL. Heating at 70°C (ethanol) or 95°C (1-butanol) was necessary to get homogeneous dispersions. For the largest BCP, sonication was needed to induce micellization. The suspensions became translucent when micelles were formed. The micellar suspensions were stable for months.

3.2.3 Sol-gel formulation and film deposition

Silica was synthesized under acidic catalysis. In a standard procedure, given amounts of TEOS, water and hydrochloric acid (HCl) 1M were added to the solvent (ethanol or 1-butanol) at a molar ratio of 1:4:0.02:42, respectively, and stirred at room temperature (20°C) for 2 h. Micelle suspensions and silica sol aliquots from the previous sol were mixed under magnetic stirring to obtain different suspensions with specific weight ratios of silica-PS-P2VP. The silica-micelle suspension was then spin coated onto borosilicate glass slides (previously cleaned and activated by O₂ plasma treatment) at different speeds for 60 s. Then the samples were heat treated in an air furnace at 550°C for 20 min.

3.2.4 Micelle size measurements

Atomic Force Microscopy (AFM, Dimension Icon with ScanAsyst, Bruker): Micellar suspensions of 1-2 mg/mL were prepared from 50 mg/mL suspensions and spin coated onto glass slides. Measurements were performed on these films (tapping mode).

Dynamic Light Scattering (DLS): Dilutions from 50 mg/mL micellar suspensions are prepared and measured by DLS (Zeta PALs, Brookhaven Instruments).

Transmission Electron Microscopy (TEM, Philips/FEI CM12): A drop of 2 mg/mL micellar suspension was poured onto copper grids and dried in a laboratory hood. Once dried, the grids were placed in a closed vial containing iodine for 30 minutes at 40°C.

3.2.5 Rheology

Steady and oscillatory shear rheology was performed using a Physica MCR rheometer (Anton Paar, Germany) with a cone/plate geometry. The fixture was completely enclosed during the measurements, and the solvent trap was filled with the appropriate solvent.

3.2.6 Nanostructure characterization

Silica porous films were observed by Scanning Electron Microscopy, SEM (XL30 ESEM-FEG, Philips). Thickness values were obtained from cross-section images.

3.2.7 Post-functionalization

Silica porous films were placed into a desiccator and in an oven for 2h at 120°C. 100 μ L (3-Aminopropyl)triethoxysilane (APTES) was poured in a bottom half of a glass Petri dish equally dried for 2h. Vacuum was applied until the silane was fully evaporated. After 2 hours, the films were taken from the desiccator and placed in an oven at 120°C for 10 minutes. No further rinsing was performed.

3.2.8 Estimation of available amino groups

The characterization of post-functionalized films with APTES was performed by a method proposed by Coussot et al.¹⁷⁶. Briefly, the functionalized films were immersed in a staining solution containing excess of Commassie brilliant blue G (CBB) at acidic pH. After immersion, the films were rinsed with the same solution without dye to remove the excess of non-adsorbed dye. The amine functions are recycled by desorbing the dye with an alkaline buffer. The amount of dye desorbed is quantified colorimetrically; the concentration is obtained using a calibration curve for CBB by comparing the absorbance intensity at λ_{max} of 611 nm.

3.2.9 Enzyme immobilization and enzymatic activity

Films post-functionalized with APTES were dipped in a solution of glutaraldehyde (Sigma-Aldrich) at 5% (v/v) in a phosphate buffer 0.01M at pH 7 for 10 minutes. Then, they were thoroughly rinsed with deionized water. Glutaraldehyde-modified films were then dipped for 2h in a horseradish peroxidase EC 1.1.11.7 solution (Sigma-Aldrich) at 10 μ g/mL prepared in deionized water. The enzyme-functionalized films are rinsed thoroughly with phosphate buffered saline Tween (PBST, Sigma-Aldrich), phosphate buffered saline (PBS, Sigma-Aldrich), and deionized water and finally dried with compressed air. Enzymatic activity tests are based on the ability of HRP to oxidize 3,3',5,5'-tetramethylbenzidine (TMB) in the presence of hydrogen peroxide. HRP-loaded films were placed in a 24-multiwell plate and a given volume of TMB solution (Sigma-Aldrich) was poured into each well containing a film and let to react in darkness for 30 minutes. Absorbance in the wells was then directly measured at 650 nm using a microplate reader (TECAN@infinite M200). Subsequently, the films were removed and sulfuric acid 0.5 M was then added to each well; absorbance is measured at 450 nm after 2 min. A calibration curve is built for known amounts of HRP in solution with TMB, just as

Chapter 3. Mesopore Size and Processability of Transparent Enzyme-Loaded Silica Films

described for the enzymatic test. The HRP concentrations calculated for the films using this curve correspond to apparent concentrations of HRP in solution.

3.3 Results and discussion

3.3.1 Synthesis of silica sol

The silica sol synthesized under acidic conditions following the molar ratios reported in the experimental section was transparent. Besides, the sol showed good stability after several months of preparation: the solution remained transparent with no evidence of precipitation and gelation. Additionally, the synthesized films using this sol showed the same characteristics independently of the time of preparation. Nevertheless, for comparative studies, the sol was always used 2 h after adding the catalyst (hydrochloric acid).

3.3.2 Formation and characterization of block-copolymer micelles as pore templates

To define the pore structures in the final inorganic films, careful control of the initial porogenic templates was necessary. The aim at this stage was to obtain a stable dispersion of homogeneous spherical micelles of PS-P2VP in a solvent compatible with the silica sol.

Whereas the use of selective solvents for the PS block are widely found in the literature¹⁷⁷⁻¹⁷⁹, no reports could be found regarding the formation of micelles in selective solvents (aliphatic alcohols) for the P2VP block. This is the first report where a study of micelle formation and characterization is made using selective solvents for the P2VP block. Therefore, we first investigated the relationship between the molecular weight of different BCP, the solvent parameters, and the resulting micelles, focusing on the formation of uniform, spherical micelles suitable to synthesize pores of 20-100 nm in diameter. The molecular weights of the PS-P2VP block copolymers studied are summarized in Table 3.1.

Table 3.1 – Overview of the PS–P2VP block copolymers used to form micellar pore templates

Sample	PS block size, kg/mol	P2VP block size, kg/mol	P2VP/PS
1	13,5	24	1.77
2	25.5	23.5	0.92
3	28	36	1.28
4	102	97	0.95
5	190	190	1.00

PS-P2VP solubility in ethanol and 1-butanol

According to the available information, PS-P2VP micelles can be prepared in methyl ethyl ketone¹⁸⁰, toluene¹⁷⁷, dimethylformamide¹⁸¹, tetrahydrofuran¹⁸², chloroform, methanol and ethanol, the last two depending on the polymer composition. No information was found

regarding the solubilization of PS-P2VP in 1-butanol. From the few options of short-chain aliphatic alcohols used to prepare PS-P2VP micelles, ethanol and 1-butanol were chosen, mainly because they are adequate with the synthesis of silica¹⁸³ and less toxic compared to methanol. P2VP is dispersible in low-aliphatic chain alcohols and other polar solvents except water, increasing solubility from shorter to longer aliphatic chain (Table 3.2). However, polystyrene is not soluble in any of these solvents, hence ethanol and 1-butanol are selective solvents for the P2VP block. In previous reports dealing with the nanostructuring of materials using PS-P2VP, the followed strategy consisted in either the selection of selective solvents for the PS block^{177;178} or the use of good solvents for both blocks, relying on EISA.¹⁸¹ The explanation about the different solubility behavior and the resulting micelle size of PS-P2VP in ethanol and 1-butanol can be explained theoretically from the available data of Flory-Huggins interaction parameters for these systems.

Table 3.2 – Solubility data for P2VP at 25°C ($M_w = 300.8$ kg/mol and $M_w/M_n = 2.32$)¹⁸⁴

Solvent	Intrinsic viscosity [η]	Flory-Huggins parameter χ
1-heptanol	1.22	0.400
1-butanol	1.15	0.445
Ethanol	1.03	0.473

In this work, PS-P2VP of low molecular weights were readily solubilized at room temperature in ethanol, forming micelles by magnetic stirring; however, the dispersion and micellization in butanol does not take place as rapidly. Interestingly, at higher temperature (i.e. 95°C), 1-butanol promotes a faster solubilization of the block copolymer compared to ethanol. This behavior can be quantify with the Flory-Huggins interaction parameter χ . This parameter measures the interaction in thermal energy units of the polymer chains and the solvent molecules. The critical value of χ for the miscibility of a polymer in a solvent is 0.5 (theta temperature). For values of χ greater than 0.5, the polymer will not be soluble in the solvent¹⁸⁵. The χ values for P2VP reported by Arichi et al.^{184;186;187} (Table 3.2) fully support the observations made here; both ethanol and 1-butanol showed values lower than 0.5. The value for 1-butanol (0.445) is slightly smaller as compared to ethanol (0.473); in other words, 1-butanol is a better solvent for P2VP than ethanol at room temperature. However, this does not coincide with our observations with ethanol. This result may be explained by the Flory-Huggins parameters of the PS blocks. Flory-Huggins parameter values¹⁸⁸ χ in aliphatic alcohols decrease with increasing temperatures (see Table 3.3) and with the number of carbons from methanol to hexanol. Therefore, even if polystyrene will not be miscible in 1-butanol at high temperature, smaller PS-P2VP micelle sizes under the experimental conditions used in this work could be expected when 1-butanol is used as a solvent (lower aggregation number) as compared to ethanol.

P2VP is a weak base and the solubility of P2VP is therefore due to the formation of hydrogen bonding¹⁹⁰. Arichi et al.^{184;186;187;191} observed higher than expected values for the intrinsic viscosity of P2VP in different aliphatic alcohols, which is due to hydrogen bonding between pyridine and alcohol moieties. Larger molecular weight PS-P2VP block copolymers would dissolve faster in 1-butanol at high temperature, where the contribution of the solvent quality of 1-butanol for polystyrene could play a role over the instable hydrogen bonding at higher

Chapter 3. Mesopore Size and Processability of Transparent Enzyme-Loaded Silica Films

Table 3.3 – Flory–Huggins parameters of ethanol and 1-butanol with respect to polystyrene; average molecular weight 129.7 kg/mol^{188;189}

Solvent	Flory-Huggins parameter, χ
Ethanol	1.75, 75°C
1-Butanol	1.20, 95°C 1.44 ,75°C

temperatures¹⁹⁰.

From this first theoretical description about solubility of PS-P2VP in aliphatic alcohols and the first qualitative dissolution tests performed over the different PS-P2VP block copolymers listed in Table 3.1, a clear difference in solubility and viscosities were observed, particularly depending on the P2VP/PS length ratio. First, block copolymers with larger PS blocks than the P2VP counterparts were soluble in neither ethanol nor 1-butanol. Second, suspensions of block copolymers with larger P2VP blocks than the PS counterparts were qualitatively more viscous than those with symmetrical blocks. From these observations, and as a first step in the characterization of this behavior from micelle suspensions with different block compositions, a rheological study of these systems is proposed.

Rheology of PS-P2VP micelle suspensions

As a first investigation towards the preparation of stable silica-micelle suspensions, the rheological properties of the micelle suspensions were studied. These mixed dispersions are then intended to be deposited by spin coating. By spin coating a PS-P2VP dispersion on a flat substrate, a free surface flow is created, where the sample is only in contact with one solid surface formed by the rotating support. Because the upper surface is free, the overall shear rate within the sample is expected to be small^{192;193}. In contrast, the rheometry experiments are always performed with the samples confined between *two* solid surfaces. Therefore, the more useful parameter to understand the behavior of the sample is not the shear *rate*, but the shear *stress*: it directly influences the force balance of the fluid film, which is determined by an interplay of centrifugal forces created by the spinning disk and the shear stress.

Figure 3.1 presents the viscosity of samples 1, 2, and 3 as a function of the shear stress. The viscosity of the micelles suspension for asymmetric block copolymers (P2VP/PS >1) was considerably higher compared to other suspensions from almost symmetric block copolymers (P2VP/PS \approx 1), as shown in the rheology measurements (Figures 3.1 and 3.2). The viscosity of sample 2 effectively does not depend on shear stress (or shear rate). The dispersion viscosity is slightly higher as compared to the pure solvent (4 vs 1 mPa·s), but the Newtonian behaviour of sample 2 is retained throughout the entire range of shear stresses and rates. However, samples 1 with P2VP/PS of 1.77 shows a shear-thinning behaviour with a very high viscosity at low shear rates.

The solvation of P2VP chains in sample 1 not only increases the viscosity of the micelles suspension, but also causes formation of a gel-type material with a yield stress and viscoplastic

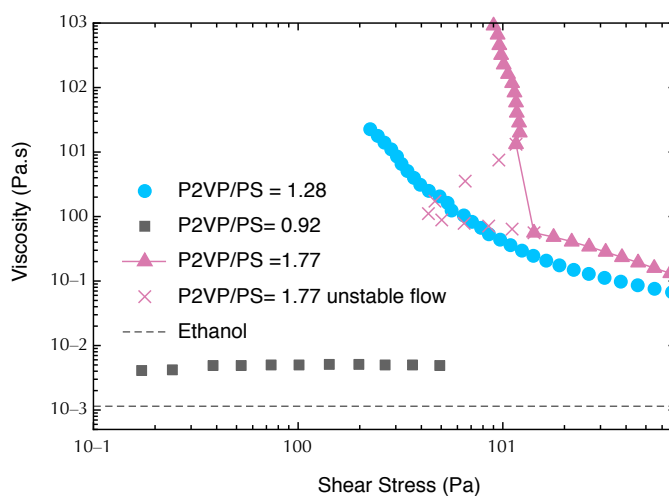


Figure 3.1 – Flow curves of PS-P2VP micellar suspensions in ethanol. Newtonian behavior is observed for symmetrical PS-P2VP (sample 2, squares) block copolymer whereas asymmetrical blocks (sample 1, triangles; sample 3, circles) show a shear thinning behavior. Unstable flow is shown for highly asymmetrical block copolymer around 10 Pa.

flow behavior (Figure 2). In this figure, the predominantly viscous behavior of sample P2VP/PS = 0.92 is observed, whereas sample P2VP/PS = 1.77 shows a typical gel-like behavior at low strain amplitudes, where the elastic modulus dominates. The linear viscoelastic behavior is limited to small deformations (<1%), with a cross over of the moduli at a deformation around 7%. Above this point the viscous modulus dominates, indicating the transition from a gel-like to a viscous liquid. This drop in the elastic modulus is observed more clearly when plotting the storage (elastic) modulus vs. shear stress (inset graph, figure 2), confirming the point where the gel yields at a stress value around 10 Pa. The critical level of the stress is virtually identical to the value found in the steady flow curve at the point where the viscosity increases dramatically.

In conclusion, the non-Newtonian rheological behavior of the asymmetric block copolymers with larger P2VP blocks will strongly affect the film casting: even at the highest rotation rate of 6000 rpm (corresponding to an angular velocity of 628.3 rad/s), the block copolymer mixture does not flow during spin coating (test performed, data not shown). This undesirable flow behavior is represented by the onset of viscoplasticity in the rheology data as the asymmetry of the block copolymer increases. In controlled shear rate experiments, where the sample is forced to flow, unstable, non-monotonic flow behavior is observed^{194;195} (Figure 3.1); in stress-controlled experiments, the sample simply does not flow below a stress of around 10 Pa in the example shown in Figure 3.2. Therefore, the individual blocks are chosen with identical molecular weights ($P2VP/PS = 1.0 \pm 0.1$) and according to their ability to form micelles with a size range close to the targeted pore size.

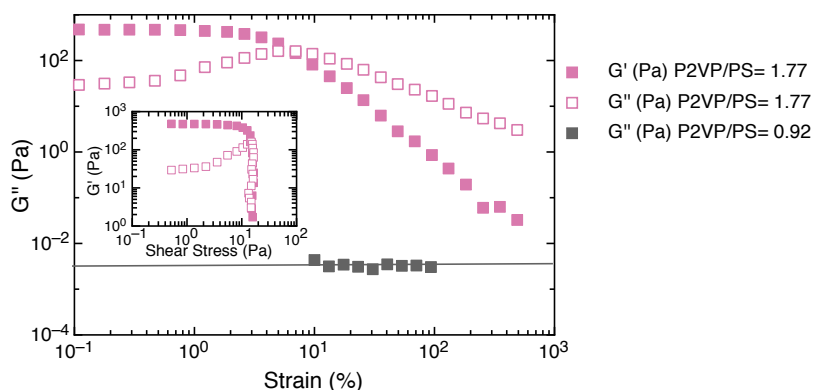


Figure 3.2 – Limiting cases of rheological behavior of the block copolymer templates: Amplitude sweep of samples PS/P2VP= 0.92 (red) and PS/P2VP= 1.77 (green) in ethanol. Sample PS/P2VP= 1.77 behaves as a gel at small strain amplitudes. Sample PS/P2VP= 0.92 shows purely viscous and linear flow behavior. Inset graph: moduli plotted vs. shear stress, indicating the linear viscoelastic regime up to stresses around 1 Pa and a dramatic drop in the elastic modulus around 10 Pa, suggesting gel yielding.

Micelle size and morphology

To assess the effect of solvent on the micelle sizes, size measurements were performed by DLS on the native micelle dispersions. Additionally, dilutions from these dispersions were deposited onto copper grids and silicon wafers, and TEM and AFM size measurements, respectively, were performed on the deposited micelles after solvent evaporation. The choice of selective solvent for the P2VP block strongly influenced the micelle size and shape, as shown in Table 3.4 and Figure 3.3. Independently of the measurement technique, the micelles of PS-P2VP prepared in ethanol are larger than those prepared in 1-butanol. Additionally, the micelle sizes obtained from DLS measurements showed higher values than those obtained from the other two techniques: the DLS values correspond to the size of solvated micelles in suspension. The values obtained from TEM and AFM reflect the size of the micelles in a dried state.

Table 3.4 – Summary of size measurements for PS-P2VP block copolymer micelles in ethanol and 1-butanol by different techniques.

Sample	DLS (nm)		TEM (nm)		AFM (nm)	
	Ethanol	Butanol	Ethanol	Butanol	Ethanol	Butanol
2	81±1	46±1	36 ±4	26±2	40±6	20±3
4	183±2	142±2	79±10	63±5	99 ±14	86 ±9
5	304±4	187±4	136±20	88±11	120±13	87±12

The micelle size is determined by the solvent capacity for each block, as explained by Antonietti et al.¹⁹⁶. They found that the micelle size of PS-P4VP BCP in selective solvents for polystyrene decreased with increasing solvent capacity for P4VP, the insoluble core. Consistent with these observations, the same tendency is observed for PS-P2VP micelles in selective

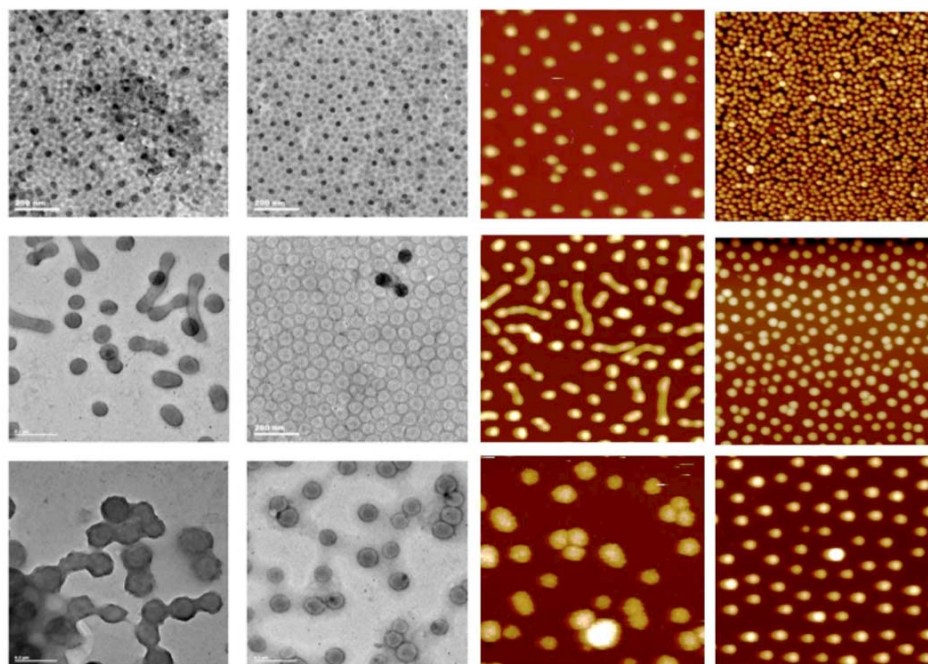


Figure 3.3 – TEM and AFM images of micelles of samples 2, 4 and 5 in descending order prepared in: ethanol (left side of each set of images) and 1-butanol (right side). Image size of AFM is $2 \times 2 \mu\text{m}$.

solvents for P2VP, where micelles sizes are smaller in 1-butanol, which is a better solvent for PS. Lower PS-P2VP micelle sizes are therefore expected when 1-butanol is used as a solvent (lower aggregation number) as compared to ethanol.

In addition, the size of the micelles also increased with the length of the nonsoluble block (PS) as observed in Table 3.4 and Figure 3.3. Moreover, rod-like morphologies were observed in both AFM and TEM images for ethanolic micelle suspensions. In contrast, micelles of PS-P2VP prepared in 1-butanol are spherical and highly monodispersed in size.

In Figure 3.4, the relationship between the micelle diameter obtained by TEM and the micelle core given by the PS block molecular weight of symmetrical block copolymer is presented. In this graph, an almost linear relationship is observed between PS block length and micelle sizes for suspensions prepared in ethanol. However, micelles prepared in 1-butanol showed smaller sizes for PS-P2VP of 190 kg/mol. This result is due to the processing temperature difference to produce micelles in ethanol (75°C) or 1-butanol (95°C) for sample 5. As shown in Table 3.3, the Flory-Huggins parameter of 1-butanol for PS at 95°C is smaller than ethanol at 75°C , indicating a better solvent capability of 1-butanol at the experimental conditions followed in this study. A better solvent for the core block results in smaller micelle sizes¹⁹⁶.

Considering the micelle size and shape of PS-P2VP micelles dissolved in ethanol or 1-butanol, a direct consequence in terms of pore sizes and morphologies can be expected after mixing these suspensions with a silica sol. Either option seems suitable to synthesize porous silica

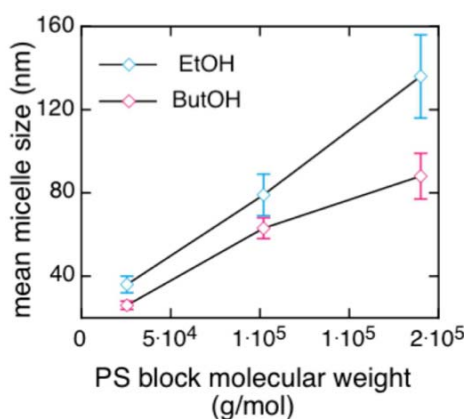


Figure 3.4 – Micelle mean diameter (measured by TEM) as a function of the PS block molecular weight in ethanol and 1-butanol.

films within the aimed range of pore sizes (20-100 nm); however, dispersions of PS-P2VP micelles in 1-butanol are more homogeneous in shape than those prepared in ethanol. For this reason, in the following sections, only results concerning silica films synthesized from micelles prepared in 1-butanol are discussed. However, silica films were synthesized from ethanolic formulations (data not shown) and a qualitative comparison is made in the following sections to emphasize the choice of 1-butanol over ethanol for film synthesis.

3.3.3 Formulation of silica-PS-P2VP mixtures

A one-pot procedure to synthesize porous silica films was first attempted, resulting in the synthesis of silica particles. A possible explanation for these results lies in the participation of pyridine groups present at outer surface of PS-P2VP micelles in hydrolysis/condensation reactions with silica species. Previous work by Yamauchi et al.¹⁹⁷⁻²⁰¹ demonstrated the interaction of inorganic species from silica and titania with the P2VP block from micelles formed by triblock copolymers PS-P2VP-PEO. In their studies, fully protonated micelles reduced their size measured by DLS after addition of metal alkoxides under acidic catalysis. The reduction in size was associated with the neutralization of fully protonated pyridine groups from the P2VP block, leading to reduced electrostatic repulsion between them. In addition, the formation of a silica wall around P2VP was further characterized by zeta potential measurements, before and after addition of TEOS, revealing a significant decrease from 35 to 5 mV.¹⁹⁸ Taking into account our own findings and the reported observations from similar systems, in this work a two-step procedure was proposed, preparing in parallel a silica sol and a micelle suspension and mixing them before casting to avoid silica particle formation. In this process, the micelles are considered stable during the pore formation. In a strict sense, there is an equilibrium in the self-assembly process between the micelle and the surrounding medium; however and according to Nagaran²⁰², the micelles are "frozen" in a kinetic sense if one block of the copolymer has a high enough transition temperature or large enough hydrophobicity, so as to cause a large activation energy barrier for molecular exchange. This is the case of PS, which is hydrophobic and after micelle preparation becomes glassy, thus rendering the micelle frozen.

Effect of silica to polymer ratio

The silica moieties in the sol form the solid framework and pore walls in the final films. Therefore, the ratio between the porogenic species (PS-P2VP blocks) and the silica precursors is expected to influence the porous structure of the resulting films. Ratios of silica to PS-P2VP in weight were varied from 0.33 to 1.33 (Figure 3.5). The impact of this ratio on the porous structure was assessed by SEM. At low silica content (ratio 0.33), open pores can be observed; nevertheless, their structures are not well defined and the silica framework is fractured. Images from ratios of 0.66 to 0.83 show a well-defined nanostructure: open porosity from the surface and no fractures. Due to the lack of silica, micelles have probably merged due to very thin silica walls, leading to the formation of larger pores. Images of films prepared with radii from 0.66 to 0.83 show a well-defined nanostructure: open porosity from the surface and no fracture of the silica framework. The pore wall increases when increasing the silica content. Finally, at a ratio of 1.33, the silica content is too large, so that only a few pores are open from the surface and most of the pores are probably closed.

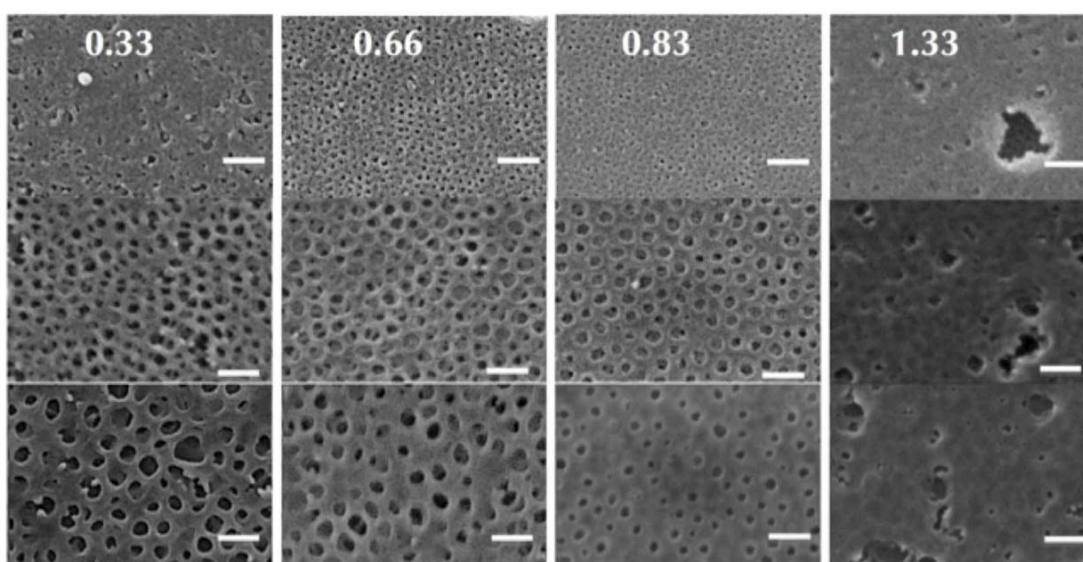


Figure 3.5 – Silica thin film nanostructures obtained from PS-P2VP micelle templating. From top set to bottom: samples 2, 4 & 5. Numbers at the top of each column indicate the silica to polymer mass ratio. Scale bar: 200 nm.

The image analysis from top view SEM pictures reveals large mesopores and small macropores, ranging from 20 to 90 nm in diameter for samples 2,4 and 5 (Figure 3.6). This result confirms the choice of block copolymer sizes and the selection of 1-butanol as solvent. Moreover, the pore size distribution is relatively narrow, as the initial micelle size dispersion. The size distribution becomes wider with the molecular weight of the block copolymer (Figure 3.6). A deviation from linearity in pore size diameter can be observed in Figure 3.7 where the micelle size diameters by TEM are compared to the pore sizes observed by SEM. For bigger block copolymer micelles, the variation in size for micelles and resulting pores is bigger compared to smaller block copolymers. Considering spherical micelles and assuming equal volumes for the core and the corona, the following relation is obtained (Figure 3.8): $V_s = V - V_c = V_c$ and then $V = 2V_c$, where V_s is the volume of the shell (P2VP), V is the total volume of the micelle, and V_c

Chapter 3. Mesopore Size and Processability of Transparent Enzyme-Loaded Silica Films

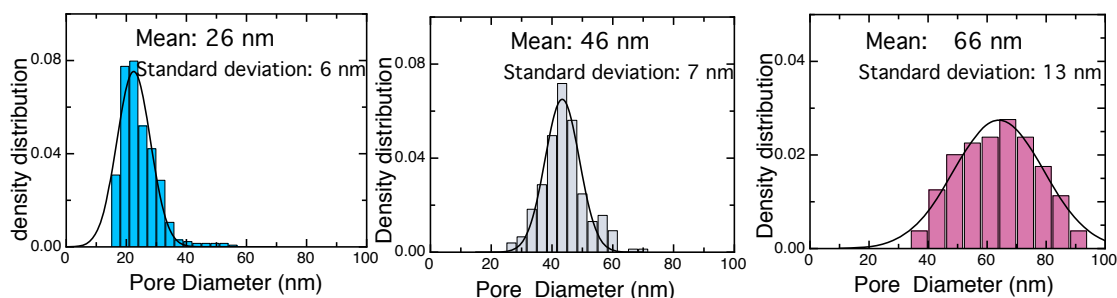


Figure 3.6 – Pore diameter distribution of nanoporous films from image analysis for sample 2 (blue), 4 (red) and 5 (green) at a silica/BCP ratio of 0.66.

is the volume of the PS core. Defining x as the ratio between the diameters of the full micelle (core and corona) and the core, and considering the volume of a sphere: $x = R/r = \sqrt[3]{2} \approx 1.26$

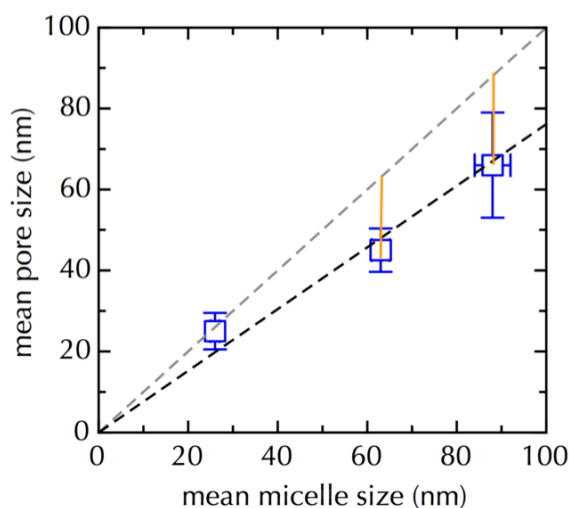


Figure 3.7 – Mean pore diameter as a function of the original micelle size for butanol-based systems measured by TEM. The upper dashed line (slope 1) indicates the ideal case of identical sizes of templating micelles and resulting pores. The lower dashed line (slope 0.76) is a linear fit of the data forced through the origin, fitting the data well above 40 nm but slightly underpredicting the pore size obtained from small micelles. Red segments represent the deviation to the equality dashed line.

This value is close to the values of the ratio between the micelle size and the pore size calculated from Fig. 3.7 namely, 1.36 and 1.33 for samples 4 and 5, respectively. This result confirms that the pore size is mainly defined by the PS core size of the micelles.¹⁹⁶ Indeed, the silica precursors infiltrate the P2VP shell. The additional contribution to this size difference may be attributed to the pore shrinking during the annealing step. For smaller micelles (sample 2), the difference between the micelle size by TEM and the resulting pore size is not as clear as with the larger block copolymers. This might be attributed to a more condensed P2VP shell, which becomes denser as the micelle decreases in diameter. Finally, the expected reduction from linearity in the films depending on the micelle is shown in Fig. 3.7. This prediction can

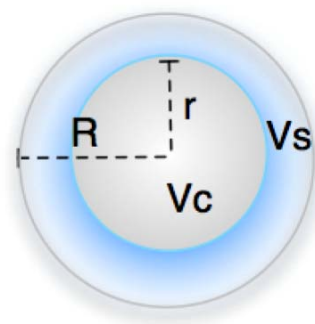


Figure 3.8 – Schematization of a PS-P2VP micelle. R and r correspond to the ratios of the whole micelle and the PS core respectively, whereas V_c and V_s are the volumes of the PS core and the corona respectively.

be useful to estimate the final pore size depending on the original micelle size.

3.3.4 Effect of solvent evaporation during spin coating

Films obtained from butanolic formulations yielded homogeneously distributed porous films with less thickness variation (striations) along the film compared to ethanolic suspensions (see supporting information in the Appendix). According to Birnie²⁰³ there are certain strategies that could be applied to reduce striations in complex mixtures (i.e., sol-gel formulations), where water is a key component for hydrolysis-condensation reactions. From his comprehensive study^{203–207}, he describes the evaporation process of a sol-gel mixture as a combination of two processes, one concerning the change of concentration of solvents at the surface and another as a cooling effect affecting the surface tension. Surface tension gradients produce a fluid flow from high to low surface tension areas, which progresses causing the thickness variations along the film (striations). As a part of the described strategy, the solvent mixture should contain a solvent with lower vapor pressure and lower surface tension compared to water. Ethanol is not the best choice following this strategy, since it has a higher vapor pressure than water (see supporting information in the Appendix). In contrast, 1-butanol does not show this result due to the effect of a low vapor pressure as main solvent during spin coating.

Moreover, the 1-butanol resulting films are highly transparent, i.e., defect free (high homogeneity in thickness and in pore size distribution). By fixing the spinning speed of the spin coater in the 1000–6000 rpm range, the film thickness can be adjusted in the 20–600 nm range. This range is higher than the reported values, usually lower than 100 nm.^{202;208} In conclusion, butanolic sol-gel-derived films were reproducibly produced with very homogeneous porosity and thickness.

3.3.5 Film post-functionalization

To assess the suitability of the silica films to be used as supports for enzyme immobilization, the as-synthesized films were successively postfunctionalized with an aminosilane and

Chapter 3. Mesopore Size and Processability of Transparent Enzyme-Loaded Silica Films

glutaraldehyde. The results presented in the previous sections serve as a guide to select the appropriate block copolymer templates and coating conditions suitable for HRP immobilization. The polymer described as sample 2 (Table 3.1) is used as a model for the following sections at a silica to polymer ratio of 0.66. This configuration exhibits the smallest pore size and yet the highest surface area. Additionally, the pores from these films are still large enough to allow the enzyme to diffuse. Different films with three different thicknesses are synthesized by adjusting the deposition parameters. A summary of the films used and their characterization after functionalization is shown in Table 3.5.

Table 3.5 – Description of samples used for enzyme immobilization

Sample	Thickness (nm)	Coomassie brilliant blue G concentration (mol/L)	HRP concentration ($\mu\text{g/mL}$)
Reference (flat)	–	$2.76 \cdot 10^{-6}$	0.06
A	333	$9.02 \cdot 10^{-6}$	0.84
B	434	$1.37 \cdot 10^{-5}$	1.21
C	562	$2.46 \cdot 10^{-5}$	2.09

Amino-functionalization of silica films

Aminosilane-functionalized porous silica is widely used in bioconjugation techniques for the covalent immobilization of enzymes. In this case, APTES in the vapor phase is used to post-modify the bare silica films with amino functionalities as it has been reported²⁰⁹. This post-functionalization step is evaluated colorimetrically using CBB (see Experimental Section). This dye binds electrostatically and quantitatively to available protonated primary amino groups in the same way as it is used to quantify proteins¹⁷⁶. At the acidic pH of the staining solution, the dye is negatively charged while the amino groups are positively charged. This method is simple, reproducible and non-destructive, allowing the reusability of the films for further enzyme coupling experiments. The spectrum of the dye in the staining solution showed a $\lambda_{\text{max}} = 611 \text{ nm}$. From the calibration curve at this wavelength, a value of extinction coefficient of $42'617 \text{ L mol}^{-1} \text{ cm}^{-1} \text{ nm}$ is found, which is not far from the value of $43'000 \text{ L mol}^{-1} \text{ cm}^{-1}$ reported at 620 nm ²¹⁰. An increase in CBB adsorption is observed by increasing the film thickness. This increase clearly indicates that the higher the thickness, the higher the grafted aminosilane amount on the porous surface. This result confirms that the porosity generated by the PS-P2VP is open and interconnected. A film with a half-micrometer thickness shows 9 times higher dye adsorbed compared to an aminosilane treated flat glass surface used as a reference (Figure 3.9).

3.3.6 Enzyme immobilization and enzymatic test

The suitability of the amino-functionalized films to be used as enzyme supports is tested using HRP, a model enzyme. Glutaraldehyde is used as a linker between available amino groups from both the enzyme and the porous silica films previously amino-functionalized⁷⁹.

This method of immobilization is unspecific, single or multipoint attachment could occur, and loss of enzymatic activity after immobilization is a common and well-known phenomenon.⁹¹

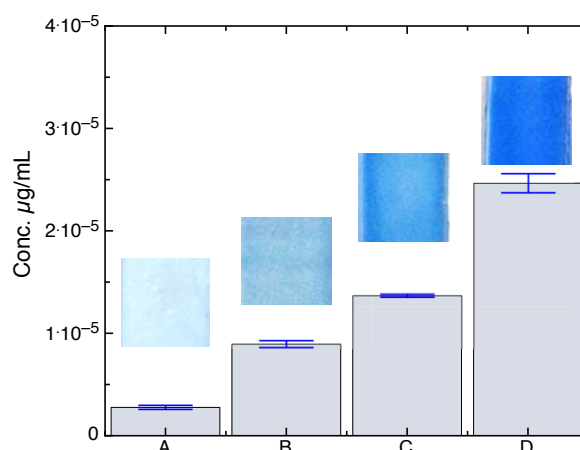


Figure 3.9 – Estimation of available amino groups: Quantification of Coomassie brilliant blue G from amino-functionalized silica films (A-B, table 3.5). The amount of adsorbed dye increases with the thickness of the films. Inset images: CBB adsorption in silica films casted on glass squares of 1 cm^2 . The intensity of blue color is a reflection of the amount of dye adsorbed, which increases with the thickness of the films.

In addition, conformational changes from the enzyme can occur as a consequence of immobilization, independently of the method selected leading to loss of enzymatic activity. Several techniques to characterize these conformational changes have been recently addressed in a review dedicated to enzyme immobilization.²¹¹ However, the advantage of covalent binding is the stability against leaching, which could lead to progressive loss of enzyme over time. For the purpose of this study, the covalent method of immobilization using glutaraldehyde was chosen. The main goal is to demonstrate that the porosity designed in the films is accessible to the enzyme and to prove the suitability of these films as enzyme supports. HRP is a glycoprotein with a diameter of 4-5 nm²¹² and with 6 lysine residues available for conjugation²¹³. There are several isozymes with isoelectric points ranging from 3 to 9. At pH 7.4 (immobilization buffer) electrostatic interactions can occur between the functionalized silica films and HRP. However, the relatively small size of the enzyme compared to the pore size in the films is expected to allow the transportation of these biomolecules through the pores.

HRP catalyzes the oxidation of redox indicators by H_2O_2 , involving the transfer of 2 electrons²¹⁴. In this study, TMB is a chromophore used as the redox indicator, with a characteristic change from colorless (reduced state) to blue (partly oxidized state), and quantitatively measured at the absorbance wavelength 650 nm. Moreover, the fully oxidized TMB is a diimine derivative with a yellow color and with a maximum absorption at 450 nm. The amount of oxidation products was measured photometrically. For this purpose, the medium was previously acidified to a pH below 1, favoring the equilibrium among all the oxidations species from TMB towards the diimine derivative²¹⁴.

The enzymatic activity of HRP immobilized in porous silica films was monitored through the oxidation of TMB during 30 minutes (Figures 3.10 and 3.11). With no acidification of the medium, the characteristic blue product was formed with a maximum absorbance at 650

Chapter 3. Mesopore Size and Processability of Transparent Enzyme-Loaded Silica Films

nm²¹⁴. The increase in the concentration of oxidized species of TMB (higher absorbance values at 650 nm) was directly related to the increase thickness of the films. Hydrochloric acid 2M was used to lower the pH below 1. The absorbance measured from porous films loaded with HRP showed in all cases higher values as compared to the flat reference. These absorbance values from porous films are proportional to their thicknesses, as previously observed from the adsorption of CBB (Figure 3.9).^b

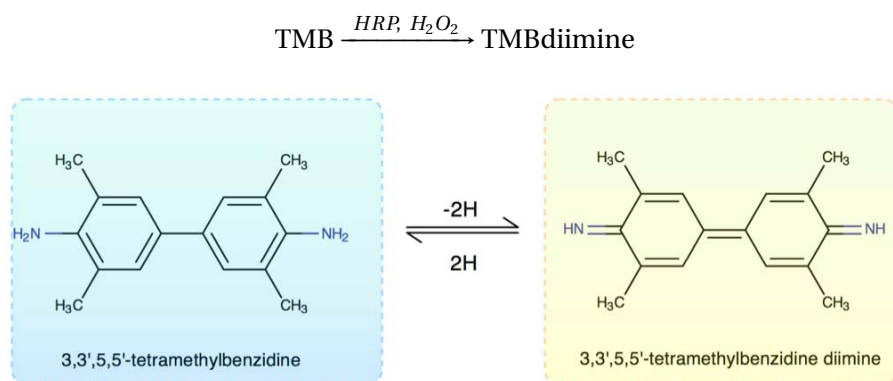


Figure 3.10 – Conversion of TMB into its diimine derivative in an acidic medium.

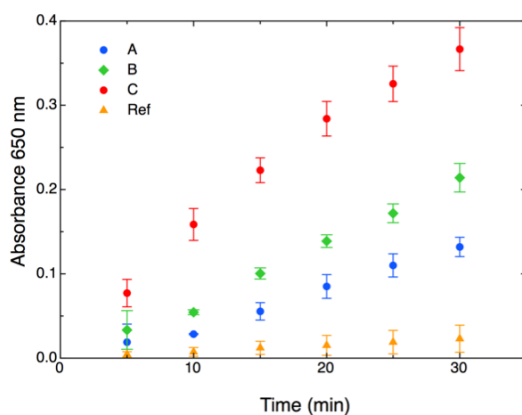


Figure 3.11 – Monitoring of the oxidation of 3,3',5,5'-tetramethylbenzidine (TMB) from HRP-loaded porous silica films. Higher enzymatic activity is observed from all the films evaluated with different thicknesses (red circles: 562 nm, green diamonds: 434 nm, blue circles: 333 nm) as compared to a flat surface used as reference (orange triangles).

After addition of hydrochloric acid, the oxidation products from TMB are converted into a diimine derivative with a λ_{max} at 450 nm²¹⁴. A calibration curve is built for known concentrations of HRP in solution with TMB, leading to the calculation of apparent concentration of

^bFrom the data in Fig. 3.11, it is also possible to obtain the rate of change of the absorbance dA/dt (see Appendix). A comparison for each film shows that the same overall trend is observed for the rate of change as for the absorbance values themselves. Therefore, the thickest film not only yields the highest product concentration, but also the fastest production rate of the detected reaction product. For the thinner films A and B, the slope dA/dt takes about 15-20 minutes to increase to the maximum rate, while the thickest film C already produces at the fastest rate from the beginning.

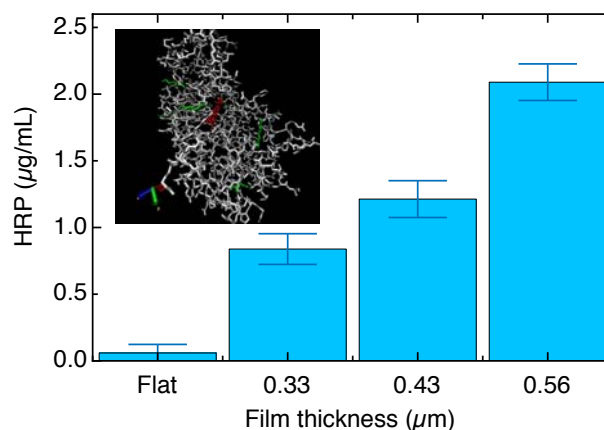


Figure 3.12 – Evaluation of the efficiency of immobilized HRP films in comparison to the free enzyme in solution. For each mesoporous film, the figure shows the activity that can be reached in terms of the equivalent free enzyme concentration. The equivalent concentration increases with the thickness of the films and is much higher for the mesoporous films as compared to a flat glass support. The area of the immobilized films is 1 cm^2 . Inset picture: graphic representation of HRP, pdb 1w4w, using the VMD visualization program from the University of Illinois²¹⁵. In green, lysine groups available for conjugation, in red hemoglobin group of the enzyme structure.

HRP in the films (Figure 3.12). These values represent the equivalent concentrations of free enzyme in solution. From Figure 3.12, the enzymatic activity increases proportionally to the thickness of the film. These values are 14, 20 and 35 times higher than those obtained for a flat surface. They confirm the previous findings about pore accessibility from the CBB adsorption. Despite the low loading concentration (only $10 \mu\text{g/mL}$ of HRP), the effect of film thickness on the enzymatic activity was observed. In addition, the accessibility of the pores to the enzymes is confirmed.

3.4 Conclusions

A highly reproducible method to synthesize transparent nanoporous silica films with pore sizes ranging from large mesopores to small macropores up to 100 nm has been developed. A new method has been developed, based on the entrapment of PS-P2VP micelles preliminary formed in a selective solvent. The influence of the solvent and block copolymer size selection on both the nanostructure and the homogeneity of the film has been demonstrated. In particular, the control of the porous structure was achieved by selecting symmetrical PS-P2VP block copolymers and 1-butanol as the selective solvent for P2VP blocks. Symmetric PS-P2VP-based micellar suspensions behave as Newtonian fluids at the studied concentration, whereas rheology measurements showed that asymmetric block copolymer suspensions at the same concentration form gels, which are unable to be casted as films. Regarding the film casting, 1-butanol is highlighted as an alternative main solvent to the commonly used ethanol for the synthesis of silica. 1-Butanol-based silica formulations led to even-textured films with homogeneously distributed pores. The silica to polymer ratio is adjusted to each block copolymer formulation to build up an interconnected porous network accessible from the surface of the films, highly transparent, and with thicknesses up to submicrometer scale. Finally, the as-synthesized films were successfully tested as enzyme carriers using HRP as a model. Mesoporous silica films with a submicrometer-scale thickness show an enzymatic activity up to 35 times higher than a functionalized flat support. This reliable method is relevant for the preparation of mesoporous supports for efficient immobilization of large bioentities. These functional mesoporous supports constitute promising patches for the reliable, accurate, and selective detection of analytes in biological media. More specifically, such enzyme-loaded patches will enable the highly sensitive and noninvasive detection of lactate, glucose, and glutamate in body fluids.

4 Formation of hierarchically porous silica films: screening and summary of different approaches

This chapter summarizes an exploratory screening of different approaches to form hierarchically porous silica films. In addition to the bottom-up sol-gel synthesis of silica films with colloidal mesopore templates described in the previous chapter, the evaluated approaches include powder-based methods, emulsion templating, electrospinning, and their combination. A summary and comparison of this evaluation is provided in this chapter, with a brief description of the different explored methods, stressing their advantages and disadvantages. In particular, a 'top-down' approach to form hierarchically porous silica films from dispersed silica particles combined with polymeric macropore templates was selected for the design of the enzyme-loaded biosensing films to be described in the subsequent chapters.^a

^aDr. Rolf Steiger (CSEM) is acknowledged for helpful discussions contributing to the development of the powder-based approaches to form silica films described in the following chapters.

4.1 Introduction

Over the last years significant efforts have been dedicated to the development of strategies to synthesize hierarchically porous materials. Their impact in catalysis, separation, energy and life science applications has motivated these developments. The presence of a multi-scale porous network combines the advantages of each pore length scale: the micro- and mesopores provide a size and shape selective network where a large amount of molecules can be hosted owing the large surface area, while macropores enhance the diffusion and accessibility of larger molecules. An exploratory screening of different approaches was carried out at an early stage of this PhD work to synthesize hierarchically porous silica films. The resulting insights are summarized in this chapter, stressing the advantages and disadvantages of the different evaluated formulations, processes and structures that can be achieved. Finally, based on this screening the most relevant methodology to synthesize hierarchically porous silica films was selected and will be described in more detail in Section 4.3. The methods described here will subsequently be used to form hierarchically porous films as supports for enzyme immobilization in the next chapters.

4.2 Powder approach for the formation mesoporous silica films

In a first approach to form mesoporous silica films, a top-down method based on a silica nanopowder is evaluated. This nanopowder is made of aggregated primary nanoparticles. Following a route originally used to form thin ceramic coatings¹⁵⁸, an aqueous, polymer-stabilized suspension of these silica aggregates is cast into films by different deposition techniques (spin, dip, bar-coating) and sintered at high temperatures, yielding mesoporous silica films. Fig. 4.1 shows a schematic representation of the method. The main process steps are: (1) the preparation of a stable water-based suspension of silica aggregates using PVA as a binder and boric acid as a crosslinker, (2) film formation from this suspension using different deposition techniques (e.g. spin, dip, or bar-coating), and (3) sintering at high temperatures to remove organic compounds, resulting in mesoporous silica films.

4.2.1 Experimental section

Materials

CAB-O-SIL[®] M5 silica nanopowder was purchased from Cabot. 2-aminoethyl-3-aminopropyl-trimethoxysilane was purchased from Evonik GmbH. Aluminium chlorohydrate was obtained from Clariant. Polyvinyl alcohol (PVA, Mowiol 40-88) and boric acid were purchased from Sigma-Aldrich.

Preparation of positively charged silica

The silica nanopowder was moisturized with a given amount of deionized water to reduce their 'volatility'. In parallel and under mechanic stirring, 2-aminoethyl-3-aminopropyltrimethoxysilane and aluminium chlorohydrate were mixed in water leaving the mixture to react for at least 30 minutes. The pre-moisturized silica was then added to the previous mixture to get

4.2. Powder approach for the formation mesoporous silica films

a final 20 wt% aminated silica aqueous dispersion. The mixture was left to react for at least one hour under mechanic stirring. To homogenize the mixture, sonication is required. A sonication probe (Bandelin Sonopuls) was used.

Preparation of silica-PVA suspension

A 15 wt% silica suspension is then prepared from the previous mother solution of aminated silica. The formulation was prepared as follows: A given amount of previously aminosilane-modified dispersed silica aggregates was mixed with a given volume of deionized water under magnetic stirring at 40°C in a water bath. At the same time, PVA at 10% w/w was prepared by dissolving the corresponding amount of PVA in deionized water. Once dissolved, PVA was then added to the silica suspension until reaching a final concentration of 15% w/w with respect to the silica content. The mixture was homogenized using a sonication probe. Prior to the final casting of this suspension into films, boric acid in aqueous solution (5% w/w) was added to the silica-PVA suspension.

Silica films

Glass cover slips were immersed in isopropanol and sonicated, followed by rinsing with ethanol and dried with compressed air. The cleaned glass surfaces were treated with O₂ plasma for 10 minutes. Films were cast by spin coating onto the cleaned glass substrates.

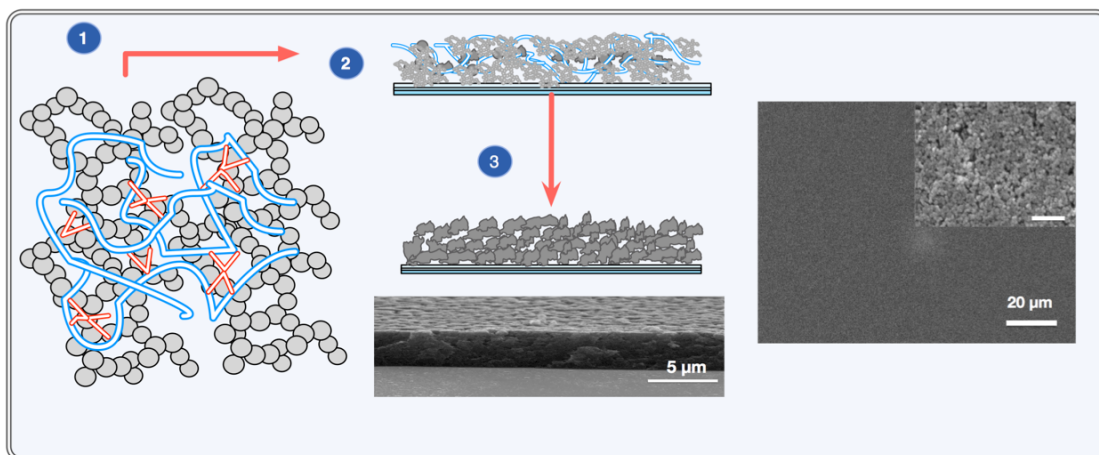


Figure 4.1 – Representation of the method followed for the synthesis of mesoporous silica films via a top-down approach. (1) A homogeneous and stable water-based suspension of silica aggregates is prepared, containing PVA as a binder and boric acid as a reticulating agent. (2) This suspension is cast into films by different deposition techniques (spin, dip, bar-coating) and (3) sintered at high temperatures, removing organic compounds from the original formulation, which finally yields mesoporous silica films.

4.2.2 Results and discussion

This method to prepare mesoporous silica films from silica powders is a top down approach. The original nanopowder is agglomerated with agglomerate sizes in the range of a few 100 nm to a few μm , based on primary silica nanoparticles with a mean diameter of 15 nm. Stabilized aqueous dispersions of these powders were obtained in deionized water (pH=5.5). At this pH value, the silica colloids are negatively charged (the isoelectric point of silica is around pH \approx 2-3), resulting in partial deagglomeration of the powder grains. The surface functionalization with aminosilane leads to positively charged $\text{SiO}_2\text{-NH}_2$ particles dispersed in water. Finally, the sonication step further reduces and homogenizes the size of the aminated silica agglomerates in dispersion to average sizes around 50-100 nm. The combination of positively charged silica particles with sizes below 100 nm leads to stable aqueous silica dispersions.

Compared to the templating method this approach has the advantage that relatively inexpensive raw materials can be used. Moreover, the aqueous solvent is more convenient at the industrial scale than 1-butanol. Films with several micrometers in thickness can be achieved by adjusting the concentration of solids, and therefore the viscosity of the dispersion, and via the coating process parameters. However, due to the use of industrially processed silica aggregates, it can be expected that the pore size distribution will not be as well controlled and homogeneous as compared to e.g. block copolymer mesopore templates. The porosity of films obtained using the approach described here will be discussed further in the next chapter.

Polyvinyl alcohol (PVA) is used as a polymeric dispersing agent in the aqueous dispersion of aminated silica particles. This polyalcohol contains pendant OH groups with a strong affinity to form hydrogen bonds with the -NH_2 , silanol (Si-OH) and siloxy (Si-O-Si) moieties on the silica surface. PVA is mainly obtained by hydrolysis of polyvinyl acetate (PVAc) (see Figure B.1 in the Appendix). PVAc hydrolysis is usually not complete, and the degree of hydrolysis is given by the ratio of hydrolyzed vinyl acetate moieties²¹⁶. It influences the chemical and physical properties, including solubility, crystallinity and hydrophilicity of the resulting PVA. The degree of hydrolysis of for the PVA used here is $\approx 88\%$ ²¹⁶, meaning it is highly hydrophilic. The abundant hydroxyl groups provide PVA with a high affinity to metal oxide surfaces. PVA therefore facilitates the dispersion of the silica nanoparticles. Besides this colloidal stabilization, the presence of PVA in the silica formulation increases the homogeneity of the final film: by interacting with the silica surface, PVA chains create a polymeric framework within the resulting films. Finally, boric acid (B(OH)_3 or B(OH)_4^- in water) crosslinks the PVA chains mainly during the drying step (see Figure B.1 in the Appendix). It strongly binds compounds with adjacent alcohol functions²¹⁷. Due to the four symmetric binding functions of boric acid, B(OH)_4^- is able to bridge closed PVA chains. In the silica dispersion before coating, the borate and PVA species do not yet form a cross-linked network. Nevertheless, their interaction in water increases the formulation viscosity and therefore the potential thickness of the resulting films (up to several μm). During the film drying step, the concentration of these compounds is increased and they form a polymeric network interpenetrated with the silica skeleton. This combination provides the hybrid film with mechanical flexibility and reduces brittleness and cracking. The resulting structures also provide a high transparency of the films.

4.3 Silica powder dispersions combined with polymeric particles as macropore templates

The powder method described in the previous section can be extended by inserting additional pore templates to form large macropores. This approach is promising for the synthesis of hierarchically nanostructured silica films. As described in Section 4.2, a stable and homogeneous dispersion of silica aggregates in water was obtained and used for the synthesis of homogeneous mesoporous silica films. Polymeric particles are added to the dispersion to generate macropores. A wide variety of particles are commercially available for this purpose. The chemistry and size of such particles are chosen in a way that the formulation remains stable and that the resulting films exhibit well-defined additional macropores. There are many advantages of this process to obtain multi-scale porous films: (i) the film thickness can be controlled by the deposition conditions and by the silica and polymer content in the dispersion, (ii) transparent films can be obtained (depending on film thickness, macropore size and macropore number density), (iii) the possibility to cast the films on large areas, (iv) the fact that these formulations can be water-based, avoiding the use of flammable or hazardous chemicals which demand implementation of safety guidelines during manipulation, limiting the up-scalability for a potential industrial synthesis, (v) the diversity of deposition techniques that can be used to cast films, and (vi) the compatibility with water-dispersible macropore templates. The process followed to obtain these films is schematized in Figure 4.2; in the example shown, polystyrene (PS) beads are used in the formulation. After their removal by pyrolysis, macropores are formed, with pores in the size range of the of the polymeric template.

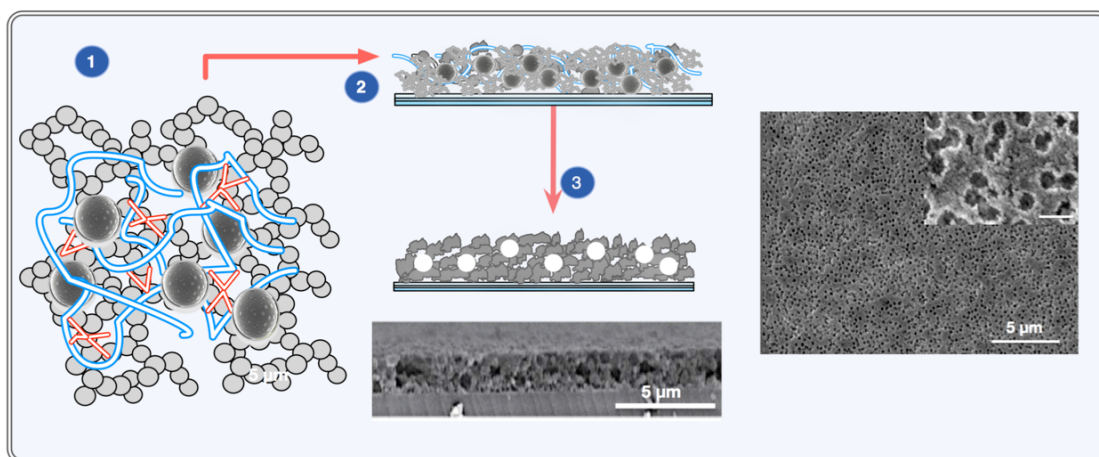


Figure 4.2 – Top-down approach for the synthesis of multi-scale porous films based on a powder method. Mesopores are formed within the silica framework due to the structure of the aggregates consisting of primary silica nanoparticles. The macropores are formed by inserting polymer beads as sacrificial templates. After removal of the polymer by heat treatment, hierarchically porous films are obtained. Scale bar of inset micrograph: 500 nm.

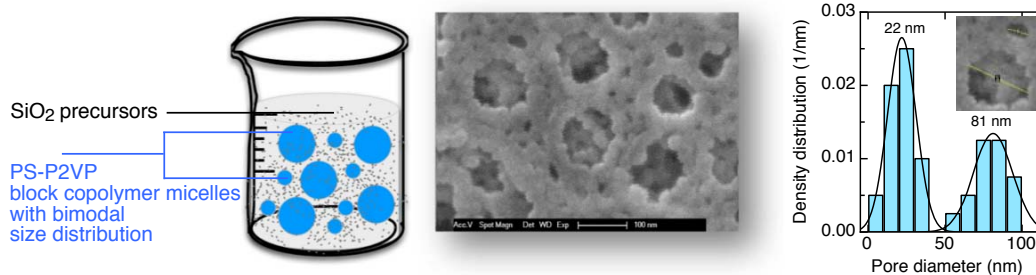


Figure 4.3 – A mixture of silica sol/PS-P2VP block copolymer micelles with a bimodal size distribution (left; silica precursors shown in black, micelles shown in blue) is cast into films and the porogenic materials are removed by calcination (middle; SEM micrograph), resulting in films with a bimodal pore size distribution with peaks around 22 nm and 81 nm (right, obtained from analysis of SEM images using the longest secant pore diameter).

4.4 PS-P2VP block copolymer templating

As discussed in Chapter 3, PS-P2VP block copolymers can be used as templating materials for the nanostructuring of silica films. Following the same procedure, spherical polymer micelles with different micelle size diameters were obtained by dissolving symmetrical block copolymers (BCP) in short chain aliphatic alcohols. The resulting micelle size diameter depended on the block copolymer molecular weight. Each block copolymer with a given molecular weight was separately dissolved and micellized. Afterwards, mixtures of micelle suspensions at different ratios were prepared. These blends of micelles with different sizes were finally mixed with a silica sol, following the method described in Chapter 3. Despite the similar chemistry, the micelles of different BCP sizes remain stable after mixing. Depending on the ratio between micelles of different sizes, a hierarchically porous film could be obtained like the one shown in Figure 4.3. A clear advantage of this method is the control over the size of the resulting pores, which directly depend on the used micelle size. Additionally, the film nanostructure can be tuned by varying the ratio between micelles with different diameters. However, a key disadvantage is the thickness of the film obtained after one deposition, which was lower than 100 nm. If thicker films are required, several deposition-calcination steps need to be performed, which increases the synthesis time and makes this approach less practical.

4.5 Porous silica particles in combination with micellar pore templates

In this strategy, polymeric colloidal templates have been used in combination with PS-P2VP block copolymer micelles to synthesize porous films (Figure 4.4). In this particular case, commercially available polymer beads made of polystyrene were used as macrotemplates to prepare porous silica particles, which in the last step were cast as films. Firstly, negatively charged polystyrene beads (a) and PS-P2VP micelles (b) were mixed in the same solvent where the micelles were prepared. A silicon alkoxide (TEOS) was added drop wise, followed by acidic water. After allowing the mixture to react, it was cast into films and the templates were removed by calcination. The detailed mechanism of formation of these porous particles (c) remains

4.5. Porous silica particles in combination with micellar pore templates

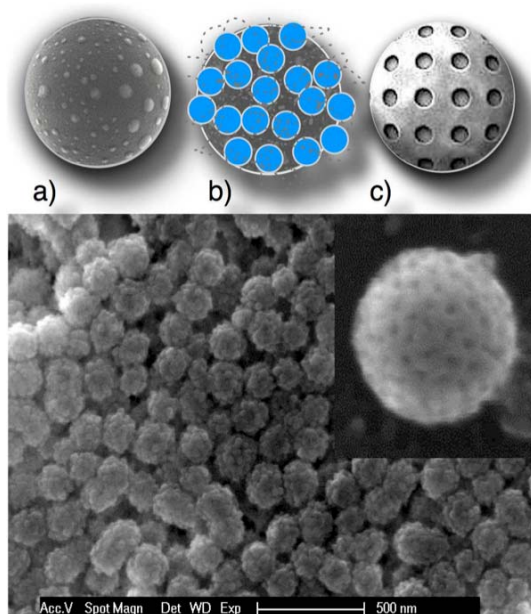


Figure 4.4 – Polymer particles in combination with PS-P2VP micelles are used as templates for the synthesis of porous silica particles, which ultimately are cast as films, producing hierarchically nanostructured silica films. Upper panel of images: schematic representation of the approach showing a) the surface of the polymer particle b) sketch of template micelles (blue) at the polymer surface and c) sketch of a resulting porous silica particle; Lower panel: resulting cast film (large micrograph) and an individual structured silica particle (inset) as observed by SEM.

challenging to explain. However, the order of addition of each component of the mixture during the synthesis was found crucial, similar to the method used in Chapter 3. In view of a mechanism proposed by Wu et al.²¹⁸ for silica structures templated with cationic surfactant micelles, the silica nanoparticles are formed by a 'seed and growth' mechanism: the templates deposit on the polymer microsphere due to surface energy, and the cationic nature of the template directs silica growth around the micelles at the surface of the beads. In the larger block copolymer micelles used in this work, basic pyridine groups are located on the outside of the micelle, suggesting that this type of catalyst and mechanism favors the formation of the particulate silica materials shown in Fig. 4.4. Casting these particles from the suspension, the procedure allowed the synthesis of porous films. The porosity consisted of mesopores within each particle and macropores formed inside and between particles, in a similar way as described in the previous section. Whereas the synthesis of porous particles seems innovative and promising, some disadvantages of this approach were recognized, among them, the lack of transparency of the resulting films, reducing the optical read-out of the resulting chemical biosensors. Assuming that these particles are hollow, similar to the ones described by Wu et al.²¹⁸, they could be of interest to encapsulate small molecules that are able to pass through the mesopores of the particle, for example in drug delivery applications. However, since the focus in this work was to immobilize large enzyme molecules of the size of a few nanometers, this approach was not followed further.

4.6 Hierarchically nanostructured films formed by emulsion templating

Emulsion templating is a versatile technique used to obtain porous thin films following an appropriate combination of surfactants, silicon alkoxide precursors and deposition conditions. The method consists in the formulation of stable emulsions as pore templates. In this example, oil-in-water (o/w) emulsions were prepared; the dispersed phase consisted of a hydrophobic compound (octane). The emulsions were stabilized by the incorporation of non-ionic emulsifiers from the family of Tween[®] and Span[®] (Table 4.1). The method followed to obtain stable emulsions was the combination of surfactants with different hydrophobic-lipophilic balance (HLB) values at low energy inputs, making this approach interesting as a low-energy emulsification procedure. Mixtures of non-ionic surfactants were dissolved with the organic phase using the relation:

$$HLB_{\text{mix}} = HLBA_x [A] + HLBB_x [B]$$

for two different surfactants A and B, where the square brackets indicate molar concentrations and the HLB scale ranges from 0 to 20 (Table 4.1). Water was added to reach the phase inversion composition (PIC) at 60°C. The emulsions were stable for months and were used as templates simply by mixing with an aqueous silica sol prepared by silicon alkoxide hydrolysis under acidic catalysis. After mixing with the sol, the formulations were cast by spin coating yielding silica gel based films containing homogeneously distributed oil droplets. Silica matrix crosslinking and drying followed by removal of the oil droplets by heating at 500°C leads to porous films with various pore sizes (Figure 4.5). These different pore sizes are defined by the polydispersity of the original emulsion. Although this approach is reported in the literature, little information is available regarding its use in real applications. A main limitation of this method is the stability of the emulsion after combination with the silica sol.

Table 4.1 – Overview of the HLB scale and values for specific surfactants

HLB scale		Values for specific surfactants	
HLB	Type	HLB	Surfactant
0-3	Anti foaming agent	16	Tween 20
4-6	w/o emulsifier	14.9	Tween 60
7-9	Wetting agent	15.6	Tween 40
8-18	o/w emulsifier	4.3	Span 20
13-15	Typical of detergents	6	Span 40

Droplets tend to coalesce due to the solvents present in the silica sol, limiting the applicability of this method in particular for small drop sizes below 100 nm. Additionally, the final nanostructure is difficult to control as the evaporation of the solvents during casting can destabilize the emulsion.

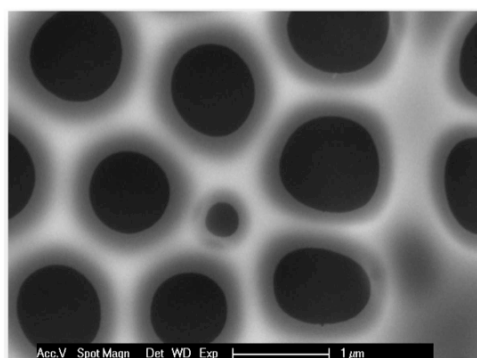


Figure 4.5 – An example of an emulsion-templated silica film synthesized from an oil in water emulsion in combination with pre-hydrolyzed silicon alkoxide. Octane droplets were emulsified in water with non-ionic emulsifiers (see Table 4.1) using the phase inversion method. The resulting stable emulsion was mixed with an aqueous silica sol prepared by acidic silicon alkoxide hydrolysis, and the mixture cast by spin coating, crosslinked and dried. Heating at 500°C yielded macroporous silica films with various pore sizes defined by the polydispersity of the original emulsion.

4.7 Electrospinning-based approaches: direct deposition and template fibers

Electrospinning is a technique used for the nanostructuring of materials into fibers. In this technique, an electric field is used to create a charged jet of a complex fluid formulation. Under suitable experimental conditions, the jet solidifies and forms dry fibers. This process therefore requires the formulation to contain ionizable compounds such as electrolytes. The electric field produces a movement of the ions transferring a force to the polymer containing liquid²¹⁹. As this jet travels in the air, the solvent evaporates leaving a charged fiber that can be electrically deflected and collected on a metal screen Figure 4.6²²⁰. Here, two strategies have been explored to produce hierarchically structured coatings with electrospinning: a) deposition of a polymeric network used as sacrificial macrotemplates by embedding in a mesoporous silica framework; b) direct deposition of a network of mesoporous silica fibers, the macropores being the voids between the fibers.

The morphology and diameter of electrospun fibers depend on various factors which can be divided as a) the intrinsic parameters from the fluid to be electrospun, b) the operational parameters for obtaining fibers and c) the ambient parameters²²¹. Among the intrinsic parameters are: (i) the properties of the polymer (such as molecular weight, molecular-weight distribution, glass-transition temperature, solubility and conformation of polymer chain²²²), (ii) the viscosity (or concentration); (iii) elasticity; (iv) electrical conductivity and (v) the polarity and surface tension of the solvent. The operational parameters comprise the i) strength of applied electric field (usually 1-30 kV)²²¹, (ii) the distance between spinneret and collector (10-25 cm²²² in most lab set-ups), and the feeding rate for the polymer solution. Finally the ambient parameters include i) the humidity, (ii) temperature of the fluid to be electrospun and from the chamber's setup and (iii) the air flux in the chamber for electrospinning. Despite the apparent complexity, this technique has been widely used over the last 10 years to produce

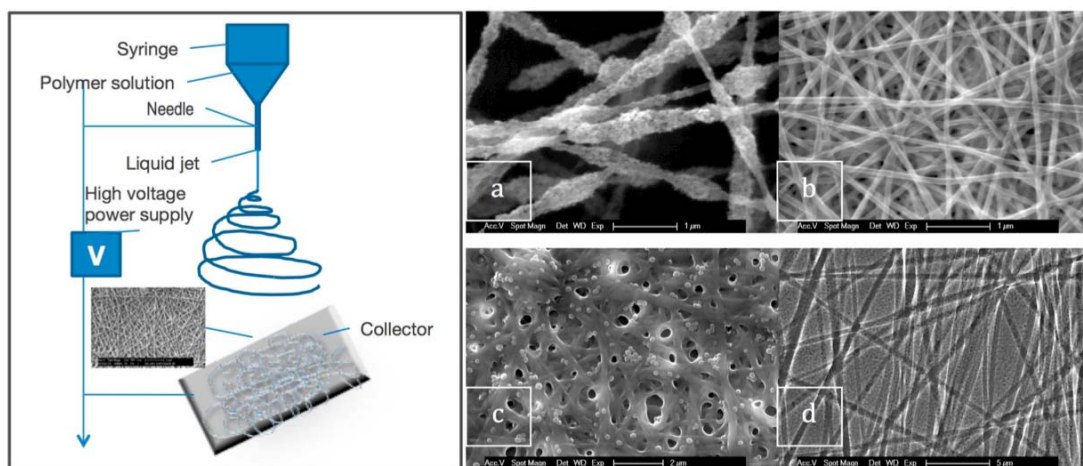


Figure 4.6 – Left: Electrospinning setup. Right: Examples of different nanostructures as obtained with the electrospinning setup built for this work: a) mesoporous silica fibers, b) gelatin fibers as macroporous templates, c) cross-linked gelatin fibers, and d) half-embedded polystyrene fibers in a mesoporous silica film.

polymeric, inorganic (metallic, metal oxide) or hybrid organic-inorganic fibers; moreover, this process has been implemented at the industrial level and is used to produce technical textiles^{219–222}.

Figure 4.6 shows a representation of an electrospinning set-up and some of the diverse nanostructures which have been achieved using the technique, ranging from porous silica fibers (Figure 4.6a), organic fibers which serve as macropores templates (Figure 4.6b), crosslinked fibers to be used as enzyme supports with no further modification (Figure 4.6c) to mesoporous silica matrixes template with PS electrospun fibers. Although the range of possibilities is huge, there are challenges to master this technique on the industrial scale.

4.8 Conclusion

Different approaches were evaluated to synthesize hierarchically porous films with a focus on the following required properties:

- Transparency of the films
- Control over thickness, pore size and pore size distribution
- Accessible porosity
- Facility to synthesize large mesopores (>100 nm)
- Inexpensive
- Up-scalable

A summary of the results is presented in Table 4.2. The method using silica powder dispersions was selected as the most promising approach to synthesize porous films with the necessary characteristics listed before. This method is relatively inexpensive, produces a highly interconnected mesoporous matrix, which in combination with porogenic macrotemplates can generate hierarchically porous materials with large macropore sizes; this approach is versatile to produce films with tuneable thickness on supports of different nature: glass, metal, paper, etc. Additionally, the formulations are water-based and stable, which enable the scale-up of the process to coat large-surface areas. In view of these features, this method will be used in the following chapters to investigate their suitability as supports in the design of lactate biosensors.

Chapter 4. Hierarchically porous silica films: screening of approaches

Table 4.2 – Overview of different approaches screened to synthesize hierarchically porous films with a focus on the required properties in view of enzyme-based biosensors.

Method	Advantages	Disadvantages	Conclusion
Powder dispersion	<ul style="list-style-type: none"> • Water-based • Stable formulations • Interconnected porosity • Large macropore sizes embedded in mesoporous network • Control over thickness and macropores' size • Up-scalable • Transparent 	<ul style="list-style-type: none"> • Colloidal stability needed (manageable via formulation and processing time) 	Suitable method for further investigations in biosensor design
PS-P2VP block copolymer templating	<ul style="list-style-type: none"> • Control over pore size and distribution • Interconnected porosity • Transparent • Particles and films can be synthesized • Accessible porosity 	<ul style="list-style-type: none"> • Use of solvents • Expensive raw materials • Limit in thickness • Large macropores (>100 nm) are difficult to synthesize 	Not further considered for biosensor design in this thesis
Electrospinning	<ul style="list-style-type: none"> • Control over fibre size • Useful for templating and porous fibres • Accessible porosity 	<ul style="list-style-type: none"> • Requires specific safety conditions: high tension, toxic solvents • Uncontrolled deposition of fibres • Lack of transparency 	Not further considered for biosensor design in this thesis
Emulsion templating	<ul style="list-style-type: none"> • Relatively inexpensive • Low energy consumption 	<ul style="list-style-type: none"> • Unstable formulations • Difficult to control pore size, connectivity and accessible porosity 	Not further considered for biosensor design in this thesis

5 Lactate detection based on hierarchically porous silica films functionalized with L-lactate dehydrogenase

In this chapter, a silica powder approach in combination with polymer particles as porogenic templates is followed for the development of multiscale porous patches for lactate biosensing. In this multiscale system, macropores of a size dependent on the polymer particle are surrounded by a mesoporous interconnected network formed by silica aggregates. The introduction of different pore scales in the films and the consequences on enzyme immobilization and optical lactate biosensing performances are the central topics in this chapter. Their performance for lactate detection has been compared to a similar material with monomodal porosity. This detection is based on the activity of lactate dehydrogenase (LDH) immobilized in the films. A multiscale porosity in the same silica system is advantageous for the transportation of enzymes during their immobilization, as revealed by an analysis of their diffusivities in media with different pore size scales. Additionally, the inclusion of a dual range of porosity in the films improves the response time of the films towards lactate detection. Visual modelling of enzyme diffusion reveals the importance of macropore location and connectivity within the film. This procedure is versatile, relatively inexpensive and compatible with more than one deposition technique, making it relevant for industrial applications.

5.1 Introduction

Hierarchically porous materials exhibiting multiscale pore sizes find application as enzyme supports primarily for their combination of high surface area and improved mass transport. In the last years, research has been devoted to the development of procedures to synthesize multiscale porous systems and the work on this field has been extensively reviewed^{99;223}. Methods based on the self-organization of soft and hard materials as templates are the most frequently cited in the literature^{99;224;225}.

Several developments of hierarchically porous materials specifically for enzyme immobilization have already been reported in the literature. For instance, a concept based on the preparation of a double emulsion has been described²²⁶. This technique allowed the synthesis of porous silica with meso and macropores to immobilize lipase by entrapment.

In another report²²⁷, a sol-gel process with a combination of pore templating materials and phase separation led to the synthesis of monolithic silica with hierarchical porosity. The resulting material was used as a bioreactor, immobilizing invertase, a relevant enzyme in food industry. The functionalized monoliths possessed extensive systems of micrometric channels connected with mesoporous networks embedded in the silica framework, resulting in large activated surface area and very short diffusion paths.

Hierarchical porous silica with pore diameters between 10 and 40 nm and 0.5 and 10 μm , and variable glyoxyl group content on its surface²²⁵ was used as support for immobilization of beta-galactosidase from *Bacillus circulans*, through multipoint covalent attachment. A higher loading capacity and enzymatic activity in comparison with other known supports was promoted by the presence of macropores and large mesopores, which were assumed to improve the diffusion of the enzyme into the mesopores.

The kinetic parameters of enzymes from the Michaelis-Menten model K_M and V_{max} describe the behaviour of a given concentration of enzyme towards the substrate. In a general manner, V_{max} is a reflection of the maximum rate of substrate conversion into product. Higher concentrations of substrate in the medium, once the V_{max} is reached, will not affect this rate of conversion. K_M is often considered as a parameter that indicates the affinity of the enzyme for the substrate, but also the accessibility of the substrate to the active site of the enzymes. The lower the K_m values, the faster the enzyme will be saturated with substrate, which ultimately represents a higher affinity of the enzyme for the substrate. Under the context of biosensors, it would be desirable to maintain high V_{max} and low K_m values after immobilization. This could be translated into faster response times and higher sensitivity, respectively. Nevertheless, the kinetic parameters are also affected by the immobilization of enzymes.

The role of the pore size in the immobilization of lipase in polymer-based support materials was reported by Li et al.¹⁰⁹. Polystyrene porous particles with different average pore sizes in the range of 15 nm to 314 nm were used. The kinetic parameters of the enzyme, K_m and V_{max} in solution were 0.441 mM and 70.4 ($\mu\text{mol/l}$)/min, respectively. Using a fluorescent probe linked to the enzyme, it was found that lipase reached the core of the macroporous particles. In contrast, the enzyme was retained as a shell in the mesoporous particles, demonstrating the limit of the pore size in the diffusion of the enzyme. After immobilisation, the values of K_m were higher and V_{max} became smaller in particles with smaller pore sizes. However, the

K_m from the enzyme immobilised in macroporous supports were lower than those of free lipase. These results indicated that the diffusion of substrate was not affected due to the large pores, which allowed the substrate to reach the immobilised lipase. In contrast, the higher K_m values for the enzyme immobilised in mesoporous supports was considered an indication of a weaker affinity of the enzyme for substrate and a result of diffusion limitations in the small pore material. In a similar study, invertase was immobilized by entrapment in sodium alginate, showing a higher value for K_m and a lower value V_{max} as compared to the free enzyme⁹². Similarly, β -glucuronidase was covalently immobilized in porous silicon. The values of V_{max} and K_m calculated were 0.076 nmol/min (or 19 nM/min if molar concentration units are used) and 0.05 mM, respectively. These values were in the same range as those from the same enzyme in solution (1.55 nmol/min and 0.078 mM). However, the value for V_{max} for the immobilized enzyme was slightly lower²²⁸.

The short overview given here shows that many approaches exist to create immobilized enzyme systems in bulk materials or on particles. In contrast, an efficient method to form robust, inexpensive and efficient biosensing surfaces in the form of thin, optically transparent films with multiscale porosity and suitable for L-lactate biosensing is still missing. The results presented in Chapter 3 showed that silica films with pore sizes in the large mesoporous range (30-50 nm), templated with block copolymer (BCP) micelles, can successfully entrap a model enzyme, horseradish peroxidase (HRP, diameter 4-5 nm²¹²). LDH is a larger enzyme requiring the incorporation of macropores for its diffusion and immobilization. In this chapter, the synthesis of thin, transparent and LDH functionalized patches is described. A combination of a templating approach to synthesize macropores together with the formation of large mesopores using silica aggregates has been demonstrated, providing an interconnected mesopore network, large surface area and macropores to allow the diffusion of enzymes. This procedure employs the use of water based formulations which can be scaled-up and which are safer and more eco-friendly. The following sections describe the characterization steps towards the use of these films as responsive surfaces in lactate biosensing.

In summary, the objectives addressed in this chapter, are: (i) to synthesize in a versatile and robust way multiscale porous films with interconnected porosity and high transparency, (ii) to immobilize LDH for optical lactate biosensing, (iii) to characterize the functionalized materials before and after enzyme loading and (iv) to demonstrate the effect of macropores in the sensor performance. LDH has a diameter of 15 nm at its largest three-dimensional length, representing three times the size of HRP. Therefore the importance of incorporating a second pore length scale in the macropore range becomes pertinent for efficient transportation and immobilization. Additionally, the known mechanism of LDH described in the background chapter follows a multistep process for substrate and co-factor binding, and requires a three dimensional conformation change of the enzyme during its activity. This information supports the hypothesis that pores in the meso-scale are not large enough to allow an efficient performance of the enzyme. In the next sections, this hypothesis is supported by scientific evidence obtained during the performance evaluation of mesoporous vs multiscale porous films for lactate biosensing.

5.2 Materials and methods

5.2.1 Film synthesis and casting

Support treatment: Borosilicate slides were cleaned by sonication using isopropanol for 10 minutes. They were then rinsed with ethanol, dried with compressed air and placed into an oxygen plasma chamber for 10 minutes. *Film preparation:* Silica films were synthesized following a top-down approach. In a typical procedure, silica aggregates (Cabosil M5) are dispersed in deionized water at a concentration of 10% w/v. For hierarchically nanostructured films, poly(methyl methacrylate) (PMMA) beads (280 nm in diameter, Polymer source) were used as macroporous templates. A given volume of polymer beads (10% w/v) was incorporated dropwise to the silica suspension with strong agitation. Polyvinyl alcohol (PVA) was used as a binder at a concentration of 15% w/w with respect to the total solids content of the formulation. The resulting suspension was spin-coated onto cleaned borosilicate slides. Heat treatment was applied to remove the porogenic templates (550°C for 20 minutes).

5.2.2 Film characterization

The films nanostructure was observed using Scanning Electron Microscopy (SEM XL30 ESEM-FEG, Philips). Cross-sectional images were taken to measure the thickness of the films. The porosity was characterized using an accelerated surface area and porosity analyser by nitrogen sorption porosimetry using BET analysis (ASAP, Micrometrics) and using a mercury intrusion porosimeter (MIP; Pascal 440, Thermo Fischer Scientific). For N₂ sorption measurements, the films deposited on glass were scraped using a blade and the product obtained was used for analysis. For MIP measurements, a monolith of the suspension was obtained by drying first a suspension in a vial to obtain a pellet and then by removing the organic templates and other compounds by calcination.^a

5.2.3 Post-functionalization of silica films

Silanization: Prior to the post-functionalization steps, the uncoated side of the support was protected with adhesive tape. Amino-propyltriethoxysilane (APTES) in the vapour phase was used to functionalize silica films with amino groups. Amino-functionalized silica films were then immersed in a solution of glutaraldehyde at 5% v/v in phosphate buffer 0.01mM at pH 7. After 10 minutes, the films were thoroughly rinsed with deionized water, and then dried with compressed air. If not used immediately, they were stored in a refrigerator covered with aluminium foil for maximum 2 hours before use. *Enzyme immobilization:* A stock solution of lactate dehydrogenase (LDH, EDM Millipore Calbiochem[®]) at a concentration of 100 U/mL was prepared in deionized water. It was diluted in phosphate buffer 0.01mM to reach a final concentration of 10 U/mL. The post-functionalized silica films were immersed in this solution for 2 hours at room temperature. Afterwards, they were thoroughly rinsed with phosphate buffered saline –Tween 20 solution (PBS-T, Sigma Aldrich), PBS and water, and dried with compressed air. The protecting tape of the film was removed and the enzyme-conjugated films were placed in a 24-multiwell plate for further experiments.

^aDr. Elise Berodier (EPFL-IMX-LMC) is acknowledged for her help in performing MIP measurements.

5.2.4 Streaming potential

Streaming current measurements were performed with the SurPASS instrument by Anton Paar (Graz, Austria) using the Adjustable Gap Cell Sample holder for the accommodation of planar samples with dimensions of 10 mm x 10 mm. For each measurement a pair of glass slides with identical top layers was fixed on these sample holders using double-sided adhesive tape. The sample holders were inserted in the cell such that the surfaces of the glass slides were precisely facing each other. A gap of 100 μm was adjusted between the sample surfaces. Before starting each measurement, the samples were carefully rinsed with the corresponding measuring electrolyte. A 0.001 mol/L KCl solution was used as the standard electrolyte. In addition a phosphate buffered saline (PBS) with ionic strength of 0.01 mol/L was used. The pH of these aqueous solutions was adjusted with 0.05 mol/L HCl and 0.05 mol/L NaOH, respectively.^b

5.2.5 Quartz crystal microbalance measurements

The adsorption of LDH was tracked by time-dependent measurements using a quartz crystal balance (E4 QCM, Q-sense). The QCM technique offers nanogram sensitivity and allows quantitative analysis of the adsorption and surface interaction of biomolecules and surface-active polymer in real-time²²⁹⁻²³¹. The method is based on the detection of small changes in the resonance frequency of quartz crystal oscillator when mass is adsorbed on its surface. An oscillating AC voltage is applied using two gold electrodes on the quartz crystal, and the shift of the resonance frequency $-\Delta f$ to smaller frequencies measured.

A film of mesoporous or hierarchically porous silica was deposited by spin coating on top of silica-coated quartz sensors, protecting the electrodes on the sensors. The organic templates from the formulation were removed by calcination at 550°C during 1 hour. Subsequently, the sensors were cleaned with deionized water, dried with N₂ and exposed to O₂ plasma (10min) before measurements. A solution of 10 U/mL of LDH in PBS was pumped through the chambers and let to equilibrate for several hours. The unadsorbed enzyme was removed by pumping PBS in a rinsing step.

5.2.6 Thermogravimetry (TGA) measurements

TGA analysis (Mettler Toledo TGA/SDTA model 851e) was performed to assess the functionalization of the films after each step and to estimate the loading of the enzyme in the hierarchically nanostructured film using a ramp from 30 to 1000 °C in air.

5.2.7 Enzymatic tests

A TRIS-hydrazine buffer solution was prepared with a concentration of 0.1M for TRIS and 0.5M for hydrazine. The pH was adjusted to 8.8 with HCl. L-lactate and NAD⁺ solutions at 0.1M were prepared in deionized water. Calculated aliquots of NAD⁺ and TRIS-hydrazine buffer were poured into 24-well transparent plates containing a functionalized porous film.

^bDr. Thomas Luxbacher (Anton Paar, Graz Austria) is acknowledged for his support with streaming potential measurements.

Chapter 5. Lactate detection based on nanostructured and transparent hybrid silica films

L-lactate was added as the final step. Approximately every 5 minutes the absorbance at 340 nm was measured (TECAN® infinite M200). A program with previous agitation (orbital shaking) was set to homogenize the solutions in each well, therefore the solutions can be considered as well-mixed.

5.2.8 Visual modelling of enzyme and solute transport

Visual simulation of LDH and L-lactate diffusing through mesoporous and hierarchically porous silica films and adsorbing on the surface was performed using the 3D graphics software Blender™ (Blender version 2.72b using Mac OS X, available at www.blender.org as open source software).

5.3 Results and discussion

In this section, the synthesis of bimodal porous silica films is evaluated towards lactate detection. The structures of mesoporous silica films and hierarchically structured films will first be described and compared using SEM micrographs and porosimetry. To further characterize the suitability of the hierarchically structured films for enzyme immobilization, their surface charge behavior will be analyzed using streaming potential data measurements under conditions relevant for the surface functionalization. The enzyme loading will be characterized using TGA curves. The adsorption and desorption of LDH on the different films will be compared using quartz crystal microbalance measurements. Finally, the enzymatic response curves of the final enzyme-functionalized surfaces at different substrate concentrations will be presented and discussed.

5.3.1 Nanostructure and Porosity

SEM micrographs of mesoporous and hierarchically nanostructured silica films are shown in Figure 5.1. In comparison to the mesoporous silica film formed from a stable dispersion of silica aggregates (without addition of polymeric templates for the larger pores), the hierarchically porous film clearly exhibits macropores in the size range of the spherical PMMA pore templates (i.e. around 280 nm). The thickness measured from cross sectional images was $\approx 1.3 \mu\text{m}$ for both. A similar thickness was expected since the formulations were designed in a way that their viscosity would be similar by matching the PVA concentration in each formulation to account for the presence of polymer beads.

Two different methods to obtain quantitative information about the pore sizes, pore volume and porosity were used: nitrogen sorption porosimetry (with BET isotherm analysis) is sensitive for micro and mesopores (because N_2 first condensates in the smallest pores while the partial pressure is increased during the measurement), whereas mercury intrusion porosimetry (MIP) is sensitive to meso and macropores (because larger pores are filled first while the liquid mercury is pressed into the material). Table 5.1 summarizes the main results from the analysis of the synthesized films using both techniques.

Table 5.1 – Summary of porosity and surface area measurements by N_2 sorption and mercury intrusion porosimetry (MIP). d_p : average pore diameter, S_s : specific surface area (BET analysis), V_p : pore volume. ^aaverage diameter d_{50} of the entire distribution; ^bmean diameter of the macroporous range only (i.e. only pores > 50 nm; see right-hand peak of the pore size distribution in Fig. 5.3).

Sample	Method	d_p (nm)	S_s (m^2/g)	V_p (cm^3/g)	Total porosity (%)
Mesoporous	MIP	17	209.0	1.14	73.27
	N_2 adsorption	31	194.2	1.50	85.6
Hierarchical	MIP	15^a ; 181^b	226.0	2.85	84.05
	N_2 adsorption	27	178.6	1.21	68.9

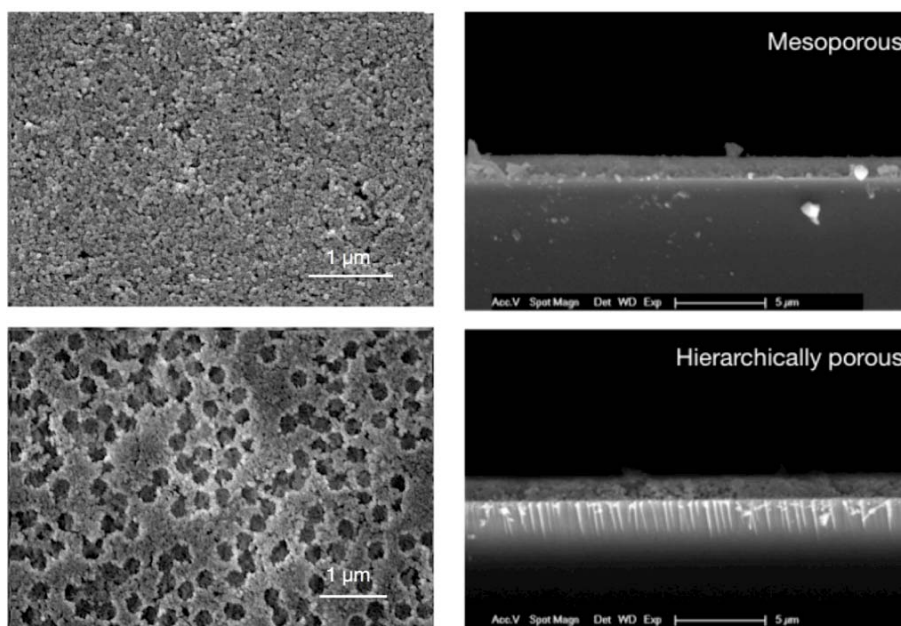


Figure 5.1 – SEM images of hierarchically nanostructured films. Upper pictures: Mesoporous silica film (top and cross-section views) formed from a dispersion of silica aggregates. Lower pictures: hierarchically porous silica film formed using PMMA particles as porogenic templates.

N₂ adsorption data reported in table 5.1 have been extracted from representative adsorption and desorption isotherms obtained for the standard mesoporous films Figure 5.2 along with the resulting pore size distribution. Average pore sizes around 30 nm (Figure 5.2 right) are observed for both types of films. The porosity in the mesoporous range is similar between the two films. This mesoporosity is determined by the spaces created between the silica aggregates after being cast as films. The curve shown in Figure 5.2 (left) is a typical type IV isotherm for mesoporous materials²³² with type H1 hysteresis, indicating a uniform mesoporous system with narrow distribution²³³. Sharp capillary condensation steps have been

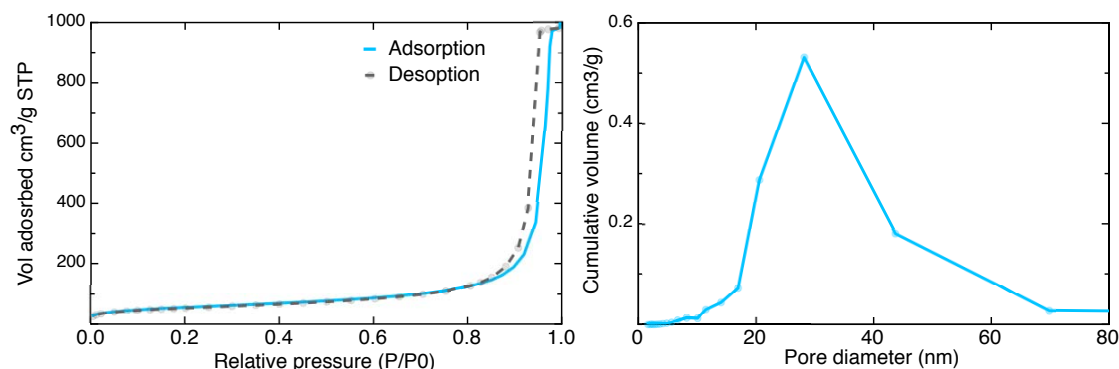


Figure 5.2 – Pore size distributions in the mesopore size range as measured by nitrogen sorption porosimetry, shown here for the mesoporous films.

interpreted as an indication of highly uniform mesopores²³⁴. Unlike pore size distribution, the results from surface area and pore volume differ between both types of films. Both values are smaller in films prepared using macroporous templates (PMMA particles) compared to purely mesoporous films (Table 5.1). Smaller surface area in bimodal porous films can be expected, as the inclusion of macropores reduces the total surface area of the material. Smaller pore volume values for bimodal porous films using the N₂ adsorption technique can be explained considering that the pore volume is calculated after the condensation of the adsorbate takes place. The probe (N₂) size is very small to condensate in the macropores created by the PMMA particles, and in this way the result for total volume can be miscalculated by N₂ adsorption. These results lead to the conclusion that this technique is not the most appropriate to compare both types of porosity in the films.

Mercury porosimetry is generally accepted as the most useful available method for the textural analysis of macropores²³⁵. The results obtained using mercury intrusion porosimetry show a clear difference between the two films in the macroporous range (Figure 5.3). In this case, the PMMA-templated large pores are markedly confirmed in the pore size distribution. The first change of the slope in the intrusion curves from Figure 5.3 (left) is referred to as the threshold or critical pore size, which is related to the size of the first pores where mercury penetrates. The shape of the curves can be compared between similar materials revealing differences in their structures²³⁶ and it reflects the distribution of pores. In the case of the materials evaluated here, a critical pore size around 1 μm can be observed for the hierarchically nanostructured silica (red line). The shape of this intrusion curve shows a change in the slope at around 250 nm. The curve concerning the mesoporous material shows a critical pore size of 100 nm but a first clear slope at 30 nm and finally a steep slope at 10 nm. The figure 5.3 upper right is the derived curve where Dv is the volume pore-size distribution, defined as the pore volume per unit interval of pore radius. Comparing both curves, the bimodal distribution of pores in the hierarchically nanostructured material is evident as compared to the narrowed distributed porosity in the mesoporous material. The pore network structure significantly influences the outcome from MIP measurements. Large pores, referred as ink-bottle pores, may be only accessible to mercury by smaller pores (neck entrances). These pores therefore may not be filled up with mercury until the pressure is increased. This leads to an underestimation of the size of these pores²³⁷ and may be the reason of the lower than expected values for macropores (100 nm in average according the derivative curve in Figure 5.3, upper right). The total surface area and pore volume values for bimodal porous films obtained using mercury intrusion porosimetry are bigger than for the mesoporous films (Table 5.1), which are contradictory to the values obtained by the N₂ adsorption technique. In the case of mercury intrusion porosimetry, the probe (mercury) is able to enter the sample and fill in all the available spaces from a low to high pressure. In this sense, the contribution of macropores as windows to access smaller pores within the material can be a reason why higher values of surface area and pore volume were obtained for the multiscale porous material compared to the mesoporous counterpart. Another way to compare these results is shown in Figure 5.3 (lower panel), where the pore size distribution in relative volume is presented. The hierarchically porous sample showed a larger bimodal porosity, as expected, with half of the total pore volume corresponding to macropores. In contrast, the mesoporous films showed monomodal porosity.

Hierarchically porous silica monoliths were previously synthesized by Sun et al.²³⁴ by a com-

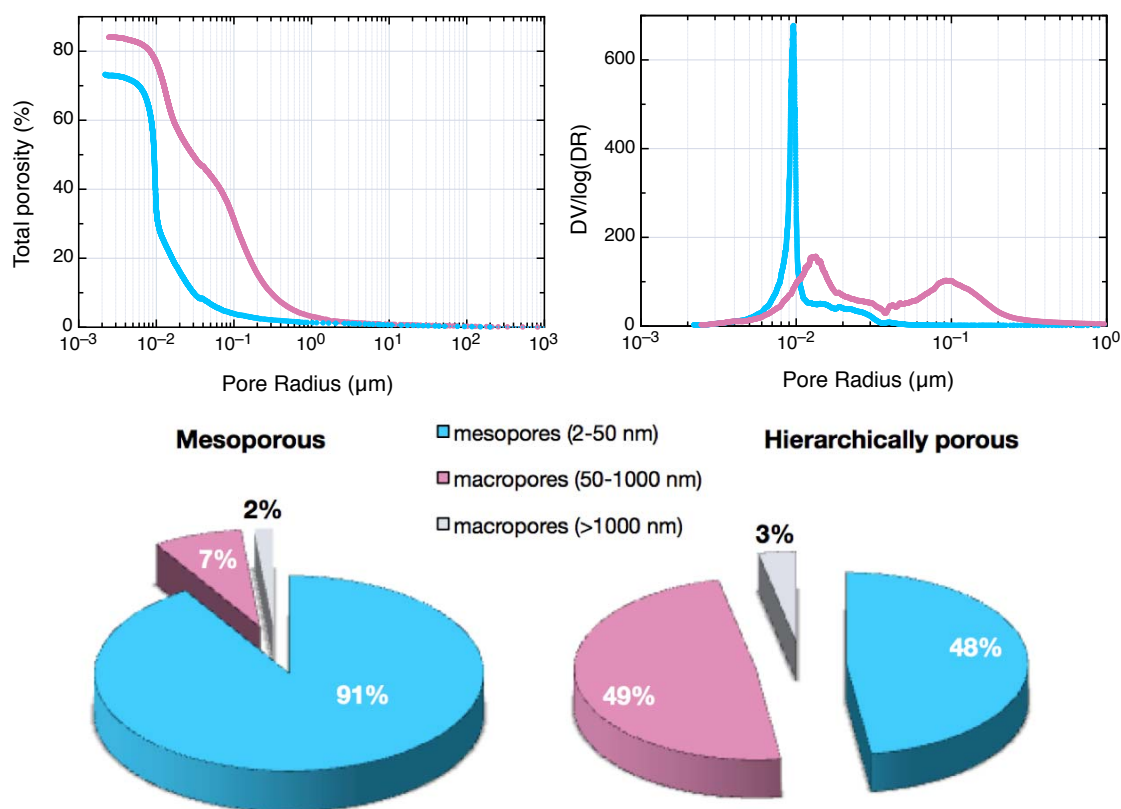


Figure 5.3 – Pore size distributions of mesoporous and hierarchically structured silica films by MIP. Upper panel: Cumulative porosity curve by intrusion (left) and its derivative (right). Lower panel: Pore size distribution (relative volume) from MIP measurements for mesoporous (left) and hierarchically porous films (right)

bination of templates: a highly ordered polymer particle colloidal crystal as macroporogenic templates and plurionics® block copolymers as mesoporogenic templates. Their materials showed high surface area ($330 \text{ m}^2/\text{g}$), with a pore volume of $0.36 \text{ cm}^3/\text{g}$, mesopores in the range of 3.6 - 4.7 nm and macropores up to 200 nm.²³⁴ In comparison to the results obtained here, the total surface area achieved was around $200 \text{ m}^2/\text{g}$, which is lower than the reported values by Sun et al. However, the sizes of mesopores obtained with our method are larger (20-40 nm), as well as the pore volume (values of 1.2 to $2\text{-}8 \text{ cm}^3/\text{g}$, depending on the method).

Finally, the porosity results obtained by these two techniques (N_2 adsorption and MIP) are complementary; the interpretation of these results takes into account the characteristics of each technique, their advantages and limitations and therefore each technique provides valuable information to describe the porous systems in this work.

As a conclusion, polymer templates have successfully contributed to create large macropores in the films. These macropores appear to be well interconnected through mesopores, as observed in the high porosity values obtained for multiscale films (84% total porosity) and well distributed within the film (as observed by SEM imaging). The macropore sizes in the 100-300 nm range perfectly complete the mesoporous framework (below 40 nm in diameter).

The balance between the surface area ($> 200 \text{ m}^2/\text{g}$) and the pore volume ($> 2.5 \text{ cm}^3/\text{g}$) can be considered an excellent compromise for enzyme loading and transportation. The mesoporous films, despite showing relatively similar surface area and total porosity, have monodispersed porosity with average pore sizes below 30 nm. This represents a potential limitation for enzyme diffusion and immobilisation. To investigate further the role of pore size in the diffusion and immobilization of enzymes, quartz crystals microbalance (QCM) measurements will be the focus of the following section.

5.3.2 Tracking of enzyme adsorption and desorption by QCM

QCM experiments were performed at a pH 7.4. At this value, the silica surface from the films is predominantly negatively charged whereas the enzyme, which has an isoelectric point of 8.4, is expected to be positively charged. In these conditions, the electrostatic adsorption of the protein onto the films can be investigated (see Figure 5.4) with two objectives: firstly, to track the time-dependent adsorption of the enzyme onto the two different types of porous films (mesoporous and bimodal meso- and macroporous patches); secondly to study the effect of the pore sizes itowards enzyme diffusion, ultimately affecting their immobilization.

The sensor coated with a mesoporous silica film required several hours for stabilization in buffer (data not shown). After pumping the enzyme into the chamber, the films were incubated for about 10 hours. A sharp drop in the frequency of the crystal quartz resonator was observed in both films as soon as the enzyme solution entered the sensor's chamber, related to the adsorption of enzyme. The mesoporous film showed stabilization after a couple of hours. Conversely, the frequency for the hierarchically porous film kept decreasing, indicating continued adsorption of enzyme over time. This observation can be linked to the diffusion of the enzyme through the porosity of the film via the macropores, which otherwise was not observed in monomodal porous films. However, this interpretation of results regarding the effect of macropores in the transportation of the enzymes is not conclusive. Macropores are considered advantageous for the fast diffusion of species in a multiscale porous material^{109;225}. QCM is very sensitive to changes in mass adsorbed at the surface of the sensors. Whereas the films with mesoporosity do not take up any more enzymes after the first hour of incubation, those with macropores continue to adsorb for several hours despite a lower surface area.

After incubation, the films were rinsed with buffer to remove the non-adsorbed or loosely adsorbed enzyme. The frequency change due to mass loss upon rinsing was larger in the mesoporous film than in the bimodal porous film. Both films stabilized quickly after the rinsing step, indicating no significant mass loss due to enzyme desorption once the rinsing was completed. However, the bimodal film showed a higher enzyme loading after rinsing, demonstrating the advantage of the macropores in the film structure.

In the classic analysis based on the Sauerbrey equation²³⁸, the adsorbed mass is simply proportional to the decrease in the resonance frequency $\Delta m = (-C/n) \cdot \Delta f$. C is the mass sensitivity constant and $n = 1,3,5,\dots$ is the number of the harmonic (overtone) frequency that is analyzed. The quartz crystals used here have a resonance frequency of 5 MHz, and $C = 17.7 \text{ ng cm}^{-2} \text{ Hz}^{-1}$ according to Hook et al.²²⁹. The Sauerbrey equation was developed for solid-like thin films, and its values need to be interpreted with care for soft polymer multilayers,

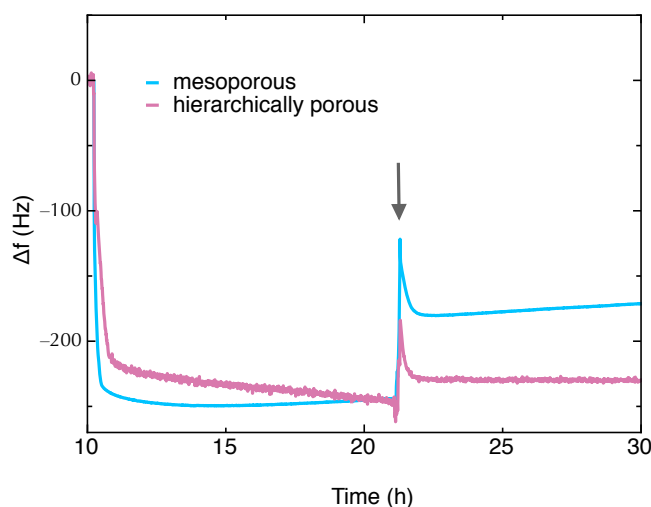


Figure 5.4 – QCM analysis of LDH adsorption and desorption on mesoporous (blue) and hierarchically porous (red) films. QCM sensors were coated with mesoporous and hierarchically porous silica films. The negative frequency shift Δf is related to the adsorbed mass at the surface. The arrow indicates the beginning of the rinsing step with pure PBS buffer at pH 7.4, leading to protein desorption. The hierarchically porous film takes more time to be saturated with the enzyme during adsorption, but it retains significantly more protein during the buffer rinse as compared to the traditional mesoporous film.

which are often highly flexible and viscoelastic²²⁹. In that case, simultaneous monitoring of the dissipation can provide additional information about the softness and viscoelastic properties of the layer^{231;239}.

Comparing the frequency shift due to the enzyme adsorbed on mesoporous and hierarchically porous films following the washout step in Figure 5.4, the ratio $(-\Delta f_{\text{hierarchical}})/(-\Delta f_{\text{meso}})$ is approximately 1.35 for the two films. This suggests that enzyme adsorption on the hierarchically structured films is about 35% higher than for the mesoporous films. If the Sauerbrey equation²³⁸ is used, the adsorbed mass of enzyme is approximately 1360 ng/cm² for the hierarchical films vs. 1005 ng/cm² for the mesoporous films. This is much higher than the typical values around 40-150 ng/cm² published for protein layers on flat surfaces²²⁹. However, these adsorbed mass values should only be used as an approximation for two reasons: 1. the Sauerbrey equation neglects flexibility and dissipation of the protein layers, i.e. a higher mass than the measured value might be adsorbed, but it is not detected²³¹. 2. Hook et al.²³⁰ found that QCM adsorption values were ca. 1.75-3.2 times higher than those measured with optical techniques. According to these authors, the difference is due to the strong hydration of the proteins: mass uptake and hydrodynamic coupling of water to the proteins increases the detected mass. Swelling effects were also discussed by Vogt et al.²³¹

The difference between the QCM curves also indicates that the enzyme is not adsorbed identically in the two different silica films: For the mesoporous film, there is a significant loss of mass during rinsing. This suggests that a part of the enzyme is only loosely adsorbed. By analogy with known QCM data from protein and lipid layers²⁴⁰⁻²⁴², this behaviour can be

explained by the build-up of secondary adsorption layers of enzyme, which are only weakly bound and detach easily during rinsing (on the mesoporous film, some mass loss of LDH is even evident before rinsing, since Δf increases again slightly between 5-10h in Fig. 5.4). In contrast, the enzyme adsorbed on the hierarchically porous film shows much smaller loss during rinsing, suggesting that a higher fraction of the enzyme is directly adsorbed on the silica in a stable manner. If this hypothesis is correct, both a higher enzymatic activity and less experimental variation would be expected for the hierarchical film. This will be assessed later in this chapter in the lactate biosensing tests.

These results reveal qualitatively the positive effect of macropores in the film on the enzyme adsorption on silica films, suggesting that their presence might allow diffusion of a larger amount of enzymes within the film, with possible beneficial repercussions for the final biosensing of lactate. For the assessment of the effect of the nanostructure in the final biosensing application, the post-modification of these silica films with organic functionalities is necessary. This post-functionalization is a multistep process requiring first the incorporation of amino groups, which further react with glutaraldehyde molecules. After each step of this process, a change in the surface charge of the films is expected, which not only can be monitored to evaluate the correct post-modification of the silica films, but allows to better understand the consequences regarding the enzyme diffusion and immobilization. To investigate this in detail, streaming surface potential measurements were performed and their results are presented in the next section.

5.3.3 Streaming potential

The understanding of the surface charge at the solid-liquid interface and the isoelectric point of the films is important considering that enzymes are charged biomolecules. When a surface is charged, ions or larger molecules of opposite charge can be attracted to it, independently if this phenomenon is desired or not. The zeta potential is a property directly related to the electrokinetic charge density of a material surface²⁴³. For particles, it can be measured via the electrophoretic mobility. In contrast, for flat surfaces or porous bodies, the zeta potential can be obtained from measurements of the streaming potential:²⁴⁴ the surface of a film has a charge, and a distribution of both anions and cations at the surface is found at equilibrium. When a liquid flows tangentially to the surface, this equilibrium is disrupted and creates a potential difference known as streaming potential. The measurements of streaming potential at different pressures are then converted into zeta potential values²⁴⁵.

In this work, streaming potential measurements were performed to evaluate both the post-functionalization of silica films and the charge of the films at the pH at which the immobilization of the enzymes takes place (pH 7.4). These measurements enable the evaluation of any potential interaction between these proteins and the films. The synthesized nanostructured films were functionalized successively with an aminosilane (APTES) and with glutaraldehyde after APTES modification. Figure 5.5 shows the pH dependence of zeta potential for functionalized hierarchical porous silica films in the pH range relevant for their isoelectric point (IEP). The zeta potential values for amino-functionalized and bare porous silica were within the expected values. Silica exhibits negatively charged Si-OH groups at neutral pH whereas the amine groups render the surface charge positive. The IEP at pH 3.5 for silica is charac-

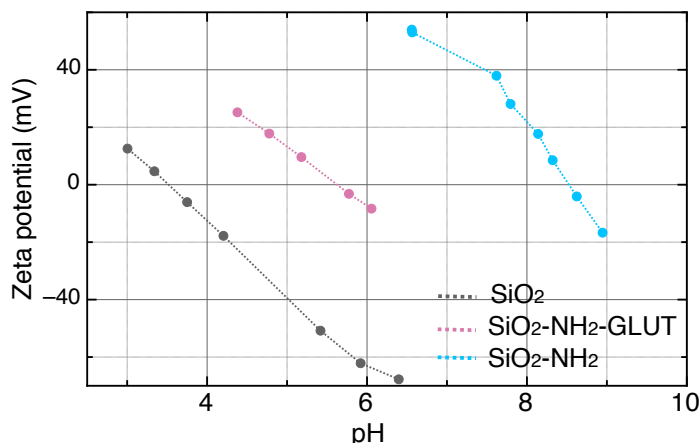


Figure 5.5 – Streaming potential measurements for bare and functionalized hierarchically porous films

teristic for an acidic surface whereas the IEP at pH 8.6 for the amino-functionalized sample represents a basic surface behaviour. From the literature similar values have been reported; for instance, Deere et al. reported values of 3.6 for bare mesoporous silica²⁴⁶. Regarding amino-functionalized porous silica, Dong. et al.²⁴⁷ found that the IEP was dependent on the amount of APTES used for functionalization, ranging from 7.9 to 8.7 for molar concentrations of 0 to 0.2M in solution following a co-condensation method. From the outcomes of these measurements, it can be concluded that bare silica films were suitably functionalized with amino-functionalities.

Finally, the IEP value found for glutaraldehyde-functionalized silica was 5.7. For aldehyde-functionalized silica, the scientific literature appears to lack any reference data. The corresponding zeta potential shown in Figure 5.5 therefore represents the first data for such functionalities on this type of surface film. LDH from rabbit muscle has an isoelectric point between 8.4-8.6²⁴⁸ and the bare silica and glutaraldehyde-modified films showed an isoelectric point around 3.5 and 5.5 respectively. In PBS buffer at pH 7.4, the enzyme and films surface have positively and negatively charged surfaces respectively, allowing electrostatic adsorption of LDH on the porous silica films.

In combination with the knowledge of the enzyme known isoelectric point, the streaming potential measurements therefore provide valuable information in terms of surface charge of the films to allow successful enzyme diffusion in the porous supports. At physiological pH, the enzyme is expected to have a general positive charge whereas the bare silica and glutaraldehyde-modified films have a negative charge. As a consequence, the adsorption of the enzyme onto the silica porous films can be anticipated. This effect competes with the diffusion of the enzyme into the films. Another aspect of this competition is the role of the pore size for enzyme diffusion vs. adsorption. The effect of the nanostructure on the transport of the enzyme molecules during immobilization, and the transport of solutes (substrate and product) in the films will be discussed in more detail in Section 5.3.7.

5.3.4 Thermogravimetry analysis

TGA analyses were performed to investigate the functionalization efficiency of the hierarchically nanostructured films. The resulting curves are shown in Figure 5.6 and a summary of these results is presented in Table 5.2.

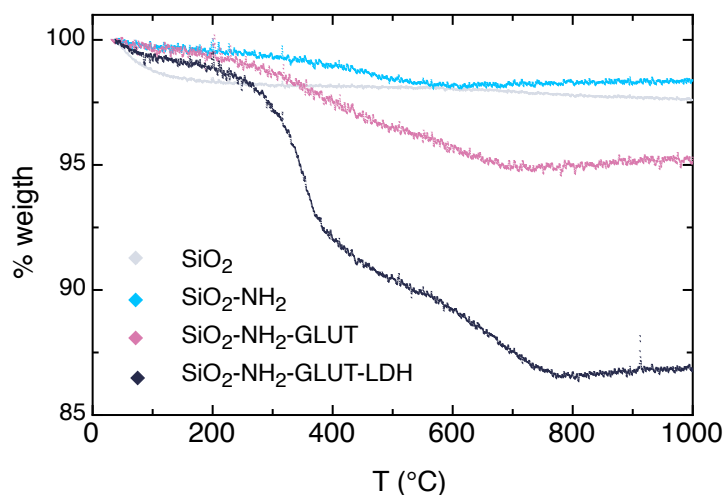


Figure 5.6 – TGA analysis of functionalized hierarchically nanostructured films (red) with APTES (blue), APTES+Glutaraldehyde (green) and APTES+Glutaraldehyde+LDH (orange).

A loss of 2.56% was observed for the bare silica film. This loss corresponds to condensed water (humidity) in the pores, as the weight remained stable after 100°C.

The loss of the amino-functionalized films represents 1.5% of the total silica film weight, corresponding to 25.86 mmol of aminopropyl groups per 100g of silica. The cumulative loss of the glutaraldehyde-functionalized films yields 4.0%. By subtracting the 1.5% contribution of the aminated groups, the mass loss for glutaraldehyde represents 2.5% of the total silica film weight, i.e. 25.27 mmol of glutaraldehyde per 100 g of silica. Due to the close values of amine and glutaraldehyde functionalities in the film, it can be concluded that almost all the amino functionalities from the film reacted with glutaraldehyde.

Results from biomacromolecule adsorption studies in hierarchically porous silica showed that porous silica monoliths with a macropore entrance of about 50 nm retain about 16.6 mg/g of bovine serum albumin (BSA, ≈ 10 nm in size). This amount is much higher than that ≈ 3.4 mg/g of the mesoporous silica materials without such macropore entrances²³⁴. Furthermore, porous materials with or without macropore entrances exhibited similar adsorption capacity

Table 5.2 – Summary of TGA results. Evaluation of the functionalization steps of hierarchically porous films towards enzyme functionalization.

	Cumulative weight loss %	Weight loss per functional group %	mmol/100g SiO ₂
SiO ₂ (H ₂ O)	2.6	2.5	142.22
Amino-silica	1.5	1.5	25.86
Glutaraldehyde	4.0	2.5	25.27
L-lactate dehydrogenase	13.3	9.3	$6.61 \cdot 10^{-2}$

Chapter 5. Lactate detection based on nanostructured and transparent hybrid silica films

for cytochrome C with an average size of 3 nm, (≈ 36.8 mg/g), suggesting that large guest molecules were excluded by the porous silica monoliths without the macropore entrances. When converted into the same units used in this work (mmol/100g of silica), considering that BSA has a molecular weight of 66'463 g/mol, they correspond to $2.5 \cdot 10^{-2}$ mmol/100 g silica for hierarchically structured films and $5.1 \cdot 10^{-3}$ mmol/100 g silica for purely mesoporous films. The values of enzyme concentration in our bimodal porous silica films are higher than the reported values in the literature for typical enzyme loadings in bulk silica²⁴⁹. Finally, the mass loss related to LDH in the film was 9.25 %, representing $6.61 \cdot 10^{-2}$ mmol/ 100g of silica. This value is considerably smaller than the molar amount of glutaraldehyde functionalities in the film, which is predictable as enzymes are biomolecules with larger molecular weights compared to glutaraldehyde. If the weight loss is compared instead for these two functionalities (glutaraldehyde and protein), it can be observed that the amount of enzyme was almost four times larger than glutaraldehyde. Using the molar amount of protein per mass of silica obtained by TGA, a simple approximation of enzyme coverage in the hierarchical and mesoporous films can be made (see Table 5.3) assuming a monomolecular protein adsorption layer and a mean molecular area of adsorption^{230;250} of $1.96 \cdot 10^{-16}$ m² (based on the longest dimension of the LDH molecule of 14 nm⁶¹). For the hierarchical film, this rough estimate suggests that a fraction of approximately 43% of the overall surface area in the porous film is covered by the enzyme, whereas for the mesoporous film the value is around 30%. These values should be understood as approximations only: for a detailed picture of protein adsorption, specialized techniques such as radio-labelling²⁵¹ and surface plasmon resonance (SPR)²²⁹ are necessary. Moreover, for further investigations regarding the optimal loading of enzyme in the films, a study dealing with several film nanostructures would be required. In particular, it is important to optimize the number of macropores per film area and the film thickness in view of the specific application; however, such a study was out of the scope of the present thesis and should be the subject of future optimization work.

Table 5.3 – Approximation of enzyme coverage in the hierarchical and mesoporous films (assuming monomolecular coverage and a mean molecular area of adsorption of $1.96 \cdot 10^{-16}$ m²).

	Hierarchical	Mesoporous
LDH loading, from TGA (mol/100g SiO ₂)	$6.60 \cdot 10^{-7}$	$4.89 \cdot 10^{-7}$
S _s , from BET analysis (m ² /g)	178	194
LDH per specific surface area (mol/m ²)	$3.71 \cdot 10^{-9}$	$2.52 \cdot 10^{-9}$
LDH per specific surface area (molecules/m ²)	$2.23 \cdot 10^{15}$	$1.51 \cdot 10^{15}$
Fraction of S _s covered by LDH (-)	0.43	0.30

5.3.5 Characterization of the enzymatic response of lactate dehydrogenase in solution

To provide the necessary calibration curve to detect lactate with LDH, the enzyme was first characterized in solution. The enzymatic reaction follows the conversion of L-lactate into pyruvate with the concomitant reduction of NAD⁺ into NADH by LDH:



This reaction is reversible. To minimize the effect of accumulation of the product while boosting the conversion of lactate into pyruvate, the buffer TRIS-hydrazine was used. According to the literature, at 25°C and pH 7, the reaction constant of LDH and L-lactate leading to pyruvate and NADH is $2.76 \cdot 10^{-6} \text{M}$, which is low and indicates that the inverse reaction (pyruvate to lactate) is favoured. By raising the pH, the reaction towards products can be enhanced. Additionally, hydrazine reacts with pyruvate producing pyruvate-hydrazone. This compound is not a substrate for LDH and so its involvement in the inverse reaction can be neglected²⁵².

NADH is the analyte optically measured from the LDH activity, as it can be tracked optically with a characteristic absorbance maximum at 340 nm⁶⁵. Figure 5.7 shows the effect of the pH from the medium on the activity of LDH in TRIS-hydrazine buffer. An optimal pH was found by following the activity of the enzyme over time. Sets of [NADH] vs pH curves were obtained. The activity of LDH exhibited a maximum between pH 8.6 and 9.0. From these observations, a value of 8.8 was chosen to build up a calibration curve to be used for further characterizations.

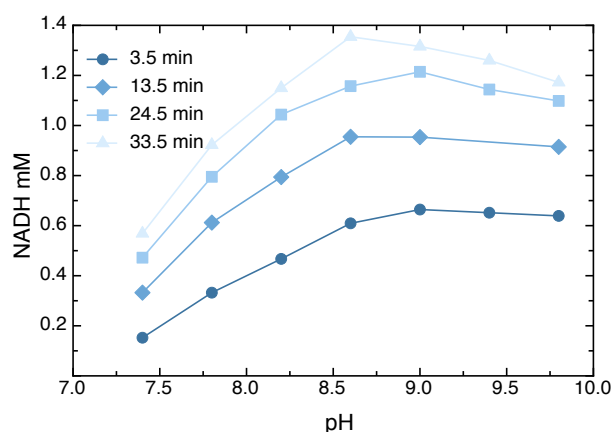


Figure 5.7 – Effect of the pH on the activity of LDH in tris-hydrazine buffer. The activity of a given concentration of enzyme (1 U/mL) in TRIS-hydrazine buffer was followed over time by the accumulation of NADH. The activity of LDH exhibited a maximum between pH 8.6 and 9.0.

The calibration curve for NADH is shown in the Appendix in Figure C.2a. Additionally, the Michaelis-Menten curve for LDH in solution at a concentration of 1 U/mL was obtained (Figure C.2b). The double reciprocal of this graph (Lineweaver-Burk plot, shown in the inset of the graph) was built and from it the values of $V_{\max} = 0.21 \mu\text{mol}/\text{min}$ and $K_M = 5.66 \text{mM}$ were obtained. Nakae and Stoward²⁵³ found values of K_M and V_{\max} from pure LDH isolated from liver and skeletal muscle tissues from mice and compared them to immobilized LDH in polyacrylamide gels. They found values ranging from 8 to 21 mM and 4 to 96 $\mu\text{mol}/\text{min}$ for K_M and V_{\max} , respectively. These values varied depending on the location of the enzyme. Generally, V_{\max} values from LDH in tissues were higher than those obtained from gels and, at the same time, K_M values were higher for LDH in polyacrylamide gels. Values of V_{\max} were remarkably lower in samples with PVA. These results were interpreted as a consequence of the increased viscosity caused by PVA addition, which retarded the diffusion of substrate towards the enzyme. In another report by Powers et al.²⁵⁴, experimental results using LDH as a model to study enzyme kinetics were compared. LDH solutions with concentrations ranging from 6

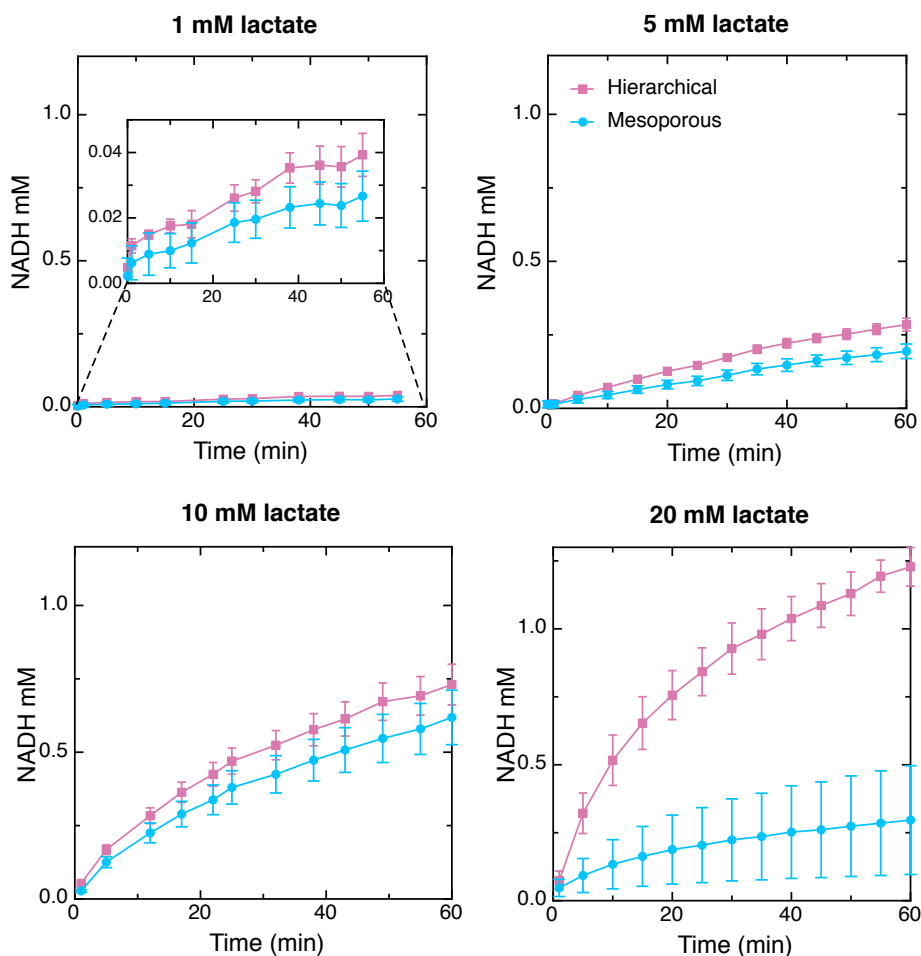


Figure 5.8 – Response curves of enzymatic activity for LDH immobilized in mesoporous and hierarchically porous films. The concentration of NADH was measured over time at different initial lactate concentrations within a range of physiological relevance.

to 19 U/mL were used. The obtained K_M and V_{max} values oscillated around 15 to 46 $\mu\text{mol}/\text{min}$ and 13 to 60 mM respectively. The concentration of LDH used to obtain kinetic parameters in this work is 1 U/mL and the kinetic constants obtained (V_{max} 0.21 $\mu\text{mol}/\text{min}$, K_M 5.66 mM) are reasonable if compared to those reported in the literature for a lower concentration of enzyme.

5.3.6 Enzymatic response of the lactate dehydrogenase-loaded transparent silica films

The enzymatic response of two different types of functionalized enzyme-loaded supports was evaluated as a function of the substrate concentration. Figure 5.8 shows the obtained curves of LDH activity immobilized in mesoporous and hierarchically porous films. The concentration of the reaction product NADH was measured over time at different initial lactate concentrations within a range of physiological relevance. Porous silica films deposited

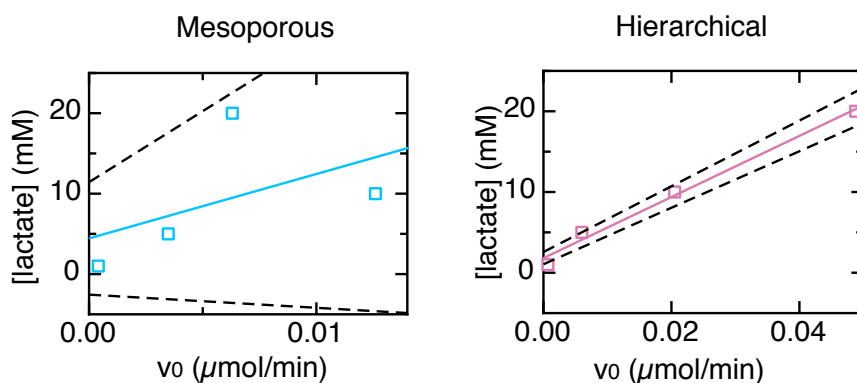


Figure 5.9 – Sensor response curves for lactate detection with LDH immobilized on mesoporous (left) and hierarchically structured (right) films. The data were obtained by extrapolating v_0 from the lactate concentration vs time data from fig. 4.9 at different substrate concentrations. The solid lines are fits obtained by linear regression to the equation $[lactate] = a \cdot v_0 + b$. The dashed lines indicate the maximum error range obtained with the linear fits for $a \pm \Delta a$ and $b \pm \Delta b$.

on glass were immersed in a TRIS-hydrazine buffer at pH 8.8, and the conversion of NAD^+ into NADH was followed over time. The measured concentration of NADH increases with the initial concentration of lactate in solution. Generally, LDH-loaded hierarchically porous films produced higher concentrations of NADH than mesoporous films at a given time. Typical standard deviations of these values are below 6% for the hierarchical films. For the mesoporous, standard deviations are considerably higher if the films are used repeatedly, as in this study, possibly due to changes in the enzyme activity after several rinsing cycles during the biosensing measurements. This observation was confirmed in all cases at any initial concentration of lactate.

The produced NADH by enzymes immobilized in mesoporous and hierarchically porous films has been plotted for four different lactate concentrations (Figure 5.8). Then, the lactate concentration was plotted as a function of v_0 , i.e. of dc/dt as $t \rightarrow 0$ (Figure 5.9). An example for the extrapolation of v_0 from the dc/dt data is shown in the Appendix in Fig. C.3. Linear regression fits show that the hierarchically porous films provide reproducible data quality with low error compared to mesoporous films. The slope $a \pm \Delta a$ of the $[lactate]$ vs. v_0 curve is a characteristic response constant for each biosensing surface, and its ‘quality’ is indicated by the dashed lines, indicating the range given by the standard deviations for the slope $\pm \Delta a$ and for the offset $\pm \Delta b$ in Figure 5.9. The specific numerical values for a and b need to be determined for a given surface. For the example shown here, the curve for the hierarchically porous films is significantly better defined than for the mesoporous film ($\Delta a/a \approx 7.3\%$ vs. 125%), indicating that the hierarchical films are far more robust for biosensing application.

Note that the presentation of data in the form of plots of analyte concentration vs. v_0 is used here because it provides the relevant information that the user needs during the utilisation of the films for lactate biosensing: $[lactate]$ is wanted, and v_0 is measured. The known value of the slope (e.g. $a \approx 3.79 \cdot 10^5$ min/L for the hierarchical film) and offset value then allow the user or the software to convert the measured v_0 into concentration values. For sensor calibration and

Chapter 5. Lactate detection based on nanostructured and transparent hybrid silica films

benchmarking, the inverse plot of v_0 vs. [lactate] is used⁷, i.e. output vs. input (measurable quantity vs. analyte concentration), and the value of its slope $s=a^{-1}$ is the sensitivity constant of the sensor. For example, the sensitivity constant of the hierarchical film is $2.65 \cdot 10^{-6}$ L/min, and for the mesoporous film it is $1.25 \cdot 10^{-6}$ L/min, meaning that the hierarchical film provides roughly a two-fold increase in sensitivity when tested on supports of identical size. A direct comparison of these slopes between different types of sensors is not meaningful because the measured properties are physically different, and the used enzymes, physicochemical detection schemes and scales of the sensor are not standardized (for example, a characteristic sensor curve of a cell-based optical fiber sensor is given in relative light intensity vs. [lactate]⁷, or amperometric biosensors¹ are characterized by plotting the measured current in μA vs. [lactate]). The key is therefore to obtain a well-defined and robust response curve for the range of concentrations relevant to the application under the given constraints (here: optically transparent thin films with sub-micrometer thickness), rather than just the optimization of its slope.

In the present study, the near-linear part of the v_0 vs. [lactate] curves is obtained, whereas the stabilization plateau is never reached. Therefore, these curves indicate that K_M would be in a range above the substrate concentrations studied here, which were selected for their physiological relevance. This phenomenon was previously observed in mesoporous materials and in alginate gels, where higher K_M and lower V_{max} were found as compared to the free enzyme⁹². According to Laidler and Bunting²⁵⁵, there are several reasons to explain why the apparent kinetics of an enzyme can be different when it is immobilized: firstly, the immobilization may impose a different protein conformation, which may cause the enzyme to behave kinetically different. Secondly, the environment around the enzyme is different compared to the enzyme in solution. Thirdly, the availability of the substrate locally in the pores may be different to the concentration in solution. Lastly, diffusion effects play a role, restricting the accessibility of the substrate to the enzyme and thus affecting the kinetics when it is immobilized. Since the objective here has been to develop a transparent functionalized surface to detect lactate via immobilized enzymes at physiologically relevant concentrations (and not to obtain the full range of Michaelis-Menten kinetics), the v_0 vs. [lactate] curves provide enough information as long as a clear, reproducible relationship between substrate concentration and the measurable quantity v_0 can be obtained.

The difference in performance of mesoporous vs hierarchically porous films is considered to be related to the effect of the films nanostructure on the enzyme diffusion during immobilisation, which ultimately results in higher enzyme loadings in milt-scale porous films. Moreover, the difference in stability regarding multiple measurements on a single functionalized patch can possibly be related to the same reasons. In the following sections, a discussion regarding mass transport differences in these two materials is presented to support these hypotheses.

5.3.7 Discussion of mass transport of enzyme and reactants in the nanostructured silica films

As shown in the previous sections, LDH-loaded hierarchically porous films produced higher concentrations of NADH than mesoporous films in all cases at any initial concentration of lactate. An explanation for this behaviour can be related to a difference in the enzyme loading for the different films. Higher enzyme loading is therefore expected in hierarchically nanostructured films as compared to mesoporous films, in agreement with the QCM results discussed above.

Mass transport for lactate biosensing with the nanostructured silica films described in this chapter can be considered important in three different situations:

1. *Enzyme transport* to the silica surface during immobilization;
2. *Diffusion of the substrate and the cofactor* to the immobilized enzyme during sensing experiments; and
3. *Transport of the reaction product* used for detection away from the enzyme.

The restriction in pore size from mesoporous films might limit the diffusion of the enzyme through the film, reducing the access to the pores and therefore affecting the immobilization. In hierarchically porous films, the macropores could facilitate this diffusion, increasing the access of the enzyme to the pores and resulting in higher amount of immobilized enzyme. Additionally, macropores can facilitate a faster diffusion of lactate to the immobilized enzyme and consequently, promote a faster production of NADH towards the solution as compared to mesoporous films.

In the following sections, the role of diffusion of the different components will be assessed both for the transport of the enzyme during immobilization, and for the transport of the substrate and the product during sensing experiments. First, the roles of pore size and tortuosity will be discussed. Both effects have been investigated in the literature; Veith, Pratsinis and coworkers¹⁴² investigated the restricted diffusion in silica particles and measured diffusivity by pulsed field gradient diffusion NMR. These authors summarized different approximation correlations commonly used for the tortuosity^{139–141} and pointed out that these correlations all give similar trends, but they only provide approximations, rather than rigorous predictions. Following the model from Suzuki and Smith¹⁴¹, the tortuosity τ as defined in the background chapter can be estimated if the porosity ϵ is known as

$$\tau = \epsilon + 1.5(1 - \epsilon). \quad (5.1)$$

Using the porosity values ϵ from Table 5.1, the resulting tortuosity values are all in a rather narrow range from $\tau = 1.072$ to $\tau = 1.115$. The ratio ϵ/τ serves as a correction factor^{84;142} allowing to estimate the effective diffusivity through tortuous materials as $D_t \approx D_0 \cdot \epsilon/\tau$. For the films synthesized here, the resulting factors are $\epsilon/\tau \approx 0.64$ for the mesoporous films and $\epsilon/\tau \approx 0.80$ for the hierarchical films.

Chapter 5. Lactate detection based on nanostructured and transparent hybrid silica films

In addition to tortuosity, the ratio of the molecule size vs. pore size $\lambda=r_{\text{molecule}}/r_{\text{pore}}$ also influences diffusion, as described in the background section. This pore size effect is reflected in a second correction factor $F(\lambda)$. Different theories are available in the literature to calculate $F(\lambda)$ ^{84;129;130;142}. Here, the numerical results from Paine and Scherr¹³⁰ given in the background chapter in Fig. 2.18 are used, i.e. $F=1/\kappa$ with $\kappa(\lambda)$ from Fig. 2.18. Using an average pore diameter around 30 nm (Table 5.1), this pore size factor can be assumed to strongly slow down diffusion of the enzyme through the mesopores, but not the diffusion of lactate or NADH: The diameter ratio enzyme:mesopore $\lambda \approx 0.3 - 0.7$, resulting in $F(\lambda) < 0.2$, meaning that the diffusivity of LDH through 30 nm mesopores is significantly reduced. In contrast, the diameter ratio between lactate and the mesopores or between NADH and the mesopores is much smaller ($\lambda < 0.1$), meaning $F \approx 1$.

Taking into account both the tortuosity and the pore size effect, the overall effective diffusivity can be estimated from the bulk value D_0 and the corrections in Table 5.4 as

$$D_{\text{eff}} \approx D_0 \cdot (\epsilon/\tau) \cdot F(\lambda). \quad (5.2)$$

The resulting D_{eff}/D_0 values are summarized in Table 5.4. The strongest reduction in diffusion is found for LDH in the mesoporous films, where it is about an order of magnitude slower than in the free solution. Comparing the pore size factor F with the tortuosity effect (ϵ/τ) it seems that the molecule:pore size ratio makes the biggest contribution to this reduction. For all other cases, the reduction is relatively moderate.

The estimation given above follows the assumptions made for 3D materials. For thin films, it is important to keep in mind that the total size (thickness) is not much bigger than the macropores. Inside the large macropores close to the the surface of the film, it is likely that the tortuosity effect is even smaller than the τ given above suggests and can then be neglected. Also, the strong reduction in diffusion of LDH into the mesopores means that the immobilized enzyme is located close to the open surface of the silica films. A side effect of this is that the tortuosity might become less relevant for the biosensing experiments because the enzymatic reaction does not occur deep inside the mesoporous structure.

Table 5.4 – Summary of parameters for the estimation of effective diffusivity in mesoporous and hierarchically porous silica films. ϵ : porosity (from Table 5.2), τ : tortuosity (from Equation 5.1), F : pore size factor for the effective diffusivity¹³⁰ (with $F=1/\kappa$ from Fig. 2.18. $F = 1$ corresponds to free diffusion), d_p : pore diameter used to estimate F (for mesopores: d_p from porosimetry, for hierarchical/macropores: d_p from SEM images).

Molecule	Medium	ϵ	τ	(ϵ/τ)	d_p (nm)	F	D_{eff}/D_0
L-lactate	mesoporous	0.732	1.130	0.64	30 nm	0.93	0.60
NADH						0.87	0.56
LDH						0.17	0.11
L-lactate	hierarchical	0.856	1.072	0.80	250 nm	0.99	0.79
NADH						0.99	0.79
LDH						0.87	0.70

Diffusion of lactate (or the cofactor NADH) is important for biosensing, but it can be assumed that this is not the limiting factor for the quality of the biosensing films: lactate and NADH easily diffuse through the pore sizes relevant here as they are much smaller than both the mesopores and the macropores. Tortuosity of the mesopore network may slightly slow down lactate diffusion deep inside the film, but this is not relevant if there is no enzyme present in those 'deep' pores. Therefore, the important restriction to diffusion is the one for the enzyme during loading/immobilization, since the films are actually only functional in places where the LDH can penetrate. This point will also be discussed further below using visual modelling results.

5.3.8 Visual modelling of enzyme immobilization and solute transport

Blender™ is an open source software that can be used to build 3D models using mesh structures. The software contains a particle physics module that allows to perform simple simulations of particles moving in the designed 3D geometries, including Brownian motion, and interaction with objects such as adhesion and repulsion (wall potential), friction, external flow, etc. Extensions to biophysics simulations are also available²⁵⁶.

For the study of enzyme and solute diffusion, silica films are schematized as a three-dimensional close packed assembly of silica aggregates, each of them formed by spherical silica particles. Electronic micrographs from the silica as treated and used in this work to synthesize films revealed nanostructures ranging from 40 to 60 nm in diameter (see micrographs in the appendix). These "small" silica nanostructures will be used here as the basic unit for the visual modelling of the films. In the visual model developed here, they are schematized as spherical silica spheres of 50 nm.^c Simulated silica aggregates are created in the software from multiple copies of the unit silica spheres, and these aggregates are then arranged in random orientation to form a model of the mesoporous film. For hierarchically porous films, additional macropores (diameter \approx 260 nm) were included, following the different shapes observed in the SEM images (single spherical pores, double pores, merged spherical pores). The films have a thickness of about 800 nm. For the simulation, the porous film is placed in a thin 3D box with impermeable walls (x dimension = 1.95 μ m, z dimension = 1.5 μ m, y dimension = 200 nm)

Moreover, LDH molecules are represented by spherical particles of 15 nm in diameter, the size of the largest dimension from LDH 3D structure. The diffusion of the enzyme molecules was simulated with the 'particle physics' module in Blender. 6000 LDH molecules were generated as spheres emitted from a plane above the film in the first frame of the simulation. Gravity and all other external forces and initial velocities were set to zero, 'Brownian dynamics' was chosen to generate random motion of the particles, 'size deflect' using the sphere radius was chosen for the collision behavior, and 'RK4' (4th order Runge-Kutta) was selected as the integration method to calculate the particle movement. To make sure that the numerical values for the Brownian motion in the Blender software are realistic, they were 'calibrated' using the bulk diffusivity D values from the Background chapter (see Fig. C.10 in the appendix).

^cAccording to the specifications from the supplier, the untreated silica powder used to form these films is composed of aggregates with an average size of 200-300 nm, which again consist of linear chains of primary silica nanoparticles of 14 nm in diameter (bulk density of 2.2 g/m³). It is likely that the 40-60 nm spheres observed by SEM are composed of those primary particles, however, they could not be observed individually and for the visualization the 50 nm unit will be used to allow efficient modelling.

Chapter 5. Lactate detection based on nanostructured and transparent hybrid silica films

Chemical interactions with the wall can be accounted for by different means: 1. as an effect that changes the considered size scale (e.g. salt concentration changes the hydrodynamic radius of the protein, or the effective pore radius including electric double layer), or with a partition coefficient⁸⁴. In the present case, physical protein adsorption at the wall is considered to be the relevant interaction. Part of it is due to electrostatic effects, which can be reversed by changes in solution conditions. However, protein adsorption also has an important thermodynamic component, and it is known to be effectively irreversible²⁵⁷ under mild solution conditions^{229;230;246;258} (very low negative free energy of adsorption due to changes in protein conformation upon adsorption). For the overall diffusion, this means that diffusive motion of the enzyme ends once it comes into contact with the walls. In the visual modelling described below, this effect will be included by using a "sticky" wall (hard wall potential) to simulate protein adsorption, i.e. the wall of the pore traps the enzyme upon contact.

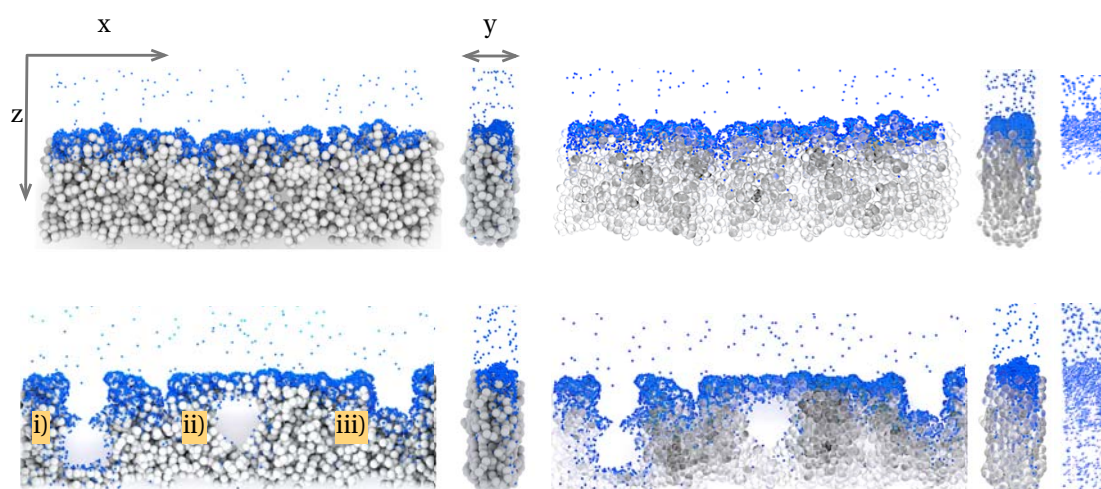


Figure 5.10 – 3D visualization of enzyme adsorption in meso- (top) and multiscale (bottom) porous silica films, and as solid (left) or transparent (right) objects visualized by BlenderTM (front and side view images). The enzyme molecules are shown as blue spheres. A transparent thin box is used for the simulation region (x dimension = $1.95 \mu\text{m}$, z dimension = $1.5 \mu\text{m}$, y dimension = 200 nm). In hierarchically porous films: i) two macropores connected and accessible from the surface, ii) a buried macropore, and iii) a single macropore accessible from the surface. Images correspond to $\approx 500 \text{ s}$ after the start of the visualization.

Figure 5.10 shows representations of mesoporous (top) and hierarchically porous (bottom) films immersed in a solution of LDH. The film structures are displayed in two different set of images: solid objects (left images) and transparent objects (right images), with the same modelling parameters. Transparent images allow to better visualize adsorption of the enzyme inside the film. The side view images of the films allow to locate over time the enzyme molecules along the z axis (film thickness). The images are taken after the enzyme has been homogeneously distributed around the medium by diffusion (see Appendix for a sequence of images). In mesoporous films, LDH molecules are observed at the upper section of the silica film after exposure to the LDH solution and to a depth of 150 to 200 nm within the film. In hierarchically porous films, LDH molecules were found at deeper lengths from the surface of the film compared to the mesoporous films and due to the presence of macropores. Different

possibilities of localization of these macropores are illustrated in Figure 5.10 (bottom images):

- i) In a first scenario, a macropore at the surface of the film is connected to another macropore "buried" within the silica film. In this case, LDH molecules are observed all along the walls of these two macropores. The presence of these two larger voids increases the surface area of the film to allow higher amount of enzyme to bind the surface of the pore, as compared to mesoporous films. The presence of macropores facilitates the bulk-like diffusion of the enzymes through the macropores, allowing LDH to reach the macropores' walls and diffuse to a certain depth in the film as observed in figure 5.10 (top images). In this later case, the diffusion is restricted by the silica film nanostructure. An additional factor is the connection window between macropores. As an example, a narrow window was chosen to demonstrate the effect on enzyme diffusion. As this connection becomes narrower, it is also more restrictive to allow the enzyme to diffuse in a bulk-like diffusion fashion. The amount of LDH at the surface of the second macropore appears slightly smaller compared to the macropores from the surface.
- ii) In a second scenario, a macropore is buried within the film and only accessible by a network of mesopores created by the silica aggregates. After diffusion, LDH molecules are observed mostly at the surface of the film. However, some of them went through the mesopores and reached the macropore, and were able to adsorb along its surface. Additionally, some of the LDH molecules could also diffuse deeper in the z axis and along the x and y axes through the mesopores. However, it can be noticed that the amount of enzyme at the surface of the macropore is smaller, as compared to the first scenario, as LDH molecules diffuse first in a restrictive way through the mesopores before reaching the macropore.
- iii) Finally, a third scenario consists of a single macropore accessible from the surface. As in the first scenario, the surface of the macropore is exposed to the LDH solution and its surface is fully covered with LDH. Some of the enzyme molecules diffuse through the mesoporous network within the film.

The side view images of the films, particularly the transparent version of them, reveal a higher amount of LDH along the z axis (thickness) of hierarchically porous films compared to mesoporous films. These visual simulations support the hypothesis made during the discussion of QCM results. In that section, LDH was assumed to deposit on top of the films, and after the incubation time, the enzyme was no longer able to diffuse through the mesopores. During the washing step, the non-adsorbed enzyme was removed from the silica surface, and only LDH strongly bound to the surface remained. In a hierarchically porous system, the adsorption of LDH required a longer stabilization time than the mesoporous system, and after the washing step, the amount of enzyme retained was higher.

The 3D models shown here can also be used to plot a distribution profile through the film (Figure 5.11). Two profiles of adsorbed enzyme amount vs. film depth obtained from the side view image of the particle-based visual modelling. Both profiles were plotted from the particle data along the z axis, starting with the identical number $n = 6000$ of enzyme molecules diffusing from the bulk solution and adsorbing on the film after letting the visualization run for

Chapter 5. Lactate detection based on nanostructured and transparent hybrid silica films

500 s. Confirming the visual information in the previous figure, the profile of the hierarchical film shows that a higher amount of enzyme is adsorbed and that the loading penetrates deeper into the film. Besides, higher amount of enzyme unable to diffuse through the film is observed in mesoporous films at the surface (0-200 nm) compared to hierarchically porous films, confirming the results from QCM analysis where loosely adsorbed enzyme is washed away after the incubation period of several hours (enzyme not adsorbed within the pores).

Additionally, the simulations also provide the location over time of the diffusing molecules. This allows to compare the trajectories of selected molecules in different locations. An example is shown in Figure 5.12. Five LDH molecules were placed in the solution and let to diffuse with Brownian motion according to the diffusivity in free solution D_0 . The same five molecule were also placed inside the mesoporous region of the film (adsorption was neglected, i.e. the silica particles in this simulation were not "sticky"). Parameters for Brownian motion of LDH were exactly the same in both cases (using D_0 in the free solution), therefore the restriction of diffusion for the mesoporous case is entirely due to the presence of the porous film. The "random walk" trajectories for both cases are plotted, as well as the mean squared displacement (MSD) vs. time curves obtained from these trajectories. The slope of the MSD curve for the LDH trapped in the film is considerably lower, meaning the effective diffusivity inside the film is strongly reduced.

Considering the structure of the films and the visualization of diffusion presented here, the following conclusions can be formulated:

- i) The presence of macropores enhance the loading of enzyme in the films as these voids:

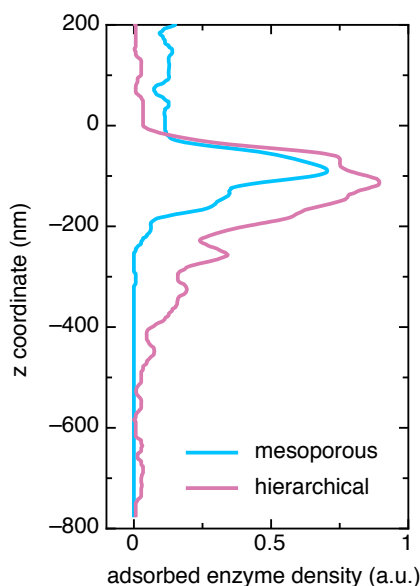


Figure 5.11 – Profile of adsorbed enzyme amount vs. film depth obtained from the side view image of the particle-based visual modelling. Both profiles were obtained starting with the identical number $n = 6000$ of enzyme molecules diffusing from the bulk solution and adsorbing on the film after letting the visualization run for 500 s.

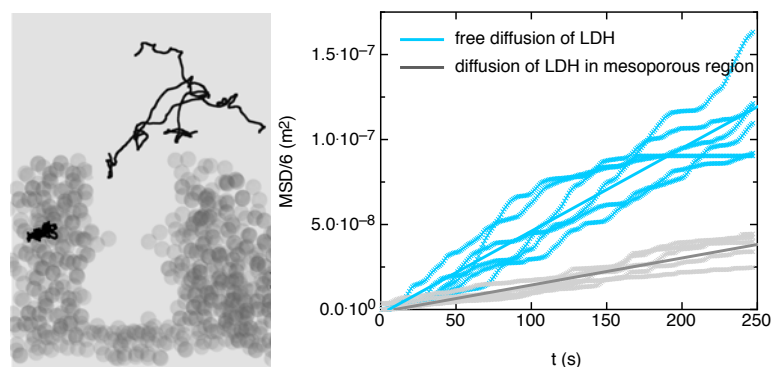


Figure 5.12 – Left: Visualization of Brownian motion of five LDH molecules in the free solution vs. trapped inside the schematized mesoporous film. Note that for this visualization the adsorption of LDH on the solid surface was switched off (i.e. LDH collides with the solid, but does not stick). Right: Mean squared displacement (MSD or $\langle \Delta x^2 \rangle$) for the two cases shown in the image. D_0 is set as $5 \cdot 10^{-11} \text{ m}^2/\text{s}$ in both cases and the only difference is the location of the LDH molecules. The free LDH moves according to D_0 (blue line), but the trapped LDH moves according to D_{eff} (green line).

- Increase the surface area of the film directly exposed to the enzyme in solution
 - Increase the amount of enzyme that can diffuse within the film via the macropores' walls and through the mesopores and smaller macropores created by the silica aggregates
- ii) Macropores accessible from the surface and connected to other macropores enhance the loading of enzymes. Wider connecting windows among macropores reduce diffusion constraints of the enzyme
 - iii) In the absence of macropores, LDH is able to diffuse only to a certain depth of the film due to the restriction of enzyme size vs pore size. The competition between diffusion and adsorption discussed already in the previous sections is confirmed visually. A loosely adsorbed LDH on top of the films could be possibly removed from the surface after several rinsing cycles, affecting the amount of enzyme at each measurement made and increasing the error (low sample to sample reproducibility). This effect was observed more drastically in mesoporous films. See figure 5.8
 - iv) Concerning the examples of macropore localization in the film and the amount of enzyme which is able to diffuse along the thickness of the film, it is plausible that thicker films would not guarantee higher loadings, unless the macropores are highly connected. However, another constraint related to the transparency of films must be taken into account, as thicker films following the approach presented in this work become opaque. Also, a practical consideration is to keep the time for the enzyme loading step short, as thicker films need much longer loading times. Optimization work on the loading process would then be required to improve loading of enzymes in these systems.

Finally, based on the schematic simulation of LHD immobilization, an additional visualization was performed to better understand the transport and enzyme reaction with lactate during

Chapter 5. Lactate detection based on nanostructured and transparent hybrid silica films

biosensing. While actual reaction kinetics can not be simulated using the Blender™ software used here, Fig. 5.13 shows an illustration of diffusion and substrate/enzyme contact during biosensing. LDH (blue spheres; 3000 molecules were used for the example) was made to adsorb in the modelled double pore of a hierarchically porous film (spherical macropore near the surface of the film, connected to a deep 'buried' macropore), as was done previously in Fig. 5.10. The ratio between the diameter of the window connecting the pores vs. the macropore diameter is 0.25. Then, this adsorbed LDH layer was used as a new collision boundary (i.e. now the enzyme is part of the pore geometry). Then lactate was made to diffuse from the solution using the diffusivity of lactate in water from Table 5.4. For the modelling, lactate was defined as a sphere of 0.75 nm diameter (5000 lactate molecules were used; note that the green spheres representing lactate in Fig. 5.10 are scaled up by factor 5 for better visibility. For reference, their actual size is shown in the Appendix). While the lactate disappears during the reaction, the close-up images in the figure are here to illustrate all lactate molecules that have collided with the enzyme. These images demonstrate that enzyme/substrate contact strongly decreases along the depth of the pore, meaning that most of the substrate is already consumed before it reaches the deepest portion of the pore. The narrow connection window between the two cavities has a strong influence on the diffusion of lactate within the films. The visualization shown here is therefore expected to be helpful for future work aiming at the optimization of the macropore geometries in enzyme supports.

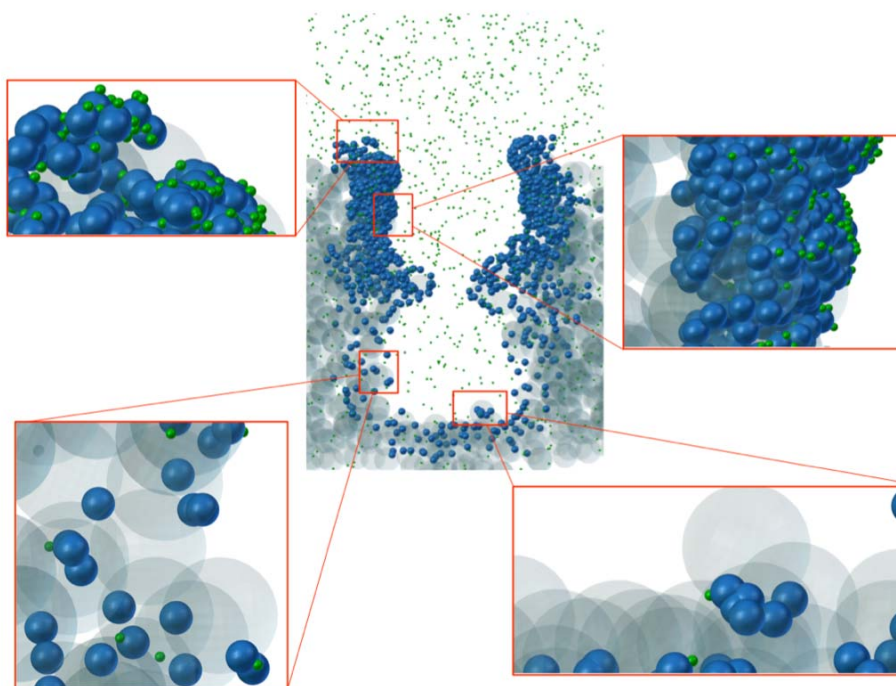


Figure 5.13 – Visual modelling of diffusion and substrate/enzyme contact during biosensing. LDH (blue spheres) was made to adsorb on the surface of the hierarchically porous film, as in Fig. 5.10. Then, the adsorbed LDH layer was re-used as a new collision boundary, and this time the lactate (green spheres) was made to diffuse from the solution. While the lactate disappears during the reaction, the close-up images here illustrate all lactate molecules that have collided with the enzyme. For reference, their actual size is shown in the Appendix.).

5.4 Summary and Conclusions

In this chapter, the synthesis of mesoporous and hierarchically nanostructured films was described. The films were synthesized by a simple top-down approach using silica powders and polymeric particles as porogenic materials to synthesize macropores. The porosity analysis revealed the presence of two length-scale pores: mesopores (10 nm) formed inside and between silica nanoparticles aggregates (30 nm) and macropores (230 nm) produced from the inclusion of polymer particles as templates in the formulation. The functionalization of these silica films (IEP 3.5) with amino functionalities rendered the surface positively charged with an IEP of 8.6, whereas the reaction of the amino groups with glutaraldehyde changed the IEP to 5.7. Adsorption and desorption of lactate dehydrogenase tracked using QCM measurements show that LDH loading is higher and more stable in hierarchically porous films compared to mesoporous ones. Lactate dehydrogenase was immobilized on the silica films covalently using glutaraldehyde as a linker between the amino-functionalized silica and the enzyme. The films with immobilized enzyme were characterized by measuring the reduction of the cofactor (NADH) over time at different lactate concentrations. Hierarchically nanostructured films are advantageous for increased enzyme loading and overall performance as compared to traditional mesoporous ones. Higher enzymatic activity on the hierarchical films allowed more sensitive and more robust detection of lactate. This advantage is evident from the better precision in the linear response of the biosensing films, as obtained by linear regression.

Diffusion of LDH in mesopores is slowed down mostly due the pore size effect. This was confirmed both by estimation of the effective diffusivities and by visual modelling. Mesoporosity provides a high specific surface area, which is beneficial for enzyme immobilization if the mesopores are large enough so that enzyme diffusion is still feasible. In hierarchical films, macropores make more of the high specific surface area provided by the mesoporous structure by rendering this surface area accessible for the enzyme immobilization. The most effective macropore geometries are those which are accessible from the films surface. Buried pores are less effective: although the substrate and product can diffuse with only small reductions in effective diffusivity, enzyme transport into deep and buried macropores is strongly limited and only small amounts of enzyme are expected to be immobilized in the deepest pore regions. In conclusion, the hierarchically porous films synthesized here are highly suitable as optical coatings e.g. on measuring cells (cuvettes), optical fibers, or glass windows while retaining transparent properties. The macropore size range and number of macropores per film area are expected to be important parameters for design optimisation in view of biosensing efficiency and optical transparency.

6 Layer-by-layer assembled nanocomposite films and particles for enzyme-based lactate biosensors

In the previous chapter, sensitive porous patches functionalized with the enzyme lactate dehydrogenase were obtained for optical lactate detection by the incorporation of multi-scale porosity in thin silica films. While those biosensing films were sensitive to L-lactate, they required the presence of a cofactor (NAD^+) in solution. An alternative choice for the enzyme, lactate oxidase (LOx), does not require a cofactor. Instead, its reaction product H_2O_2 can be optically detected using an oxidation-reduction scheme, monitoring the oxidation state of separate indicator molecules, such as cytochrome C (CytC), a heme-containing protein. Here, a novel biosensing scheme for lactate detection is presented, using LOx in combination with CytC to synthesize not only lactate sensitive patches, but also micrometric particles and thus addressing the general objectives of this work towards the development of particle based systems for lactate detection. For the synthesis of lactate sensitive patches, their incorporation into the system is achieved by the layer-by-layer deposition technique, forming polyelectrolyte layers composed of polyethylene imine (PEI) and polyacrylic acid (PAA), allowing the adsorption of CytC on top of the enzyme-functionalized silica films. Both mesoporous and hierarchically porous silica films are evaluated and compared as the basis for these multilayer structures using quartz crystal microbalance (QCM) experiments, absorbance spectra and by evaluation of the time dependend oxidation of CytC. In addition to the film-based detection approach, a final part of this chapter focuses on the formation of LOx–CytC particles using porous calcium carbonate particles as sacrificial templates for the synthesis of lactate micrometric probes. The resulting protein-based particles can be used directly for optical detection of lactate. Moreover, they are interesting materials for future developments of rapid optical detection methods in liquid suspensions, for example in cell media.^a

^aThis chapter is the result of a 6-months research stay at the laboratory of Nanostructured Interfaces and Materials Science Group (NIMS) led by Prof. Frank Caruso at the University of Melbourne, Australia. The funds for this stay were generously obtained from the Swiss National Science Foundation via a granted proposal within the framework of their Doc.Mobility programme. All the experimental work has been entirely performed by the PhD candidate, with the exceptions explicitly mentioned.

6.1 Introduction

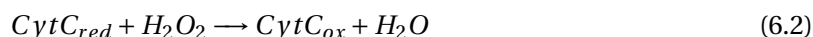
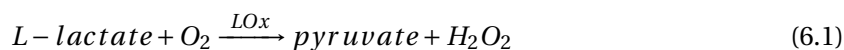
Some of the challenges of this thesis concerning the reproducible synthesis of transparent, porous supports for the immobilisation of enzymes have been addressed in previous chapters. This study has led to the development of responsive patches for lactate quantification. However, others challenges remain to be tackled. In particular, the design of more flexible lactate sensing schemes for (i) the formation of 'all-in-one' materials containing both the biocatalyst and the secondary sensing elements needed for detection (e.g. cofactors or chromophores); (ii) accurate control over the location and local concentration of different sensing elements in structured materials and (iii) the highly relevant extension of these biosensing materials to micrometric particle based probes specifically identified as a current need in biotechnological applications. To obtain a more widely applicable lactate biosensing platform, these points need to be addressed.

In this context, the layer-by-layer (LbL) technique is one of the most promising methods to incorporate multiple biological components into sensor devices^{259;260}. It is a versatile method involving the sequential deposition of materials of various chemistries onto supports of diverse chemical and morphological nature²⁶¹⁻²⁶³. Originally described as a method to sequentially deposit macroparticles of opposite charge²⁶⁴, it was later extended to the deposition of polyelectrolytes²⁶⁵. The most simplified explanation about the fundamentals of this technique is the electrostatic interaction among ionic side-groups of the polymer backbones. However, the deposition of materials by LbL can rely on other molecular interactions such as hydrophobic interactions²⁶⁶, hydrogen bonds²⁶⁷, coordination chemistry²⁶⁸, biologically specific interactions²⁶⁹, etc. A comprehensive description about molecular interactions driving LbL systems has been reviewed by Borges and Mano²⁷⁰. The flexibility of the LbL technique allows combining different materials for tailored applications. Its use to synthesize enzyme-containing systems has demonstrated an increase in enzymatic activity as compared to the free enzyme in solution²⁷¹. The optical properties from an assembly of polymer-sensing elements can be monitored following a biochemical reaction. Among the existing optical methods, there are those based on absorption and reflection of light in the UV-Visible range, fluorescence spectroscopy, Raman scattering and surface plasmon resonance. In some cases, the measurements are straightforward, as in low-cost sensors based on colorimetry²⁶⁰. Altering the number of layers deposited can exert a control on the thickness (amount) of the deposited materials, if required²⁷². The use of LbL assembly has a number of advantages. For example, LbL assembly can be performed in entirely aqueous solutions, a large range of polymers can be used to create multilayers, resulting in the ability to finely tune the composition, permeability, stability, and surface functionality of the films. The assembly process is relatively cheap, requiring only simple laboratory equipment, and can be performed with inexpensive materials.

Despite the selectivity and suitability of lactate dehydrogenase as a biosensing element for lactate detection, the sensing scheme as demonstrated in the previous chapter required the use of a cofactor, nicotinamide adenine dinucleotide NAD⁺ in solution. It participates directly in the enzymatic reaction by binding to the active site of the enzyme, together with the substrate. This specific interaction between the active site-substrate-cofactor, as described in detail in the background chapter, produces a conformational change in the enzyme, which is essential, but difficult to promote if both enzyme and cofactor are immobilized in the same support. In contrast, an alternative enzyme choice, lactate oxidase (LOx), does not require a cofactor. Its

mechanism of reaction involves the consumption of oxygen and hydrogen peroxide (reaction 6.1). The evolution of oxygen depletion or hydrogen peroxide concentration are the methods to monitor the activity of LOx. The latter can be followed by the incorporation of another independent biosensing element into the system: cytochrome C (CytC), a biomolecule, which in presence of hydrogen peroxide is oxidized. The optical properties of CytC depend on its oxidation state and can be coupled to the oxidation of L-lactate by LOx.

Recently, the change in light absorption of CytC depending on its oxidation state has been reported as a mean to detect the presence of H_2O_2 in stressed cells, and an extremely low limit-of-detection down to the subnanomolar range was achieved^{51;52}. The H_2O_2 produced by the enzyme after exposure to lactate reacts with CytC oxidizing it and consequently changing its optical properties. This behavior is due to the change in oxidation state of the iron center from its heme group, from ferrous Fe^{2+} ($\lambda_{abs} = 550$ nm) to ferric Fe^{3+} .^{273;274} This method is promising for lactate detection due to the narrow absorption peak from its reduced state and the constant absorption of CytC independently of its oxidation state (isosbestic points at wavelengths $\lambda = 542$ nm and $\lambda = 556$ nm).



Another alternative technique to detect the oxidation state of CytC is based on the fluorescence produced by CytC in its reduced state⁵⁰. When excited at 350 nm and at a pH value of 7²⁷⁵, CytC emits at 402 nm and 437 nm. Only the reduced state of CytC has fluorescence properties and thus the decay in fluorescence intensity can be interpreted as a direct response from the oxidation of CytC by hydrogen peroxide.

In this chapter, a novel scheme for lactate detection is proposed and developed in the form of responsive lactate patches and microparticles. This scheme involves the integration of LOx in combination with CytC into LbL functionalized systems. The co-immobilized CytC does not directly participate in the enzymatic reaction but only serves as an indicator molecule, making this approach more versatile. In the case of patches, the integration of the different components into one system is achieved by the layer-by-layer deposition of oppositely charged polyelectrolyte layers, allowing the adsorption of CytC on top of the enzyme-functionalized porous silica films developed in the previous chapter. Both mesoporous and hierarchically porous materials are compared here to validate the results observed before. The implementation of a coupled LOX-CytC biosensing arrangement within a hybrid responsive material to lactate is therefore proposed and developed as an integrated responsive system without the need for additional reactants during biosensing, i.e. with all necessary reacting components other than the analyte molecule included permanently in the system. In the specific case of the lactate responsive patches developed here, the polyelectrolyte system should fulfill several purposes: (i) it should provide additional stability and protect the covalently immobilized LOx enzyme layer in the porous silica film; (ii) at the same time, it should not limit diffusion

of the reactants and products through the multilayer; and (iii) the multilayer should serve as a scaffold for the optical sensing element, CytC, accessible to the reaction product H_2O_2 . For the development of lactate micrometric probes, a porous support is used to synthesize protein-based lactate responsive microparticles by the sequential adsorption of LOx and CytC onto porous CaCO_3 particles. The advantages from using CaCO_3 particles as templates have been described at the corresponding section in the background chapter. Among them, the removal of the support by dissolution under mild conditions is highly important as it yields protein-based microparticles with active LOx and CytC closely bound together, allowing the detection of lactate in a single microparticle.

6.2 Materials and methods

6.2.1 Film synthesis, casting and characterization

Support treatment: Borosilicate cover glasses No. 5, diameter 19 mm (ProSciTech Pty Ltd) were cleaned by sonication using isopropanol for 10 minutes. Afterwards they were rinsed with ethanol, dried with compressed air and placed into an oxygen plasma chamber for 10 minutes.

Film preparation: Silica films were synthesized following a top-down approach. Silica aggregates (Cabosil M5, Cabot Corporation) were dispersed in deionized water at a concentration of 10% w/v. For hierarchically nanostructured films, poly(methyl methacrylate) (PMMA) beads (280 nm in diameter, Polymer Source, Inc.) were used as macropore templates. A given volume of the polymer beads (10% w/v) was incorporated dropwise to the silica suspension with strong agitation. Polyvinyl alcohol was incorporated to the suspensions from a solution at 10% w/v in water (Mowiol[®] 40-88, Sigma-Aldrich). The ratio of polyvinyl alcohol was adjusted to the solid content of the suspension to avoid changes in the viscosity. The resulting suspensions were spin-coated onto previously cleaned borosilicate supports. Heat treatment was applied to remove the porogenic templates (550°C for 20 minutes).

Film characterization: The films nanostructure was observed using Scanning Electron Microscopy (SEM XL30 ESEM-FEG, Philips).

6.2.2 Post-functionalization of silica films

Silanization: Prior to the post-functionalization steps, the uncoated side of the support was protected with adhesive tape. Amino-propyltriethoxysilane (APTES) in vapour phase was used to functionalize silica films with amino groups. A desiccator was placed into an oven at 120°C for 2h with the samples to be silanized. The desiccator was then taken out from the oven, and 100 μL of APTES were then added into the chamber using a dried half-Petri dish as a container. Vacuum was applied and the samples were left for 2h. Finally, the silanized samples were placed in an oven at 100°C for 10 minutes.

Glutaraldehyde-functionalization: Amino-functionalized silica films were then immersed in a solution of glutaraldehyde at 5% v/v in phosphate buffer 0.01 mM at pH 7. After 10 minutes, the films were rinsed thoroughly with deionized water, dried with compressed air and were

then ready for enzyme conjugation. If not used immediately, they were placed in a refrigerator covered with aluminium foil for maximum 2 hours before use.

Enzyme immobilization: A stock solution of lactate oxidase (LOx, Toyobo) at a concentration of 100 U/mL was prepared in deionized water. The post-functionalized silica films were immersed in this solution for 2h at room temperature. Afterwards, they were thoroughly rinsed with phosphate buffered saline – Tween 20 (PBS-T, Sigma Aldrich), PBS and water, and dried with compressed air. The protected side of the film was removed and the enzyme-conjugated films were placed in a 12-multiwell plate for further experiments.

6.2.3 Layer-by-layer deposition of cytochrome C

Cytochrome C (CytC) from equine heart (Calbiochem[®], Merck Millipore) was reduced with ascorbic acid and purified using a desalting column (Zeba spin desalting, <7000 Da, 10 mL). Polyethyleneimine (PEI) branched (Mw \approx 25'000 Sigma-Aldrich) and polyacrylic acid (PAA), sodium salt 35% (Mw 60'000, Polysciences) were used to prepare solutions at 1 mg/mL in PBS at a pH value of 7.4. Dipping the enzyme functionalized silica films in the previously prepared solution first created a layer of PEI. Rinsing three times by dipping the films in deionized water removed the excess of non-adsorbed PEI. Afterwards, the same procedure was applied to adsorb PAA and CytC (3 mg/mL).

Evaluation of layer-by-layer adsorption: To track the adsorption of polymers and CytC, measurements were performed using a quartz crystal microbalance (E4 QCM, Q-sense) using silica-coated sensors. Experimental details of the QCM method and data evaluation can be found in the previous chapter. For the data shown in this chapter, the third overtone of the resonance frequency shift Δf was used.

6.2.4 Detection of lactate in porous silica films

The LOx–CytC functionalized films were immersed in solutions of lactate at different concentrations. PBS buffer at a pH value of 7.4 was used as reaction detection medium. The oxidation of cytochrome C was followed measuring the absorbance in situ over time using a plate reader (Tecan Infinite 200 PRO).

6.2.5 Assembly of LOx–CytC particles

Porous calcium carbonate CaCO₃ particles were used as templates for the formation of protein particles. They were prepared according to the work of Imai et al.^{108*} by a precipitation and aggregation process, initiated by mixing two solutions at room temperature: CaCl₂ [Ca²⁺] at a concentration of 32 mM and NaCO₃ [CO₃²⁻] at a concentration of 16 mM in a solution of polystyrene sulfonate (PSS). PSS was removed from the particles by calcination. Particles with an average diameter of approximately 5 μ m were used. The particles were calcined at 550 °C

*Dr. Jiwei Cui from the University of Melbourne is acknowledged for providing the CaCO₃ particles as templates for this study. A detailed characterisation of these particles has previously been published by Imai et al.¹⁰⁸, and more information is provided in the Appendix.

for 6h, rinsed with deionized water three times and resuspended again in PBS at pH = 7.4. LOx was labeled with Alexa-Fluor[®] 488 dye (life technologies) and purified using a desalting column (Zeba spin desalting column, 40K MWCO, 2 mL). A suspension of CaCO₃ particles were mixed with LOx-Alexa[®]-Fluor 488 and placed in a tube rotator for 2 hours, then rinsed three times with buffer to remove unabsorbed enzyme. CytC was then absorbed in the same way. The dissolution of CaCO₃ was performed by adding ethylenediaminetetraacetic acid (EDTA) 0.2 M at pH 8 into the dispersion. The protein particles were then rinsed with PBS to remove the dissolved CaCO₃ and EDTA.

Microscopy: the loading of LOx and CytC in the particles before and after dissolution of the template was observed by microscopy (Inverted Microscope Olympus IX71) at 60x magnification with an oil immersion objective. Fluorescently labeled particles were observed using the corresponding filter set.

6.2.6 Detection of lactate using protein particles

The activity of lactate oxidase in the particles was evaluated firstly by incubating them in buffer with CytC. 5 μ L of protein capsules (from a suspension with a concentration of 10 mg/mL) were added into a 96-well plate. 5 μ L of CytC in PBS (3 mg/ml) followed by 85 μ L of PBS at pH = 7.4 were added. Finally, 5 μ L of lactate at 0.25 M were added to the mixture. The oxidation of CytC was monitored over time measuring the absorbance spectra (see Figure D.1 for reference spectra) with a plate reader (Tecan Infinite 200 PRO). In a second method, the decay in fluorescence from CytC was monitored by fluorescence microscopy directly in the protein particle. Numerical values of the relative fluorescence decay were evaluated by image analysis of the micrographs using the software ImageJ (available from The National Institutes of Health, <http://imagej.nih.gov>).

6.3 Results and discussion

6.3.1 Lactate responsive LOx-CytC hybrid patches

Porous silica supports were prepared following a powder approach and using polymer particles as macropore templates. Their nanostructure features, porosity characterization and post-functionalization with enzymes were described in the previous chapter. In this particular case, LOx was immobilized instead of LDH. LOx is 4-subunit enzyme with an isoelectric point (IEP) of 4.2 and a molecular weight of 160 kDa. The crystallographic size of the enzyme reveals a structure unit with dimensions of 11 x 13 x 18 nm⁷¹. This tetrameric enzyme belongs to the α -hydroxy acid oxidase flavoenzyme family. It contains a flavin nucleotide as a prosthetic group (the non-protein part of the enzyme) which performs as a cofactor integrated in the enzyme (details can be found in the background chapter of this thesis)⁷⁰.

The scheme for lactate detection based on LOx–CytC functionalized patches is shown in Figure 6.1. A LOx-functionalized porous silica support was coated with CytC embedded in a layer of polyelectrolytes. In a first step, lactate reaches the enzyme and it is converted into pyruvate and hydrogen peroxide. In a second step, the hydrogen peroxide diffuses out reaching the CytC molecules embedded in a network of polymers. As a consequence, CytC becomes oxidized, changing its optical properties, decreasing its light absorbance at 550 nm, and producing a color change from brilliant orange-pink (CytC-Fe²⁺) to red (CytC-Fe³⁺).

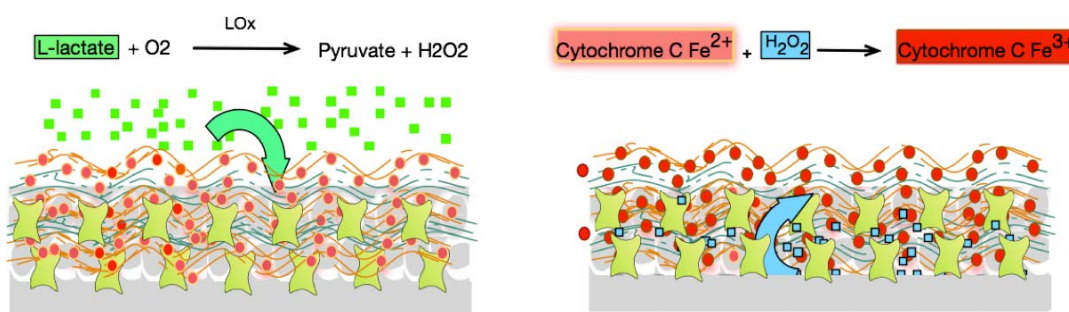


Figure 6.1 – Scheme for the approach developed in this study to assemble a hybrid functionalized porous silica film for lactate detection. Lactate oxidase (yellow) is covalently immobilized in a porous silica film (grey). A layer-by-layer system of oppositely charged polymers (PEI–PAA, green and orange) and integrating cytochrome C (red-pink) is adsorbed on top of the enzyme-functionalized porous film. Lactate oxidase converts lactate (green squares) into pyruvate and hydrogen peroxide (blue squares).

Deposition of PEI-PAA

The conditions to bring the polyelectrolytes and CytC onto the LOx-functionalized films with the minimum number of deposition cycles were established using QCM experiments. These conditions were sought to (i) efficiently immobilize a large amount of CytC adsorbed in a single step, (ii) to avoid extra processing time and (iii) to limit the exposure of the enzyme immobilised in the film to chemically changing environments with a potential loss of its activity. In this first study, the influence of pH and NaCl content in the polyelectrolyte solution

were evaluated. Solutions of PEI at pH = 9 and PAA at pH = 4 were prepared at a concentration of 1 mg/mL. Müller et al. showed that at these pH values a multilayer system using these polymers could be obtained in a reproducible way²⁷⁶. They reported the selective adsorption of a mixture of proteins: concanavalin A (IEP = 5.4 and lysozyme IEP = 11.1) on a polyelectrolyte multilayer system consisting of PEI and PAA. They found that at pH = 7.3, when PEI was the outermost layer, negatively charged proteins (concanavalin A) were adsorbed. However, when PAA was the outermost layer at the same pH, positively charged proteins (lysozyme) were adsorbed instead²⁷⁶. For the multilayer films to be synthesized here, the charges and deposition conditions of these two polyelectrolytes need to be matched to build up a stable multilayer and to allow subsequent adsorption of CytC. Additionally, PEI has also shown to be beneficial for enhancing colloidal stability and preventing degradation of enzyme activity²⁷⁷. The isoelectric point (IEP) of CytC from horse heart is 10²⁷⁸ and at physiological conditions it is assumed to be positively charged. Therefore, PAA is selected as the outermost layer where CytC is adsorbed.

Figure 6.2 shows the QCM results for the adsorption of polyelectrolytes with and without NaCl. The graphs reveal that moderate concentrations of NaCl influence the mass deposition of polyelectrolytes and the final adsorption of CytC only very weakly. Consecutive mass adsorption of polymers can be observed, as well as a final uptake of CytC from the outer PAA layer. However, the deposited amount of CytC was not high enough to be detected by spectrophotometry.

The layer-by-layer system was built up here in a relatively simple arrangement, with the enzyme LOx first immobilized as the primary layer on the silica support, followed by one cationic PEI layer and one anionic PAA layer, and with the CytC as the closing top layer, and

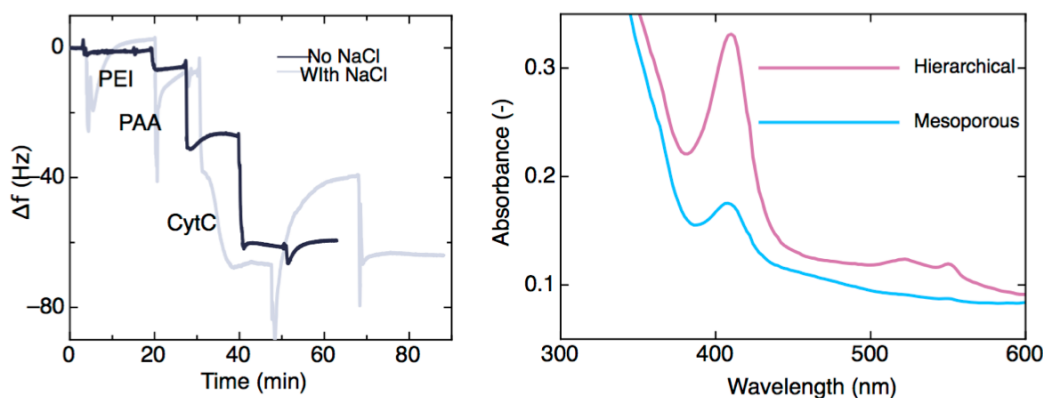


Figure 6.2 – Left: Layer-by-layer adsorption of a PEI–PAA–CytC multilayer on silica coated QCM sensors, following a traditional adsorption procedure²⁷⁶ with pH = 9 (PEI) and pH = 4 (PAA), followed by adsorption of CytC at pH = 7.4. Curves are shown for a salt-free procedure and with a NaCl concentration of 0.15 M. Δf: frequency shift. Right: Spectra of hierarchically porous and mesoporous films with immobilized LOx, coated with PEI–PAA–CytC following the adsorption procedure shown on the left. The characteristic absorbance of CytC between 500 and 600 nm, which is necessary for biosensing, is not achieved here due to the low concentration adsorbed using this protocol.

which remains strongly adsorbed at physiological pH in view of its opposite IEP compared to PAA. This arrangement provides protection to the enzyme layer and allows sufficiently strong adsorption of CytC while creating an overall system that is sufficiently thin to retain transparent optical properties²⁷⁹.

The effect of NaCl in the polymer conformation in solution can have an influence on the mass deposited by the LbL process. The ions can mask the surface charge of polyelectrolytes, reducing their attraction between chains and stretching the molecules²⁸⁰. In this study, increased salt concentrations can interfere with the enzyme, producing denaturation and causing loss of activity. For this reason, a concentration of 0.138 M (PBS) was selected for QCM evaluation.

While Figure 6.2 demonstrates that PEI–PAA–CytC multilayers can be formed under the conditions shown (pH = 9 for PEI, pH = 4 for PAA, pH = 7.4 for CytC), the evolution of the QCM curves also indicates that the repeated changes in the pH value induce slow changes in adsorption each time the polyelectrolyte solution is changed. To avoid these changes in the degree of dissociation during buildup of the layers, it would therefore be desirable to form more stable multilayers under more mild and constant conditions.

In contrast to strong polyelectrolytes, for which the charge density does not depend on the pH of the medium, the degree of ionization of weak polyelectrolytes such as PEI and PAA strongly depends on the pH. At a pH value of 7.4, PEI is positively charged while PAA is negatively charged. The pK_a value reported for PAA is 4.5²⁸¹ whereas an equivalent values for the branched PEI used here could not be identified in the literature; previously reported values for the degree of protonation of branched PEI at pH = 7.4 were 20%²⁸² and 30%²⁸³, respectively. Therefore, to further increase the amount of adsorbed CytC in the films, an additional QCM study was performed, this time maintaining the pH at 7.4 for both polymers in PBS. These results are shown in Figure 6.3. The adsorption of CytC is considerably higher than in the previous experiments. At pH 7.4, both polymers are highly ionized and exhibit opposite charges. At the same time, CytC is positively charged. The long time for stabilization observed in the QCM adsorption curves may be the result of competitive adsorption between PEI and CytC for PAA. Also, CytC multilayer formation is possible. The Sauerbrey approximation gives a mass per surface area of 103 ng/cm² for the PEI–PAA polyelectrolyte layer. Once the CytC adsorption arrives at a steady value after 10 hours, the adsorbed mass is much higher, with values > 2000 ng/cm². As discussed in the previous chapter, these mass values are not precise because the Sauerbrey model does not perform well for soft, thick adsorption layers. Nevertheless, these QCM results clearly indicate that significant quantities of CytC are adsorbed, and in comparison with the literature for globular proteins it is likely that CytC multilayers are formed on top of the PEI–PAA. In comparison to the non-buffered initial QCM experiments without optimized pH and ionic strength shown above, the adsorption conditions shown in Figure 6.3 also result in CytC layers that are more stable against desorption during rinsing.

These new PEI–PAA–CytC adsorption conditions were tested directly on enzyme-functionalized porous films deposited on glass disks. Figure 6.4 shows the pictures of glass slides of 19 mm diameter coated with polyelectrolytes and with CytC adsorbed. A much more intense orange color can be observed in the multi-scale porous films (Figure 6.4c) compared to the

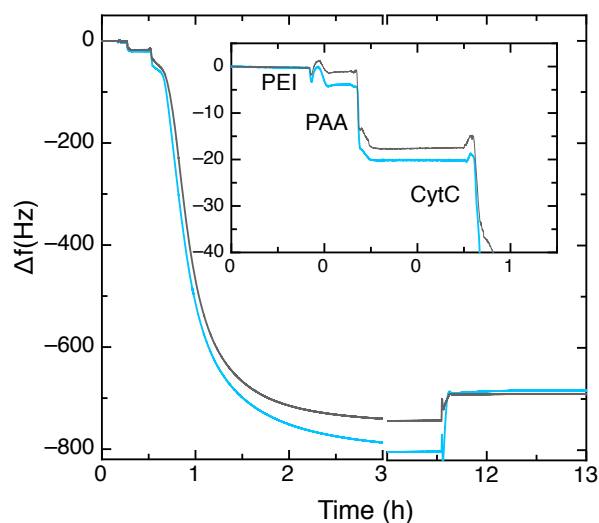


Figure 6.3 – QCM study of polymer adsorption on top of a silica coated sensor with improved deposition conditions and optimized buffer concentration and pH for all components. PEI solution (1 mg/mL) in 0.138 M PBS buffer at pH = 7.4 is adsorbed in first place and the excess is rinsed. PAA (1 mg/mL) is adsorbed consecutively in the same manner. Finally, a solution of cytochrome C (3 mg/mL) is let to flow into the chamber and left to stabilize for several hours, then finally rinsed.

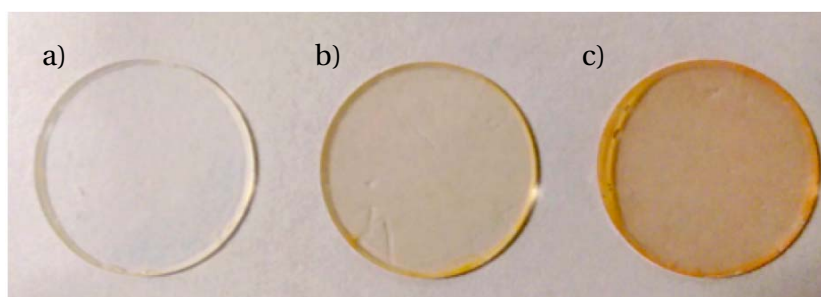


Figure 6.4 – Images of circular glass slides (19 mm in diameter) a) bare glass, b) mesoporous functionalized silica and c) hierarchically porous silica; both of the coated surfaces are loaded with immobilized lactate oxidase and coated by a PEI–PAA–CytC multilayer. The hierarchically porous silica shows a stronger red-pink color, indicating a higher adsorption of cytochrome C.

monomodal porous films (Figure 6.4b). This outcome may be a result of the polyelectrolytes coating the inner porous surface of the films, where the created macropores facilitate the diffusion and the adsorption of the layer-by-layer system. Regarding the effect of mass transport for PEI, PAA and CytC during the formation of the LbL multilayers, it can be assumed that the relevant transport process is bulk diffusion from the solution to the previously adsorbed enzyme or polyelectrolyte layer: on the mesopore level, the silica films have already been covered with significant amounts of the LOx during the immobilization. In contrast, on the macropore level, the PEI, PAA and CytC molecular sizes are small with respect to the macropores, therefore the pore size effect is not expected to influence the LbL process significantly.

Lactate detection in porous films

With the LOx–CytC functionalized multilayer films at hand, L-lactate sensing tests were performed at different analyte concentrations. The lactate solutions were directly brought in contact with the transparent films and the change of the absorbance spectra over time was recorded to infer the oxidation state of the CytC in the films.

Figure 6.5 shows sets of spectra of CytC in the layer-by-layer assembled films over time during immersion in lactate solutions with physiologically relevant concentrations. The inset graphs show a magnification of the spectra within the wavelength range where the oxidation of CytC can be monitored. In general terms, lactate was detected in both functionalized porous hybrid films, independent of monomodal and bimodal porosity. However, in hierarchically porous films, the oxidation of lactate occurred more rapidly. Considering a ratio between the difference of absorbance at 550 nm and one of the isosbestic points at 556 nm, an oxidation coefficient of CytC can be obtained⁵¹ and compared for both porous systems (Figure 6.6):

$$\Phi = \frac{\text{CytC}_{550nm} - \text{CytC}_{556nm}}{\text{CytC}_{556nm}} \quad (6.3)$$

For lactate detection in LbL-functionalized mesoporous films, the oxidation coefficient Φ evolves only very slowly, and the performance and sensitivity is poor compared to hierarchically porous films. In Fig. 6.7, the initial slope of the $d\Phi/dt$ curves is shown as a function of the lactate concentration for PEI–PAA–CytC coated films with immobilized lactate oxidase. The mesoporous multilayer films exhibit poor performance and do not provide a useable sensor response, with very low initial slopes that cannot be linked to the L-lactate concentrations. In contrast, the Φ data from the hierarchical film allow to obtain a sensor response curve (slope of $|d\Phi/dt| = 3.2 \cdot 10^{-1} \text{ l}/(\text{mol} \cdot \text{min})$, corresponding to the sensitivity constant) for lactate sensing.

While this difference in performance between mesoporous and hierarchically porous films confirms the trends discussed in the previous chapter for a smaller enzyme, the results observed here suggest that the combined use of LOx as the enzyme and LbL-multilayer formation on top of the LOx-loaded films further amplifies the differences in performance, sensitivity and robustness between hierarchical and mesoporous enzyme-loaded systems. A possible explanation for these different results is that for the mesoporous case the LOx is not transported efficiently inside the silica mesopores, as discussed in the corresponding section from the previous chapter. Indeed, LOx is a large 4-subunit enzyme with a higher molecular weight and its longest dimension is about 35% larger than LDH. Therefore its effective diffusivity in the mesopores is likely to be restricted even more strongly than that of LDH because of the pore size effect. Consequently, significant amounts of LOx can be expected to be immobilized in the form of enzyme aggregates or enzyme multilayers, rather than directly on the SiO₂ surface within the mesopores. This type of loose adsorption can be the reason for the poor robustness during rinsing and bad reproducibility, as compared to proper covalent immobilization on the silica as in the case of the hierarchically porous films, where the macropores make more of the high specific surface area of the silica accessible to the enzyme.

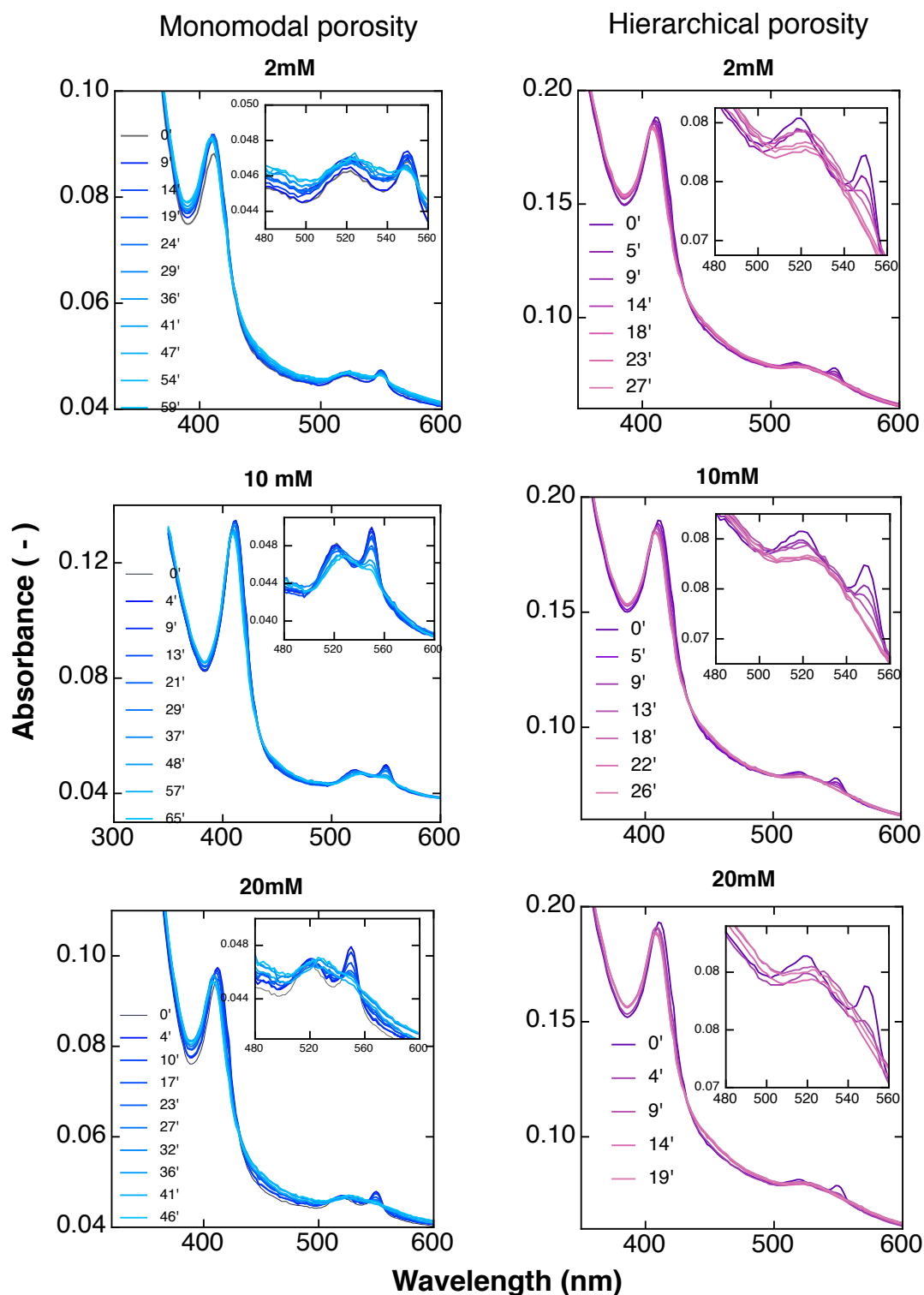


Figure 6.5 – Response curves of mesoporous (blue) and hierarchically porous silica films (red) functionalized for lactate detection. The spectra show the absorbance of CytC (Fe^{2+}), with characteristic peaks of absorption at 520 and 550 nm. When immersed in lactate solutions at different concentrations (2, 10, 20 mM), the hydrogen peroxide produced by the enzyme oxidizes CytC and thus decreases the absorbance at these characteristic wavelengths.

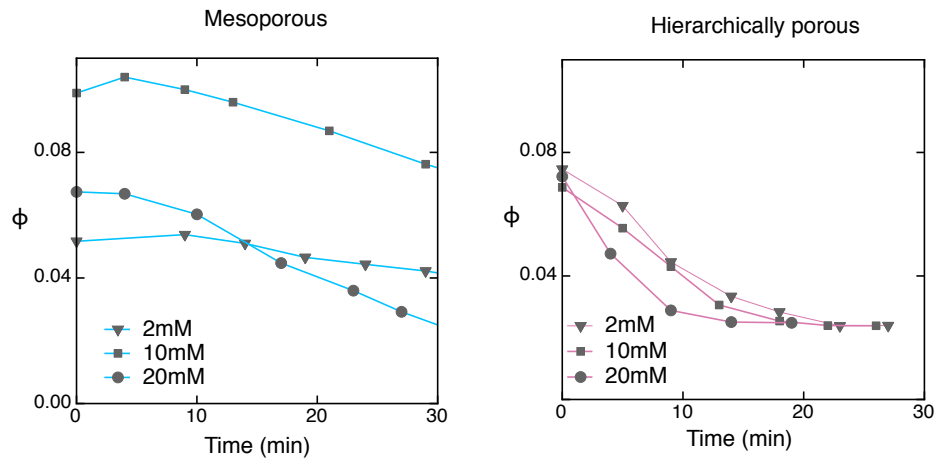


Figure 6.6 – Oxidation coefficient Φ over time for LOx–CytC functionalized mesoporous and hierarchically porous films. A faster oxidation of CytC was observed in the multi-scale porous films immersed in solutions of lactate at physiologically relevant concentrations.

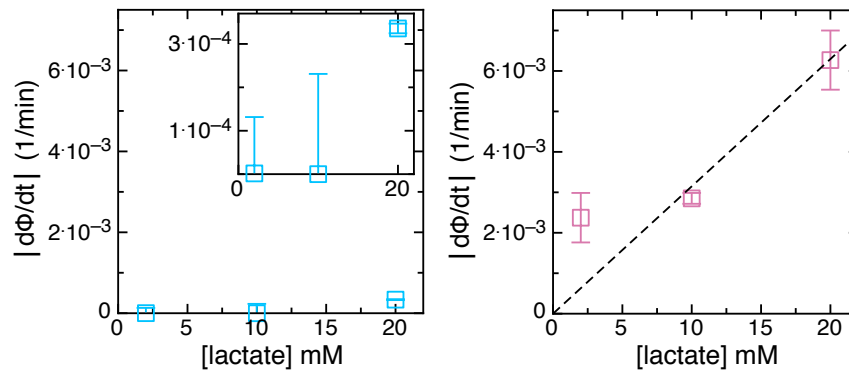


Figure 6.7 – Absolute value of the initial slope $d\Phi/dt$ as a function of the lactate concentration for PEI–PAA–CytC coated mesoporous (left) and hierarchically porous films (right) with immobilized lactate oxidase. The mesoporous multilayer films exhibit poor performance and do not provide a useable sensor response (very low response values with a large error). In contrast, from the Φ data of the hierarchical film a sensor response curve (dashed line) for lactate sensing was obtained.

Using the same approximations discussed in the previous chapter for enzyme transport in the nanostructured films, the effective diffusivity of LOx in the mesoporous films is reduced to $D_{\text{eff}}/D_0 \approx 0.05$ (assuming $r_{\text{molecule}}/r_{\text{pore}} \approx 0.63$ for LOx in a typical mesopore, leading to a pore size factor¹³⁰ $F \approx 0.07$, and using the same factors for the tortuosity of the silica films as in the last chapter). For comparison, the value estimated for the smaller LDH enzyme used in the last chapter was $D_{\text{eff}}/D_0 \approx 0.11$, meaning that for the larger LOx molecule the mesoporous structure is a stronger diffusion barrier. In contrast, in the hierarchically porous films with their large macropores, diffusion of LOx is only slightly reduced to $D_{\text{eff}}/D_0 \approx 0.67$ (which is again very close to the value of 0.69 found for LDH in the previous chapter).

6.3.2 Micrometric lactate-responsive particles

A second alternative for lactate detection combining LOx and CytC was developed in the form of micrometric particles using sacrificial inorganic templates as porous supports. CaCO₃ microspheres with average diameters around 5 μm were used as templates for this synthesis. These particles are particularly developed in this work to contribute with an innovative solution to the existing need of particle based systems for lactate biosensing, as revealed by the state of the art on this field presented in the introduction section.

CaCO₃ microparticles used here are composed of radially oriented branches of nanocrystals of 20 nm size in average, confirming other studies reporting on the synthesis of CaCO₃ microparticles by a similar method¹⁰³. These microparticles have been characterized as vaterite from their XRD patterns. Although the vaterite species is considered a metastable phase of CaCO₃ and less stable than calcite at ambient conditions, it has been reported that acidic polyelectrolytes such as PSS are effective for the construction of mesostructured vaterite, stabilizing it and allowing the aggregation of nanoparticles²⁸⁴. The mechanism of formation of these microparticles is still under debate²⁸⁵, nevertheless two possible explanations are found in the literature. One supports the idea of the simultaneous formation of single nanocrystals, which rapidly aggregate to form a microparticle. A second theory supports that vaterite microparticles grow from a single nucleus crystal that branches from it, and where both crystallization process (nucleus and branches) can occur at the same time. In any case, the result is the precipitation of microparticles of different diameter which can be tuned by modifying synthesis parameters such as stirring speed and pH of the solution¹⁰⁸. The porosity of such microparticles is created in a similar way to the porous silica films addressed in this and the previous chapters. Mesopores originate from the space between CaCO₃ nanoparticles; large mesopores and macropores are created after removal of a porogenic material (PSS) by heat treatment (a SEM micrograph of the particle structure is shown in Figure 6.8a, and reference information from the literature on the nanocrystal arrangement and the pore sizes is shown in the Appendix in Figure D.2). As shown previously by Imai et al.¹⁰⁸ the microparticles before polymer removal contained small mesopores below 20 nm in diameter, while particles as used here where the polymer had been removed revealed a much larger pore volume fraction, with the presence of both large mesopores and macropores up to 80 nm.

In Figure 6.8 a schematic representation of the method developed and evaluated is shown. In a first step towards the preparation of LOx-CytC protein microparticles, CaCO₃ templates (IEP 8.5¹⁰³) were mixed in PBS with the larger protein (LOx, IEP 4.2). After a couple of hours of incubation at room temperature, they were thoroughly rinsed with excess PBS buffer to remove the non-absorbed LOx. CytC (IEP 10) was subsequently absorbed in the same way. In a final step, EDTA at pH = 8 was added to remove the sacrificial CaCO₃ core of the particles.

LOx was labelled with a fluorophore (Alexa-Fluor 488) to track their absorption into the porous CaCO₃ template particles by fluorescence microscopy. The hybrid particles exhibited fluorescence emission at 525 nm (green); CytC was not labelled since it is fluorescent itself when excited in the UV range with emission maxima at 440 nm (blue). A set of images from CaCO₃ particles loaded with LOx and CytC before and after removal of the inorganic core template using by EDTA are shown in Figure 6.9. These images confirm that (i) the particles are loaded with both LOx and CytC (as indicated by the fluorescence signal), and (ii) even

after removal of the CaCO_3 core, the particles remain assembled in a roughly spherical shape. The intensity in fluorescence decreases after the core removal, indicating slow leaking of the protein. To demonstrate the dissolution of the core, images of a CaCO_3 loaded particle were taken along time showing the progressive dissolution of the core in Figure 6.10.

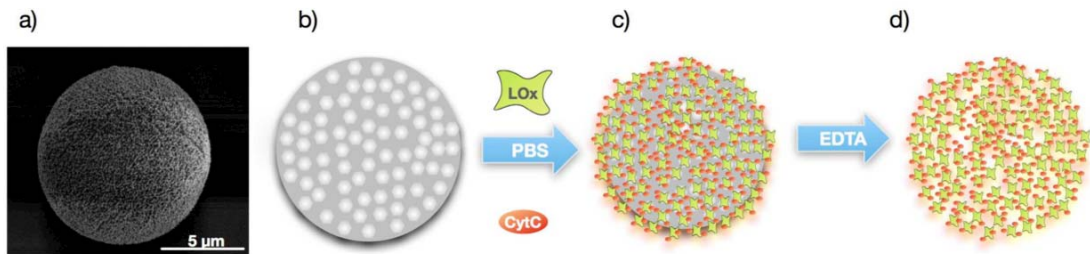


Figure 6.8 – Preparation of CaCO_3 -templated LOx–CytC particles. Porous CaCO_3 is used as a template for the synthesis of LOx–CytC particles; a) and b) SEM image and schematic drawing of a porous CaCO_3 particle; c) LOx is absorbed in PBS at pH = 7.4 and rinsed. CytC is absorbed afterwards under the same conditions; d) the porous template is removed with EDTA at pH 8.

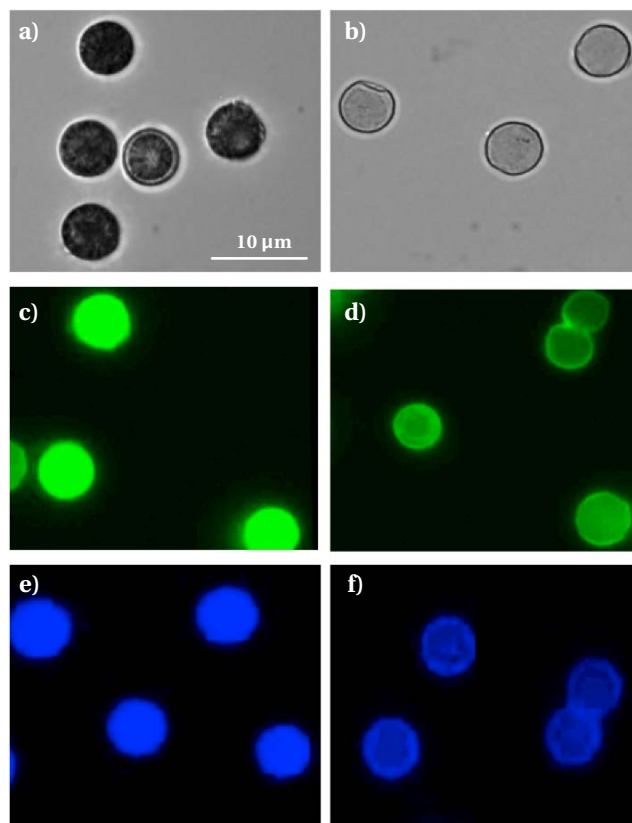


Figure 6.9 – Micrographs of LOx–CytC protein particles. a) bright field image of protein loaded CaCO_3 particles and b) protein particles after CaCO_3 removal by EDTA. Fluorescence images from CaCO_3 particles loaded with c) LOx-Alexa Fluor 488 and e) LOx–CytC; LOx-CytC particles after CaCO_3 removal: d) LOx-Alexa Fluor 488 fluorescence and f) CytC fluorescence.

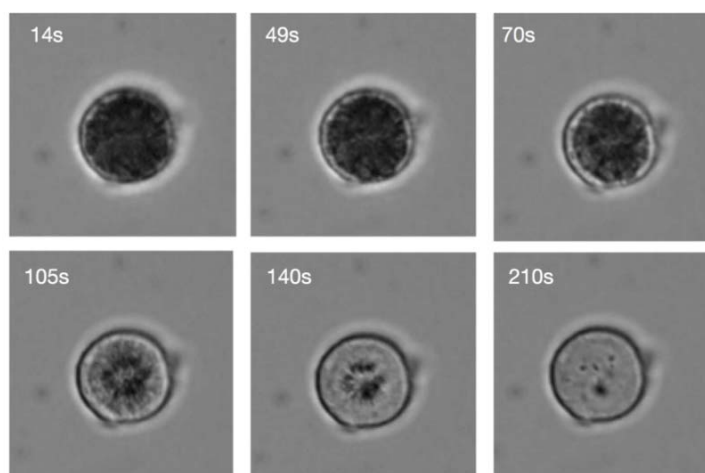


Figure 6.10 – Time course sequence of the dissolution of the sacrificial CaCO_3 core from CaCO_3 particles loaded with LOx–CytC, as observed by bright field microscopy (removal with EDTA 0.2 M at pH 8.)

There are two main aspects for the evaluation of the enzyme particles formed here: (i) the stability and integrity of the protein microspheres following removal of the sacrificial core, and (ii) their ability to exhibit enzymatic activity of the LOx even after particle formation and assembly with CytC. Both aspects are required for lactate sensing using these particles, and they will be discussed in the following section. To understand the mechanism of stabilization of the LOx–CytC assemblies after dissolution of the CaCO_3 core, the amphoteric nature of the LOx and CytC molecules should be taken into account. In particular, comparing the isoelectric points of both proteins allows to explain electrostatic interactions between them at a specific pH value. At physiological pH, at which the assembly of the particles took place, both proteins have opposite charge (the IEP of LOx is 4.2 and the IEP of CytC is 10). The net opposite charge of these molecules can therefore be expected to be the main influence for the stability of their assemblies^{95;259}. Since the IEPs of LOx and CytC are separated by almost six pH units, these two proteins and the chosen conditions are therefore an ideal combination for complex formation at the selected pH value of 7.4.

The polymer-templated CaCO_3 microspheres were chosen as templates because of their suitability to entrap guest molecules, as shown previously for different dyes and proteins^{108;286;287} and for the facility to be removed under mild conditions, avoiding damage to the enzyme. LOx has an approximate molecular diameter of 19 nm and the inorganic microsphere templates show pores between 20 nm and 100 nm (see the reference data mentioned in the Appendix), therefore diffusion of the enzyme into the larger pore fractions is expected to occur. A simple assessment can be made to confirm whether the proteins were actually able to penetrate inside the template particle, or if they were only adsorbed as a "shell" at the surface: by following the time course images in Figure 6.10 taken during dissolution of the CaCO_3 core using EDTA, it appears that the shape and volume of the microparticles remain constant. This stability of the particle shape during mass transfer from the inside to the outside indeed suggests that the LOx–CytC assembly indeed penetrates deeply into the template to form a matrix particle, rather than just forming an adsorbed protein multilayer. In contrast, soft polyelectrolyte,

protein or DNA shells are well-known^{286–289} to be mechanically unstable and buckle during volume transfer from the core to the outside, which is not observed here.

Moreover, TEM images obtained from samples drawn at different time of dissolution with EDTA (Figure 6.11) suggest that some CaCO₃ could remain inside the particle. Since the pure inorganic template particles are easily dissolved by EDTA, the presence of this residual material indicates that the protein complex formed around and in the pores of the inorganic particles acts as a barrier towards the CaCO₃ dissolution process. Additionally, some shrinkage of the particle is observed during dissolution of the template core, which has been also observed in similar systems^{290;291}.

The enzymatic activity of lactate oxidase in LOx–CytC particles is evaluated by two different methods: indirectly via the oxidation of free CytC in solution, and directly via fluorescence microscopy on the particles themselves.

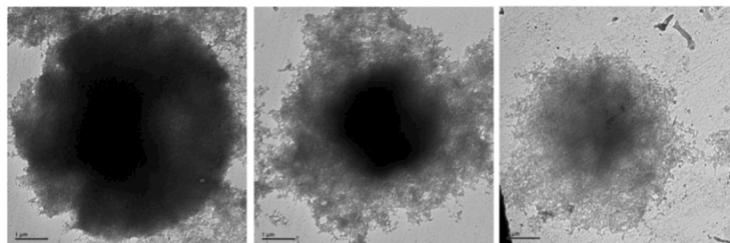


Figure 6.11 – TEM micrographs of a) CaCO₃ particles after LOx–CytC absorption b) CaCO₃ particles isolated during dissolution by EDTA; some CaCO₃ remains at the core and c) LOx–CytC, with most of the CaCO₃ having been removed. Scale bar 1 μm

Firstly, to assess their biocatalytic activity in suspension, an aliquot of particles is mixed with a solution of free CytC and L-lactate in excess (the direct evaluation of CytC oxidation by spectrophotometric means within the particles themselves was not possible; however, the goal was to verify that the LOx remains active even after all the processing steps to form the particles). To verify that the oxidation of CytC was due to LOx activity and not to any other external factor (for example, oxygen from the air), a control experiment was performed in parallel without LOx–CytC particles. The results are shown in Figure 6.12.

Oxidation of the free CytC added in the solution is clearly visible over time as shown in Figure 6.12a. The control remains stable, with negligible oxidation during the same experiment. These results confirm that LOx remains active even after the formation of the protein particles. Moreover, the fluorescence of the solution was measured to evaluate the effect of LOx activity on the CytC fluorescence (Figure 6.12b). The control shows no decay of fluorescence over time; in contrast, the solution with protein particles shows a decrease in fluorescence. The oxidation of CytC by spectroscopy and the decay of fluorescence are correlated. After 30 minutes of measurements no further significant oxidation of CytC is observed (either by decrease of absorption or by fluorescence emission).

Secondly, the fluorescence decay of CytC in LOx–CytC particles was also evaluated directly using fluorescence microscopy. In Figure 6.13, a time sequence tracking directly the decay in fluorescence intensity of the particle-bound CytC upon addition of L-lactate is shown.

Chapter 6. Layer-by-layer assembled films and particles for lactate biosensors

This last experiment demonstrates that the particles can indeed be used as a stand-alone detection system for L-lactate, independent of additional reactants, with a fast response time in less than a minute. Normalized fluorescence intensity values obtained by image analysis from the average of multiple particles in these micrographs are shown in Figure 6.14. In an actual application for lactate detection, a biosensing assay can be performed either based on microscopy as shown in Figures 6.13 and 6.14; alternatively, these microparticle suspensions also allow facile detection using bulk fluorescence analysis, as it can be performed easily using inexpensive portable single-channel fluorometers.

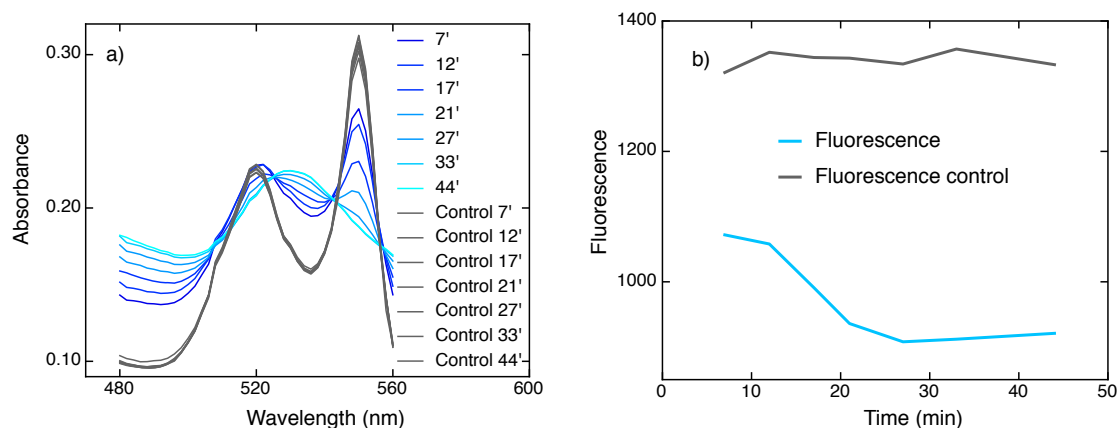


Figure 6.12 – Oxidation of free CytC in solution by LOx–CytC particles. (a) Spectra of a solution of CytC measured over time. CytC is oxidized by the hydrogen peroxide produced from LOx activity in the particles. Control samples show no oxidation of CytC over time, indicating that the change in absorbance corresponds to the activity of the enzyme. (b) Fluorescence decay from the same solution of CytC in the presence of LOx–CytC particles. Fluorescence intensity decreases with the increase in concentration of H_2O_2 in solution.

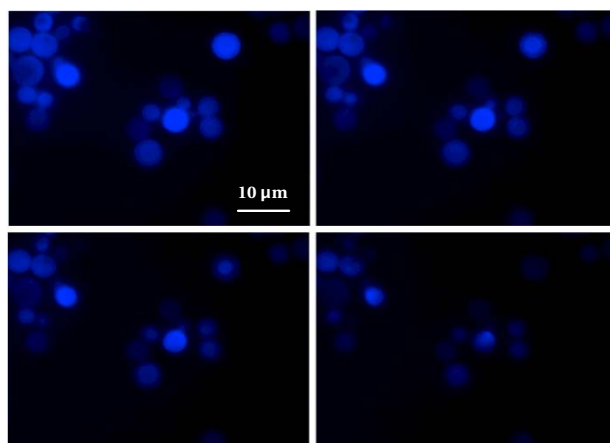


Figure 6.13 – Oxidation of CytC due to H_2O_2 formed by LOx activity in the presence of L-lactate, tracked via fluorescence microscopy of LOx–CytC particles. Fluorescence excited in the UV range (350 nm) with emission at 460 nm (blue). Images taken at times 0, 10, 20 and 30 sec, [L-lactate] = 12.5 mM.

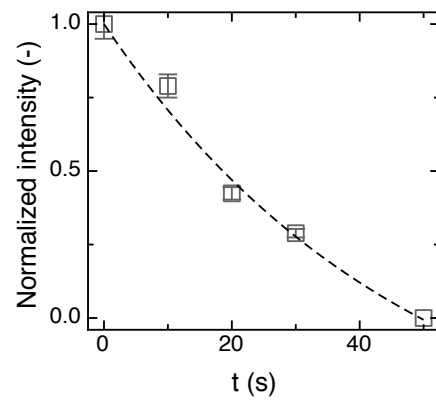


Figure 6.14 – Evolution of the normalized fluorescence intensity averaged over the particles, obtained from image analysis of the fluorescence micrographs shown in the previous figure. A fast response from the particles is observed within a minute after exposure to lactate.

6.4 Summary and conclusions

In this chapter, a new scheme for optical lactate detection has been conceived, developed and implemented for the fabrication of responsive patches and micrometric particles. In the case of patches, hybrid enzyme-silica films were synthesized: lactate oxidase (LOx) was covalently immobilized within the silica porous structure synthesized, and cytochrome C (CytC) was immobilized by adsorption with a polyelectrolyte layer-by-layer technique, serving as a reporting biomolecule for the activity of LOx. The polyelectrolyte dissociation degree and charge, and the protein adsorption were dependent on the pH of the medium. High CytC uptake was found under electrostatically attractive conditions. L-lactate was detected by the oxidative effect of hydrogen peroxide over CytC co-adsorbed in the films. Mesoporous and hierarchically porous silica films were evaluated. Both functionalized films were sensitive to lactate, however, the hierarchical system exhibited a faster and more reliable response. The layer-by-layer assembly scheme was then further developed towards particle-based detection systems, forming LOx–CytC protein particles instead of films. Calcium carbonate porous particles were used as templates. LOx was found to remain active even after the particle formation and removal of the template core. The enzymatic activity was monitored both via the decay of fluorescence from CytC in the particles and in solutions of excess CytC in the presence of the biocatalytic particles. The LOx–PEI–PAA–CytC multilayer films are suitable for the development of biosensing surfaces, for example on optical flow cells, microscopy surfaces, or optical fibers. On the other hand, the LOx–CytC protein microspheres are suitable for detection of lactate in rapid tests, either using particle image analysis by fluorescence microscopy, or with bulk fluorescence measurements in laboratory-based or portable fluorometry devices. An interesting practical and economical aspect of the two biosensing schemes presented in this chapter is the reversibility of CytC oxidation: after use, the multilayer films or the enzymatically active LOx–CytC hybrid particles can be ‘recycled’ easily by reducing the oxidized CytC with an inexpensive electron transfer molecule such as ascorbic acid.

7 Conclusions and Outlook

The main focus of this thesis has been the optical detection of L-lactate using immobilized enzymes via the design of nanostructured thin films and particles. While most current studies for lactate quantification are dominated by amperometric methods, an optical biosensing approach for lactate detection was implemented in this thesis, offering advantages such as a wide applicability for different instrumental configurations, including coated glass surfaces or optical fibers, high specificity and minimum interference with competing analytes, as well as straightforward calibration. The general research approach proposed in this work has been the design of two different schemes for lactate detection: the development of i) lactate responsive patches and ii) micrometric particles, both functionalized with lactate-consuming enzymes, whose activity could be followed by optical transducing technologies finding applications in the medical, agro-food and biotech fields.

Summary of Research Achievements

In the first part of this work, the exploration of different strategies for the synthesis of porous thin films as enzyme supports was presented. In Chapter 3, it was shown that optically transparent silica films with pores in the large mesopore size range, suitable for enzyme immobilization, can be synthesized in a robust manner using sol-gel chemistry in combination with block copolymer templates. This method follows a bottom-up approach for the synthesis of silica via sol-gel chemistry and utilizes amphiphilic block copolymer micelles as sacrificial templates for the formation of pores. It was found that PS-P2VP block copolymer micelles from polymers with different molecular weight have been originally used to create pores within a range of 20–100 nm. Low-chain aliphatic alcohols, ethanol and 1-butanol, were chosen as solvent media to prepare PS-P2VP micelles (they are good solvents for the P2VP block) as they are also conveniently used for the synthesis of silica. The choice of the solvent had a major influence not only on the micelle size and shape, but also on the flow behaviour and the homogeneity of the films after deposition. Additionally, it was found that the architecture of the block copolymers to form micellar pore templates had a strong influence on the suitability of the material to form stable micelle suspensions, where only block copolymers with equivalent block lengths could be used for the synthesis of good quality films (homogeneously distributed pores, uniform in size and highly transparent). The enzyme horseradish peroxidase (HRP) was used as a model enzyme to show the suitability of these synthesized porous films as enzyme

supports. With film thicknesses of only half a micrometer, the apparent enzymatic activity measured from the films was quantified as 35 times higher compared to a non-porous support. The high transparency of these films and their suitability to host enzymes and to keep them active after their immobilization was proven, showing that this approach to produce films is highly useful in biosensing applications. Moreover, the different deposition processes which can be used to fabricate thin films using the proposed method make them very relevant for realistic industrial applications. While the most important challenges established in this work for the porosity design in the large mesopore size range were accomplished at this stage of the research, some important topics remained to be addressed in the subsequent chapters. For example, the need to incorporate larger macropores in the films, and the limitation in thickness are among them. These points are important because whereas HRP is a relatively small protein with only 5 nm in diameter, the relevant enzymes for lactate detection are 3 to 4 times larger than HRP. For this reason, further explorations were required for the synthesis of transparent films including large meso- and larger macropores in the same film, and with the possibility to tune the thickness for higher enzyme loadings.

In Chapter 4, an exploratory screening of different approaches for the synthesis of multi-scale porous systems was presented. Several routes to synthesize in the same material pores with different relevant sizes for biosensing (specifically large meso- and macropores) were investigated, emphasizing their potential to be used as enzyme carriers for lactate biosensors. In this evaluation, the advantages and disadvantages of each synthetic path were described. A powder approach for the synthesis of meso and multi-scale porous films was distinguished among the various possibilities as a simple and highly suitable method to synthesize hierarchically porous films. This method followed a top-down approach using pre-synthesized silica aggregates which, in combination with polymer particles as porogenic templates, offered the possibility to obtain multi-scale porous films via water-based formulations. In these porous systems, the macropores size was found to depend on the polymer particle used, and they were surrounded by an interconnected network of mesopores, formed by the interstitial spaces between silica aggregates. The high transparency of the films obtained by this method, together with the possibility to control the macropore size, the film thickness and the scalability of the process were among the most important criteria to select this method for further investigations in this work as enzyme supports for lactate biosensing applications.

In the second part of this work, described in Chapters 5 and 6, mesoporous and hierarchically nanostructured silica films were post-functionalized for enzyme immobilization and compared as enzymes supports for the development of optically responsive patches for L-lactate detection. Additionally, a method to assemble enzyme-based biosensing particles using porous CaCO₃ microsphere scaffolds was developed. The two most reported enzymes for lactate detection, L-lactate dehydrogenase (LDH) and L-lactate oxidase (LOx) were immobilized in these porous materials and the resulting systems were characterized in terms of their response towards lactate detection.

In Chapter 5, a comparative study of mesoporous and multi-scale porous films as enzyme supports for LDH was performed. Their nanostructure, porosity and surface charge behavior were investigated, described and analyzed with an emphasis on their consequences for enzyme diffusion and loading, thereby addressing the key challenge of transport limitation of large molecules in mesoporous materials. Films with surface area values of 194 m²/g and 179

m^2/g were obtained for mesoporous and multi scale porous films, respectively, and with a total porosity higher than 80%. Large mesopores of 30 nm in size were measured by nitrogen adsorption porosimetry and BET analysis in the films, and the presence of macropores was confirmed by mercury intrusion porosimetry measurements in the multi-scale systems. SEM images showed macropores of 250 nm in diameter, using polymer template particles of approximately 280 nm in size. Adsorption and desorption of LDH in these porous films could successfully be tracked using quartz crystal microbalance measurements, confirming higher enzyme loadings and better stability against desorption in hierarchically porous films. LDH was immobilized on amino-functionalized silica films by covalent attachment using glutaraldehyde. To characterize the behaviour of these systems in the context of biosensing for lactate, formation of the reaction product (NADH) was followed over time at different lactate concentrations. Hierarchically nanostructured films were found to be advantageous for increased enzyme loading, better stability, and more reliable and faster response compared to simple mesoporous ones. In particular, the higher enzyme activity on the hierarchical films allowed a two times more sensitive and much more robust detection of L-lactate than using the mesoporous counterparts. The estimation of effective diffusivities of LDH in the porous films showed that its diffusion was slowed down in the mesopores mostly due to the pore size effect, while tortuosity was found to play only a minor role. To maximize the benefits of the films high surface area for enzyme immobilization, the incorporation of macropores in the film structure was found pertinent. Such macropores facilitated the diffusion of LDH to access such high surface area through connected windows between macropores. A theoretical analysis of different macropore locations in the film showed that those available at the surface were the most effective at attaining higher enzyme loadings; in the case of macropores connected to other macropores buried within the film, the access of the enzyme to the high surface area of the film was facilitated and higher enzyme loadings could be explained compared to mesoporous films. In summary, LDH was found to be a highly suitable enzyme for L-lactate biosensing, in particular when immobilized on hierarchically porous silica supports. However, a disadvantage of using LDH in the development of lactate biosensors is the need of a cofactor, the NAD^+ molecule, which binds the active site of the enzyme, producing a three-dimensional conformation change of the biomolecule in order to perform its catalytic activity. The immobilization of both LDH and NAD^+ in the same material has proven to be not feasible in view of this required interaction. Therefore, as a next step in this thesis, the challenge was to design a biosensing material for L-lactate with all the necessary elements integrated in the same matrix.

In Chapter 6, a different concept of biosensing films was developed using an alternative enzyme, lactate oxidase (LOx). While it does not need the presence of a cofactor for its reaction scheme, the reaction product hydrogen peroxide needs to be detected indirectly; therefore, a key challenge of Chapter 6 was the development of combined 'all-in-one' biosensing films in which both the enzyme and an indicator molecule, cytochrome C (CytC), are immobilized. This challenge was solved by using a layer-by-layer polyelectrolyte deposition technology in combination with porous silica substrates. For the development of patches, hybrid enzyme-silica films were synthesized first by covalently immobilizing LOx within the porous silica supports. Secondly, cytochrome C (CytC) was co-immobilized by adsorption via a polyelectrolyte layer-by-layer technique. High CytC loads could be achieved under suitable electrostatic conditions during the layer-by-layer deposition. Both mesoporous and

Chapter 7. Conclusions and Outlook

hierarchically porous silica films were evaluated as enzymes supports. While both types of films allowed enzyme immobilization, the hierarchical system exhibited a faster and more robust response, analogous to the previous results obtained using LDH. The pore size effect on the LOx diffusion was considered the reason of the poor performance of mesoporous systems. In addition to the film-based biosensing materials, the developed layer-by-layer approach was also used to assemble particle-based detection systems, forming LOx-CytC protein particles with intact enzymatic activity. To form these particles, calcium carbonate microspheres were used as templates and LOx and CytC were adsorbed one after the other into the porous particles. LOx remained active even after the inorganic core particle was removed. Their capability to detect the presence of lactate was demonstrated in a single particle by fluorescence microscopy. This microparticle-based system represents a clear contribution towards the development of lactate biosensors in inhomogeneous media, where the size of the probe represents a challenge for a reliable quantification next to the source, such as in cell cultures.

General Conclusions and Outlook

This work reports on the design, the synthesis and the performance characterization of multi-scale porous materials for lactate biosensing. Methods for a robust and reproducible synthesis of multi-scale porous films and particles were developed with an emphasis on the inclusion of large mesopores (10-50 nm) and macropores (50-300 nm). These materials have been functionalized with lactate-consuming enzymes towards the optical detection of L-lactate within concentrations relevant for real applications (0-20 mM) in the food, health care and biotech fields. Overall, the utilization of multi-scale porous materials enhanced the transport of enzymes during immobilization and facilitated their access to the high surface area of the materials, resulting in better performance for L-lactate detection compared to purely mesoporous matrices. Two optical-biochemical detection schemes were developed: A first one comprised the use of L-lactate dehydrogenase for the detection of lactate in solution through the immobilization of the enzyme in porous silica films, with optical detection of the reaction product NADH in the bulk solution. A second scheme involved the use of L-lactate oxidase, co-immobilized with cytochrome C as an optical indicator molecule. This second scheme allowed to form 'all-in-one' materials, with all catalytic and optically active molecules integrated into the same hybrid film. This scheme resulted in the successful formation and evaluation of two lactate-responsive materials: colorimetric patches and micrometric probe particles. This achievement is expected to bring significantly more flexibility for the design of possible detection systems and instrumentation, resulting in the advancement of this work towards the development of novel biosensing materials for lactate detection with realistic applications. A summary of the challenges vs achievements of this work is presented in Table 7.1

Based on the broad concepts developed here, future work in the area lactate detection with enzyme-based biosensors should include (i) further optimization of the nanostructures for enhanced enzyme loads; (ii) the development of alternative immobilization protocols and their evaluation on enzyme loading; (iii) the application to more complex media, e.g. real physiological fluids or industrial reaction media; (iv) the exploration of additional sensing schemes to track enzyme activity while keeping the same porous films as support (e.g. lumi-

Table 7.1 – General overview of challenges, approaches and achievements of this thesis.

Challenges	Approach	Achievements
Porosity	Block copolymer templating Powder & polymer particle templating	<input checked="" type="checkbox"/> Multiscale porous films <input checked="" type="checkbox"/> Interconnected pores <input checked="" type="checkbox"/> Robust, reproducible <input checked="" type="checkbox"/> Biocompatible silica formulations
Mass transport	Large mesopores, hierarchical porosity	
Interconnectivity	Formulation, casting	
Biocompatibility	Silica, protein-based particles	
Immobilization	Grafting, adsorption	<input checked="" type="checkbox"/> Loading of enzymes
Selectivity	Enzyme-based detection with LDH, LOx	<input checked="" type="checkbox"/> Enzyme activity retained in films & particles <input checked="" type="checkbox"/> LOx/CytC films, cofactor-free detection <input checked="" type="checkbox"/> No cross-talk evaluation
Transparency	Thickness, nanostructuring	<input checked="" type="checkbox"/> 100 nm - few μm thick <input checked="" type="checkbox"/> Homogeneous coating
Sensitivity	0-20 mM	<input checked="" type="checkbox"/> Targeted range achieved for medical, biotech, food applications

nescence). An important step for further investigations will be the integration of the films discussed here into actual biosensor devices. A key advantage of the materials developed here is that their readout can be performed with standard optical methods. Therefore, the instrumental implementation for viable biosensor devices is expected to be relatively inexpensive. For example, a straightforward implementation of the concepts proposed in this work is the adaptation of the films to patches readable by portable spectrophotometer that could be used to measure directly the concentration of lactate in a given sample, as shown in Figure 7.1. A portable photometric device would then facilitate the prompt analysis of samples, giving straightforward information about the process or product evaluated, for instance, for quality control measurements, in field studies, or for mobile clinical applications. This implementation can be extended to other metabolites by modifying the functionalization of the patches according to the analyte of interest.

A second implementation consists in the use of paper as in the principle of origami for the development of 3-D paper-based microfluidic devices. The applicability of these devices has been demonstrated by colorimetric and fluorescence assays using multilayer systems based on paper folding. The methods to produce porous films in this work are compatible with existing printing techniques on paper, which would enable the fabrication of large surface areas of coated paper in a facile, fast, cost-effective and reproducible way. Additionally, the assembly of such devices would not require additional equipment or advanced skills, which is beneficial in remote areas where access to such resources is limited. This represents an outstanding opportunity to develop biosensing materials for point of care applications in less-favored countries where access to advanced technologies is limited.

Finally, an implementation of the microparticle-based detection of lactate can be envisaged

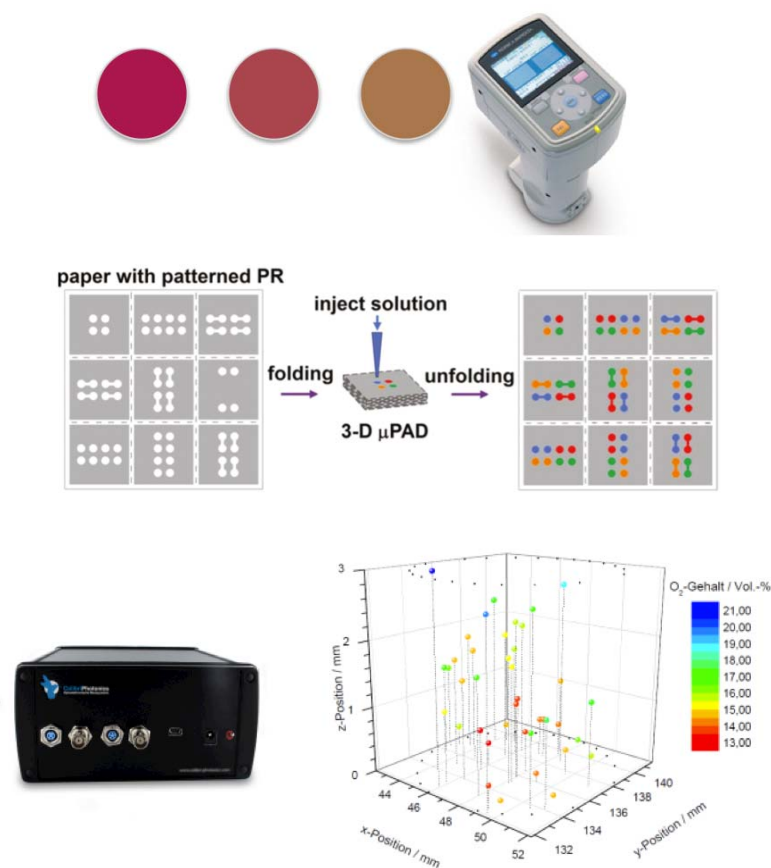


Figure 7.1 – Outlook: schematic overview of possible implementations of the biosensing materials developed in this thesis. *Top panel:* Representation of the colorimetric patches developed in this work. A straightforward application of these biosensing materials can be achieved using portable spectrophotometers (Konica Minolta model CM-700d, image obtained from the manufacturer’s website²⁹²). *Middle panel:* Origami-based 3-D fabrication of one-piece, single step biosensing devices. This speeds up the fabrication process and reduces cost. Parallel analyses are possible. (reprinted with permission from Liu et al.²⁹³, ©American Chemical Society). *Lower panel:* Fluorescence-based device for 3-D oxygen detection via optical particle localization²⁹⁴. This approach allows real-time, non-invasive measurements from distances up to 1 meter, which could be extended to lactate and other relevant analytes based on the enzyme microparticle approach developed in this thesis (Image from Colibri Photonics, obtained from the company’s website²⁹⁵)

in combination with commercially available fluorometers, which are able to measure fluorescence in a bulk solution in an inexpensive way, as the cost of typical single-channel devices is low. Additionally, an important and current application of the developed microparticles is the analysis of complex media where inhomogeneous distribution of lactate is often a challenge for representative measurements. The scheme developed in this work may contribute to a solution in this area. For example, current non-invasive oxygen sensor systems are able to locally detect micrometric probes in a 3-D medium^{294;295} (see for example Colibri Photonics

(<http://www.colibri-photonics.com>). While those commercially available technologies have focused on the quantification of oxygen at different depths in a 3-D sample, an extension of this technology can be obtained if other micrometric probes are developed, like in this work, for the monitoring of relevant analytes in the agro-food and biotech industries. In this sense, the results of this work represent a realistic contribution to the field of lactate biosensing for real applications.

In summary, the combined investigation of suitable support materials, including the porosity design and processing aspects, the functionalization of these support materials with enzymes, and the performance characterization of the resulting materials for the detection of physiologically relevant analyses have led to novel inorganic/organic films and microparticles for biosensing. These results are expected to be widely applicable for inexpensive optical biosensing in a wide range of industrial and medical scenarios.

A Supporting Information for Chapter 3

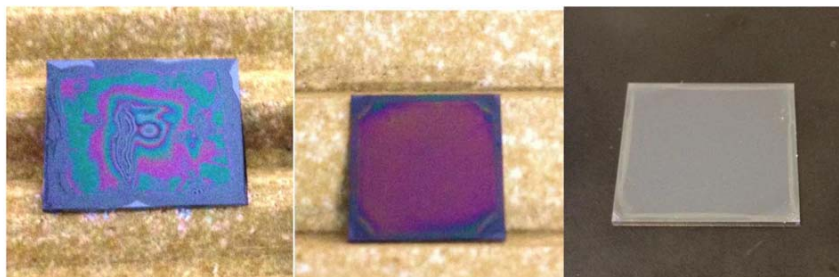


Figure A.1 – Images of PS-P2VP-silica coatings deposited by spin coating on silicon substrates. Silica films formed from sols in different solvents. Left: ethanol, middle: 1-butanol, and right: 1-butanol after heat treatment. Color variations indicate inhomogeneities in the film thickness. Film dimensions: 2 cm².

Table A.1 – Calibration curve data from Commassie brilliant blue G solutions.

Conc. $\mu\text{g/mL}$	Conc. mol/L	Abs corr.
0	0	0.0000
0.01	$1.17 \cdot 10^{-8}$	0.0084
0.05	$5.85 \cdot 10^{-8}$	0.0073
0.1	$1.17 \cdot 10^{-7}$	0.0093
1	$1.17 \cdot 10^{-6}$	0.0339
5	$5.85 \cdot 10^{-6}$	0.1319
10	$1.17 \cdot 10^{-5}$	0.2300
15	$1.76 \cdot 10^{-5}$	0.3973
20	$2.34 \cdot 10^{-5}$	0.5304
25	$2.93 \cdot 10^{-5}$	0.6705
30	$3.51 \cdot 10^{-5}$	0.7987

Appendix A. Supporting Information for Chapter 3

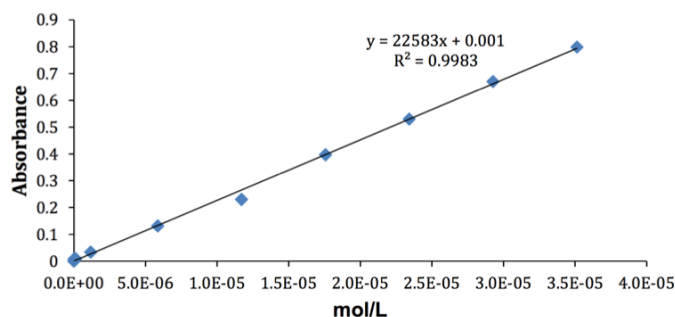


Figure A.2 – Calibration curve from Coomassie brilliant blue G for the estimation of available amino groups in mesoporous silica films.

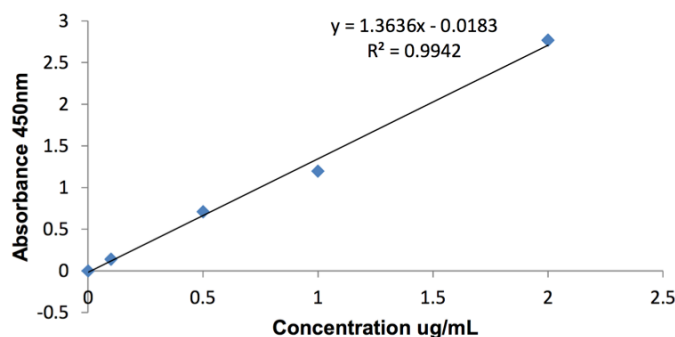


Figure A.3 – Calibration curve from TMB after acidification of the medium.

Table A.2 – Spectrophotometric measurements of desorbed Coomassie brilliant blue G from amino-functionalized porous silica films.

	Flat sample	Sample A	Sample B	Sample C
Absorbance	0.05531	0.1893	0.3096	0.5536
	0.0668	0.2064	0.3099	0.5565
	0.0650	0.2091	0.3106	0.5578
	0.0667	0.2097	0.3110	0.5590
		0.2086	0.3130	0.5620
Average	0.0634	0.2046	0.3108	0.5578
Std. dev	0.00550	0.00865	0.00134	0.00310
Conc. mol/L	$2.77 \cdot 10^{-6}$	$9.02 \cdot 10^{-6}$	$1.37 \cdot 10^{-5}$	$2.47 \cdot 10^{-5}$
Ratio Ref.	1.0	3.3	5.0	8.9

Table A.3 – Spectrophotometric measurements from the oxidation of TMB by HRP immobilized in porous silica films and measured at 650 nm.

Time min	Flat sample	Sample A	Sample B	Sample C
	Average	Average	Average	Average
5	0.0463 ± 0.0170	0.0648 ± 0.0214	0.0792 ± 0.0230	0.1230 ± 0.0163
10	0.0080 ± 0.0743	0.0743 ± 0.007	0.1002 ± 0.0029	0.2044 ± 0.0189
15	0.1358 ± 0.0168	0.1013 ± 0.0103	0.1462 ± 0.0066	0.2687 ± 0.0147
20	0.1798 ± 0.0347	0.1308 ± 0.0141	0.1846 ± 0.0075	0.3298 ± 0.0205
25	0.2111 ± 0.0394	0.1558 ± 0.0137	0.2176 ± 0.0111	0.3712 ± 0.0211
30	0.2350 ± 0.0464	0.1777 ± 0.0115	0.2598 ± 0.0169	0.4125 ± 0.0255

Table A.4 – Apparent concentration of HRP in the films obtained from calibration curve (measured at 30 min at a wavelength of 450nm).

	Flat sample	Sample A	Sample B	Sample C
Abs corr	0.0991	1.1617	1.6723	2.8674
Conc ($\mu\text{g HRP/mL}$)	0.0593	0.8385	1.2130	2.0894
Std dev.	0.0337	0.0709	0.0878	0.0871
Ratio	1	14.2	20.5	35.3

Table A.5 – Equivalent enzyme activity normalized with film thickness. For each film, the apparent activity is shown as the equivalent HRP concentration $c_{eq(HRP)}$ of a free enzyme solution is shown in mol/mL (assuming a nominal relative molecular weight of HRP of 44173 g/mol). $c_{eq(HRP),norm}$ is the equivalent HRP concentration normalized with film thickness.

	Sample A	Sample B	Sample C
Film thickness (nm)	330	430	560
$c_{eq(HRP)}$ (mol/mL)	$1.83 \cdot 10^{-11}$	$2.81 \cdot 10^{-11}$	$4.98 \cdot 10^{-11}$
$c_{eq(HRP),norm}$ (mol/mL)/nm	$5.56 \cdot 10^{-14}$	$6.53 \cdot 10^{-14}$	$8.89 \cdot 10^{-14}$

Table A.6 – Physical properties of solvents present in the sol-gel formulations²⁹⁶.

Solvent	Molar volume ($\text{cm}^3 \cdot \text{mol}^{-1}$)	Surface tension ($\text{mN} \cdot \text{m}^{-1}$)	Vapor pressure (Pa)	Viscosity (mPa·s)
Water	18	72.86	2306	1
Ethanol	58.5	22.39	5866	1.114
Butanol	91.5	24.6	560	2.947

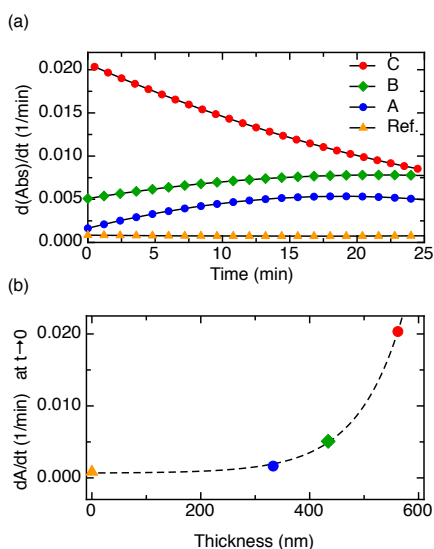


Figure A.4 – (a) Slope of the absorbance vs. time curves in Fig. 3.11 for the oxidation of TMP from HRP-loaded porous silica films (C, red circles: film thickness 562 nm; B, green diamonds: 434 nm; A, blue circles: 333 nm; D, orange triangles: flat surface used as reference). For the thinner films A and B, dA/dt takes about 15-20 minutes to increase to the maximum rate, while the thickest film C already produces at the fastest rate from the beginning. (b) Initial value of the slope at zero time plotted against the film thickness.

B Supporting Information for Chapter 4

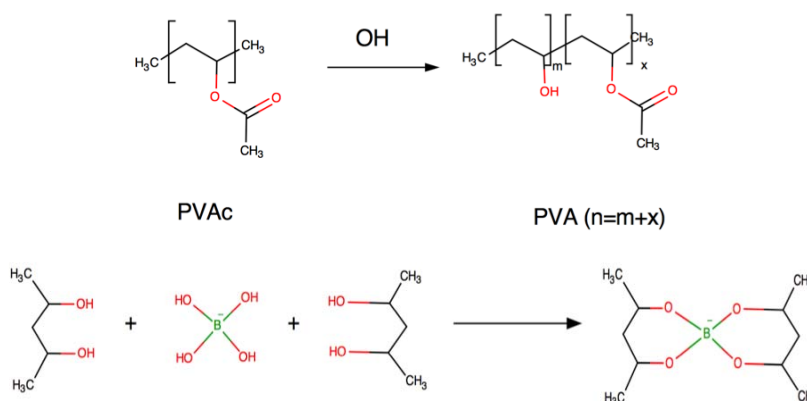


Figure B.1 – Top: Hydrolysis of polyvinyl acetate (PVAc) yields polyvinyl alcohol (PVA) with different degrees of alcohol functionalities. Hydrolysis of PVAc is usually incomplete ($x > 0$), influencing the feasibility of cross-linking with boric acid. m/n is the degree of hydrolysis; for the PVA used in this work, its value is $m/n \approx 88\%$ ²¹⁶. Bottom: PVA cross-linking with boric acid.

C Supporting Information for Chapter 5

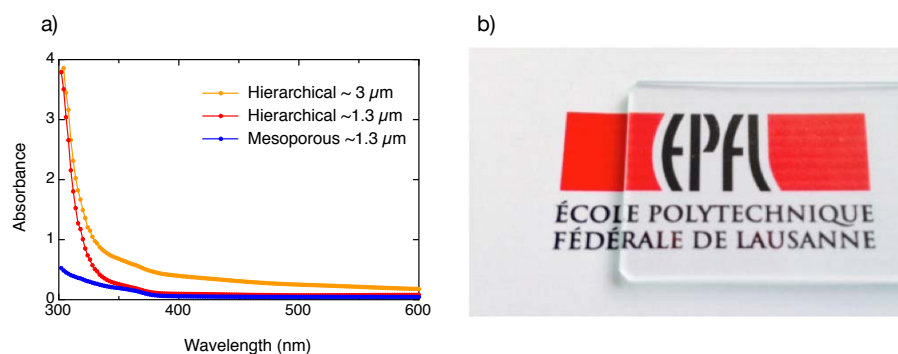


Figure C.1 – a) Spectra of transparent mesoporous and hierarchically porous films on glass, demonstrating transparency in the range of interest; b) image of a hierarchically porous film of about 1.3 μm thickness

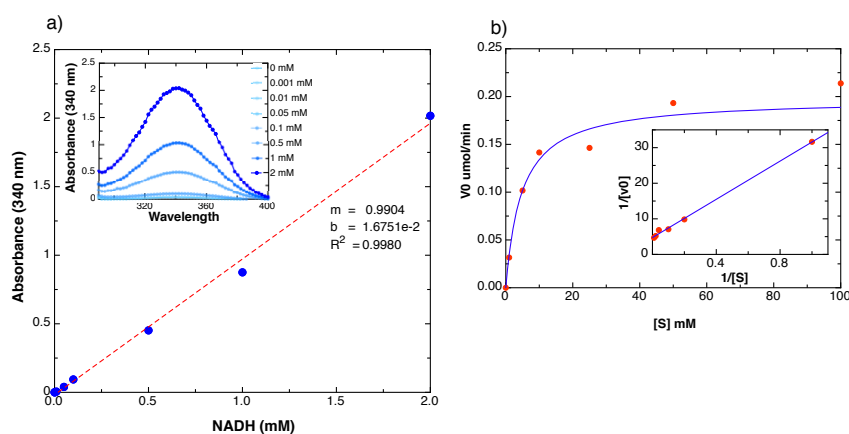


Figure C.2 – a) Calibration curve of LDH. The inset graph shows the spectra of NADH at different concentrations. b) Michaelis-Menten fit for LDH. The inset picture shows the double reciprocal of the Michaelis-Menten curve, the Lineweaver-Burk plot, from which kinetic parameters are obtained.

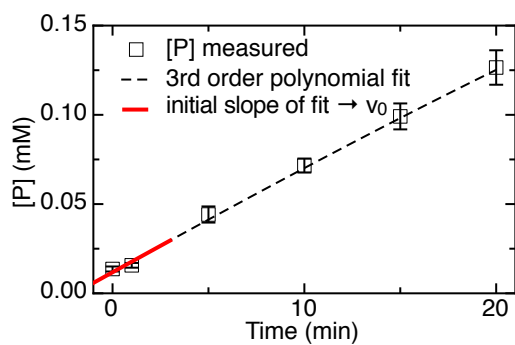


Figure C.3 – Example for the derivation of the initial reaction rate v_0 from the product concentration [P] vs. time data. A third order polynomial is fitted to the concentration vs. time data using the data analysis software ProFit (Quansoft, Mac OS X), and the initial reaction rate is obtained numerically from its slope.

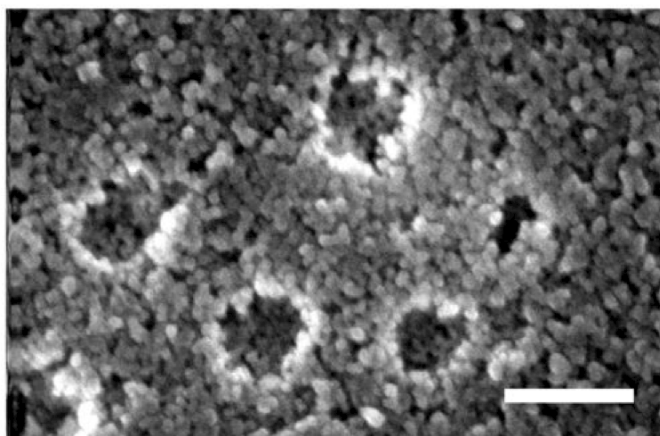


Figure C.4 – SEM image of a hierarchically porous silica film. Scale bar: 1 μm

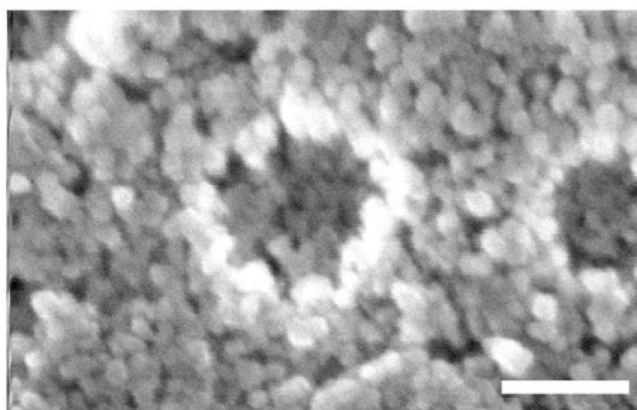


Figure C.5 – SEM image with higher amplification of a hierarchically porous film. Macropores are surrounded by silica aggregates. Each aggregate each composed of silica nanoparticles. The image shows small spherical aggregates with an average size of 40-50nm. Scale bar: 200 nm

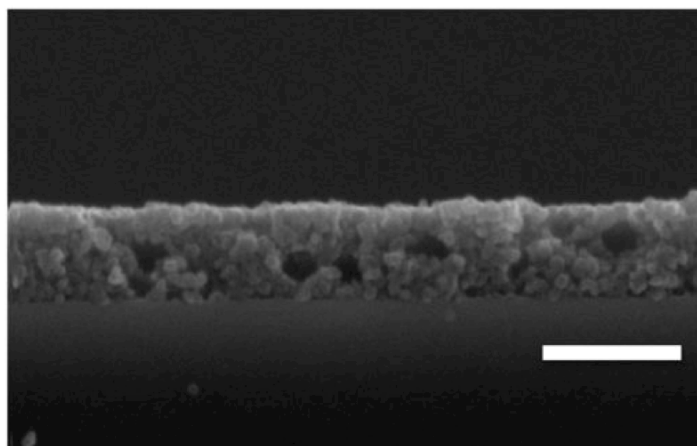


Figure C.6 – SEM image of the cross section from a hierarchically porous silica film. The macropores are around 250nm. Scale bar: 1 μm

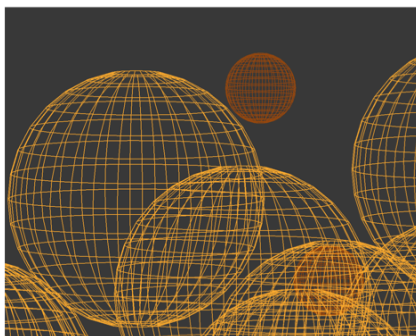


Figure C.7 – Example for the mesh structure used in the visual modelling of silica aggregates and enzyme molecules. Each particle or molecule was created as a spherical mesh with 512 faces and scaled according to the SEM images or known molecular diameter. Yellow: mesh of the silica sphere units; orange: mesh used to model the enzyme

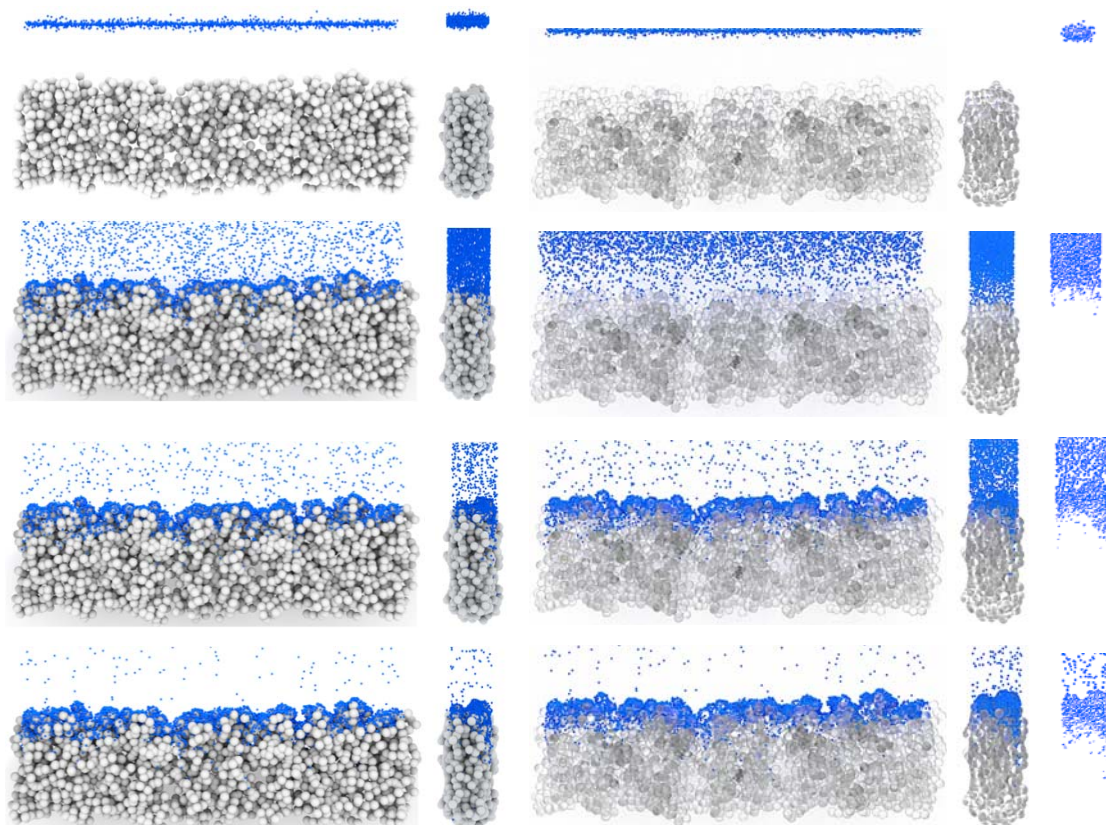


Figure C.8 – Example for a sequence of images generated for the visual modelling approach. LDH diffusion over time in mesoporous films represented as solid (left) and transparent (right) materials. From top to bottom: 1. blank film at the start of the simulation, 2. generation of 6000 enzyme molecules as spherical particles in a plane 200 nm above the film at time $t=0$ s, 3. intermediate step of enzyme diffusion and adsorption to the film, 4. final step after the sequence was stopped after 500 s. The side view of the films shows the diffusion of the enzyme molecules along the z axis (film thickness).

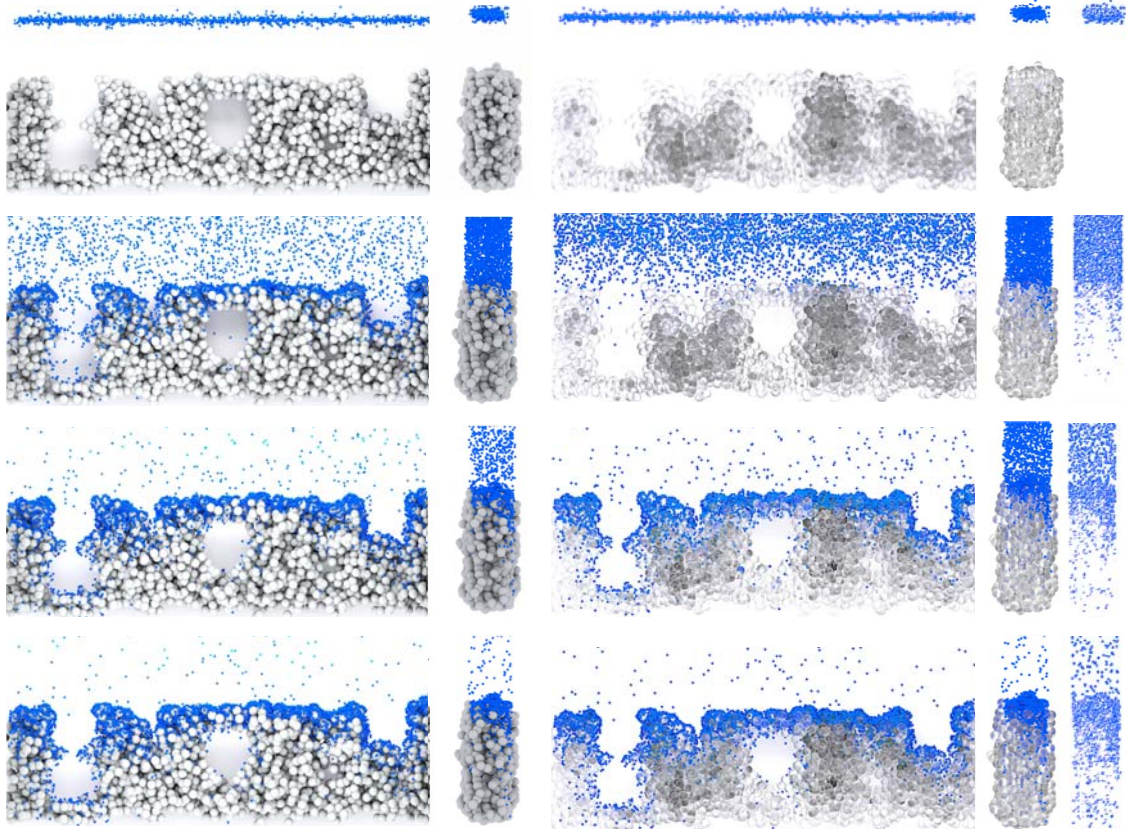


Figure C.9 – Example for a sequence of images generated for the visual modelling approach. LDH diffusion over time in multiscale porous films represented as solid (left) and transparent (right) materials. From top to bottom: 1. blank film at the start of the simulation, 2. generation of 6000 enzyme molecules as spherical particles in a plane 200 nm above the film at time $t=0$ s, 3. intermediate step of enzyme diffusion and adsorption to the film, 4. final step after the sequence was stopped after 500 s. The side view of the films shows the diffusion of the enzyme molecules along the z axis (film thickness).

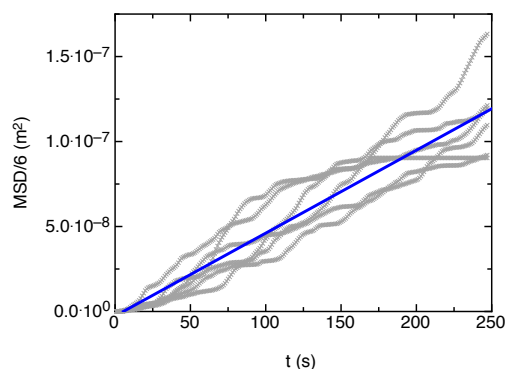


Figure C.10 – Calibration of Brownian motion for visual modelling. Mean squared displacement (MSD or $\langle \Delta x^2 \rangle$) for lactate dehydrogenase obtained from the simulated Brownian motion images. Grey curves show the Δx^2 for several simulated particles given by the Blender™ software. The solid line is the averages, and its slope is related to the diffusivity by $\langle \Delta x^2 \rangle = 6Dt$. To obtain realistic motion of the enzyme molecules in the visualization, the parameters for Brownian motion were set in the software to match the bulk diffusivity from literature for lactate dehydrogenase⁸⁴ ($D \approx 5 \cdot 10^{-11} \text{ m}^2/\text{s}$).

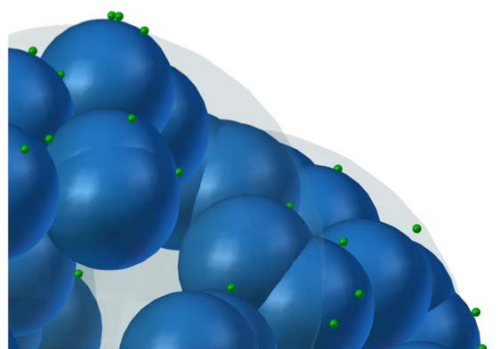


Figure C.11 – Schematic visualization from Fig. 5.13, shown here with the actual size scale of L-lactate vs. LDH (blue spheres: LDH, green spheres: L-lactate, opaque grey spheres: silica film). In Chapter 5 the spheres representing lactate were scaled by a factor of 10 for better illustration; here, the original size is shown).

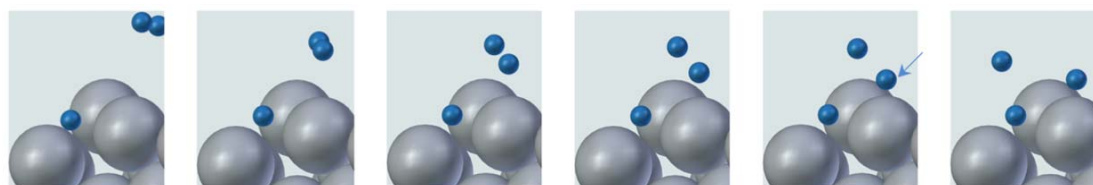


Figure C.12 – Close-up images of the visual modelling performed visualized using the Blender™ software. Grey spheres are schematized silica unit particles (50 nm diameter) within an aggregate. Blue spheres are lactate dehydrogenase molecules moving by diffusion (Brownian motion model). The arrow shows the moment of collision of an enzyme molecule on the silica surface. To visualize adsorption, the silica surface is adhesive (attractive hard wall potential).

D Supporting Information for Chapter 6

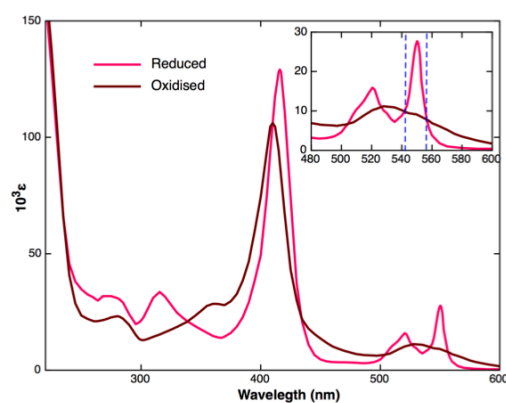


Figure D.1 – Reference spectra of reduced and oxidized CytC in solution. Data obtained from Margoliash²⁷³.

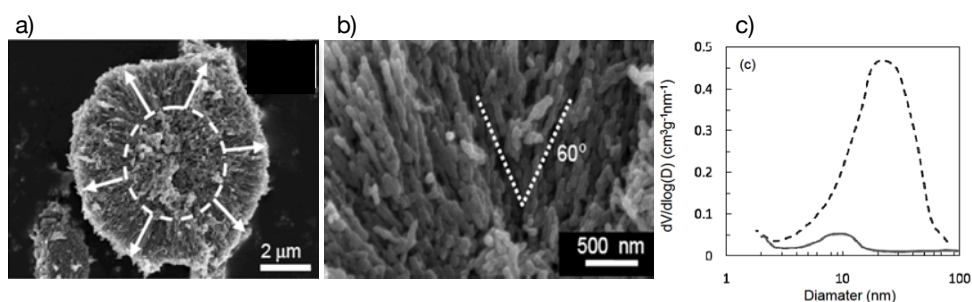


Figure D.2 – Reference information for the calcium carbonate microparticles based on images from the publication by Imai et al.¹⁰⁸ a) Cross-section SEM image showing branches of nanocrystals growing radially from the core of the microparticle, b) close-up of CaCO_3 branches composed of single nanoparticles and c) pore size distribution of the microparticles: continuous line shows porosity before PSS removal by heat treatment; dashed line shows porosity after PSS removal. Reprinted with permission, ©American Chemical Society.

Bibliography

- [1] C. Boero, S. Carrara, G. Del Vecchio, L. Calzà, and G. De Micheli. Highly sensitive carbon nanotube-based sensing for lactate and glucose monitoring in cell culture. *IEEE Transactions on NanoBioscience*, 10(1):59–67, 2011.
- [2] M. Brandstetter, L. Volgger, A. Genner, C. Jungbauer, and B. Lendl. Direct determination of glucose, lactate and triglycerides in blood serum by a tunable quantum cascade laser-based mid-ir sensor. *Applied Physics B*, 110(2):233–239, 2013.
- [3] W. C. Clegern, M. E. Moore, M. A. Schmidt, and J. Wisor. Simultaneous electroencephalography, real-time measurement of lactate concentration and optogenetic manipulation of neuronal activity in the rodent cerebral cortex. *The Journal of Visualized Experiments (JoVE)*, 70:e4328, 2012.
- [4] J. M. Goran, J. L. Lyon, and K. J. Stevenson. Amperometric detection of L-lactate using nitrogen-doped carbon nanotubes modified with lactate oxidase. *Analytical Chemistry*, 83(21):8123–8129, 2011.
- [5] D. Groegel, M. Link, and O. S. Duerkop, Axel A. Wolfbeis. A new fluorescent pet probe for hydrogen peroxide and its use in enzymatic assays for L-lactate and D-glucose. *ChemBioChem*, 12(18):2779–2785, 2011.
- [6] Z. H. Ibupoto, S. M. U. A. Shah, K. Khun, and M. Willander. Electrochemical l-lactic acid sensor based on immobilized zno nanorods with lactate oxidase. *Sensors*, 12(3):2456–2466, 2012.
- [7] S. G. Ignatov, J. A. Ferguson, and D. R. Walt. A fiber-optic lactate sensor based on bacterial cytoplasmic membranes. *Biosensors and Bioelectronics*, 16(1):109–113, 2001.
- [8] W. Jia, A. J. Bandodkar, G. Valdés-Ramírez, J. R. Windmiller, Z. Yang, J. Ramírez, G. Chan, and J. Wang. Electrochemical tattoo biosensors for real-time noninvasive lactate monitoring in human perspiration. *Analytical Chemistry*, 85(14):6553–6560, 2013.
- [9] X. Liu and W. Tan. Development of an optical fiber lactate sensor. *Microchimica Acta*, 131(1-2):129–135, 1999.
- [10] S. de Marcos, J. Galbá, and J. R Castillo. An enzyme fluorescence quenching method for the determination of lactate in synthetic blood serum. *Analytical Sciences*, 11(2):233–238, 1995.

Bibliography

- [11] C. A. Marquette, B. D. Leca, and L. J. Blum. Electrogenerated chemiluminescence of luminol for oxidase-based fibre-optic biosensors. *Luminescence*, 16(2):159–165, 2001.
- [12] M. M. Rahman. Fabrication of l-lactate biosensor based on redox species mediated lactate oxidase using micro-device. *International Journal of Biological and Medical Research*, 1(3):9–14, 2010.
- [13] C-Cit AG. Citsens bio lactate sensor, URL: <http://www.c-cit.ch/en/katalog/citsens-bio-laktat-sensor/>, August 9th, 2013.
- [14] Pinnacle Technology. Lactate biosensor; <http://www.pinnaclet.com/lactate.html>, August 9th, 2013.
- [15] E. Naylor, D. V. Aillon, B. S. Barrett, G. S. Wilson, D. A. Johnson, D. A. Johnson, H. P. Harmon, S. Gabbert, and P. A. Petillo. Lactate as a biomarker for sleep. *Sleep*, 35(09):1209–1222, 2012.
- [16] L. A. Newman, D. L. Korol, and P. E. Gold. Lactate produced by glycogenolysis in astrocytes regulates memory processing. *PLoS ONE*, 6(12):e28427, 2011.
- [17] B. Phypers and J. M. T. Pierce. Lactate physiology in health and disease. *Continuing Education in Anaesthesia, Critical Care & Pain*, 6(3):128–132, 2006.
- [18] M. R. Romero, F. Ahumada, F. Garay, and A. M. Baruzzi. Amperometric biosensor for direct blood lactate detection. *Analytical Chemistry*, 82(13):5568–5572, 2010.
- [19] N. Nikolaus and B. Strehlitz. Amperometric lactate biosensors and their application in (sports) medicine, for life quality and wellbeing. *Microchimica Acta*, 160(1-2):15–55, 2008.
- [20] A. Philp, A. L. Macdonald, and P. W. Watt. Lactate—a signal coordinating cell and systemic function. *Journal of Experimental Biology*, 208(24):4561–4575, 2005.
- [21] F. Zagari, M. Jordan, M. Stettler, H. Broly, and F. M. Wurm. Lactate metabolism shift in cho cell culture: the role of mitochondrial oxidative activity. *New Biotechnology*, 30(2):238–245, 2013.
- [22] X. T. Zheng, H. B. Yang, and C. M. Li. Optical detection of single cell lactate release for cancer metabolic analysis. *Analytical Chemistry*, 82(12):5082–5087, 2010.
- [23] T. B. Goriushkina, A. P. Soldatkin, and S. V. Dzyadevych. Application of amperometric biosensors for analysis of ethanol, glucose, and lactate in wine. *Journal of Agricultural and Food Chemistry*, 57(15):6528–6535, 2009.
- [24] Servier Medical Art. <http://www.servier.com/powerpoint-image-banks>, accessed March 10th 2015.
- [25] K. Hosoya, T. Kondo, M. Tomi, H. Takanaga, S. Ohtsuki, and T. Terasaki. Mct1-mediated transport of l-lactic acid at the inner blood–retinal barrier: a possible route for delivery of monocarboxylic acid drugs to the retina. *Pharmaceutical Research*, 18(12):1669–1676, 2001.

- [26] T. Shimomura, T. Sumiya, M. Ono, T. Ito, and T.-a. Hanaoka. Amperometric l-lactate biosensor based on screen-printed carbon electrode containing cobalt phthalocyanine, coated with lactate oxidase-mesoporous silica conjugate layer. *Analytica Chimica Acta*, 714(0):114–120, 2012.
- [27] S. H. Choi and K. B. Chin. Evaluation of sodium lactate as a replacement for conventional chemical preservatives in comminuted sausages inoculated with listeria monocytogenes. *Meat Science*, 65(1):531–537, 2003.
- [28] S. Smaoui, H. B. Hlima, and R. Ghorbel. The effect of sodium lactate and lactic acid combinations on the microbial, sensory, and chemical attributes of marinated chicken thigh. *Poultry Science*, 91(6):1473–1481, 2012.
- [29] R. H Schmidt and G. E. Rodrick. *Food Safety Handbook*. John Wiley & Sons, 2003.
- [30] L. A. Palomares, S. Estrada-Moncada, and O. T. Ramírez. Production of recombinant proteins. In *Recombinant Gene Expression*, pages 15–51. Humana Press, 2004.
- [31] J. J. Greene. Host cell compatibility in protein expression. In *Recombinant Gene Expression*, pages 3–14. Humana Press, 2004.
- [32] B. Nagel, H. Dellweg, and L. Gierasch. Glossary for chemists of terms used in biotechnology (IUPAC recommendations 1992). *Pure and Applied Chemistry*, 64(1):143–168, 2009.
- [33] Transparency Market Research. Biosensors market. electrochemical, optical, thermal, piezoelectric. global industry analysis, size, share, growth, trends and forecast 2014-2020, <http://www.transparencymarketresearch.com>, November 2014.
- [34] R. Monošík, M. Stredanský, and E. Šturdík. Biosensors - classification, characterization and new trends. *Acta Chimica Slovaca*, 5(1):109–120, 2012.
- [35] Markets and Markets. Biosensors market by application (point of care, home diagnostics, research labs, biodefense, environmental monitoring, food industry), product (wearable, non-wearable), technology (electrochemical, piezoelectric, optical) & geography - analysis & forecast to 2020, report code: SE 3097, <http://www.marketsandmarkets.com>, January 2015.
- [36] J. Anzai, H. Takeshita, Y. Kobayashi, T. Osa, and T. Hoshi. Layer-by-layer construction of enzyme multilayers on an electrode for the preparation of glucose and lactate sensors: elimination of ascorbate interference by means of an ascorbate oxidase multilayer. *Analytical Chemistry*, 70(4):811–817, 1998.
- [37] I. H. Boyaci and M. Mutlu. Amperometric biosensors in food processing, safety, and quality control. In *Biosensors in Food Processing, Safety, and Quality Control*. CRC Press, 2012.
- [38] C. R. Ispas, G. Crivat, and S. Andreescu. Review: recent developments in enzyme-based biosensors for biomedical analysis. *Analytical Letters*, 45(2-3):168–186, 2012.

Bibliography

- [39] B. Liu, Y. Cao, D. Chen, J. Kong, and J. Deng. Amperometric biosensor based on a nanoporous zro 2 matrix. *Analytica Chimica Acta*, 478(1):59–66, 2003.
- [40] C. Qin, C. Chen, Q. Xie, L. Wang, X. He, Y. Huang, Y. Zhou, F. Xie, D. Yang, and S. Yao. Amperometric enzyme electrodes of glucose and lactate based on poly (diallyldimethylammonium)-alginate-metal ion-enzyme biocomposites. *Analytica Chimica Acta*, 720:49–56, 2012.
- [41] L. Rassaei, W. Olthuis, S. Tsujimura, E. R. Sudhölter, and A. Berg. Lactate biosensors: Current status and outlook. *Analytical and Bioanalytical Chemistry*, 406(1):123–137, 2014.
- [42] G. De Micheli, C. Boero, C. Baj-Rossi, I. Taurino, and S. Carrara. Integrated biosensors for personalized medicine. In *Proceedings of the 49th Annual Design Automation Conference*, pages 6–11. ACM, 2012.
- [43] I. A Ges and F. Baudenbacher. Enzyme-coated microelectrodes to monitor lactate production in a nanoliter microfluidic cell culture device. *Biosensors and Bioelectronics*, 26(2):828–833, 2010.
- [44] A. Heller and B. Feldman. Electrochemical glucose sensors and their applications in diabetes management. *Chemical Reviews*, 108(7):2482–2505, 2008.
- [45] S. Spichiger and U. E. Spichiger-Keller. New single-use sensors for online measurement of glucose and lactate: The answer to the pat initiative. In *Single-Use Technology in Biopharmaceutical Manufacture*, pages 295–299. John Wiley & Sons, Inc., 2010.
- [46] M. M. Rahman, M. J. A. Shiddiky, M. A. Rahman, and Y.-B. Shim. A lactate biosensor based on lactate dehydrogenase/nicotinamide adenine dinucleotide (oxidized form) immobilized on a conducting polymer/multiwall carbon nanotube composite film. *Analytical Biochemistry*, 384(1):159–165, 2009.
- [47] M. Gamella, S. Campuzano, F. Conzuelo, J. A. Curiel, R. Muñoz, A. J. Reviejo, and J. M. Pingarrán. Integrated multienzyme electrochemical biosensors for monitoring malolactic fermentation in wines. *Talanta*, 81(3):925–933, 2010.
- [48] S. Bell and F. Dunand. A comparison of amperometric and optical dissolved oxygen sensors in power and industrial water applications at low oxygen levels ($< 5 \mu\text{g} \cdot \text{kg}^{-1}$). *Power Plant Chemistry*, 12(5):296–303, 2010.
- [49] G. Broder and M. H. Weil. Excess lactate: an index of reversibility of shock in human patients. *Science*, 143(3613):1457–1459, 1964.
- [50] A. Esteve-Núñez, J. Sosnik, P. Visconti, and D. R. Lovley. Fluorescent properties of c-type cytochromes reveal their potential role as an extracytoplasmic electron sink in *geobacter sulfurreducens*. *Environmental Microbiology*, 10(2):497–505, 2008.
- [51] G. Suárez, C. Santschi, S. Dutta-Gupta, L. Juillerat-Jeanerret, and O. J. F. Martin. Biophotonic tool for sensing the dynamics of h₂o₂ extracellular release in stressed cells. *Proc. SPIE 8229, Optical Diagnostics and Sensing XII: Toward Point-of-Care Diagnostics; and Design and Performance Validation of Phantoms Used in Conjunction with Optical Measurement of Tissue IV, 822908 (February 1, 2012)*, 8229:822908–822908–7, 2012.

- [52] G. Suárez, C. Santschi, O. J. F. Martin, and V. I. Slaveykova. Biosensor based on chemically-designed anchorable cytochrome c for the detection of h₂o₂ released by aquatic cells. *Biosensors and Bioelectronics*, 42(0):385–390, 2013.
- [53] Z. Wang, C. Zhao, D. Han, and F. Gu. Luminol chemiluminescence actuated by modified natural sepiolite material and its analytical application. *Analytical Methods*, 7(6):2779–2785, 2015.
- [54] N. Shimojo, K. Naka, C. Nakajima, C. Yoshikawa, K. Okuda, and K. Okada. Test-strip method for measuring lactate in whole blood. *Clinical Chemistry*, 35(9):1992–1994, 1989.
- [55] T. Karapinar, O. Kaynar, A. Hayirli, and M. Kom. Evaluation of 4 point-of-care units for the determination of blood L-lactate concentration in cattle. *Journal of Veterinary Internal Medicine*, 27(6):1596–1603, 2013.
- [56] T. Hassell, S. Gleave, and M. Butler. Growth inhibition in animal cell culture. *Applied Biochemistry and Biotechnology*, 30(1):29–41, 1991.
- [57] Persistence Market Research. Global market study on biosensors: Asia-Pacific to witness highest growth by 2020, <http://www.persistencemarketresearch.com/market-research/biosensor-market.asp>, October 2014.
- [58] R. Silverman. *Enzyme Kinetics. In: The Organic Chemistry of Enzyme-Catalyzed Reactions*. Academic Press, 2002.
- [59] J. M. Berg, J. L. Tymoczko, and L. Stryer. *Biochemistry (5th Ed.)*. W H Freeman, New York, 2002.
- [60] D. E. Koshland. The key-lock theory and the induced fit theory. *Angewandte Chemie – International Edition*, 33(23-24):2375–2378, 1995.
- [61] H. M. Berman, J. Westbrook, Z. Feng, G. Gilliland, T. N. Bhat, H. Weissig, I. N. Shindyalov, and P. E. Bourne. The protein data bank. *Nucleic acids research*, 28(1):235–242, 2000.
- [62] D. Schomburg. BRENDA: The comprehensive enzyme information system, <http://www.brenda-enzymes.org>, accessed: March 10th, 2015.
- [63] Enzyme Nomenclature. Recommendations of the nomenclature committee of the international union of biochemistry and molecular biology on the nomenclature and classification of enzymes. *NC-IUBMB Academic*, 1992.
- [64] K. Swiderek, A. Panczakiewicz, A. Bujacz, G. Bujacz, and P. Paneth. Modeling of isotope effects on binding oxamate to lactic dehydrogenase. *The Journal of Physical Chemistry B*, 113(38):12782–12789, 2009.
- [65] R. B. McComb, L. W. Bond, R. W. Burnett, R. C. Keech, and G. N. Bowers Jr. Determination of the molar absorptivity of NADH. *Clinical Chemistry*, 22(2):141–150, 1976.
- [66] J. R. Lakowicz, H. Szmecinski, K. Nowaczyk, and M. L. Johnson. Fluorescence lifetime imaging of free and protein-bound nadh. *Proceedings of the National Academy of Sciences*, 89(4):1271–1275, 1992.

Bibliography

- [67] E. T. Pineda Jr., R. Callender, and S. D. Schwartz. Ligand binding and protein dynamics in lactate dehydrogenase. *Biophysical Journal*, 93(5):1474–1483, 2007.
- [68] Y. Umena, K. Yorita, T. Matsuoka, A. Kita, K. Fukui, and Y. Morimoto. The crystal structure of L-lactate oxidase from aerococcus viridans at 2.1 Å resolution reveals the mechanism of strict substrate recognition. *Biochemical and Biophysical Research Communications*, 350(2):249–256, 2006.
- [69] Toyobo Co. Ltd. L-lactate oxidase from microorganism, product specification. http://www.toyobo-global.com/seihin/xr/enzyme/pdf_files/2010_189_192_LCO_301.pdf, accessed March 10th 2015.
- [70] D. Edmondson and S. Ghisla. Flavoenzyme structure and function. In S. Chapman and G. Reid, editors, *Flavoprotein Protocols*, volume 131 of *Methods in Molecular Biology*, chapter 12, pages 157–179. Humana Press, 1999.
- [71] I. Leiros, E. Wang, T. Rasmussen, E. Oksanen, H. Repo, S. B. Petersen, P. Heikinheimo, and E. Hough. The 2.1 Å structure of aerococcus viridans L-lactate oxidase (LOx). *Acta Crystallographica Section F*, 62(12):1185–1190, 2006.
- [72] A. Mattevi. To be or not to be an oxidase: challenging the oxygen reactivity of flavoenzymes. *Trends in Biochemical Sciences*, 31(5):276–283, 2006.
- [73] P. Macheroux, V. Kieweg, V. Massey, E. Söderlind, K. Stenberg, and Y. Lindqvist. Role of tyrosine 129 in the active site of spinach glycolate oxidase. *European Journal of Biochemistry*, 213(3):1047–1054, 1993.
- [74] T. Soderberg. Enzymatic reactions with free radical intermediates. In *Organic Chemistry with a Biological Emphasis*. University of Minnesota, Morris, 2010.
- [75] G. I. Berglund, G. H. Carlsson, A. T. Smith, H. Szoke, A. Henriksen, and J. Hajdu. The catalytic pathway of horseradish peroxidase at high resolution. *Nature*, 417(6887):463–468, 2002.
- [76] A. Henriksen, A. T. Smith, and M. Gajhede. The structures of the horseradish peroxidase C-ferulic acid complex and the ternary complex with cyanide suggest how peroxidases oxidize small phenolic substrates. *Journal of Biological Chemistry*, 274(49):35005–35011, 1999.
- [77] Sigma Aldrich Corp. Peroxidase from horseradish, Online product data sheet, <http://www.sigmaaldrich.com/content/dam/sigma-aldrich/docs/sigma/datasheet/2/p8375dat.pdf>, Accessed January 27th, 2014.
- [78] N. C. Veitch. Horseradish peroxidase: a modern view of a classic enzyme. *Phytochemistry*, 65(3):249–259, 2004.
- [79] G. T. Hermansson. Homobifunctional crosslinkers. In G. T. Hermansson, editor, *Bioconjugate Techniques*, pages 234–275. Academic Press, New York, 2008.
- [80] G. W. Bushnell, G. V. Louie, and G. D. Brayer. High-resolution three-dimensional structure of horse heart cytochrome C. *Journal of Molecular Biology*, 214(2):585–595, 1990.

- [81] C. Giulivi and E. Cadenas. The reaction of ascorbic acid with different heme iron redox states of myoglobin: antioxidant and prooxidant aspects. *FEBS Letters*, 332(3):287–290, 1993.
- [82] P. L. Vandewalle and N. O. Petersen. Oxidation of reduced cytochrome C by hydrogen peroxide: implications for superoxide assays. *FEBS Letters*, 210(2):195–198, 1987.
- [83] R. Radi, L. Thomson, H. Rubbo, and E. Prodanov. Cytochrome c-catalyzed oxidation of organic molecules by hydrogen peroxide. *Archives of Biochemistry and Biophysics*, 288(1):112–117, 1991.
- [84] G. A. Truskey, G. Yuan, and D. F. Katz. *Transport Phenomena in Biological Systems (2nd Ed.)*. Pearson, Upper Saddle River, NJ, 2009.
- [85] M. Hartmann and X. Kostrov. Immobilization of enzymes on porous silicas - benefits and challenges. *Chemical Society Reviews*, 42(15):6277–6289, 2013.
- [86] E. Magner. Immobilisation of enzymes on mesoporous silicate materials. *Chemical Society Reviews*, 42(15):6213–6222, 2013.
- [87] K. E. Cassimjee, M. Trummer, C. Branneby, and P. Berglund. Silica-immobilized his6-tagged enzyme: Alanine racemase in hydrophobic solvent. *Biotechnology and Bioengineering*, 99(3):712–716, 2008.
- [88] L. Cao. Covalent enzyme immobilization. In *Carrier-Bound Immobilized Enzymes*, pages 169–316. Wiley-VCH, 2005.
- [89] U. Hanefeld, L. Cao, and E. Magner. Enzyme immobilisation: Fundamentals and application. *Chemical Society Reviews*, 42(15):6211–6212, 2013.
- [90] R. A. Sheldon and S. van Pelt. Enzyme immobilisation in biocatalysis: Why, what and how. *Chemical Society Reviews*, 42(15):6223–6235, 2013.
- [91] M. D. Trevan. Enzyme immobilization by covalent bonding. In *New Protein Techniques; J. Walker, Ed. (Chapter 37)*, pages 495–510. Humana Press: Clifton, NJ, 1988.
- [92] C. N. Khobragade and S. G. Chandel. Comparative study of catalytic activity of immobilized invertase in sodium alginate gel on sucrose hydrolysis. *Indian Journal of Chemical Technology*, 9(6):535–539, 2002.
- [93] Biorad Laboratories. Affi-gel, URL: <http://www.bio-rad.com/en-au/product/affi-gel-10-gel>, October 3rd, 2014.
- [94] S. Cantone, V. Ferrario, L. Corici, C. Ebert, D. Fattor, P. Spizzo, and L. Gardossi. Efficient immobilisation of industrial biocatalysts: criteria and constraints for the selection of organic polymeric carriers and immobilisation methods. *Chemical Society Reviews*, 42(15):6262–6276, 2013.
- [95] K. Ariga, J. P. Hill, and Q. Ji. Layer-by-layer assembly as a versatile bottom-up nanofabrication technique for exploratory research and realistic application. *Physical Chemistry Chemical Physics*, 9(19):2319–2340, 2007.

Bibliography

- [96] E. J. Calvo. Electrochemically active LbL multilayer films: From biosensors to nanocatalysts. In *Multilayer Thin Films*, pages 1003–1038. Wiley-VCH, 2012.
- [97] N. Ferreyra, L. Coche-Guerente, and P. Labbe. Construction of layer-by-layer self-assemblies of glucose oxidase and cationic polyelectrolyte onto glassy carbon electrodes and electrochemical study of the redox-mediated enzymatic activity. *Electrochimica Acta*, 49(3):477–484, 2004.
- [98] J. V. Alemán, A. V. Chadwick, J. He, M. Hess, K. Horie, R. G. Jones, P. Kratochvíl, I. Meisel, I. Mita, G. Moad, S. Penczek, and R. F. T. Stepto. Definitions of terms relating to the structure and processing of sols, gels, networks, and inorganic-organic hybrid materials (IUPAC recommendations 2007). *Pure and Applied Chemistry*, 79(10):1801, 2007.
- [99] C. Sanchez, P. Belleville, M. Popall, and L. Nicole. Applications of advanced hybrid organic–inorganic nanomaterials: From laboratory to market. *Chemical Society Reviews*, 40(2):696–753, 2011.
- [100] C. J. Brinker and G. W. Scherer. *Sol-Gel Science, the Physics and Chemistry of Sol-Gel Processing*. Academic Press, Boston, 1990.
- [101] R. H. Iler. *The Chemistry of Silica*. John Wiley & Sons Inc, 1979.
- [102] A. A. Antipov, Y. Fedutik, A. I. Petrov, G. B. Sukhorukov, and H. Möhwald. Carbonate microparticles for hollow polyelectrolyte capsules fabrication. *Colloids and Surfaces A: Physicochemical and Engineering Aspects*, 224(1):175–183, 2003.
- [103] G. B. Sukhorukov, D. V. Volodkin, A. M. Günther, A. I. Petrov, D. B. Shenoy, and H. Möhwald. Porous calcium carbonate microparticles as templates for encapsulation of bioactive compounds. *Journal of Materials Chemistry*, 14(14):2073–2081, 2004.
- [104] D. V. Volodkin, R. von Klitzing, and H. Möhwald. Pure protein microspheres by calcium carbonate templating. *Angewandte Chemie International Edition*, 122(48):9444–9447, 2010.
- [105] A. L. Becker, A. Johnston, and F. Caruso. Layer-by-layer-assembled capsules and films for therapeutic delivery. *Small*, 6(17), 2010.
- [106] J. Guo, Y. Ping, H. Ejima, K. Alt, M. Meissner, J. J. Richardson, Y. Yan, K. Peter, D. von Elverfeldt, C. E. Hagemeyer, and F. Caruso. Engineering multifunctional capsules through the assembly of metal–phenolic networks. *Angewandte Chemie International Edition*, 53(22):5546–5551, 2014.
- [107] Y. Yan, M. Björnalm, and F. Caruso. Assembly of layer-by-layer particles and their interactions with biological systems. *Chemistry of Materials*, 26(1):452–460, 2013.
- [108] H. Imai, N. Tochimoto, Y. Nishino, Y. Takezawa, and Y. Oaki. Oriented nanocrystal mosaic in monodispersed CaCO₃ microspheres with functional organic molecules. *Crystal Growth & Design*, 12(2):876–882, 2012.
- [109] Y. Li, F. Gao, W. Wei, J.-B. Qu, G.-H. Ma, and W.-Q. Zhou. Pore size of macroporous polystyrene microspheres affects lipase immobilization. *Journal of Molecular Catalysis B: Enzymatic*, 66(1-2):182–189, 2010.

- [110] J. Cheng, R. Bordes, E. Olsson, and K. Holmberg. One-pot synthesis of porous gold nanoparticles by preparation of ag/au nanoparticles followed by dealloying. *Colloids and Surfaces A: Physicochemical and Engineering Aspects*, 436:823–829, 2013.
- [111] H. Zhou, S. Xu, H. Su, M. Wang, W. Qiao, L. Ling, and D. Long. Facile preparation and ultra-microporous structure of melamine–resorcinol–formaldehyde polymeric microspheres. *Chemical Communications*, 49(36):3763–3765, 2013.
- [112] B.-L. Su, C. Sanchez, and X.-Y. Yang. Insights into hierarchically structured porous materials: From nanoscience to catalysis, separation, optics, energy, and life science. In *Hierarchically Structured Porous Materials*, pages 1–27. Wiley-VCH, 2011.
- [113] U. Schubert and N. Hüsing. *Synthesis of Inorganic Materials*. Wiley-VCH, 2004.
- [114] C. M. A. Parlett, K. Wilson, and A. F. Lee. Hierarchical porous materials: Catalytic applications. *Chemical Society Reviews*, 42(9):3876–3893, 2013.
- [115] M. E. Franke, T. J. Koplín, and U. Simon. Metal and metal oxide nanoparticles in chemiresistors: Does the nanoscale matter? *Small*, 2(1):36–50, 2006.
- [116] S. Tao, Z. Shi, G. Li, and P. Li. Hierarchically structured nanocomposite films as highly sensitive chemosensory materials for TNT detection. *ChemPhysChem*, 7(9):1902–1905, 2006.
- [117] Q. Li, M. Retsch, J. J. Wang, W. G. Knoll, and U. Jonas. Porous networks through colloidal templates. In P. Broekmann, K. H. Dotz, and C. A. Schalley, editors, *Templates in Chemistry III*, volume 287 of *Topics in Current Chemistry*, pages 135–180. Springer Verlag, 2009.
- [118] Y. Wan and D. Zhao. On the controllable soft-templating approach to mesoporous silicates. *Chemical Reviews*, 107(7):2821–2860, 2007.
- [119] Y. Wan, H. Yang, and D. Zhao. Host-guest chemistry in the synthesis of ordered non-siliceous mesoporous materials. *Accounts of Chemical Research*, 39(7):423–432, 2006.
- [120] G. J. Soler-Illia, P. C. Angelome, M. C. Fuertes, A. Calvo, A. Wolosiuk, A. Zelcer, M. G. Bellino, and E. D. Martinez. Mesoporous hybrid and nanocomposite thin films. a sol-gel toolbox to create nanoconfined systems with localized chemical properties. *Journal of Sol-Gel Science and Technology*, 57(3):299–312, 2011.
- [121] G. J. Soler-Illia, P. C. Angelome, M. C. Fuertes, D. Grosso, and C. Boissiere. Critical aspects in the production of periodically ordered mesoporous titania thin films. *Nanoscale*, 4(8):2549–2566, 2012.
- [122] G. J. Soler-Illia, C. Sanchez, B. Lebeau, and J. Patarin. Chemical strategies to design textured materials: From microporous and mesoporous oxides to nanonetworks and hierarchical structures. *Chemical Reviews*, 102(11):4093–4138, 2002.
- [123] G. J. Soler-Illia, E. L. Crepaldi, D. Grosso, and C. Sanchez. Block copolymer-templated mesoporous oxides. *Current Opinion in Colloid & Interface Science*, 8(1):109–126, 2003.

Bibliography

- [124] C. T. Kresge, M. E. Leonowicz, W. J. Roth, J. C. Vartuli, and J. S. Beck. Ordered mesoporous molecular sieves synthesized by a liquid-crystal template mechanism. *Nature*, 359(6397):710–712, 1992.
- [125] R. B. Bird, W. E. Stewart, and E. N. Lightfoot. *Transport Phenomena*. Wiley, New York, 2007.
- [126] D. Iber. Numerical solution of reaction–diffusion problems (PDF tutorial, computational biology group (CoBi), ETH Zürich), www.bsse.ethz.ch, Accessed January 2015.
- [127] W. M. Deen. *Analysis of Transport Phenomena*. Oxford University Press, UK, 2011.
- [128] H. S. Fogler. *Elements of Chemical Reaction Engineering (4th Ed.)*. Prentice Hall, 2009.
- [129] J. L. Anderson and J. A. Quinn. Restricted transport in small pores: A model for steric exclusion and hindered particle motion. *Biophysical Journal*, 14(2):130, 1974.
- [130] P. L. Paine and P. Scherr. Drag coefficients for the movement of rigid spheres through liquid-filled cylindrical pores. *Biophysical Journal*, 15(10):1087–1091, 1975.
- [131] J. Fu, M. Liu, Y. Liu, N. W. Woodbury, and H. Yan. Interenzyme substrate diffusion for an enzyme cascade organized on spatially addressable DNA nanostructures. *Journal of the American Chemical Society*, 134(12):5516–5519, 2012.
- [132] H. R. Zare and S. M. Golabi. Caffeic acid modified glassy carbon electrode for electrocatalytic oxidation of reduced nicotinamide adenine dinucleotide (NADH). *Journal of Solid State Electrochemistry*, 4(2):87–94, 2000.
- [133] A. C. F. Ribeiro, V. M. M. Lobo, D. G. Leaist, J. J. S. Natividade, L. P. Verissimo, M. C. F. Barros, and A. M. T. D. P. V. Cabral. Binary diffusion coefficients for aqueous solutions of lactic acid. *Journal of Solutions Chemistry*, 34:1009–1016, 2005.
- [134] B. Ghanbarian, A. G. Hunt, R. P. Ewing, and M. Sahimi. Tortuosity in porous media: a critical review. *Soil Science Society of America Journal*, 77(5):1461–1477, 2013.
- [135] P. Van Cappellen and J.-F. Gaillard. Biogeochemical dynamics in aquatic sediments. *Reviews in Mineralogy and Geochemistry*, 34(1):335–376, 1996.
- [136] P. M. Adler. *Porous Media: Geometry and Transports*. Butterworth–Heinemann, New York, 1992.
- [137] L. Shen and Z. Chen. Critical review of the impact of tortuosity on diffusion. *Chemical Engineering Science*, 62(14):3748–3755, 2007.
- [138] S. C. Carniglia. Construction of the tortuosity factor from porosimetry. *Journal of Catalysis*, 102(2):401–418, 1986.
- [139] J. S. Mackie and P. Meares. The diffusion of electrolytes in a cation-exchange resin membrane. i. theoretical. *Proceedings of the Royal Society of London. Series A. Mathematical and Physical Sciences*, 232(1191):498–509, 1955.

- [140] N. Wakao and J. M. Smith. Diffusion in catalyst pellets. *Chemical Engineering Science*, 17(11):825–834, 1962.
- [141] M. Suzuki and J. M. Smith. Axial dispersion in beds of small particles. *Chemical Engineering Journal*, 3:256–264, 1972.
- [142] S. R. Veith, E. Hughes, G. Vuataz, and S. E. Pratsinis. Restricted diffusion in silica particles measured by pulsed field gradient NMR. *Journal of Colloid and Interface Science*, 274(1):216–228, 2004.
- [143] Y. Lu, R. Ganguli, C. A. Drewien, M. T. Anderson, C. J. Brinker, W. Gong, Y. Guo, H. Soyez, B. Dunn, M. H. Huang, and J. I. Zink. Continuous formation of supported cubic and hexagonal mesoporous films by sol-gel dip-coating. *Nature*, 389(6649):364–368, 1997.
- [144] C. Lei, Y. Shin, J. Liu, and E. J. Ackerman. Entrapping enzyme in a functionalized nanoporous support. *Journal of the American Chemical Society*, 124(38):11242–11243, 2002.
- [145] M. Hartmann. Ordered mesoporous materials for bioadsorption and biocatalysis. *Chemistry of Materials*, 17(18):4577–4593, 2005.
- [146] A. Taguchi and F. Schüth. Ordered mesoporous materials in catalysis. *Microporous and Mesoporous Materials*, 77(1):1–45, 2005.
- [147] I. I. Slowing, B. G. Trewyn, S. Giri, and V. Y. Lin. Mesoporous silica nanoparticles for drug delivery and biosensing applications. *Advanced Functional Materials*, 17(8):1225–1236, 2007.
- [148] C. C. Chen, J. S. Do, and Y. Gu. Immobilization of HRP in mesoporous silica and its application for the construction of polyaniline modified hydrogen peroxide biosensor. *Sensors*, 9(6):4635–4648, 2009.
- [149] D. Chen, F. Huang, Y. B. Cheng, and R. A. Caruso. Mesoporous anatase TiO₂ beads with high surface areas and controllable pore sizes: A superior candidate for high-performance dye-sensitized solar cells. *Advanced Materials*, 21(21):2206–2210, 2009.
- [150] M. Kruk. Access to ultralarge-pore ordered mesoporous materials through selection of surfactant/swelling-agent micellar templates. *Accounts of Chemical Research*, 45(10):1678–1687, 2012.
- [151] B. G. Trewyn, S. Giri, I. I. Slowing, and V. S. Y. Lin. Mesoporous silica nanoparticle based controlled release, drug delivery, and biosensor systems. *Chemical Communications*, 31:3236–3245, 2007.
- [152] S. Giri, B. G. Trewyn, and V. S. Y. Lin. Mesoporous silica nanomaterial-based biotechnological and biomedical delivery systems. *Nanomedicine*, 2(1):99–111, 2007.
- [153] K. Suzuki, K. Ikari, and H. Imai. Synthesis of mesoporous silica foams with hierarchical trimodal pore structures. *Journal of Materials Chemistry*, 13(7):1812–1816, 2003.

Bibliography

- [154] M. C. Fuertes and G. J. Soler-Illia. Processing of macroporous titania thin films: From multiscale functional porosity to nanocrystalline macroporous TiO₂. *Chemistry of Materials*, 18(8):2109–2117, 2006.
- [155] A. C. Fournier, H. Cumming, and K. M. McGrath. Assembly of two- and three-dimensionally patterned silicate materials using responsive soft templates. *Dalton Transactions*, 39(28):6524–6531, 2010.
- [156] C. Triantafillidis, M. S. Elsaesser, and N. Hüsing. Chemical phase separation strategies towards silica monoliths with hierarchical porosity. *Chemical Society Reviews*, 42(9):3833–3846, 2013.
- [157] J. Nestor, A. Vilchez, C. Solans, and J. Esquena. Facile synthesis of meso/macroporous dual materials with ordered mesopores using highly concentrated emulsions based on a cubic liquid crystal. *Langmuir*, 29(1):432–440, 2012.
- [158] P. Bowen, H. Hofmann, M. Staiger, R. Steiger, P. A. Brugger, and K. Peternell. Colloidal processing of nanoceramic powders for porous ceramic film applications. *Euro Ceramics VII, Pt 1-3*, pages 1977–1980, 2002.
- [159] D. Zhao, J. Feng, Q. Huo, N. Melosh, G. H. Fredrickson, B. F. Chmelka, and G. D. Stucky. Triblock copolymer syntheses of mesoporous silica with periodic 50 to 300 angstrom pores. *Science*, 279(5350):548–552, 1998.
- [160] F. Eder and N. Hüsing. Mesoporous silica layers with controllable porosity and pore size. *Applied Surface Science*, 256(3, Suppl.):S18–S21, 2009.
- [161] E. Krämer, S. Förster, C. Göltner, and M. Antonietti. Synthesis of nanoporous silica with new pore morphologies by templating the assemblies of ionic block copolymers. *Langmuir*, 14(8):2027–2031, 1998.
- [162] S. Polarz and M. Antonietti. Porous materials via nanocasting procedures: Innovative materials and learning about soft-matter organization. *Chemical Communications*, 22:2593–2604, 2002.
- [163] C. Aubery, C. Solans, S. Prevost, M. Gradzielski, and M. Sanchez-Dominguez. Microemulsions as reaction media for the synthesis of mixed oxide nanoparticles: Relationships between microemulsion structure, reactivity, and nanoparticle characteristics. *Langmuir*, 29(6):1779–1789, 2013.
- [164] Y. Deng, J. Wei, Z. Sun, and D. Zhao. Large-pore ordered mesoporous materials templated from non-pluronic amphiphilic block copolymers. *Chemical Society Reviews*, 42(9):4054–4070, 2013.
- [165] K. M. McGrath, D. M. Dabbs, N. Yao, I. A. Aksay, and S. M. Gruner. Formation of a silicate l3 phase with continuously adjustable pore sizes. *Science*, 277(5325):552–556, 1997.
- [166] P. Feng, X. Bu, G. D. Stucky, and D. J. Pine. Monolithic mesoporous silica templated by microemulsion liquid crystals. *Journal of the American Chemical Society*, 122(5):994–995, 2000.

- [167] P. Feng, X. Bu, and D. J. Pine. Control of pore sizes in mesoporous silica templated by liquid crystals in block copolymer-cosurfactant-water systems. *Langmuir*, 16(12):5304–5310, 2000.
- [168] J. L. Blin and B. L. Su. Tailoring pore size of ordered mesoporous silicas using one or two organic auxiliaries as expanders. *Langmuir*, 18(13):5303–5308, 2002.
- [169] J. P. Hanrahan, M. P. Copley, K. J. Ziegler, T. R. Spalding, M. A. Morris, D. C. Steytler, R. K. Heenan, R. Schweins, and J. D. Holmes. Pore size engineering in mesoporous silicas using supercritical CO₂. *Langmuir*, 21(9):4163–4167, 2005.
- [170] J. R. Matos, M. Kruk, L. P. Mercuri, M. Jaroniec, L. Zhao, T. Kamiyama, O. Terasaki, T. J. Pinnavaia, and Y. Liu. Ordered mesoporous silica with large cage like pores: Structural identification and pore connectivity design by controlling the synthesis temperature and time. *Journal of the American Chemical Society*, 125(3):821–829, 2003.
- [171] T.-W. Kim, R. Ryoo, M. Kruk, K. P. Gierszal, M. Jaroniec, S. Kamiya, and O. Terasaki. Tailoring the pore structure of sba-16 silica molecular sieve through the use of copolymer blends and control of synthesis temperature and time. *Journal of Physical Chemistry B*, 108(31):11480–11489, 2004.
- [172] A. Sayari, P. Liu, M. Kruk, and M. Jaroniec. Characterization of large-pore mcm-41 molecular sieves obtained via hydrothermal restructuring. *Chemistry of Materials*, 9(11):2499–2506, 1997.
- [173] Y. V. Kolen'ko, V. D. Maximov, A. V. Garshev, P. E. Meskin, N. N. Oleynikov, and B. R. Churagulov. Hydrothermal synthesis of nanocrystalline and mesoporous titania from aqueous complex titanyl oxalate acid solutions. *Chemical Physics Letters*, 388(4-6):411–415, 2004.
- [174] C. Sanchez, C. Boissiere, D. Grosso, C. Laberty, and L. Nicole. Design, synthesis, and properties of inorganic and hybrid thin films having periodically organized nanoporosity. *Chemistry of Materials*, 20(3):682–737, 2008.
- [175] J. D. Bass, E. Belamie, D. Grosso, C. Boissiere, T. Coradin, and C. Sanchez. Nanostructuring of titania films prepared by self-assembly to affect cell adhesion. *Journal of Biomedical Materials Research Part A*, 93A(1):96–106, 2010.
- [176] G. Coussot, C. Perrin, T. Moreau, M. Dobrijevic, A. Le Postollec, and O. Vandenabeele-Trambouze. A rapid and reversible colorimetric assay for the characterization of aminated solid surfaces. *Analytical and Bioanalytical Chemistry*, 399(3):1061–1069, 2011.
- [177] S. Krishnamoorthy, R. Pugin, J. Brugger, H. Heinzelmann, A. C. Hoogerwerf, and C. Hinderling. Block copolymer micelles as switchable templates for nanofabrication. *Langmuir*, 22(8):3450–3452, 2006.
- [178] J. Q. Lu and S. S. Yi. Uniformly sized gold nanoparticles derived from PS-B-P2VP block copolymer templates for the controllable synthesis of si nanowires. *Langmuir*, 22(9):3951–3954, 2006.

Bibliography

- [179] A. Frömsdorf, A. Kornowski, S. Pütter, H. Stillrich, and L. T. Lee. Highly ordered nanostructured surfaces obtained with silica-filled diblock-copolymer micelles as templates. *Small*, 3(5):880–889, 2007.
- [180] Y.-H. Cho, J.-E. Yang, and J.-S. Lee. Size control of polymeric nanoparticles from polystyrene-*b*-poly(2-vinylpyridine). *Materials Science and Engineering: C*, 24(1-2):293–295, 2004.
- [181] W.-J. Shin, J.-Y. Kim, G. Cho, and J.-S. Lee. Highly selective incorporation of SiO₂ nanoparticles in PS-*B*-P2VP block copolymers by quaternization. *Journal of Materials Chemistry*, 19(39):7322–7325, 2009.
- [182] C. C. Yang, P. T. Wu, W. C. Chen, and H. L. Chen. Low dielectric constant nanoporous poly(methyl silsesquioxane) using poly(styrene-*block*-2-vinylpyridine) as a template. *Polymer*, 45(16):5691–5702, 2004.
- [183] T. N. M. Bernardis, M. J. C. H. Janssen, and M. J. van Bommel. Influence of butanol on the hydrolysis-condensation behaviour of teos. *Journal of Non-Crystalline Solids*, 168(3):201–212, 1994.
- [184] S. Arichi, H. Matsuura, Y. Tanimoto, and H. Murata. Studies of poly-2-vinylpyridine. ii. solubilities in various solvents. *Bulletin of the Chemical Society of Japan*, 39(3):434–439, 1966.
- [185] R. P. Danner and M. S. High. *Handbook of Polymer Solution Thermodynamics*. John Wiley & Sons, 1993.
- [186] S. Arichi. Studies of poly-2-vinylpyridine. iii. intrinsic viscosity and molecular weight. *Bulletin of the Chemical Society of Japan*, 39(3):439–446, 1966.
- [187] S. Arichi, S. Mitsuta, N. Sakamoto, and H. Murata. Studies of poly-2-vinylpyridine. i. suspension polymerization and molecular weight distribution. *Bulletin of the Chemical Society of Japan*, 39(3):428–434, 1966.
- [188] G. Bernardo and D. Vesely. Equilibrium solubility of alcohols in polystyrene attained by controlled diffusion. *European Polymer Journal*, 43(3):938–948, 2007.
- [189] J. Brandrup, E. H. Immergut, and E. A. Grulke. Polymer handbook, vol. ii. *New York: Willey*, page 282, 1999.
- [190] P. L. Dubin. A polymer-solution "thermometer": A demonstration of the thermodynamic consequences of specific polymer-solvent interactions. *Journal of Chemical Education*, 58(11):866, 1981.
- [191] S. Arichi, M. Yoshida, and Y. Ogawa. The specific refractive index increment and the partial specific volume of atactic poly(2-vinylpyridine). *Bulletin of the Chemical Society of Japan*, 48(5):1417–1422, 1975.
- [192] C. J. Lawrence and W. Zhou. Spin coating of non-newtonian fluids. *Journal of Non-Newtonian Fluid Mechanics*, 39(2):137–187, 1991.

- [193] S. L. Burgess and S. D. R. Wilson. Spin-coating of a viscoplastic material. *Physics of Fluids*, 8(9):2291–2297, 1996.
- [194] P. Fischer. Time dependent flow in equimolar micellar solutions: Transient behaviour of the shear stress and first normal stress difference in shear induced structures coupled with flow instabilities. *Rheologica Acta*, 39(3):234–240, 2000.
- [195] V. Herle, P. Fischer, and E. J. Windhab. Stress driven shear bands and the effect of confinement on their structures - a rheological, flow visualization, and rheo-sals study. *Langmuir*, 21(20):9051–9057, 2005.
- [196] M. Antonietti, S. Heinz, M. Schmidt, and C. Rosenauer. Determination of the micelle architecture of polystyrene/poly(4-vinylpyridine) block copolymers in dilute solution. *Macromolecules*, 27(12):3276–3281, 1994.
- [197] Y. Li, B. P. Bastakoti, M. Imura, S. M. Hwang, Z. Sun, J. H. Kim, S. X. Dou, and Y. Yamauchi. Synthesis of mesoporous TiO₂/SiO₂ hybrid films as an efficient photocatalyst by polymeric micelle assembly. *Chemistry – A European Journal*, 20(20):6027–6032, 2014.
- [198] B. P. Bastakoti, Y. Li, N. Miyamoto, N. M. Sanchez-Ballester, H. Abe, J. Ye, P. Srinivasu, and Y. Yamauchi. Polymeric micelle assembly for the direct synthesis of functionalized mesoporous silica with fully accessible pt nanoparticles toward an improved co oxidation reaction. *Chemical Communications*, 50(65):9101–9104, 2014.
- [199] Y. Li, B. P. Bastakoti, M. Imura, N. Suzuki, X. Jiang, S. Ohki, K. Deguchi, M. Suzuki, S. Arai, and Y. Yamauchi. Synthesis of a large- sized mesoporous phosphosilicate thin film through evaporation-induced polymeric micelle assembly. *Chemistry – An Asian Journal*, 10(1):183–187, 2015.
- [200] B. P. Bastakoti, R. R. Salunkhe, J. Ye, and Y. Yamauchi. Direct synthesis of a mesoporous TiO₂-ruo2 composite through evaporation-induced polymeric micelle assembly. *Physical Chemistry Chemical Physics*, 16(22):10425–10428, 2014.
- [201] B. P. Bastakoti, N. L. Torad, and Y. Yamauchi. Polymeric micelle assembly for the direct synthesis of platinum-decorated mesoporous TiO₂ toward highly selective sensing of acetaldehyde. *ACS Applied Materials & Interfaces*, 6(2):854–860, 2013.
- [202] R Nagarajan. Frozen micelles: polymer nanoparticles of controlled size by self-assembly. *Nanoparticles: Synthesis, Stabilization, Passivation, and Functionalization*, 996:341–56, 2008.
- [203] D. P. Birnie III. Rational solvent selection strategies to combat striation formation during spin coating of thin films. *Journal of Materials Research*, 16(4):1145–1154, 2001.
- [204] D. P. Birnie III and M. Manley. Combined flow and evaporation of fluid on a spinning disk. *Physics of Fluids*, 9(4):870–875, 1997.
- [205] D. E. Haas and D. P. Birnie Iii. Evaluation of thermocapillary driving forces in the development of striations during the spin coating process. *Journal of Materials Science*, 37(10):2109–2116, 2002.

Bibliography

- [206] D. J. Taylor and D. P. Birnie III. A case study in striation prevention by targeted formulation adjustment: Aluminum titanate sol-gel coatings. *Chemistry of Materials*, 14(4):1488–1492, 2002.
- [207] D. P. Birnie III, D. M. Kaz, and D. J. Taylor. Surface tension evolution during early stages of drying of sol-gel coatings. *Journal of Sol-Gel Science and Technology*, 49(2):233–237, 2009.
- [208] M. Faustini, L. Nicole, C. Boissière, P. Innocenzi, C. Sanchez, and D. Grosso. Hydrophobic, antireflective, self-cleaning, and antifogging sol-gel coatings: An example of multifunctional nanostructured materials for photovoltaic cells. *Chemistry of Materials*, 22(15):4406–4413, 2010.
- [209] H. Juvaste, E. I. Iiskola, and T. T. Pakkanen. Preparation of new modified catalyst carriers. *Journal of Molecular Catalysis A: Chemical*, 150(1-2):1–9, 1999.
- [210] H. J. Chial, H. B. Thompson, and A. G. Splittgerber. A spectral study of the charge forms of coomassie blue g. *Analytical Biochemistry*, 209(2):258–266, 1993.
- [211] F. Secundo. Conformational changes of enzymes upon immobilisation. *Chemical Society Reviews*, 42(15):6250–6261, 2013.
- [212] J. Sun, H. Zhou, Y. Jin, M. Wang, Y. Li, and N. Gu. Magnetically enhanced dielectrophoretic assembly of horseradish peroxidase molecules: Chaining and molecular monolayers. *ChemPhysChem*, 9(13):1847–1850, 2008.
- [213] Z. Zhao, J. Tian, Z. Wu, J. Liu, D. Zhao, W. Shen, and L. He. Enhancing enzymatic stability of bioactive papers by implanting enzyme-immobilized mesoporous silica nanorods into paper. *Journal of Materials Chemistry B*, 1(37):4719–4722, 2013.
- [214] R. W. Bally and T. C. J. Gribnau. Some aspects of the chromogen 3,3',5,5'-tetramethylbenzidine as hydrogen donor in a horseradish peroxidase assay. *Journal of Clinical Chemistry and Clinical Biochemistry*, 27(10):791–796, 1989.
- [215] W. Humphrey, A. Dalke, and K. Schulten. VMD: Visual molecular dynamics. *Journal of Molecular Graphics*, 14(1):33–38, 1996.
- [216] M. S. Peresin, Y. Habibi, J. O. Zoppe, J. J. Pawlak, and O. J. Rojas. Nanofiber composites of polyvinyl alcohol and cellulose nanocrystals: manufacture and characterization. *Biomacromolecules*, 11(3):674–681, 2010.
- [217] D.P. Joshi, Y. L. Lan-Chun-Fung, and J. G. Pritchard. Determination of poly (vinyl alcohol) via its complex with boric acid and iodine. *Analytica Chimica Acta*, 104(1):153–160, 1979.
- [218] X. Wu, Y. Tian, Y. Cui, L. Wei, Q. Wang, and Y. Chen. Raspberry-like silica hollow spheres: Hierarchical structures by dual latex-surfactant templating route. *Journal of Physical Chemistry C*, 111(27):9704–9708, 2007.
- [219] D. H. Reneker and I. Chun. Nanometre diameter fibres of polymer, produced by electrospinning. *Nanotechnology*, 7(3):216–223, 1996.

- [220] J. Doshi and D. H. Reneker. Electrospinning process and applications of electrospun fibers. *Journal of Electrostatics*, 35(2-3):151–160, 1995.
- [221] D. Li and Y. Xia. Electrospinning of nanofibers: Reinventing the wheel? *Advanced Materials*, 16(14):1151–1170, 2004.
- [222] A. Greiner and J. H. Wendorff. Electrospinning: A fascinating method for the preparation of ultrathin fibers. *Angewandte Chemie - International Edition*, 46(30):5670–5703, 2007.
- [223] X.-Y. Yang, Y. Li, A. Lemaire, J.-G. Yu, and B.-L. Su. Hierarchically structured functional materials: Synthesis strategies for multimodal porous networks. *Pure and Applied Chemistry*, 81(12):2265–2307, 2009.
- [224] C. Ispas, I. Sokolov, and S. Andreescu. Enzyme-functionalized mesoporous silica for bioanalytical applications. *Analytical and Bioanalytical Chemistry*, 393(2):543–554, 2009.
- [225] C. Bernal, L. Sierra, and M. Mesa. Improvement of thermal stability of β -galactosidase from *Bacillus Circulans* by multipoint covalent immobilization in hierarchical macro-mesoporous silica. *Journal of Molecular Catalysis B: Enzymatic*, 84:166–172, 2012.
- [226] J.-L. Blin, J. Jacoby, S. Kim, M.-J. Stébé, N. Canilho, and A. Pasc. A meso-macro compartmentalized bioreactor obtained through silicalization of "green" double emulsions: w/o/w and w/slns/w. *Chemical Communications*, 50(80):11871–11874, 2014.
- [227] K. Szymanska, W. Pudlo, J. Mrowiec-Bialon, A. Czardybon, J. Kocurek, and A. B. Jarzebski. Immobilization of invertase on silica monoliths with hierarchical pore structure to obtain continuous flow enzymatic microreactors of high performance. *Microporous and Mesoporous Materials*, 170:75–82, 2013.
- [228] S. E. Letant, B. R. Hart, S. R. Kane, M. Z. Hadi, S. J. Shields, and J. G. Reynolds. Enzyme immobilization on porous silicon surfaces. *Advanced Materials*, 16(8):689–693, 2004.
- [229] F. Hook, B. Kasemo, T. Nylander, C. Fant, K. Sott, and H. Elwing. Variations in coupled water, viscoelastic properties, and film thickness of a mefp-1 protein film during adsorption and cross-linking: a quartz crystal microbalance with dissipation monitoring, ellipsometry, and surface plasmon resonance study. *Analytical Chemistry*, 73(24):5796–5804, 2001.
- [230] F. Hook, J. Voros, M. Rodahl, R. Kurrat, P. Boni, J. J. Ramsden, M. Textor, N. D. Spencer, P. Tengvall, J. Gold, and B. Kasemo. A comparative study of protein adsorption on titanium oxide surfaces using in situ ellipsometry, optical waveguide lightmode spectroscopy, and quartz crystal microbalance/dissipation. *Colloids and Surfaces B: Biointerfaces*, 24(2):155–170, 2002.
- [231] B. D. Vogt, E. K. Lin, W. L. Wu, and C. C. White. Effect of film thickness on the validity of the sauerbrey equation for hydrated polyelectrolyte films. *Journal of Physical Chemistry B*, 108:12685–12690, 2004.
- [232] K. S. W. Sing. Reporting physisorption data for gas/solid systems with special reference to the determination of surface area and porosity (recommendations 1984), 1985.

Bibliography

- [233] S. Lowell, J.E. Shields, M Thomas, and M. Thommes. *Characterization of Porous Solids and Powders: Surface Area, Pore Size and Density*. Particle Technology Series. Springer, The Netherlands, 2010.
- [234] Z. Sun, Y. Deng, J. Wei, D. Gu, B. Tu, and D. Zhao. Hierarchically ordered macro-/mesoporous silica monolith: Tuning macropore entrance size for size-selective adsorption of proteins. *Chemistry of Materials*, 23(8):2176–2184, 2011.
- [235] J. Rouquerol, G. Baron, R. Denoyel, H. Giesche, J. Groen, P. Klobe, P. Levitz, A. V. Neimark, S. Rigby, R. Skudas, K. Sing, M. Thommes, and Unger K. Liquid intrusion and alternative methods for the characterization of macroporous materials (IUPAC technical report). *Pure and Applied Chemistry*, 84(1):107–136, 2011.
- [236] F. Moro and H. Böhni. Ink-bottle effect in mercury intrusion porosimetry of cement-based materials. *Journal of Colloid and Interface Science*, 246(1):135–149, 2002.
- [237] J. Kaufmann. Characterization of pore space of cement-based materials by combined mercury and wood's metal intrusion. *Journal of the American Ceramic Society*, 92(1):209–216, 2009.
- [238] G. Sauerbrey. Verwendung von schwingquarzen zur wägung dünner schichten und zur mikrowägung. *Zeitschrift für Physik*, 155:206–222, 1959.
- [239] M. Eita. Insight into the adsorption of humic acid/Gd³⁺ complex on the surface of Al₂O₃ studied in situ by QCM-D and ex situ by ellipsometry and XPS. *Soft Matter*, 7(16):7424–7430, 2011.
- [240] R. P. Richter and A. R. Brisson. Following the formation of supported lipid bilayers on mica: A study combining AFM, QCM-D, and ellipsometry. *Biophysical journal*, 88(5):3422–3433, 2005.
- [241] A. Naderi, G. Olanya, R. Makuska, and P. M. Claesson. Desorption of bottle-brush polyelectrolytes from silica by addition of linear polyelectrolytes studied by QCM-D and reflectometry. *Journal of colloid and interface science*, 323(2):223–228, 2008.
- [242] J. Rickert, A. Brecht, and W. Gopel. Qcm operation in liquids: Constant sensitivity during formation of extended protein multilayers by affinity. *Analytical Chemistry*, 69(7):1441–1448, 1997.
- [243] R. P. Danner and M. S. High. *Zeta Potential in Colloid Science. Principles and Applications*. Academic Press, UK, 1988.
- [244] L. Dongqing. Chapter 3: Electro-viscous effects on pressure-driven liquid flow in microchannels. In *Interface Science and Technology Dongqing, L. (Ed.)*, pages 30–91. Elsevier, 2004.
- [245] L. Dongqing. Chapter 3: Electro-viscous effects on pressure-driven liquid flow in microchannels. In *Interface Science and Technology, Dongqing, L. (Ed.)*, pages 30–91. Elsevier, 2004.

- [246] J. Deere, E. Magner, J. G. Wall, and B. K. Hodnett. Adsorption and activity of proteins onto mesoporous silica. *Catalysis Letters*, 85(1-2):19–23, 2003.
- [247] M. Dong, Z. Wu, M. Lu, Z. Wang, and Z. Li. Combining the physical adsorption approach and the covalent attachment method to prepare a bifunctional bioreactor. *International Journal of Molecular Sciences*, 13(9):11443–11454, 2012.
- [248] S. J. Lovell and D. J. Winzor. Effects of phosphate on the dissociation and enzymic stability of rabbit muscle lactate dehydrogenase. *Biochemistry*, 13(17):3527–3531, 1974.
- [249] C. Bernal, L. Sierra, and M. Mesa. Application of hierarchical porous silica with a stable large porosity for β -galactosidase immobilization. *ChemCatChem*, 3(12):1948–1954, 2011.
- [250] R. Mezzenga and P. Fischer. The self-assembly, aggregation and phase transitions of food protein systems in one, two and three dimensions. *Reports on Progress in Physics*, 76(4):046601, 2013.
- [251] F. Macritchie and L. Ter-Minassian-Saraga. Concentrated protein monolayers: Desorption studies with radiolabelled bovine serum albumin. *Colloids and Surfaces*, 10:53–64, 1984.
- [252] C.-I. Li, Y.-H. Lin, C.-L. Shih, J.-P. Tsaur, and L.-K. Chau. Sol-gel encapsulation of lactate dehydrogenase for optical sensing of l-lactate. *Biosensors and Bioelectronics*, 17(4):323–330, 2002.
- [253] Y. Nakae and P. J. Stoward. Kinetic parameters of lactate dehydrogenase in liver and gastrocnemius determined by three quantitative histochemical methods. *Journal of Histochemistry & Cytochemistry*, 45(10):1427–1431, 1997.
- [254] J. L. Powers, N. E. Kiesman, C. M. Tran, J. H. Brown, and V. L. H. Bevilacqua. Lactate dehydrogenase kinetics and inhibition using a microplate reader. *Biochemistry and Molecular Biology Education*, 35(4):287–292, 2007.
- [255] K. J. Laidler and P. S. Bunting. The kinetics of immobilized enzyme systems. *Methods in enzymology*, 64:227–248, 1980.
- [256] J. Schöneberg, A. Ullrich, and F. Noé. Simulation tools for particle-based reaction-diffusion dynamics in continuous space. *BMC Biophysics*, 7(11):1–10, 2014.
- [257] R. R. Van Tassel, L. Guemouri, J. J. Ramsden, G. Tarjus, P. Viot, and J. Talbot. A particle-level model of irreversible protein adsorption with a postadsorption transition. *Journal of Colloid and Interface Science*, 207(2):317–323, 1998.
- [258] E. Dickinson. Proteins at interfaces and in emulsions - stability, rheology and interactions. *Journal of the Chemical Society-Faraday Transactions*, 94(12):1657–1669, 1998.
- [259] K. Ariga, Q. Ji, and J. Hill. Enzyme-encapsulated layer-by-layer assemblies: Current status and challenges toward ultimate nanodevices. In Frank Caruso, editor, *Modern Techniques for Nano- and Microreactors/-Reactions*, volume 229 of *Advances in Polymer Science*, chapter 42, pages 51–87. Springer Berlin Heidelberg, 2010.

Bibliography

- [260] O. N. Oliveira, P. H. B. Aoki, F. J. Pavinatto, and C. J. L. Constantino. Controlled architectures in LBL films for sensing and biosensing. In *Multilayer Thin Films*, pages 951–983. Wiley-VCH, 2012.
- [261] G. Decher, M. Eckle, J. Schmitt, and B. Struth. Layer-by-layer assembled multicomposite films. *Current Opinion in Colloid & Interface Science*, 3(1):32–39, 1998.
- [262] M. Schönhoff. Self-assembled polyelectrolyte multilayers. *Current Opinion in Colloid & Interface Science*, 8(1):86–95, 2003.
- [263] G. Decher. Layer-by-layer assembly (putting molecules to work). In *Multilayer Thin Films*, pages 1–21. Wiley-VCH, 2012.
- [264] R. K. Iler. Multilayers of colloidal particles. *Journal of Colloid and Interface Science*, 21(6):569–594, 1966.
- [265] G. Decher and J.-D. Hong. Buildup of ultrathin multilayer films by a self-assembly process, 1 consecutive adsorption of anionic and cationic bipolar amphiphiles on charged surfaces. *Makromolekulare Chemie. Macromolecular Symposia*, 46(1):321–327, 1991.
- [266] N. A. Kotov. Layer-by-layer self-assembly: The contribution of hydrophobic interactions. *Nanostructured Materials*, 12(5 - 8):789–796, 1999.
- [267] W. B. Stockton and M. F. Rubner. Molecular-level processing of conjugated polymers. 4. Layer-by-layer manipulation of polyaniline via hydrogen-bonding interactions. *Macromolecules*, 30(9):2717–2725, 1997.
- [268] X. Wang, Z. Jiang, J. Shi, Y. Liang, C. Zhang, and H. Wu. Metal-organic coordination-enabled layer-by-layer self-assembly to prepare hybrid microcapsules for efficient enzyme immobilization. *ACS Applied Materials & Interfaces*, 4(7):3476–3483, 2012.
- [269] W. Muller, H. Ringsdorf, E. Rump, G. Wildburg, X. Zhang, L. Angermaier, W. Knoll, M. Liley, and J. Spinke. Attempts to mimic docking processes of the immune system: recognition-induced formation of protein multilayers. *Science*, 262(5140):1706–1708, 1993.
- [270] J. Borges and J. F. Mano. Molecular interactions driving the layer-by-layer assembly of multilayers. *Chemical Reviews*, 114(18):8883–8942, 2014.
- [271] L. Derbal, H. Lesot, J. C. Voegel, and V. Ball. Incorporation of alkaline phosphatase into layer-by-layer polyelectrolyte films on the surface of affi-gel heparin beads: Physico-chemical characterization and evaluation of the enzyme stability. *Biomacromolecules*, 4(5):1255–1263, 2003.
- [272] G. K. Such, E. Tjipto, A. Postma, A. P. R. Johnston, and F. Caruso. Ultrathin, responsive polymer click capsules. *Nano Letters*, 7(6):1706–1710, 2007.
- [273] E. Margoliash and N. Frohwirt. Spectrum of horse-heart cytochrome c. *Biochem. J.*, 71(3):570–572, 1959.

- [274] W. D. Butt and D. Keilin. Absorption spectra and some other properties of cytochrome c and of its compounds with ligands. *Proceedings of the Royal Society of London. Series B, Biological Sciences*, 156(965):429–458, 1962.
- [275] D. Löwenich and K. Kleinermanns. Porphyrin fluorescence dominates UV photoemission of folded cytochrome C. *Photochemistry and Photobiology*, 83(6):1308–1312, 2007.
- [276] M. Müller, B. Kessler, N. Houbenov, K. Bohatá, Z. Pientka, and E. Brynda. pH dependence and protein selectivity of poly(ethyleneimine)/poly(acrylic acid) multilayers studied by in situ ATR-FTIR spectroscopy. *Biomacromolecules*, 7(4):1285–1294, 2006.
- [277] M. M. Andersson and R. Hatti-Kaul. Protein stabilising effect of polyethyleneimine. *Journal of Biotechnology*, 72(1–2):21–31, 1999.
- [278] G. H. Barlow and E. Margoliash. Electrophoretic behavior of mammalian-type cytochromes c. *Journal of Biological Chemistry*, 241(7):1473–1477, 1966.
- [279] X. Cao. *Antifouling Properties of Smooth and Structured Polyelectrolyte Thin Films*. PhD thesis, University of Heidelberg, Germany, 2008.
- [280] M. Kolasinska, R. Krastev, T. Gutberlet, and P. Warszynski. Swelling and water uptake of PAH/PSS polyelectrolyte multilayers. In G. Auernhammer, H.-J. Butt, and D. Vollmer, editors, *Surface and Interfacial Forces - from Fundamentals to Applications*, volume 134 of *Progress in Colloid and Polymer Science*, chapter 88, pages 30–38. Springer Berlin Heidelberg, 2008.
- [281] J. E. Gebhardt and D. W. Fuerstenau. Adsorption of polyacrylic acid at oxide/water interfaces. *Colloids and Surfaces*, 7(3):221–231, 1983.
- [282] J. Suh, H. J. Paik, and B. K. Hwang. Ionization of poly(ethylenimine) and poly(allylamine) at various pH's. *Bioorganic Chemistry*, 22(3):318–327, 1994.
- [283] J. Nagaya, M. Homma, A. Tanioka, and A. Minakata. Relationship between protonation and ion condensation for branched poly(ethylenimine). *Biophysical Chemistry*, 60(1–2):45–51, 1996.
- [284] H. Kawaguchi, H. Hirai, K. Sakai, S. Sera, T. Nakajima, Y. Ebisawa, and K. Koyama. Crystallization of inorganic compounds in polymer solutions. Part I: Control of shape and form of calcium carbonate. *Colloid and Polymer Science*, 270(12):1176–1181, 1992.
- [285] D. B. Trushina, T. V. Bukreeva, M. V. Kovalchuk, and M. N. Antipina. CaCO₃ vaterite microparticles for biomedical and personal care applications. *Materials Science and Engineering: C*, 45:644–658, 2014.
- [286] S. De Koker, L. J. De Cock, P. Rivera-Gil, W. J. Parak, R. A. Velty, C. Vervaet, J. P. Remon, J. Grooten, and B. G. De Geest. Polymeric multilayer capsules delivering biotherapeutics. *Advanced drug delivery reviews*, 63(9):748–761, 2011.

Bibliography

- [287] B. G. De Geest, M. A. Willart, H. Hammad, B. N. Lambrecht, C. Pollard, P. Bogaert, M. De Filette, X. Saelens, C. Vervaet, J. P. Remon, et al. Polymeric multilayer capsule-mediated vaccination induces protective immunity against cancer and viral infection. *ACS nano*, 6(3):2136–2149, 2012.
- [288] A. Johnston and E. Caruso. Exploiting the directionality of DNA: controlled shrinkage of engineered oligonucleotide capsules. *Angewandte Chemie*, 119(15):2731–2734, 2007.
- [289] V. Kozlovskaya, E. Kharlampieva, I. Drachuk, D. Cheng, and V. V. Tsukruk. Responsive microcapsule reactors based on hydrogen-bonded tannic acid layer-by-layer assemblies. *Soft Matter*, 6(15):3596–3608, 2010.
- [290] A. C. Pinheiro, A. I. Bourbon, M. A. Cerqueira, E. Maricato, C. Nunes, M. A. Coimbra, and A. Vicente. Chitosan/fucoidan multilayer nanocapsules as a vehicle for controlled release of bioactive compounds. *Carbohydrate polymers*, 115:1–9, 2015.
- [291] Y. Liu, J. Yang, Z. Zhao, J. Li, R. Zhang, and F. Yao. Formation and characterization of natural polysaccharide hollow nanocapsules via template layer-by-layer self-assembly. *Journal of colloid and interface science*, 379(1):130–140, 2012.
- [292] Konica Minolta. <http://www.konicaminolta.eu>, May 3rd, 2015.
- [293] H. X. Liu and R. M. Crooks. Three-dimensional paper microfluidic devices assembled using the principles of origami. *Journal of the American Chemical Society*, 133(44):17564–17566, 2011.
- [294] C. Ast, E. Schmalzlin, H.-G. Lohmannsroben, and J. T. Van Dongen. Optical oxygen micro- and nanosensors for plant applications. *Sensors*, 12(6):7015–7032, 2012.
- [295] Colibri Photonics. <http://www.colibri-photonics-com>, May 3rd, 2015.
- [296] W. M. Haynes (Ed.). *CRC Handbook of Chemistry and Physics, 95th Edition*. Taylor and Francis, Boca Raton FL, USA, 2014.

CURRICULUM VITAE

PERSONAL INFORMATION

First name: Oswaldo Javier
Last name: Pérez Anguiano
Date of birth: 20th march 1983
Birthplace: Mexico City, Mexico
Nationality: Mexican

EDUCATION

2011 – 2015	<u>PhD Materials Science & Engineering, EPFL</u> Powder Technology Laboratory Thesis: Innovative biosensing through the design of nanostructured materials	Switzerland
2008 – 2010	<u>MSc Food Technology, Specialization European Master in Food Studies</u> Wageningen University Lund University AgroParisTech University College Cork	The Netherlands Sweden France Ireland
2001 – 2005	<u>BSc Food Chemistry, National Autonomous University of Mexico</u> Minor: Food Microbiology.	Mexico

PROFESSIONAL EXPERIENCE

2010 – 2014	PhD trainee- Life Sciences Division, CSEM SA, Neuchâtel PhD project conducted at CSEM's headquarters	Switzerland
03-09 2014	Research stay- University of Melbourne Executed collaboration between my host laboratory in Switzerland and the Laboratory of Nanostructured Interfaces and Materials Science (NIMS) led by Prof. Frank Caruso. Expanded my scientific knowledge within the scope of my PhD project in a prestigious laboratory abroad.	Australia
2009 – 2010	Master Trainee- Flavours, Firmenich SA, Geneva Developed the experimental design (DoE), lab trials, large-scale production and analytical evaluation of glassy polysaccharide delivery systems at the interface of the analytical and materials science departments and the production plant.	Switzerland
2007 – 2008	Warehouse Manager, Nestlé SA, Toluca Complex Led two-shifts (2x8h) of cross-functional operational employees, managed inventories, forecasted critical materials, coordinated distribution of supplies to both Coffee and Culinary Factories, Implemented new warehouse layout due to expansion of production lines, avoiding rental of external facilities	Mexico
2006 – 2007	Quality assurance specialist, Nestlé SA, Toluca Complex Performed physicochemical analysis of raw and packaging materials at reception. Managed non-conformities and filed complaints. Coordinated quality audits to suppliers. Trained panelists for coffee and culinary semi-finished and finished products.	Mexico
2005 – 2006	Trainee- GLOBE, Nestlé SA, Mexico City Developed technical specifications for raw and packaging materials towards the implementation of SAP for the Mexican market	Mexico

CONFERENCES AND WORKSHOPS

05. 2014 Elsevier's Biosensors Conference. Poster presentation. Synthesis of hierarchically porous silica films for applications in lactate biosensing. Melbourne, Australia
03. 2013 3rd International Conference on Multifunctional, Hybrid and Nanomaterials. Poster presentation. Synthesis and characterization of large-mesoporous silica films for biosensing applications. Sorrento, Italy
01. 2013 Nanoparticles: from fundamentals to applications in Life Sciences. Centre of Competence in Materials Sciences (CCMX). Winter school. Kandersteg, Switzerland.
07. 2011 Growth and dissolution of solids on the molecular, cellular and atomic scale. National Research Programme 62 "Smart Materials" and CCMX. Lugano, Switzerland.
11. 2006 VI International Congress in Food Safety CIATEJ-CONACyT. Oral presentation. Detection of class-1 integrons in total DNA by PCR from antibiotic-multiresistance enterococci isolated from wholesale chicken in Mexico City. Guadalajara, Mexico
10. 2006 Food Science and Food Technology in Developing Countries. Poster presentation. Isolation and characterization of antibiotic-multiresistant enterococci from wholesale chicken sellers in Mexico City. Saltillo, Mexico.
04. 2006 2nd FEMS Congress of European Microbiologists. Poster presentation. Isolation and characterization of antibiotic-multiresistant enterococci from wholesale chicken sellers in Mexico City. Scientific evidence of antibiotic-fed poultry: a threat to public health. Madrid, Spain
04. 2006 National Congress of Microbiology. Poster presentation. Isolation and characterization of antibiotic-multiresistant enterococci from wholesale chicken and pork sellers in Mexico City. Oaxtepec, Mexico.

PUBLICATIONS

Pérez-Anguiano, O. et al. Controlling Mesopore Size and Processability of Transparent Enzyme-Loaded Silica Films for Biosensing Applications. *ACS Applied Materials & Interfaces*, 2015, 7 (4), pp 2960–2971

Pérez-Anguiano, O. et. al. Hierarchically porous silica films for lactate detection. In preparation

Pérez-Anguiano, O. et. al. Layer-by-layer assembled nanocomposite films and particles for enzyme-based lactate biosensors. In preparation

LANGUAGES

Spanish (mother tongue), English (fluent, C1), French (fluent, C1), German (learning, A2).

ADDITIONAL INFORMATION

Amateur singer (baritone) and writer, long distance runner, interested in different cultures, travelling, wine, coffee, psychology and vegetarian cuisine.